The role of extracellular vesicles in the oral squamous cell carcinoma tumour microenvironment

Cathy Park

A thesis submitted in partial fulfilment of the requirements for the degree of Doctor of Philosophy

The University of Sheffield

Faculty of Medicine, Dentistry and Health

School of Clinical Dentistry

September 2023

Acknowledgements

I would first and foremost like to Dr Stuart Hunt and Dr Helen Colley for their unwavering support and guidance. From my initial application, through COVID lockdowns, project setbacks, tight deadlines and silly lab mistakes. I'm extremely grateful to have had such a great supervisory team who go above and beyond for their students and, importantly, take me for ice-cream when I finish my lab work.

I would also like to thank all members of the Hunt Group and the Colley Group who have been there to guide me in the lab as beacons of knowledge. Namely Dr Amy Harding, Dr Bethany Ollington, Dr Luna Perciato, Dr Anita Liu, and Dr Wenyi Jiang.

Thank-you to the amazing students of the DSRS past and present, for keeping morale high, you make the Dental School a great place to work with a real sense of community. I especially would like to thank Hollie, Isabel, Klaudia, and Luna for being great friends.

A huge thank you to the technicians in the Dental School; Brenka, Jason, Matt and Lisa. As well as Sarah Elliot and Sue Clark from the medical school and Ben Peacock from NanoFCM.

Thank you to Isabel and Dan for opening your home, food and gin to me. You are the most generous and disapprovingly maternal people I know.

A special mention to Sarah and Jimmy, thank-you for everything, I couldn't have done this without you.

And last but not least, thank-you to my brilliant family. Thank-you Grandad Jack and Uncle Steve for being generous supporters. Thank-you Annie and Eve for being my best friends and cheerleaders. Of course mum and dad. There is nothing I cannot thank Grandma Jean for.

This thesis is dedicated to the memory of Grandma Pat.

Abstract

Head and neck cancer is the 6th most common cancer worldwide with 90% being classified as oral squamous cell carcinoma (OSCC). Recent findings have implicated the tumour microenvironment (TME), which includes cells such as cancer-associated fibroblasts (CAFs), in cancer progression. Tumour cells are known to communicate with stromal cells via a network of cytokines, growth factors and extracellular vesicles (EVs). There is evidence that some cargo are presented on the surface of EVs, such as transforming growth factor beta 1 (TGF-β1), and can induce CAF differentiation. We therefore sought to determine the role of EVs in promoting a CAF like phenotype.

A cell panel including an immortalised normal oral keratinocyte cell line, an OSCC cell line and primary patient derived normal oral fibroblasts (NOFs) and CAFs were used in this study. An EV deficient OSCC cell line ($H357^{\Delta HGS}$) and a fluorescent EV reporter OSCC cell line ($H357^{CD63\text{-}GFP}$) were characterised and validated by nanoparticle tracking analysis (NTA), quantitative polymerase chain reaction (qPCR), western blotting and immunofluorescence microscopy (IF). GFP tagged EV uptake in NOFs was visualised by fluorescence imaging. EVs were enriched by size exclusion chromatography (SEC) and characterised by NTA and western blotting. TGF-β1 was quantified by ELISA. CAF markers and phenotype was assessed using molecular techniques and functional assays.

There were significantly higher levels of TGF-β1 associated with EVs derived from oral cancer cells (H357) compared to normal cells (FNB6). TGF-β1 levels were significantly greater in EV preparations compared to conditioned media (CM). Treatment of NOFs with soluble recombinant TGF-β1 or H357 derived EVs led to an increase in α-SMA

stress fibre formation, however this was abrogated with the use of a TGF-β neutralising antibody, indicating an EV-TGF-β dependent role in NOF activation. Furthermore, compared to untreated cells, H357 derived EVs enhanced NOF migration and contraction. The cancer derived EVs promoted greater NOF contraction at 24 and 48 hours compared to their normal cell -derived EV counterparts.. These results indicate that inhibition of EV associated TGF-β1 might be a novel strategy to reduce stromal cell activation in the TME.

Abbreviations

α-SMA	Alpha smooth muscle actin
AC	Apoptotic cell
ADSC	Adipose-derived stem cell
AGO2	Argonaute RISC Catalytic Component 2
AJ	Adherens junctions
AKT	Protein kinase B
ALI	Air-liquid interface
ALIX	Programmed cell death 6-interacting protein
ANOVA	Analysis of variance
APS	Ammonium persulphate
ARF6	ADP-ribosylation factor 6
ATP	Adenosine triphosphate
BafA1	Bafliomycin A1
BC	Breast cancer
BCA	Bicinchoninic acid
BCL2	B-cell lymphoma 2
BM	Bone marrow
BNP	Bone morphogenetic proteins
BSA	Bovine serum albumin
CAF	Cancer associated fibroblast
CAV1	Caveolin 1
CCL2	Monocyte chemoattractant protein-1
CCND1	Cyclin D1
CD	Cluster of differentiation
CDKN2A	Cyclin-dependent kinase inhibitor 1A
CER	Ceramide
CFSE	Carboxyfluorescein succinimidyl ester
CHD9	Chromodomain Helicase DNA binding protein
CHMP4	Charged multivesicular body protein 4a
CL	Cell lysate
CM	Conditioned medium
COL11A1	Collagen type XI alpha 1 chain
COL1A1	Collagen type I alpha 1 chain
CRISPR	Clustered reguarly interspaced palindromic repeats
CSC	Cancer stem cell
CXCL	Chemokine (C-X-C motif) ligand
DAPI	4′,6-diamidino-2-phenylindole
DENND2D	DENN/MADD Domain Containing 2D
DMA	Dimethyl Amiloride
DMEM	Dulbecco's Modified Eagle Medium

DMSO	Dimethyl sulfoxide
DNA	Deoxyribonucleic acid
ECM	Extracellular matrix
EDTA	Ethylenediaminetetraacetic acid
EEA1	Early endosome antigen 1
EGF	Epidermal growth factor
EGFR	Epidermal growth factor receptor
ELISA	enzyme-linked immunosorbent assay
EMT	Epithelial to mesenchymal transition
ERK	Extracellular signal-related kinase
ESCC	Esophageal cancer
ESCRT	Endosomal sorting complex required for transport
EV	Extracellular vesicle
FA	Focal adhesion
FACS	Fluorescence-activated cell sorting
FAK	Focal adhesion kinase
FAP	Fibroblast activation protein
FBS	Fetal bovine serum
FITC	Fluorescein isothiocyanate
FN	Fibronectin
FOX3P	Forkhead box P3
GAPDH	Glyceraldehyde 3-phosphate dehydrogenase
GARP	Glycoprotein A repetitions predominant
GFP	Green fluorescent protein
GTP	Guanosine triphosphate
GTPase	Nucleotide guanosine triphosphate binding protein
HEPES	4-(2-hydroxyethyl)-1-piperazineethanesulfonic acid
HGF	Hepatocyte growth factor
HGS	Hepatocyte growth factor related tyrosine kinase
HIF	Hypoxia-inducible factor
HNC	Head and neck cancer
HNSCC	Head and neck squamous cell carcinoma
HPV	Human papillomavirus
HRP	Horseradish peroxidase
HSP90	Heat shock protein 90
HSPG	Heparan Sulfate Proteoglycans
HUVEC	Human umbilical vein endothelial cells
IDA	Iminodiacetic acid
IF	Immunofluorescence
IFN	Interferon
ILV	Intraluminal vesicle
IRF	Interferon-regulatory factor
IU	International Unit

JNK	c-Jun N-terminal kinase
KD	Knockdown
kDa	Kilodalton
KIBRA	kidney and brain expressed protein
KO	Knockout
LAMP1	Lysosomal associated membrane protein 1
LAP	Latency associated peptide
LLC	Large latency complex
lncRNA	Long non-coding ribonucleic acid
LSCC	laryngeal squamous cell carcinoma
LTBP	latent TGF-β-binding protein
MAPK	Mitogen-activated protein kinases
MDSC	myeloid-derived suppressor cells
miRNA	Micro ribonucleic acid
MMP	Matrix metalloproteinase
MMT	mesothelial-mesenchymal transition
mRNA	Messenger ribonucleic acid
MSC	Mesenchymal stem cell
MTT	3-(4,5-dimethylthiazol-2-yl)-2,5-diphenyltetrazolium
MV	Microvesicle
MVB	Multivesicular body
MVD	Microvessel density
MWCO	Molecular weight cut-off
NADPH	educed nicotinamide adenine dinucleotide phosphate
NAP1	Exosomal NF-κB-activating kinase-associated protein 1
NGS	Normal goat serum
NK	Natural killer
NOF	Normal oral fibroblast
NOK	Normal oral keratinocyte
NPC	Nasopharyngeal cancer
NTA	Nanoparticle tracking analysis
OMV	Outer membrane vesicles
OSCC	Oral squamous cell carcinoma
PBMC	Peripheral blood mononuclear cells
PBS	Phosphate buffered saline
PC	Prostate cancer
PCR	Polymerase chain reaction
PDGFR	Platelet derived growth factor receptor
PDL-1	Programmed cell death ligand 1
PFA	Paraformaldehyde
PKM2	Pyruvate kinase M2
PLD2	Phospholipase D2
PMF	Primary myelofibrosis

PS	phosphatidylserines
qPCR	Quantitative polymerase chain reaction
Rab	Ras-associated binding protein
Ras	Rat sarcoma virus
RFU	Relative fluorescence unit
RIPA	Radioimmunoprecipitation assay
RISC	RNA-induced silencing complex
RNA	Ribonucleic acid
ROCK	Rho-associated protein kinase
ROS	Reactive oxygen species
SCC	Squamous cell carcinoma
SDS	Sodium dodecyl sulphate
SDS-PAGE	Sodium dodecyl sulphate-polyacrylamide gel electrophoresis
SEC	Size exclusion chromatography
SMAD	Suppressor of Mothers against Decapentaplegic
SNARE	Soluble N-ethylmaleimide-sensitive fusion attachment protein receptor
STAT	signal transducer and activator of transcription
TAM	Tumour associated macrophage
TBS	Tris buffered saline
TEM	Tetraspanin-enriched microdomains
TGF-β	Transforming growth factor beta
TGFR	Transforming growth factor receptor
TME	Tumour microenvironment
TNF	Tumour necrosis factor
TSG101	Tumour susceptibility gene 101
VEGF	Vascular endothelial growth factor
VEGFR	Vascular endothelial growth factor receptor
VPS4	Vacuolar protein sorting-associated protein 4
WT	Wildtype
YAP	Yes-associated protein
ZEB1	zinc finger E-box binding homeobox 1

Publications and presentations

Publication:

Park C, Colley H and Hunt, S. Induction of a cancer-associated phenotype in fibroblasts via oral cancer-derived extracellular vesicles is TGF-β dependent''. *In preparation.*

Presentations:

EACR Annual Congress 2023, Torino, Italy; poster presentation
''Oral cancer cells induce a cancer-associated fibroblast-like phenotype by releasing transforming growth factor beta 1 presenting extracellular vesicles''.

UKEV2022, Edinburgh, UK: poster presentation ***Runner Up Award**
''Transforming growth factor beta 1 presenting oral cancer extracellular vesicles induce a cancer-associated fibroblast-like phenotype in normal fibroblasts''.

UKEV2021, online; flash talk and poster presentation ***Runner Up Award**
''Elucidating the role of extracellular vesicles in oral cancer progression using in vitro 3D models''.

Biomaterials and Tissue Engineering Group, online, 2021; poster and flask talk
''Elucidating the role of extracellular vesicles in oral cancer progression using in vitro 3D models''.

Biomedical Engineers, Medical Engineers and Bioengineers Conference, 2021, Sheffield, UK; flash talk
''Targeting extracellular vesicle-mediated intracellular communication through the use of tissue engineered models''.

Contents

List of tables

List of figures

1 Introduction

1.1 Head and neck cancer

Head and neck cancer is a broad entity of neoplasms affecting structures such as salivary glands, skin, craniofacial bone and mucosal membranes. 90% of head and neck cancers are classified as squamous cell carcinomas (HNSCCs) that arise from the epithelium lining the sinonasal tract, oral cavity, pharynx and larynx (Pai et al., 2009). In the UK, head and neck cancer accounts for 3% of total new cancer cases, with a 10 year survival rate ranging between 19-59% ('Head and neck cancers statistics | Cancer Research UK'). Globally there were 354,864 new cases of lip and oral cavity cancers, followed by larynx (177,422) and nasopharynx (129,079) in 2018 (Bray et al., 2018). Rates in men are high in global areas such as Western Europe, Southern Europe, South Asia and Southern Africa, which follows patterns of tobacco and alcohol consumption (Parkin et al., 2005). The risk of developing head and neck cancer is 50-fold higher for users of tobacco and alcohol compared to non-users, and continued use impacts recurrence thereby contributing to lowered survival rates (Howren et al., 2013). Human papillomavirus (HPV) is another risk factor, that is shown to contribute to around 25% of HNSCCs through downregulation of tumour suppressor genes p53 and retinoblastoma (pRb) involved in cell cycle control (Chung et al., 2009). Of the 12 mucosal high-risk HPV types, HPV16 is the most common oncogenic driver, being responsible for 90% of virus associated HNSCCs (Galati et al., 2022). There are differences in patient outcomes between virus and non-virus associated HNSCCs where HPV-associated HNSCCs have significantly improved rates of disease-free and

overall survival as well as improved response to radiotherapy making it a favourable prognostic marker (Johnson et al., 2020).

HNSCC progression is initiated by epithelial cell hyperplasia followed by mild, moderate or severe dysplasia leading to carcinoma *in situ* and later, invasive carcinoma. Patients with HNSCC usually present with symptoms from the primary site such as persistent hoarseness, ulcers, oral or neck swelling and ear pain amongst others (Johnson et al., 2020).

Most HNSCC patients do not present with an antecedent pre-malignant lesion i.e dysplasia, and it is common for enlargement of the cervical lymph node to be the first clinical presentation from ‘’silent sites’’, most commonly the nasopharynx, tongue base and supraglottis (Vigneswaran et al., 2006). 80% of cervical lymph node metastases with cancer of unknown primary (CUP) originate from head and neck sites and have severely poor 5-year-survival rates ranging from 5-15% (Große-Thie et al., 2021). Around two thirds of HNSCC patients present with an advanced cancer stage with lymph node metastasis, which is associated with up to a 50% decrease in survival (Leemans et al., 2010)

The extent of the tumour, presence of lymph node and distant metastases determines the cancer stage, which largely informs the prognosis for HNSCC patients. Staging is determined by examination, imaging, cytology of lymph nodes and histopathology. In oropharyngeal tumours, risk factors of HPV status and tobacco use have been shown to have such high prognostic influence they may be of more value than traditional staging systems (Ang et al., 2010).

1.2 Oral squamous cell carcinoma

Oral squamous cell carcinoma (OSCC) accounts for the majority of HNSCCs and develops from the stratified squamous epithelium of the oral mucosa. Oral potentially malignant disorders (OPMDs) including oral leukoplakia, oral erythroplakia, oral submucosal fibrosis and oral lichen planus put patients at a higher risk of developing invasive oral carcinomas compared to those with healthy mucosa (Almangush et al., 2020). OSCC is characterised by red and/or white lesions most frequently occurring at the lateral edges of the tongue (50% of all OSCC cases), mouth floor, gingiva and buccal mucosa. Oral precursor lesions are the most commonly diagnosed of HNSCCs and of these, oral leukoplakia, a white lesion in the oral mucosa, is the most commonly observed (Kerr et al., 2021).

These lesions can be classified according to epithelial alterations including hyperkeratosis, hyperplasic and acanthosis as well as stages of dysplasia prior to the establishment of invasive carcinoma (Rivera et al., 2014). OSCC metastasis is predominantly to the lymph nodes, namely the ipsilateral followed by the bilateral nodes. Dissemination is also seen in the lungs, bones and liver (Tan et al., 2023). Cancers of the oral cavity are able to be diagnosed at a relatively early stage due to self-recognisable symptoms such as the interference of ulcers with eating and speaking (Tan et al., 2023).

The development of OSCC involves the accumulation of molecular and genetic alterations that are influenced by environmental factors, as previously mentioned, as well as genetic pre-disposition (Rivera et al., 2014). One of the earliest chromosomal aberrations is a high frequency loss of heterozygosity at chromosome 9. For example, allelic loss at 9p21 has been shown in the majority of premalignant oral lesions. This

region possesses genes that code for growth suppressing cyclin-dependent kinase inhibitors, for example CDKN2A encoding for p16 and p14 an alternative transcript is frequently deleted in malignant oral lesions (Pérez-sayáns et al., 2009). Cyclin D1, encoded by CCND1, also regulates the cell cycle by controlling progression to S phase and is amplified in 30-50% of HNSCC patients (Motokura et al., 1993). CCND1 gene amplification is also associated with tumour progression and lymph node metastasis, however cyclin D overexpression has been shown to be predictive of benefit for certain chemotherapeutics (Zhong et al., 2013; Dhingra et al., 2017). Other alterations include changes in epidermal growth factor signalling, the Ras oncogene, STAT proteins, Rb and the tumour suppressor p53 (Choi et al., 2008).

1.2.1 HNSCC Treatment

Early-stage HNSCC tumours have a more favourable prognosis and are treated with resection and radiotherapy with cure rates of around 80%. For more advanced tumours or those with nodal metastasis, post-resection radiation or chemoradiation is utilised (Oosting et al., 2019; Amaral et al., 2022). The preferred treatment regimen for patients with locoregionaly advanced HNSCC where surgery outcomes would be poor is chemoradiotherapy with high-dose cisplatin every 3 weeks. Alternative beneficial concomitant treatments include carboplatin with 5-fluorouracil (5-FU) or the EGFR inhibitor cetuximab (Oosting et al., 2019) Adjuvant chemotherapy and radiotherapy are utilised in the cases of advanced OSCC, either before or after surgery. EGFR inhibitors, namely Cetuximab, are used in the case of metastatic OSCC (Melo-Alvim et al., 2023).

Cisplatin is often used in the first instance due to its significant efficacy, however for cisplatin intolerant patients the use of docetaxel has also been shown to improve

outcomes in phase II and III clinical trials alone and in combination with cetuximab (Harari et al., 2014; Patil et al., 2023). Another candidate is Xevinapant, an antagonist of inhibitor apoptosis proteins and a promising therapeutic for enhancing chemoradiotherapy. The phase III XRAY VISION trial is currently recruiting to evaluate xevinapant efficacy in combination with radiotherapy in locally resected HNSCCs (NCT05386550).

Immunotherapeutics are growing as an attractive alternative to traditional chemotherapies, because of their potential for long-lasting anti-tumour effects (Yu et al., 2022). Anti PD-1/PDL-1 antibodies, pembrolizumab and nivolumab have shown efficacy in clinical trials for the treatment of metastatic HNSCC (Tan et al., 2023). Post-hoc analysis of Pembrolizumab efficacy in the Phase III KEYNOTE study showed that first line pembrolizumab and pembrolizumab-chemotherapy demonstrated survival benefit compared to cetuximab-chemotherapy in metastatic HNSCC (Harrington et al., 2023). Pembrolizumab and nivolumab are now recommended for second-line treatment of recurring or metastatic HNSCC following platinum-containing therapy (Harrington et al., 2023). There are multiple other potential immunosuppressive checkpoint targets for HNSCC that have been investigated. Cytotoxic T-lymphoytes-associated protein 4 (CTLA-4) binds to the antigen presenting cell (APC) surface ligands CD80 and CD86 with a higher affinity to its homolog CD28 and functions to inhibit T-cell response (Haddad et al., 2023). The CTLA-4 blocking antibody ipilimumab is currently being tested clinically in HNSCC in combination with other immunotherapies. A phase II CheckMate-651 investigated the efficacy of ipilimumab in combination with nivolumab compared to the EXTREME regimen (cisplatin and fluorouracil cycles followed by cetuximab) for first-line treatment of metastatic HNSCC, however this combination did not significantly improve overall survival (Haddad et al.,

2023). Other T-cell suppressor targets such as lymphocyte-activation gene 3 (LAG-3), T-cell immunoglobulin and ITIM domain (TIGIT) and mucin domain-3 (TIM-3) have shown promise pre-clinically and are currently being assessed in Phase I and II trials for HNSCC treatment (Yu et al., 2022).

1.2.2 HNSCC Biomarkers

Histologic grading is limited in that it cannot predict all changes present in HNSCC, development, therefore molecular biomarkers are useful to indicate the risk of progression (Perez-Ordoñez et al., 2006). Aldehyde dehydrogenase (ALDH) is a potential predictive cytosolic enzyme involved in the reduction of oxidative stress. The subtype ALDH1, induces retinoic acid signalling that causes ‘’stemness’’ of cancer stem cells. Liu *et al* used patient biopsies to reveal that just under 50% of oral lesions positive for ALDH1 progressed to invasive carcinoma compared to around 13% with ALDH1 negativity (Liu et al., 2013). There are multiple other potential markers that have been linked to HNSCC including those relating to the cell cycle for example, p53, as well as loss of heterozygosity at chromosomal loci, notably at chromosome 9p21 (Perez-Ordoñez et al., 2006).

An obstacle with immune checkpoint inhibitors is that only a subset of patients are able to respond, therefore biomarkers for treatment outcome could help inform clinicians of the best options for patient on an individual basis. PD-L1 is currently the most promising marker with PD-L1 positive HNSCC patients treated with immune checkpoint inhibitors showing improved overall survival at 6 and 12 months compared to those with negative tumours, as showed in a meta-analysis of 11 clinical trials (Huang 2021). Further indicators of immune checkpoint such as EGFR, TGF-β and PD-L2 are promising but warrant further study (Meliante et al., 2023).

Biomarkers from liquid biopsy are more favourable than surgical biopsies due to their less invasive nature and ease of patient monitoring. Analytes from blood, urine, plasma and saliva include cell-free DNA (cfDNA), circulating tumour cells (CTCs), circulating RNAs and extracellular vesicles (EVs) (Chen et al., 2023). EVs are appealing biomarkers due to their ability to harbour multiple cargo and they have been used to successfully predict outcomes in multiple cancers via protein and RNA cargo (Ciferri et al., 2021).

1.2.3 OSCC tumour microenvironment

Recent findings have implicated the tumour microenvironment (TME) as a major contributor to cancer survival and progression. The stromal components of the TME, such as cancer-associated fibroblasts (CAFs) and subpopulations of immune cells interact with the tumour cells as well as each other cells via a network of cytokines, chemokines, growth factors and extracellular matrix (ECM) proteins (Peltanova et al., 2019).

CAFs are a prevalent cell type within the tumour stroma and function to modulate the TME to create favourable conditions for tumour growth. CAFs are derived from progenitors such as fibroblasts, pericytes or endothelial cells through mesothelial-mesenchymal transition (MMT) and epithelial-mesenchymal transition (EMT), respectively (Peltanova et al., 2019). Markers for myofibroblasts include platelet-derived growth factor (PDGFR)-α, fibroblast activation protein (FAP) and the commonly used α- smooth muscle actin (α-SMA), which is correlated with a poor prognosis in oral carcinoma (Lim et al., 2011). However, it should be noted that α-SMA has varying expression between CAF subtypes and is not a specific marker due to

significant expression in pericytes and smooth muscle cells (Nurmik et al., 2020). It has previously been shown that CAFs produce high levels of chemokine CCL2, when co-cultured with OSCC cells, which enhances reactive oxygen species (ROS) production leading to increased PI3K/AKT signalling. ROS also activates nuclear transcription factor-kappa B (NF-κB) and STAT3 which leads to constitutive expression of CCL2 in CAFs, thus creating a favourable tumour growth environment (Li et al., 2014). Furthermore, senescent CAFs derived from genetically unstable OSCC have been shown to produce metalloproteinase-2 (MMP-2) which functions to disrupt epithelial adhesion and allow induction of keratinocyte invasion, a possible mechanism for metastatic dissemination (Hassona et al., 2014).

Furthermore, lysyl oxidase (LOX), shown to be highly expressed in CAFs, was significantly linked to severity of malignancy and poor prognosis in OSCC (Zhang et al., 2021a) . Invasion and EMT was increased in OSCC cells after culture with CAF conditioned medium, however the effect was lessened with conditioned media from LOX knockdown CAFs (CAF-shLOX). Collagen matrix stiffness was also increased when CAF conditioned media was added but reduced with CAF-shLOX conditioned media. OSCC cells cultured in this collagen matrix showed upregulation of FAK phosphorylation, and an inhibitor of FAK reduced the CAF-derived LOX induced proliferation and invasion ability of OSCC cells (Zhang et al., 2021a).

In terms of metabolism, it has been shown that OSCC CAFs preferentially use oxidative phosphorylation and demonstrate a significantly higher ATP production capacity compared to NOFs (Xiao et al., 2021). Proteomic analysis distinguished 183 differentially expressed proteins between mitochondria from CAFs and NOFs, and two protein associated with oxidative phosphorylation were downregulated, ATP50 and TRAP1 (Xiao et al., 2021). CAFs overexpressing TRAP1 (CAF-TRAP1) showed

reduced proliferation and oxidative phosphorylation. *In vivo,* mice were injected with OSCC cells alone, with CAFs or with CAF- TRAP1 cells. Tumours grew at a faster rate when CAFs and OSCC cells were added, however at the end of the experiment those mice bearing OSCC and CAF-TRAP1 cells has significantly smaller tumours (Xiao et al., 2021). This indicates that CAF metabolism is an important factor in promoting OSCC tumour growth.

Tumour associated macrophages (TAM) are another large component of the TME. Macrophages are mononucleated phagocytes which are involved in the adaptive and innate immune response against pathogens (Peltanova et al., 2019). Macrophages display plasticity between proinflammatory 'M1' and anti-inflammatory 'M2' phenotypes, with TAMs in the TME having been shown to display markers for both phenotypes (Peltanova et al., 2019). Previous studies have shown that higher concentrations of TAMs, mainly M2 subtype, are related to poor prognosis in OSCC (Alves et al., 2018; Kumar et al., 2019). It has been shown that TAMs possessing the $CD206^{+}$ M2 marker are located in OSCC tumours and promote proliferation and invasion of OSCC cells via EGF secretion (Haque et al., 2019). Furthermore, OSCC patients possessing this TAM subtype had a poorer prognosis, highlighting the pro-tumoural effects of the M2 phenotype (Haque et al., 2019).

Other tissue infiltrating immune cells which have been shown to contribute to OSCC prognosis are regulatory T-cells (Tregs). Tregs are a subset of T-cells which function to regulate self-immunity as well as other immune cells such as B-cells, macrophages, natural killer (NK) cells and other T-cells. Natural Tregs originating from the thymus express CD25 and CD4 markers. These cells also express the forkhead box (FOXP3) transcription factor, which is involved in regulating T-cell development and activity, to dampen the immune response. Peripheral Tregs differentiate from mature $CD4^{+}$ T-

cells outside of the thymus, and require cytokines for activation (Peltanova et al., 2019). Tregs isolated from tumours have shown to have greater inhibition of T-cell proliferation than those isolated from peripheral blood, indicating that they are induced towards a more immunosuppressive phenotype in the TME (Jie et al., 2013). Moreover, studies have shown that an increase in Tregs in the oral cancer TME or patient blood, is associated with a poorer prognosis (O'Higgins et al., 2018).

Natural killer cells make up around 10% of circulating lymphocytes and are distinguished by their $CD3^{-}CD56^{+}$ phenotype. They can be divided into two subpopulations depending on CD56/CD16 density on the cell surface. $CD56^{bright}CD16^{dim}$ immature NK cells produce cytokines such as interferon gamma (IFNγ) and tumour necrosis factor alpha (TNF-α) which contribute to immunomodulation. The majority of NK cells are mature $CD56^{dim}CD16^{bright}$ cells, which have a cytotoxic function towards invading pathogens, controlled by recognition of activating and inhibitory receptors. NK cells in cancer patients have impaired function due to downregulation of activating receptors and upregulation of inhibitory receptors (Hu et al., 2019). MHC-class I chain related protein A (MICA) is a major ligand of natural killer cell group 2 member D (NKG2D) which activates immune effector cells. It has been shown that MICA expression in OSCC cells is lower than in NOK cells and may therefore be a mechanism by which OSCC tumours evade the immune response (Chen et al., 2015). Moreover, the inhibitory receptors NKG2A and PD-1 have been demonstrated to be significantly overexpressed in tumour-associated NK cells from HNSCC patients (Korrer et al., 2019). A systematic review and meta-analysis found that higher numbers of $CD57^{+}$ NK cells, as well as CD163+ M2 macrophages, were a good prognostic marker for OSCC (Hadler-Olsen et al., 2019).

1.3 Extracellular vesicles

Extracellular vesicles (EVs) are phospholipid bilayer enclosed spherical vesicles produced by all mammalian cells, as well as prokaryotes which are typically termed outer membrane vesicles (OMVs). Eukaryotic EVs were originally thought to function as cell-waste removers, however there is evidence that EVs play important roles in signalling within and between cells (El Andaloussi et al., 2013). The term EVs refers to all secreted membrane vesicles, however they are highly heterogenous in terms of characteristics and function. EVs are commonly classified into three main types based on biogenesis; exosomes, microvesicles and apoptotic bodies/EVs (Figure 1.1) (Van Niel et al., 2018).

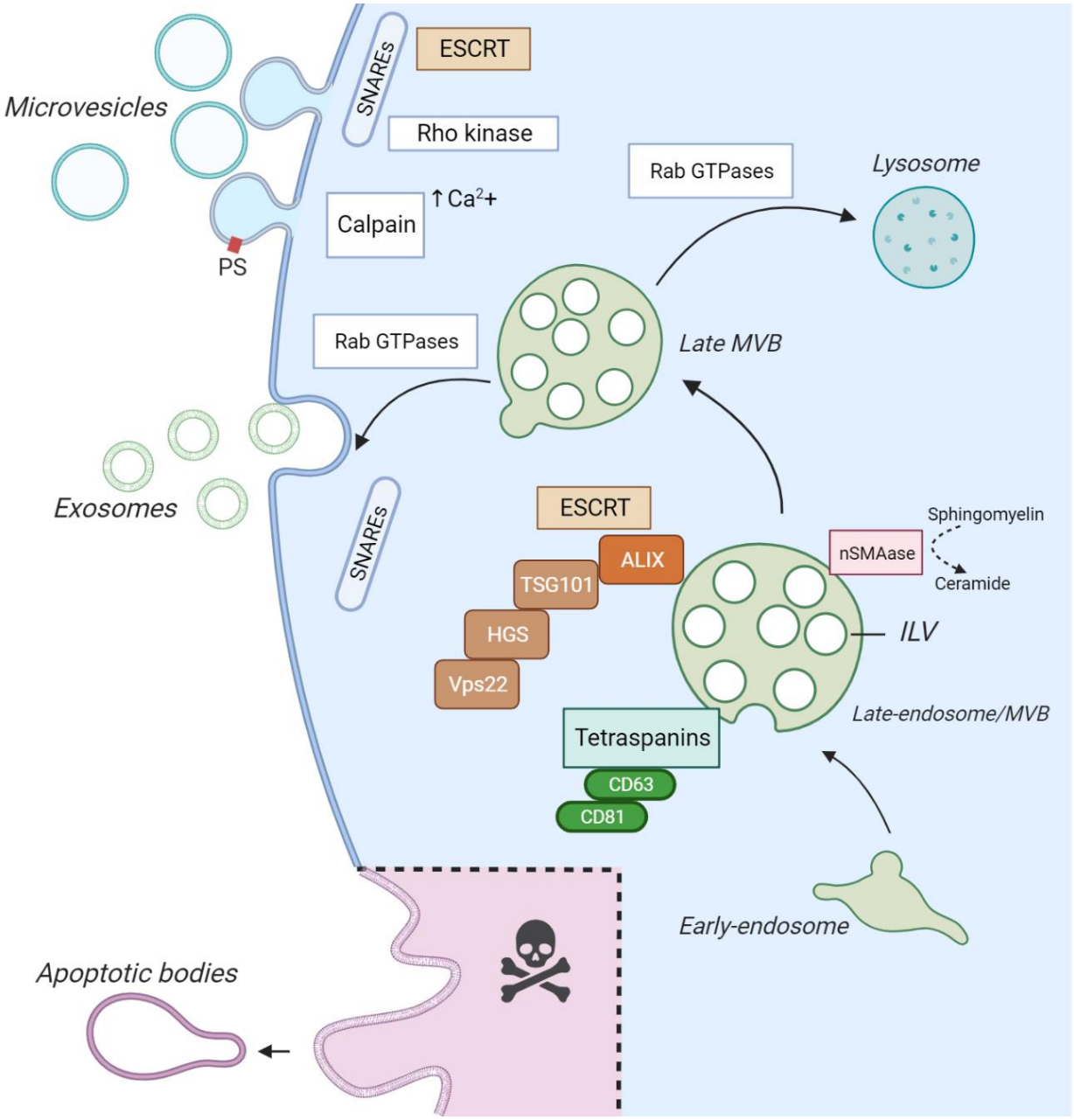

Figure 1.1 ESCRT dependent and independent extracellular vesicle biogenesis. Exosomes originate from early-endosomes formed from inward budding of the plasma membrane. Maturation of these early-endosomes into MVBs involves the formation of ILVs through ESCRT-dependent and independent mechanisms. MVBs are trafficked to lysosomes for degradation or to the cell surface by Rab GTPases. The SNARE complex facilitates fusion with the plasma membrane for release of exosomes ranging from 30-100nm in diameter. MVs are formed from outward budding of the plasma membrane resulting from a change in Ca2+ levels causing calcium dependent enzymes to modify the plasma membrane. This releases MVs typically 10-100nm in diameter.

1.3.1 EV Biogenesis

1.3.1.1 Exosomes

Initially the term ‘exosome’ was used to describe vesicles released from multivesicular bodies during reticulocyte development (Johnstone et al., 1987). However, in the 1990s Raposo *et al* demonstrated that exosomes have an immune stimulatory effect when released from B-lymphocytes, initiating further research into characterising the function of exosomes (Raposo et al., 1996). Exosomes are now defined as vesicles ranging from 30-100 nm in size, originating from inward budding of the cell membrane to form early endosomes. Multivesicular bodies (MVBs) are then formed by a second inward budding of the endosomal membrane resulting in intraluminal vesicles (ILVs)(Zhang et al., 2019).

The formation of ILVs requires the endosomal sorting complex required for transport (ESCRT) machinery, which comprises around 30 proteins in vertebrates. The ESCRT protein complexes are classified into four groups; ESCRT-0, I, II and III. ESCRT-0 comprises the subunit HGF-regulated tyrosine kinase substrate (HGS) which recognises mono-ubiquitinated proteins and sequesters them to specific domains of the endosomal membrane due to its ability to bind phosphatidylinositol 3-phosphate (PI3P). HGS recruits TSG101, a member of the ESCRT-I complex which in turn recruits ESCRT-II to the site. Both ESCRT-I and -II sort ubiquitinated cargos at ILV, as well as ESCRT-0, and bind with ESCRT-III which is involved with invagination and constriction of the membrane to form ILVs. ESCRT-III is activated via ESCRT-II or ESCRT-I which causes ESCRT-III proteins to polymerise and form helical tubular structures which deforms the membrane causing constriction (Caillat et al., 2019). The

ATPase sorting protein VPS4 disassembles ESCRT-III polymers allowing them to be recycled and separate from the MVB membrane allowing membrane fission (Maity et al., 2019).

There is some controversy concerning whether exosome release is an ESCRT-regulated mechanism. However, it has been shown that ESCRT and associating proteins are necessary for exosome formation. Alix, associated with ESCRT proteins TSG101 and CHMP4, is involved in endosomal budding and abscission as well as cargo sorting through syndecan-syntenin (Baietti et al., 2012). Moreover, inhibition of Alix impairs the ability of dendritic cells to secrete CD63 enriched exosomes (Colombo, et al., 2013).

However, depletion of ESCRT subunits does not fully ablate the formation of MVBs, indicating that there are ESCRT-independent mechanisms of exosome formation. Raft-based microdomains highly enriched in sphingomyelinases have a role in the lateral segregation of cargo within the endosomal membrane. Ceramides are formed from sphingomyelinases by hydrolytic removal of the phosphocholine group by neutral sphingomyelinase (nSMase) enzymes. The inhibition of nSMase2 enzyme has been shown to reduce the release of exosomal EGFP-CD63 from transfected prostate cells, thus implicating the role of ceramides in exosome formation (Trajkovic et al., 2008). Although the exact mechanism for this is unknown, it may be due to the cone-shaped structure of ceramide promoting domain-induced budding by spontaneous negative curvature of the endosomal membrane (Zhang et al., 2019).

The transmembrane tetraspanin proteins also play a role in exosome biogenesis via tetraspanin-enriched microdomains (TEMs). TEMs are involved in receptor and signalling protein compartmentalisation in the plasma membrane. Concomitant knock-

down of tetraspanin CD63 by CRISPR/Cas9 in HEK293 cells has been shown to reduce the secretion of exosomes, highlighting the role of tetraspanins in exosome biogenesis (Hurwitz et al., 2016). Interestingly, CD63 has been shown to co-accumulate with syndecan, syntenin and Alix in certain vesicle population, suggesting a possible interaction for the formation of a subset of exosomes (Baietti et al., 2012).

MVBs are either directed to lysosomes for content degradation or transported to the cell periphery for exosome release, requiring molecular machinery for trafficking, docking and fusion to the plasma membrane. This process requires regulation by cytoskeleton molecules, myosins and kinesins, Rab GTPases, fusion machinery and tethering factors. The Rab GTPases are the largest family of small GTPases and are implicated in vesicle budding, transport along actin and tubulin, docking and membrane fusion (Hessvik et al., 2018). The first Rab GTPase shown to be involved in exosome production was Rab11, whereby the creation of a dominant-negative Rab11 human leukemic cell line inhibited exosome release (Vidal et al., 1997). Proteomic analysis of purified oligodendrocyte exosomes showed a relativity high number of Rab GTPases, however the relative expression of Rab35 was found to be the most abundant (Hsu et al., 2010). Inhibition of Rab35 using a dominant-negative mutant Rab35 and RNAi knockdown significantly reduced exosome secretion and increased the accumulation of late endosomes, indicating that Rab35 has a role in vesicle trafficking to the plasma membrane (Hsu et al., 2010). Similar techniques were used to determine that both Rab27a and Rab27b promote exosome secretion in HeLa cells by enabling MVB docking at the plasma membrane (Ostrowski et al., 2010). More recently it has been shown that the kidney and brain expressed protein (KIBRA) stabilises Rab27a by preventing its degradation through the ubiquitin-proteasome pathway and its knockdown decreased both Rab27a expression and exosome

secretion (Song et al., 2019). In addition, the subcellular location and expression of an early endosome marker in KIBRA-KD cells was not altered compared to control cells, indicating KIBRA is involved in MVB transport rather than formation (Song et al., 2019).

The soluble N-ethylmaleimide-sensitive factor attachment protein receptors (SNAREs) are also known to be involved in vesicle-membrane fusion. A SNARE complex comprises of family members R-or Q-SNARE fused to form four coiled-coil helices (Hessvik et al., 2018). The R-SNARE protein, YKT6, plays a key role in exosome release as knockdown in two independent cell lines has been shown to reduce levels of exosome associated TSG101 (Gross et al., 2012; Ruiz-Martinez et al., 2016). Furthermore the over expression of the N-terminal domain of VAMP7 (R-SNARE), known to hinder SNARE complex formation, causes enlargement of MVBs with greater localisation at the cell periphery (Fader et al., 2009). In addition, VAMP7 co-localised with the late-endosomal marker CD63, implying it plays a role in the later stages of the MVB pathway and membrane docking (Fader et al., 2009).

1.3.1.2 Microvesicles

Microvesicles (MVs) typically range from around 100-1000 nm in diameter and are formed by outward budding or pinching of the plasma membrane (Sedgwick et al., 2018). Difficulty in distinguishing EV subtypes often arises due to overlap in sizes of smaller MVs and exosomes (100-150 nm) (Brennan et al., 2020). MVs were first described as ‘platelet dust’ as they were sedimented from blood by high-speed centrifugation and shown to possess coagulation properties (Wolf, 1967).

Outward budding and fission of the plasma membrane requires molecular rearrangements at specific sites of MV origin and includes changes in lipid and protein

composition as well as Ca^{2+} levels. MVs have distinctive lipid characteristics such as phosphatidylserines (PS) located externally rather than on the internal leaflet of the membrane (Catalano et al., 2020). PS has an upright cone shape and induces membrane fusion upon binding of divalent cations (Kinnunen et al., 2000). Lipid raft domains are also enriched in MVs and depletion of cholesterol has been shown to reduce MV formation (Del Conde et al., 2005). A change in Ca^{2+} levels induces calcium-dependent enzymes such as floppase, flippase and scramblase to modify the plasma membrane by translocating phospholipids between membrane leaflets (Catalano et al., 2020). Sustained increase in cytosolic Ca^{2+} inhibits flippase from moving PS inward causing it to be expressed on the surface and activating cytosolic proteins involved in cytoskeletal remodelling (Taylor et al., 2019) Two mechanisms of cytoskeletal remodelling involve calpains and apoptosis-induced MV release. Calpains are a family of Ca^{2+}-dependent cysteine proteases responsible for cytoskeletal remodelling and specific inhibition in cells has been shown to significantly reduce MV release (Roseblade et al., 2015). Alternatively, during apoptosis caspase-3 mediates the cleavage of ROCK1 which phosphorylates myosin light chain kinase via Rho-kinase leading to membrane blebbing (Sebbagh et al., 2001). The small GTPase Rho family play a key role in cytoskeleton contractility as well as actin assembly thereby participating in MV release from the plasma membrane. Li *et al* demonstrated that MV release in cancer cells is controlled through a Rho-dependent signalling pathway, activated by EGF (Li et al., 2012). RhoA activates downstream effectors which phosphorylate cofilin leading to the extension of actin fibres, a possible mechanism for the formation of an actin-ring structure which is implicated in MV biogenesis (Li et al., 2012).

Although the majority of research implicates the ESCRT machinery in exosome biogenesis, there is suggestion that ESCRT proteins are also involved in MV release. Nabhan *et al* showed that arrestin domain-containing protein (ARRDC1) is localised at the plasma membrane and its overexpression results in localisation of TSG101 at the surface from the cytosol. Furthermore, introduction of a mutation in the TSG101 binding motif in ARRDC1 abrogated TSG101 recruitment to the plasma membrane and inhibited MV production (Nabhan et al., 2012).

1.3.1.3 Apoptotic bodies/EVs

Apoptotic bodies are the largest EV subtype, ranging between 1-5 μm, and are secreted during programmed cell death during a process termed apoptotic cell (AC) disassembly. This involves shortening of the cell nucleus, blebbing of the plasma membrane and fragmentation of cellular components into apoptotic bodies (Anand et al., 2019). However, apoptotic membrane blebbing does not produce apoptotic bodies in certain cell types indicating the use of alternate mechanisms for apoptotic body biogenesis (Atkin-Smith et al., 2015). Such processes include the formation of microtubule spikes, apoptopodia and beaded-apoptopodia, the latter are formed after an absence of membrane blebbing (Atkin-Smith et al., 2017). ACs are also known to produce smaller EVs by similar mechanisms, however evidence for a distinguished biogenesis pathway is lacking (Grant et al., 2019). AC EVs contain signals involved in phagocyte recruitment thereby aiding in AC clearance, however more investigation is needed to characterise the function of these EVs (Grant et al., 2019). It should be noted that ‘Minimal information for studies of extracellular vesicles 2018’ (MISEV2018) guidelines suggest cell viability be estimated to ensure apoptotic EVs are minimised in MV or exosome preparations (Théry et al., 2018).

1.3.2 EV Cargo

Exosomes contain endosome-associated proteins such as Rab GTPase and SNAREs, as well as Alix and TSG101 which are involved in MVB biogenesis. Membrane proteins such as tetraspanins that cluster at microdomains on the plasma membrane are also enriched on EVs. Tetraspanins are a family of more than 30 proteins that are composed of four transmembrane domains and include members such as CD9, CD63 and CD81 which are commonly used EV markers. EVs also contain proteins that associate with lipid rafts, for example glycosylphosphatidylinositol-anchored proteins. Exosomes from a variety of cells are enriched in cholesterol, sphingomyelin and hexosylceramides which play a structural role as well as exosome formation (Skotland et al., 2019). There is less knowledge surrounding MV protein and lipid content and if cargo is enriched relative to their plasma membrane of origin (Raposo et al., 2013). Apart from proteins, EVs also carry nucleic acids including DNA and RNAs (mRNAs and non-coding RNAs). Many RNAs that have been isolated from EVs have enriched RNA profiles relative to the originating cell as well as being differentially sorted depending on their sequence, indicating that these RNAs are selectively loaded into EVs (Villarroya-Beltri et al., 2013). Components of the RNA-induced silencing complex (RISC), AGO2 and GW182, have been shown to be co-expressed with MVB markers suggesting a mechanism whereby miRNAs may be packaged in to exosomes (Bhome et al., 2018). However, further studies are necessary to uncover specific mechanisms of how RNAs are sorted into EVs are necessary and may identify potential therapeutic targets (Chen et al., 2012).

1.4 The role of EVs in cancer

It has been well established that cancer patients maintain significantly higher levels of EVs in their blood compared to their healthy counterparts (Logozzi et al., 2009; Eldh et al., 2014; König et al., 2017). This may be attributed to overexpression or hyperactivation of biogenesis components in cancer cells, for example elevated Rho-ROCK signalling observed in various tumour types (Morgan-Fisher et al., 2013). In addition, it has been shown that EGFRvIII expression in cancer cells promotes the formation of MVs (Al-Nedawi et al., 2008). These MVs were able to transfer EGFRIII and activate oncogenic signalling in recipient cancer cells, thus demonstrating the role of EVs in promoting an oncogenic switch (Al-Nedawi et al., 2008). Similarly, Lee *et al* demonstrated that the oncogene H-*ras* increases the production of EVs which contain double stranded DNA fragments including H-*ras* and N-*ras* (Lee et al., 2014). This indicates a possible positive feedback mechanism for the increase in oncogenic phenotype between cells via EVs. Furthermore, microenvironmental conditions such as hypoxia, have been shown to enhance EV release in cancer cells by different mechanisms for MVs and exosomes (King et al., 2012; Bebelman et al., 2018). Moreover, EVs derived from hypoxic tumour cells contribute to cancer progression through the transfer of miRNA to normoxic cells, inducing an epithelial mesenchymal transition (EMT) switch and promoting invasion and metastasis (Li et al., 2016).

1.4.1 The role of extracellular vesicles in head and neck cancer

The tumour mass is made up of heterogenous cancer cells which communicate via direct and indirect signalling to create a premetastatic microenvironment and promote tumour recurrence and spread. EVs have been implicated in contributing to the

progression of head and neck cancer (HNC) by facilitating cross-talk (Figure 1.2) (Qadir et al., 2018). The treatment of mice bearing pre-malignant oral lesions with exosomes isolated from HNSCC cell lines increased the tumour development and burden, as well as reducing the immune cell infiltration into the tumour (Razzo et al., 2019). This implicates EVs as contributors to OSCC development and progression.

Sento *et al* demonstrated that the oncogenic pathways; PI3K/Akt, MAPK/ERK and JNK-12 pathways were activated in OSCC cells treated with OSCC cell-derived exosomes (Sento et al., 2016). Recipient OSCC cells demonstrated a significant increase in proliferation, migration and invasion (Sento et al., 2016).

Transcriptome analysis of primary oral keratinocytes treated with HNSCC cell line-derived exosomes showed that the expression of genes associated with matrix remodelling, cell cycle, membrane remodelling, differentiation, apoptosis and transcription/translation were altered (Qadir et al., 2018). The same study also showed that cancer-derived exosomes induced a stronger upregulation of matrix metalloproteinase 9 (MMP-9), from a family of proteins involved in cell migration and invasion, in recipient cells (Qadir et al., 2018). Moreover, MMP-13 was found to be enriched in nasopharyngeal cancer (NPC)-derived exosomes in a hypoxia-induced factor-1α (HIF-1α)-dependent manner (Shan et al., 2018). These exosomes facilitated migration in equivalent NPC cells, and depletion of HIF-1α induced a decrease in exosomal MMP-13 leading to reduced invasion and migration (You et al., 2015; Shan et al., 2018). It has also been shown that HIF-1α delivered by exosomes causes

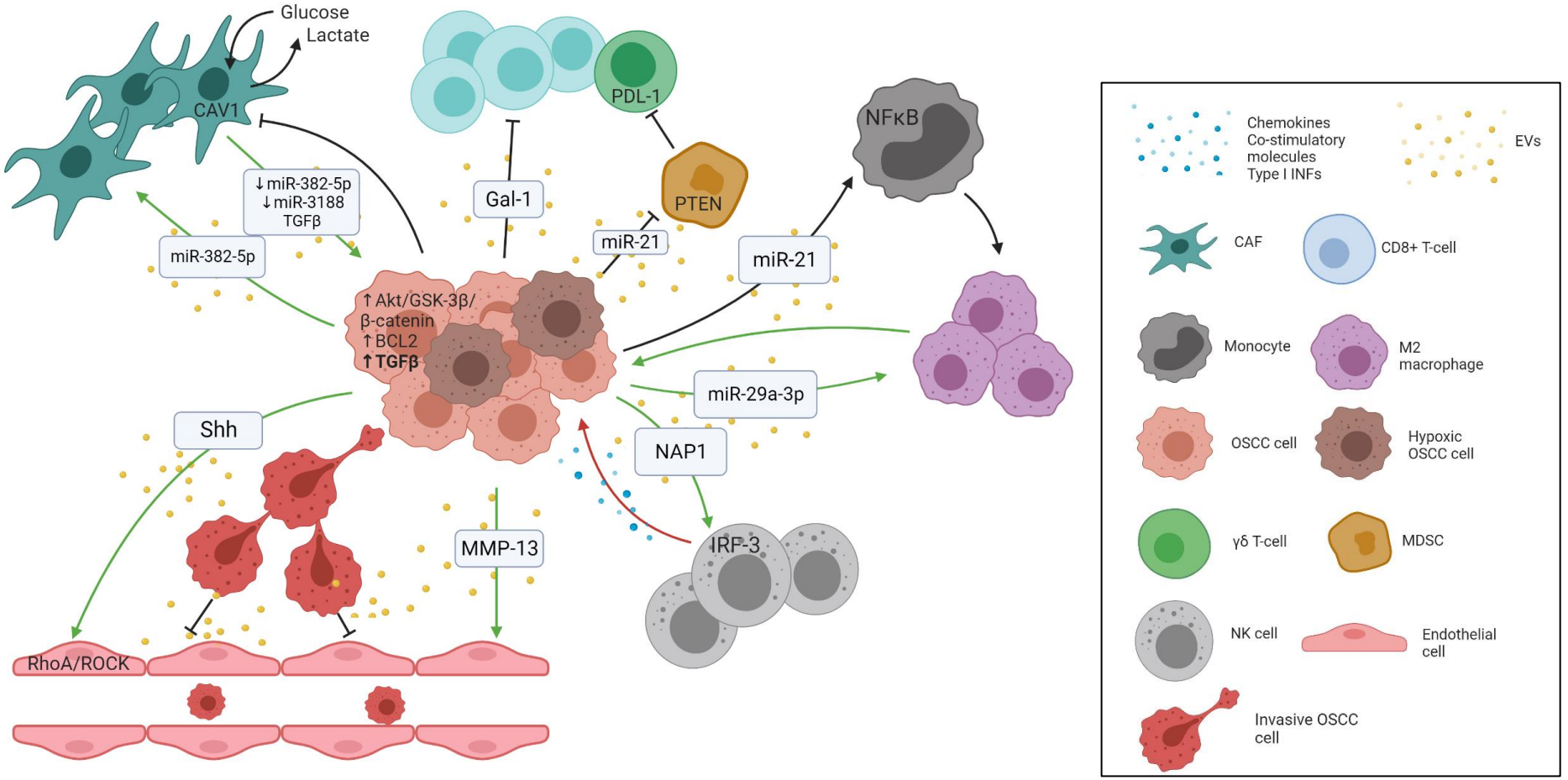

Figure 1.2 The multiple roles of extracellular vesicles in the oral cancer microenvironment. OSCC cell EVs promote the upregulation of oncogenic pathways, increase expression of MMPs involved in invasion and migration, and modulate the metabolism of CAFs via CAV1 to support tumour growth. OSCC EVs containing miR-21 promote the M2 phenotype in macrophages leading to increased tumour growth and suppression of the cytotoxic effect of T-cells via exosomal Gal-1. Hypoxic OSCC exosomes contain miR-21 that enhance the suppressive effect of MDSCs and downregulate γδT-cell toxicity via PTEN and PD-L1. NK cells receiving NAP1 from OSCC exosomes display enhanced cytotoxic activity via the release of cancer supressing factors. CAF-derived EV cargo increases TGFβ and AKT/GSK-3β/β-catenin signalling and derepress BCL2 in OSCC cells to increase proliferation. OSCC MVs abundant in Shh promote angiogenesis via the RhoA/ROCK signalling pathway in endothelial cells, however EVs from highly invasive OSCC cells inhibit endothelial cell tube formation and proliferation.

changes in the expression of E- and N-cadherins associated with the EMT phenotype in NPC cells (Aga et al., 2014).

Exosomes derived from highly metastatic OSCC cells were able to induce a metastatic phenotype in non-metastatic OSCC cell clones from the same patient (Morioka et al., 2016). This led to a reduction in mRNA expression of cytokeratin 13 in recipient cells, associated with malignant transformation (Morioka et al., 2016).

In addition to proteins, non-coding RNAs have been implicated in HNSCC tumour progression. Comparison of miRNA cargo of EVs derived from oropharyngeal cancer cell lines showed differential signatures based on HPV status, as well as multiple cancer related pathways predicted to be targeted by enriched miRNAs (Peacock et al., 2018). MiR-1246 was shown to be highly expressed in oesophageal squamous cell carcinoma (ESCC) as well as OSCC-derived exosomes and is a potential diagnostic and prognostic marker for ESCC despite not being upregulated in tissue samples (Takeshita et al., 2013; Lin et al., 2018).

Furthermore, miR-27a was found to be upregulated in laryngeal squamous cell carcinoma (LSCC) cells treated with LSCC patient serum-derived EVs (Shuang et al., 2022). These cells demonstrated increased proliferative and Wnt/β-catenin pathway activity, but also reduced SMAD4 expression. SMAD4 was shown to be targeted by miR-27a via a luciferase reporter assay and transfecting cells with miR-27a mimic increased tumourigenesis both *in vitro* and *in vivo* (Shuang et al., 2022). This implicates LSCC-derived EV cargo in further promoting cancer progression in already transformed cells. Also in LSCC, Huang *et al* confirmed the ability of LSCC cells to uptake EVs enriched with miR-1246 (Huang et al., 2020). Inhibition of miR-1246 reduced the migration and invasiveness of LSCC cells and halted cells in G1 phase of

the cell cycle (Huang et al., 2020). It has been shown that miR-1246 downregulates CCNG2 (encoding cyclin G2), leading to enhanced cancer cell proliferation (Lin et al., 2018; Huang et al., 2020). However, Sakha *et al* demonstrated that exosomal miR-1246 did not significantly increase proliferation in OSCC cells but was able to increase the motility of poorly metastatic OSCC cells via suppression of DENN/MADD Domain Containing 2D (DENND2D) (Sakha et al., 2016).

In relation to early-stage cancer, it has been shown that OSCC-EVs enhance proliferation, migration and invasion of normal epithelial cells, but inhibit their apoptosis (Liang et al., 2022). Protein expression of mesenchymal markers such as N-cadherin and vimentin were increased, and epithelial marker E-cadherin was decreased in epithelial cells receiving OSCC-EVs (Fujiwara et al., 2018; Liang et al., 2022). Along with a change in morphology from oval to spindle shaped, this suggests that normal epithelial cells undergo EMT and are transformed by OSCC-EV to a precancerous state (Fujiwara et al., 2018; Liang et al., 2022). Moreover, OSCC-EV treated epithelial cells showed a significant reduction in tumour suppressors p53 and PTEN due to the PTEN targeting EV cargo miR-let-c. Inhibition of miR-let-c increased apoptotic markers and reduced EMT markers in epithelial cells treated with OSCC-EVs, implicating EV derived miRNA cargo in malignant transformation of normal cells (Liang et al., 2022).

MiR-200c-3p is a member of the miR-200 family and has been implicated in promoting metastasis in many human cancers, however there are differing conclusions as to whether miR-200c acts as an oncogene or not in HNSCCs (Zhang et al., 2016). Microarray analysis of OSCC cell line-derived exosomes found 32 differentially expressed miRNAs (Kawakubo-Yasukochi et al., 2018). Of these, miR-200c-3p was found to enhance the invasive capacity of a non-metastatic tongue cancer cell line by decreasing expression of WRN and CHD9, involved in genetic stability and chromatin

remodelling, respectively (Kawakubo-Yasukochi et al., 2018). This study supports conclusions that upregulation of miR-200c is associated with poorer prognosis in various cancers (Zhang et al., 2016). However, a separate study showed that this was the opposite for OSCC in that the downregulation of miR-200c correlated with a later tumour stage, enhanced recurrence and a poorer overall survival (Song et al., 2020). Supporting this, Xie *et al* demonstrated that miR-200c inhibited the proliferation of OSCC cells by downregulating Akt and Glut4, involved in cell growth and glucose uptake respectively (Xie et al., 2018). Moreover, miR-200c has been shown to negatively regulate Zinc finger E-box-binding homeobox (ZEB1), thus reducing EMT and the metastatic potential of OSCC cells (Yan et al., 2018). These data would suggest that the downregulation of miR-200c is pro-oncogenic in OSCC, however it was not determined whether this is specific to EVs. It may be possible that miR-200c-3p is specifically packaged into EVs by OSCC cells as a means to enhance its expression in less metastatic cells in the heterotypic tumour microenvironment.

1.4.2 The role of EVs in the tumour microenvironment

1.4.2.1 Cancer-Associated Fibroblasts

As previously described, there is substantial evidence for the role of CAFs in tumourigenesis, invasion and metastasis (Li et al., 2014; Hassona et al., 2014) . The frequency and distribution of CAFs in OSCC of the tongue has been shown to be an independent prognostic factor, having a strong negative correlation with overall survival and disease-free survival (Li et al., 2015). Moreover, treatment with CAF conditioned media increased the proliferation and invasion of OSCC cells lines (Li et al., 2015). Studies looking to identify differences in the OSCC CAF secretome have

found that exosomes contain a higher number of cancer associated proteins involved in; tissue polarity, cell communication, wounding, cell motility, cell communication and a notably strong association of CAF exosome cargo with metabolism and energy pathways (Principe et al., 2018; Dourado et al., 2019). There is evidence that OSCC-derived MVs cause a metabolic switch in CAFs through downregulation of caveolin 1 (CAV1), causing an increase in glucose uptake and lactate production (Jiang et al., 2019). This suggests that OSCC EVs play a role in switching CAFs to aerobic glycolysis which in turn supports tumour growth.

It has been previously shown that transforming TGF-β is expressed on the surface of cancer derived exosomes and can activate the SMAD3-related signalling pathway in CAFs (Webber et al., 2010).Transforming growth factor β (TGF-β) is a secreted cytokine stored in the extracellular matrix existing as a latent complex. Upon activation it binds to the TGF-β receptor (transforming growth factor β (TβR) complex resulting in initiation of multiple downstream signalling pathways involved in growth, EMT, and many other cell functions (Pang et al., 2018). As in many cancers, the role of TGF-β in HNSCC is unclear due to its dual role as a tumour promotor and suppressor depending on the context. However, its over expression has been noted in human HNSCC samples and in a mouse model this overexpression lead to epithelial hyperproliferation amongst other pro-oncogenic effects (Lu et al., 2004). In multiple cancers TGF-β has been shown to associate with EVs, either on their surface or also within the lumen, as seen in HNSCC EVs (Webber et al., 2010; Goulet et al., 2018). TGF-β associated with cancer derived EVs have been shown to activate fibroblasts and promote angiogenic phenotypes in endothelial cells and macrophages (Ludwig et al., 2018, 2022). This information, coupled with the fact that HNSCC patient derived

EVs have been shown to associate with TGF-β in higher levels than healthy controls, points to this EV cargo being a potential drug target (Ludwig et al., 2023).

OSCC cells treated with CAF-derived EVs displayed modulated genes with SMAD3 being the most associated transcription factor (Dourado et al., 2019). Although SMAD3 was not detected in EVs, SMAD3 interacting proteins were overexpressed, indicating EV cargo interacts with the transcription factor to modulate gene expression in cancer cells (Dourado et al., 2019). Furthermore, OSCC patient derived fibroblast exosomes have been shown to contain TβRII (TGF-β type II receptor), and when incubated with TβRII SCC cells deficient in TGF-β ligand response, increased TGF-β signalling (Languino et al., 2016). Interestingly, exosome transfer increased levels of SMAD2 phosphorylation but not SMAD3, therefore it is possible that this effect is due to other components such a miRNAs present in CAF-exosomes (Languino et al., 2016)

The altered exosomal non-coding RNA (ncRNA) profile of OSCC-derived CAFs compared to NOFs has been shown to contribute to progression, invasion and metastasis of OSCC (Yap et al., 2020). The overexpression of miR-382-5p in OSCC-derived CAFs has been demonstrated to be transported by exosomes to OSCC cells and enhance migration and invasion (Sun et al., 2019). Moreover, the expression of miR-382-5p showed a positive correlation with OSCC metastasis in patients, however did not correlate with CAF density indicating a one way communication from CAFs to OSCC cells via exosomes (Sun et al., 2019).

miRNAs can also negatively regulate oncogenic gene expression, meaning a lack of specific miRNAs can contribute to OSCC. Li *et al* found that miR-34a-5p binds to and downregulates *AXL* which in turn reduces the activity of the AKT/GSK-3β/β-catenin signalling pathway responsible for proliferation (Li et al., 2018). In addition, miR-34a-

5p expression levels were shown to be low in OSCC CAF-derived exosomes, and overexpression of miR-34a-5p significantly reduced OSCC proliferation, migration and invasion (Li et al., 2018). MiR-3188 is also reduced in exosomal OSCC-derived CAFs and these exosomes are able to be transferred to HNSCC cells leading to increased proliferation and reduced apoptosis via derepression of B-cell lymphoma 2 (BCL2) (Wang et al., 2019). Therefore, the transfer of exosomes lacking inhibitory miRNAs from CAFs to HNSCC contributes to tumour progression through decreased oncogene suppression. One explanation as to how miRNAs are suppressed is the presence of miRNA sponges in exosomes. Jin *et al* revealed that miR-14 is downregulated by lncRNA TIRY, which when overexpressed in CAFs promoted invasion and metastasis of OSCC cells via miR-14 devoid exosomes activating the Wnt/β-catenin signalling pathway and enhancing EMT (Jin et al., 2020).

More recently, CAF-derived exosomes have been shown to promote metastasis and EMT of ESCC cells via long intergenic non-protein coding RNA (LINC0)-1410 (Shi et al., 2022). Further investigation found that LINC01410 contained binding sequences for miR-122-5p, with pyruvate kinase M2 (PKM2), involved in cancer metabolism, being the predicted target for this miRNA. Overexpression of LINC01410 increased migration and invasion in ESCC cells, whilst this was decreased with transfection of an miR-122-5p mimic. The addition of over expressing PKM2 rescued levels of migration and invasion, indicating that LINC01410 sponges miR-122-5p to enhance PKM2 expression (Shi et al., 2022). These data suggest that CAF-EV lncRNA cargo may sponge tumour-supressing miRNAs.

1.4.2.2 Immune cells

Intravenous injection of tumour-derived exosomes into mice bearing premalignant OSCC lesions has been shown to reduce immune cell invasion into the tumour mass, thus implicating EV communication as a method of immune evasion in OSCC (Razzo et al., 2019). It has previously been shown that exosomal transfer of the proinflammatory thrombospondin 1 (THSB1) from OSCC cells to TAMs causes polarisation to an M1-like phenotype (Xiao et al., 2018). Conditioned media from M1-TAMs was shown to have elevated IL-6 levels and increase colony formation, invasion and migratory ability of OSCC cells (Lu et al., 2022; You et al., 2022). Inhibition of IL-6 in the CM significantly blocked its pro-tumourigenic effects, namely abrogating invasion and migration of OSCC cells (You et al., 2022). In contrast, a separate study found that lncRNA HOXA transcript at the distal tip (HOTTIP) was upregulated in M1-derived exosomes, and these exosomes supressed proliferation, migration and invasion of cancer cells (Jiang et al., 2022). Mechanistically, this was revealed to be due to HOTTIP competitively sponging miR-19a-3p and miR-19b-3p and activating the TLR5/NF-κB signalling pathway (Jiang et al., 2022).

The evidence for the role of M1 derived EVs in OSCC is conflicting, however there is a larger body of literature demonstrating that macrophages in contact with OSCC EVs shift preferentially towards an M2 phenotype. Cai *et al* found that co-culture of OSCC cell lines and macrophages caused a higher expression of M2 markers, and media taken from this co-culture promoted the invasion and proliferation of OSCC cells (Cai et al., 2019).

It has been shown that monocytes treated with HNSCC-derived exosomes displayed a higher expression of M2 markers than M1 (Hsieh et al., 2018). This was due to Snail

directly activating the transcription of *MIR21* leading to miR-21 abundant HNSCC-exosomes which promoted M2 polarisation, angiogenesis and tumour growth (Hsieh et al., 2018). High levels of miR-21 have also been found in the plasma of patients with OSCC, however uptake of these into monocytes increased pro-inflammatory NFkB signalling which would suggest an M1 phenotypic shift (Momen-Heravi et al., 2018). Macrophages treated with OSCC cell line derived EVs showed increased protein expression of pro-tumourigenic IL-6, COX2 and VEGF, however the effect of this on OSCC cells functionally was not investigated (Momen-Heravi et al., 2018).

Proinflammatory related cytokines, IL-10, TNF-α and TGF-β1 have been shown to be upregulated in $CD73^+$ OSCC-EV educated TAMs, indicating a shift to an M2 phenotype (Lu et al., 2022). Co-culture of macrophages with $CD73^+$ EVs induced translocation of p65 to the nucleus indicating NF-κB pathway activation, which is an effector of the aforementioned cytokines. These EVs also influenced TAMs to express greater levels of immunosuppressive LAG3, CD279 and CD274, showing that $CD73^+$ OSCC EVs induce macrophages to aid in immune escape and tumour progression (Lu et al., 2022).

There is also increasing evidence for OSCC-EV influenced macrophages on other cell types in the TME. $TGF\beta^+$ HNSCC-EVs caused an M2 shift in macrophages and an increase in pro-angiogenic factors. Although this study did not look at the effect of HNSCC-EV programmed macrophages on endothelial cells directly, mice injected with cancer-EVs showed enhanced vascularisation (Ludwig et al., 2022).

Due to tumour cells expressing membrane bound Fas ligand (FasL), a high number of T-cells undergo apoptosis in the OSCC tumour allowing evasion of the immune system. Fas-L positive vesicles have also been detected in the sera of OSCC patients,

and induced apoptosis in Jurkat cells and T-cell blasts as indicated by caspase-3 cleavage and cytochrome *c* release (Jeong et al., 2005). In patients, a high content of FasL in MVs significantly correlated to tumour stage, implicating MVs as prognostic markers (Jeong et al., 2005).

Tumours are also known to influence $CD8^+$ T cells to display an immunosuppressive activity and reduce their cytotoxic effect (Filaci et al., 2007). HNSCC cell line-derived exosomes induce a suppressive phenotype in $CD8^+$ T cells and contain unique proteins such as galectin 1 (Gal-1), which is a recognised immunosuppressor known to stimulate apoptosis in effector T-cells (Maybruck et al., 2017). Stable knockout of Gal-1 in a HNSCC cell line produced exosomes that were less able to induce a T cell suppressive phenotype, highlighting exosomal Gal-1 as an important regulator of immune response in HNSCC (Maybruck et al., 2017). Additionally, studies investigating the importance of the hypoxic tumour microenvironment have shown that hypoxic OSCC-exosomes promote the downregulation of gamma delta (γδ) T-cell toxicity by enhancing the suppressive effect of myeloid-derived suppressor cells (MDSCs) (Li et al., 2019). This suppressive effect was achieved in a miR-21/PTEN/PD-L1-axis-dependent manner, demonstrated by treatment of miR-21 KD exosomes and anti-PDL-1 in OSCC tumour bearing immunocompetent mice significantly slowing tumour growth (Li et al., 2019).

NK cells also uptake OSCC-derived exosomes, however it has been reported that they regulate an anti-tumour response (Al-Samadi et al., 2017; Wang et al., 2018). OSCC cell line-derived exosomes have been shown to enhance the cytotoxic activity of NK cells and reduce the survival rate of OSCC cells in co-culture with NK cells (Al-Samadi et al., 2017; Wang et al., 2018). Antibody array showed that in NK-cells pre-treated with OSCC exosomes, IRF-3 was significantly upregulated, as well as downstream

inflammatory cytokines, chemokines and co-stimulatory molecules known to suppress cancer cells. Exosomal NF-κB-activating kinase-associated protein 1 (NAP1) was found to be responsible for initiating IRF-3 signalling in NK cells and enhancing their cytotoxic activity (Wang et al., 2018). A high number of CD57-positive NK cells in patients in associated with a significant survival benefit, however there was is no link when using a pan-marker indicating that exosomal cargo may be specific to NK subtypes (Hadler-Olsen et al., 2019).

1.4.2.3 Endothelial cells

Exosomes derived from HNSCC cell lines also contain angiogenesis-related proteins and are able to increase VEGF and VEGFR2 levels in recipient HUVEC cells when co-incubated (Morioka et al., 2016; Ludwig et al., 2018). Furthermore, HNSCC cell line-derived exosomes stimulated the proliferation, migration and tube formation of HUVECs *in vitro,* and *in vivo* increased pericyte coverage of blood vessels within tumours (Morioka et al., 2016; Ludwig et al., 2018). You *et al* detected the overexpression of MMP13 in NPC cell exosomes, which when internalised by HUVECs, increased tube formation (You et al., 2015). Exosomes have also been implicated in promoting OSCC lymph node metastasis by enhancing lymphangiogenesis, which is impaired by laminin-332 γ2 inhibition in exosomes (Wang et al., 2019). Moreover, laminin-332 was found in higher levels in the plasma EVs from OSCC patients with lymph node metastasis than healthy controls or OSCC patients without lymphatic metastasis (Wang et al., 2019). The Sonic Hedgehog (Shh) protein, known for its role in embryonic development and angiogenesis was also found to be positively associated with lymph node metastasis, as well as microvessel density (MVD) (Huaitong et al., 2017). The same study showed that Cal-27, tongue carcinoma, cell line releases MVs abundant in Shh, which is 5-fold higher than in parent cells

(Huaitong et al., 2017). The application of a RhoA inhibitor reduced MV-induced tube formation, indicating Cal-27 MVs promote angiogenesis via the RhoA/ROCK signalling pathway (Huaitong et al., 2017).

Most recently, literature has emerged surrounding the role exosomal miRNA in angiogenesis. One study focussed on miR-221 which was shown to be upregulated in OSSC tissue and cell line, in parallel with a downregulation of PIK3RI. It was determined that OSCC-derived exosomal miR-211 could negatively regulate PIK2RI expression and promote endothelial cell migration and angiogenesis (He et al., 2021)

This evidence suggests that HNSCC-derived EVs contribute to angiogenesis. However, de Andrade *et al* found opposing function of EVs depending on their cell of origin (de Andrade et al., 2018). The SCC15 cell line with a low invasive phenotype produced exosomes that significantly increased HUVEC tube formation, migration and number of apoptotic bodies, whereas the highly invasive HSC3 cell line EVs inhibited tube formation and proliferation (de Andrade et al., 2018). EVs derived from both cell lines were characterised as being similar in size and concentration, however there were differences in CD63 and annexin II levels which may warrant further investigation (de Andrade et al., 2018).

1.5 Investigating the role of EVs using 3D models of cancer

It is widely acknowledged that polystyrene used in 2D cell culture vessels is not representative of the biological environment present in living systems. Cellular monolayers lack complexity in terms of morphology, growth behaviour and cell-cell and ECM interactions. 3D models more closely mimic the gene expression, cell phenotype and tumour behaviour that would occur in organisms, thus improving physiological relevance and potentially reducing the necessity for animal testing (Pampaloni et al., 2007). The majority of research investigating the role of EVs in cellular communication currently utilises 2D monolayer cultures, however it has been shown that these may not be representative of *in vivo* systems in terms of secretion dynamics and molecular cargo (Rocha et al., 2019; Thippabhotla et al., 2019).

Studies employing artificial matrices to form tumour spheroids have found that culturing tumour cells in this 3D approach increases the EV secretion rate and favours the production of smaller sized EVs (Villasante et al., 2016; Rocha et al., 2019; Thippabhotla et al., 2019). Thippabhotla *et al* observed that EVs derived from cervical cancer cells cultured in a peptide hydrogel scaffold, had a small RNA content with higher similarity to those derived from patient plasma (Thippabhotla et al., 2019). Furthermore, a significant difference in miRNA expression profile between 2D and 3D culture was observed, however this may be indicative of cancer type and culture methods (Thippabhotla et al., 2019). In contrast, an agarose microwell culture method for gastric cancer spheroids, showed that in comparison to 2D culture, EVs have a similar miRNA but different protein expression profile (Rocha et al., 2019). Moreover, one of the first studies investigating the role of EVs using 3D models, demonstrated that EVs from a tissue engineered Ewing's sarcoma model were similar to those in patient plasma in terms of size distribution and Polycomb histone methyltransferase

EZH2 mRNA abundance (Villasante et al., 2016). Interestingly, EZH2 protein levels were undetectable in monolayers, but increased in tissue engineered tumours (Villasante et al., 2016). These studies demonstrate the effects of 3D composition on size, cargo and function of EVs, and highlight the clinical relevance of using such models to investigate the role of EVs.

Solid tumours often have an accumulation of myofibroblastic stromal cells which contribute to tumour progression via angiogenesis and metastasis, thereby making them a relevant inclusion to 3D models. The inclusion of bone marrow mesenchymal stem cells (BM-MSCs), able to differentiate into myofibroblasts, into prostate cancer spheroids increased their outgrowth (Chowdhury et al., 2015). Rab27a knockdown in PC cells, producing exosome deficiency, reduced the invasive capacity of BM-MSC tumour cell spheroids, showing the role of EVs in tumour invasion (Chowdhury et al., 2015). Song *et al* also showed that cancer-derived EVs promote the myofibroblast differentiation of adipose-derived stem cells (ADSCs) in both 2D culture and a collagen based 3D model of breast cancer (BC) (Song et al., 2017). BC-EVs caused enhanced contractility in a free-floating 3D collagen disc model indicating increased α-SMA and thereby a myofibroblast phenotype of ADSCs. BC-EV pre-treated ADSCs in 3D co-culture with HUVECs increased sprouting via increased VEGF secretion (Song et al., 2017) .

Transwell assays have also been utilised to determine EV uptake and EV dependent cancer promoting mechanisms. One study showed that fluorescently labelled EVs from fibroblasts and thyroid cancer donor cells, seeded in the transwell upper chamber were uptaken in recipient thyroid cancer cells seeded in the lower well (Bravo-Miana et al., 2022). Transwell co-culture of these fibroblasts and thyroid cancer cells produced EVs that had an ECM remodelling proteomic profile and induced MMP2

activation in normal thyroid cells (Bravo-Miana et al., 2022). In addition, Kang *et al* demonstrated that transwell co-culture of two BC cell lines induced increased glycolysis and exosome related genes (Kang et al., 2021). Proteomic analysis of BC-derived EVs showed that proteins capable of phosphorylating PKM2 (involved in glycolysis) were present in their lumen, indicating they may play a role in activating glucose metabolism in cancer (Kang et al., 2021).

1.5.1 Extracellular vesicles in 3D culture systems of OSCC

Previous studies investigating EVs in OSCC have used 3D-myoma organotypic models to mimic the TME (Vered et al., 2015; Dourado et al., 2019). This model is derived from a human uterus benign leiomyoma tumour and has been shown to cause differentially expressed genes in an OSCC cell line, HSC-3, compared to 2D culture (Salo et al., 2015). HSC-3 cells cultured with CAF EVs invaded a greater area in the 3D-myoma model compared to the NOF EV treated cells (Dourado et al., 2019). The treatment with CAF-EV did not increase HSC-3 proliferation, indicating that CAF EVs in the TME contribute more to invasion and metastasis (Dourado et al., 2019).

Further work has examined the participation of EV cargo in OSCC-stromal crosstalk using a transwell co-culture system. Sun *et al* cultured OSCC cells in the lower chamber of a transwell system and NOFs or CAFs in the upper chamber (Sun et al., 2019). To ascertain whether miR-382-5p is delivered from CAFs to OSCC cells via exosomes, miR-382-5p mimics were labelled with FAM and transfected into CAFs. Uptake in OSCC cells was observed after 24h, however this was attenuated with the use of an EV inhibitor. MiR-382-5p was shown to enhance OSCC cell migration and invasion, thus implicating EV cargo in cancer progression (Sun et al., 2019).

1.6 Hypothesis

We hypothesise that OSCC derived EVs contribute to the phenotypic switch of NOFs to CAFs.

1.7 Aims and objectives

The aims and objectives of this study were to:

- Characterise small molecule inhibitors against EV biogenesis; GW4869, dimethyl amiloride (DMA) and Bafilomycin A1 (BafA1). The cell viability of oral keratinocyte cell lines and primary oral fibroblasts treated with the drugs will be assessed using MTT assay, and IC_{50} doses calculated. Appropriate doses will be determined and reduction in EV release will be examined using nanoparticle tracking analysis (NTA) and EV marker protein abundance levels by western blotting.

- Establish a fluorescent-reporter cell line to assess EV association with recipient fibroblasts in 2D and dissemination throughout the multicellular 3D OSCC model. An OSCC cell line will be generated that will stably express CD63-GFP and TSG101-mCherry to label the EV membrane with green fluorescent protein and the internal compartment with red fluorescent protein, respectively. This will be generated using transfection of plasmids transferring antibiotic resistance to cells, expansion of surviving colonies and FACS via fluorescence. Stably expressing cells will be characterised for labelled protein expression by western blot and fluorescence microscopy.

- Determine if NOF activation to a CAF-like phenotype can be induced by OSCC-derived EVs. To test whether this effect is EV dependent we will use a Transwell

co-culture method incorporating NOFs and normal oral keratinocytes, OSCC cells, or OSCC cells with reduced EV secretion. We will also isolate EVs from these cell lines using size exclusion chromatography (SEC) and incubate with NOFs. A CAF-like phenotype in NOFs will be assessed by examining CAF marker gene expression by quantitative polymerase chain reaction (qPCR) and protein abundance by western blot and immunofluorescence (IF). We will also assess functional changes in NOFs by examining migration via live cell microscopy and contraction using a collagen assay.

- The levels of TGF-β1 on the surface of EVs will be assessed using enzyme linked immunosorbent assay (ELISA) and co-localisation with tetraspanins using Nano-Flow cytometry. To determine whether the induction of a CAF-like phenotype by EVs is dependent on associated TGF-β1, we will use a blocking antibody and assess protein abundance of CAF markers via IF.

2 Materials and Methods

2.1 Materials

Unless otherwise stated, general laboratory reagents, tissue culture media and supplements were purchased from Merck, UK (previously, Sigma Aldrich).

2.2 Cell Culture

2.2.1 Cell lines

H357 (purchased from ECACC) were originally isolated from a 74-year-old male patient with a squamous cell carcinoma of the tongue (Prime et al., 1990). H357 $^{\Delta HGS}$ were donated by Dr Wenyi Jiang and generated by CRISPR/Cas9 knockout of hepatocyte growth factor-regulated tyrosine kinase substrate (HGS). FNB6 (obtained from Professor Keith Hunter, The University of Sheffield), are a human oral keratinocyte cell line derived from buccal mucosa immortalised by transfection of human telomerase reverse transcriptase (hTERT) (McGregor *et al*., 2002). H357 and FNB6 cells were cultured in flavin and adenine-enriched medium (also known as Green's medium): Dulbecco's Modified Eagle Medium (DMEM) and Ham's F12 medium in a 3:1 ratio supplemented with 10% (v/v) Fetal Bovine Serum (FBS), 10 ng/mL of epidermal growth factor (EGF) (Invitrogen, UK), 0.4 µg/mL hydrocortisone, 0.18 mM adenine, 5 µg/mL insulin, 5 µg/mL transferrin, 2 mM glutamine, 0.2 nM triiodothyronine, 0.625 µg/mL amphotericin B, 100 IU/mL penicillin and 100 µg/mL streptomycin (Allen-Hoffmann and Rheinwald, 1984).

2.2.2 Primary cells

Human primary normal oral fibroblasts (NOFs) and cancer associated fibroblasts (CAFs) were kindly isolated and provided by Dr Helen Colley and Dr Amy Harding, respectively. NOFs were isolated from biopsies obtained from the oral mucosa from patients during routine dental procedures and CAFs isolated from the oral mucosa of patients undergoing cancer resection. Written, informed consent was given under approval by NHS Research Ethics Committee (Ref: 09/H1308/66 and 13/NS/0120). CAF002 (65 year old female) and CAF003 (61 year old female) were isolated from the floor of the mouth and gingiva, respectively. NOF352 were isolated from the gingiva of a 57-year-old female, non-smoker. NOF316 were isolated from the gingiva of a 22-year-old female, non-smoker. NOF and CAF cells were used up until a passage number of 10 for all experiments.

NOFs and CAFs were routinely cultured in DMEM high glucose supplemented with 10% FBS (v/v), 2 mM glutamine, 100 IU/mL penicillin and 100 µg/mL streptomycin.

2.2.3 Cell culture procedures

Cell cultures were allowed to reach 80-90% confluency before passaging. Monolayers were washed in Dulbecco's phosphate buffered saline (PBS) before incubation with trypsin at 37°C, 5% CO_2 for 3-5 min. Growth medium was used to neutralise the trypsin and the cell suspension centrifuged at 1000 x *g* for 5 min to pellet the cells. The supernatant was discarded and the cell pellet resuspended in growth medium at densities dependent on cell type and experimental requirements. Viable cells were quantified by adding 10 µl of 0.4% Trypan Blue mixed 1:1 with cell suspension to a haemocytometer. Cells unstained were counted as viable.

2.2.4 Cell doubling time

In order to calculate cell doubling times, 5 x 10^4 cells were seeded per well in a 6 well plate. At timepoints of 24, 48, 72 and 96 h cells were trypsinised and viable cells were counted as previously described (2.2.3). Doubling time was calculated using the following equations:

$$r = \frac{\ln\left(\frac{Nt}{N0}\right)}{t}$$

$$t_d = \frac{\ln(2)}{r}$$

r = Growth rate

N_t = number of cells at time t

N_0 = number of cells at time 0

T_d = doubling time (hours)

2.2.5 Transwell co-culture

NOFs were seeded into 12 well plates at a density depending on the experimental endpoint (Figure 2.1) and serum starved for 24 h. A 0.4 µm pore diameter ThinCert 12-well insert (Greiner) was then added per well in which 1 x 10^6 donor cells (H357, $H357^{\Delta HGS}$ or FNB6s) was added per insert in serum free Green's medium (Figure 2.1). Cells were incubated for 24 and 48 h, prior to either RNA extraction (Section 2.9) or immunofluorescence (IF) staining (Section 2.8.6).

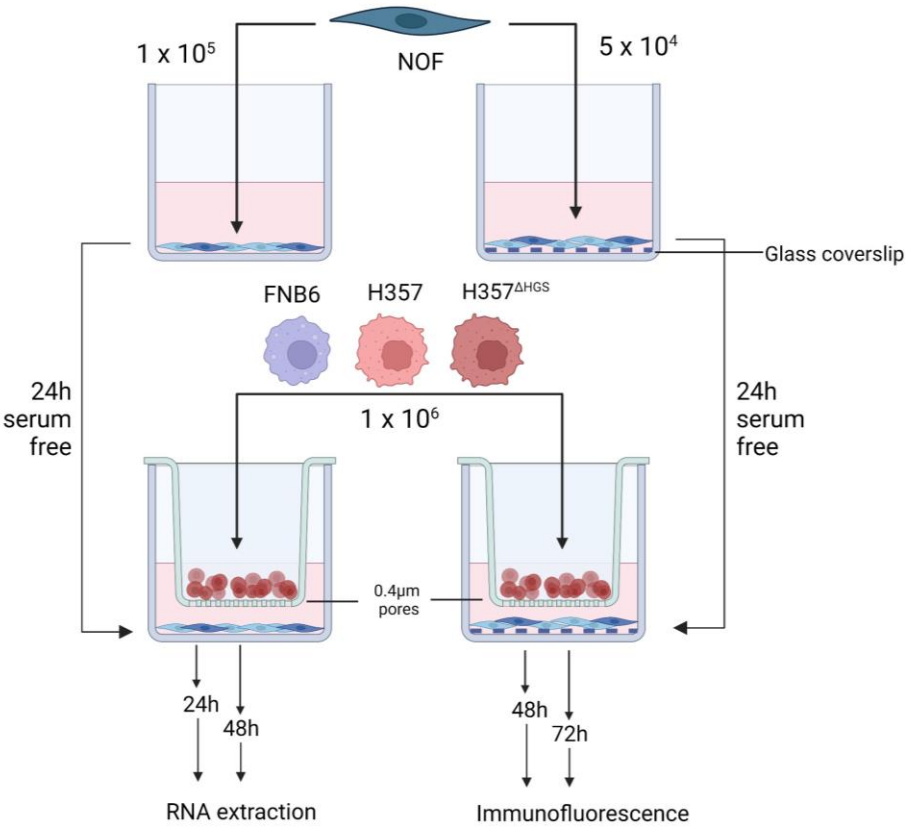

Figure 2.1 Transwell co-culture method schematic

2.3 Oral mucosa collagen models

2.3.1 Rat tail-collagen

Collagen I fibres were extracted from rat tail tendons using a scalpel and washed with PBS. Collagen was then dissolved in 0.1 M acetic acid at 4°C under mixing conditions for 7 days to obtain a sterile soluble collagen. Collagen was frozen overnight at -20°C and then freeze-dried using a VirTis 47 Benchtop K Manifold freeze drier (SP

Scientific) for 3-4 days. Dried collagen was then weighed and dissolved in sterile 0.1 M acetic acid to give a final concentration of 5 mg/mL. This solution was stored at 4°C.

2.3.2 Tissue engineered normal and dysplastic oral mucosa models

Rat tail collagen I, stored on ice to prevent solidifying, was supplemented with DMEM (10x), reconstitution buffer (2.6 M sodium bicarbonate, 0.2 M HEPES, 0.06 M NaOH, dissolved in dH_2O), FBS and L-glutamine as shown in (Table 2.1). 2 M NaOH added dropwise to neutralise the solution to pH 7.4. NOF and CAF were detached from cell culture flask using trypsin (2.2.4), counted and resuspended at a density of 6.25 x 10^6 / mL. Cells were added to models to a final concentration of 2.5 x 10^5 per model (Table 2.1)

Table 2.1 Components of collagen type I matrix

Component	Final concentration	Volume per model (µl)
DMEM (10X)	1 X	100
Reconstitution buffer (10X)	1 X	100
FBS	8%	80
L-Glutamine	2 mM	10
Collagen	3.35 mg/mL	670
Fibroblasts	2.5 x 10^5 /mL	40

Total		1000

1 mL of collagen solution with cells was added to each 0.4 µm pore diameter ThinCert 12-well insert (Greiner) and incubated at 37℃ for 1-2 h. Once set, growth medium was added above and below the model. Models were incubated for 48 h at 37℃, 5% CO_2

After 48 h normal keratinocytes (FNB6) or OSCC (H357) suspended at 2.5 x 10^5 cells in 200 µl Green's medium were added to the top of each model. Green's media was added below models. After a further 24 h models were raised to an air-to-liquid interface, by removing the media from the top of the collagen. Models were then cultured for 14 days, replacing the Green's medium every 2-3 days.

2.4 Histological analysis

Collagen models were fixed in 10% (v/v) PBS-buffered formalin for at least 24 h, processed overnight using a Leica TP1020 benchtop tissue processor (Leica TP1020 benchtop tissue processor, Leica Microsystems) using the standard processing schedule (Table 2.2). Models were then bisected and embedded perpendicular to the bottom of the mould in paraffin wax (Leica EG1160 embedding centre, Leica Microsystems, Germany). Formalin-fixed paraffin-embedded (FFPE) blocks were left to set on a cooling plate, and then sectioned using a microtome into 5 µm thick sections. Sections were placed on a water bath surface (38℃) and mounted onto microscope slides and oven dried for 20 minutes at 60℃.

Table 2.2 Standard processing schedule for model fixation

Solution	Duration
70% alcohol	1 h
80% alcohol	1 h
90% alcohol	1 h 30 min
Absolute alcohol I	1 h 30 min
Absolute alcohol II	1 h 30 min
Absolute alcohol III	2 h
Toluene I	1 h 30 min
Toluene II	2 h
Xylene	PASS
Wax I	2 h
Wax II	2 h
	Total = 16 h

2.4.1 Haematoxylin and eosin staining

Haematoxylin and eosin (H&E) staining was performed using a Leica ST4040 Shandon Linear Stainer (Leica Microsystems, Germany), using a staining schedule detailed in Table 2.3.

Table 2.3 Standard protocol for H&E staining

Bath nº	**Solution**
1-3	Xylene
4-5	99% IDA
6	70% IDA
7-8	Distilled water
9-12	Harris' haematoxylin (Shandon)
13	Running tap water
14	0.1% acid alcohol
15	Running tap water
16	Scott's Tap water substitute
17	Running tap water
18-20	Eosin Y- aqueous (Shandon)
21	Running tap water

22-24	99% IDA
25-28	Xylene

Following staining, slides were mounted onto coverslips with distyrene and xylene (DPX) mountant and left to set. Slides were visualised using an Olympus-BX51 light microscope and captured using cellSens Entry software (Olympus).

2.5 Preparation of EV-depleted FBS

Bovine extracellular vesicles (EVs) were removed from FBS by ultrafiltration using Amicon ultra-15 centrifugal filter units (100 kDa cut-off) as previously stated by Kornilov R *et al*. (2018) with minor adaption. FBS was filtered through 100 kDa filters loaded into the upper chamber of the centrifuge tubes. After centrifugation at 2,500 x *g* for 2 h at 4°C, flow-through was recovered in the lower chamber as ultrafiltered EV-depleted FBS. FBS was supplemented into appropriate media and stored at 4°C.

2.5.1 Isolation and characterisation of EVs

Conditioned media was collected from cells cultured in EV-depleted FBS supplemented media after 24 h. Cells were seeded at the same density to control for differences in EV biogenesis due to confluence, as well as between cell lines. For analysis of particles in conditioned media, collected media was subject to centrifugation for 10 min at 300 x *g* to remove cells and the resulting supernatant analysed by NTA (2.5.3) on the same day. For large scale EV preparations, conditioned media was subject to differential centrifugation; 300 x *g* 10 min, 2,000 x *g*

15 min and 10,000 x *g* 30 min. The resulting supernatant was concentrated to 0.5 mL, using Vivaspin-20 100 kDa molecular weight cut off columns (Cytiva) by centrifugation at 6,000 x *g* at 4°C for approximately 20 min.

2.5.2 Size exclusion chromatography

Size exclusion chromatography (SEC) was performed using disposable 20 mL chromatography columns (Biorad) filled with 14 mL of Sepharose CL-2B/ethanol slurry (GE Healthcare). The slurry was left for approximately 1 h for the gel beads to settle. A polystyrene filter was placed directly above the settled gel. Ethanol was drained from the column and 30 mL sterile PBS supplemented with 0.03% (v/v) Tween-20 (PBST) was used to wash and equilibrate the resin.

SEC was performed by running 0.5 mL of concentrated conditioned medium through the gel column. Once the medium soaked into the polystyrene filter, 1 mL of PBST was gently added and allowed to soak through, and throughout PBST was maintained at 1-3 mL above the gel column. Elutant from the column was collected in microcentrifuge tubes as 0.5 mL fractions. Fractions were pooled and subject to ultracentrifugation at 100,000 x *g* using a benchtop TLX ultracentrifuge (Beckman Optima). Supernatant was removed and pellets were then resuspended in an appropriate buffer depending on experimental usage.

2.5.3 Nanoparticle tracking analysis

The autofocusing nanoparticle tracking ZetaView instrument (Particle Metrix GmbH) was used to perform EV characterisation. Acquisition settings used are shown in table

2.4. The machine was calibrated with polystyrene calibration particles with a known average size of 100 nm diluted 1/500,000 in distilled water. Approximately 3 mL of sample was injected into the fluid cell and particles were analysed at 11 separate positions to give a representative average. ZetaView software (version 8.05.11 SP1) generated data of particle size and concentration in each sample.

Table 2.4 ZetaView image acquisition settings

Parameters	**Settings**
Sensitivity	85
Shutter	70
Minimum brightness	25 pixels
Maximum area	500 pixels
Minimum area	5 pixels
Frame rate	30 frame per second (fps)
Trace length	15
Positions	11

2.5.4 Nano-Flow Cytometry

Data acquisition and analysis was performed in collaboration with NanoFCM at their laboratory in Nottingham, UK.

EVs were isolated by SEC, as described previously (Section 2.6.1) and labelled with a tetraspanin (CD9, CD63 and CD81 APC-conjugated) antibody cocktail at 1/50 dilution. The anti-TGF-β (Alexa-488 conjugated) antibody was diluted 1/250. EVs and antibodies were incubated for 30 min at RT. EVs were pelleted by centrifugation at 100,000 x *g* for 45 min in a benchtop TLX ultracentrifuge (Beckman Optima) and

resuspended in 20 µl 10 mM HEPES. Samples were analysed using a Flow NanoAnalyzer (NanoFCM) instrument and associated software.

2.6 Functional assays

2.6.1 Cell viability assays

2.6.1.1 3-(4,5-dimethylthiazol-2-yl)-2,5-diphenyltetrazolium bromide (MTT) assay

To determine the viability of our cell lines in response to drug treatment in 2D, we utilised 3-(4,5-dimethylthiazol-2-yl)-2,5-diphenyltetrazolium bromide (MTT) that detects viable cells with an active metabolism. Cells were plated at 5 x 10^3 cells/well in 96-well culture plate and incubated for 24 h. Cells were treated with serially 10-fold diluted drug concentrations for 24 and 48 h. Untreated cells and vehicle controls (i.e. DMSO concentration corresponding to equivalent drug concentration) (Table 2.5) were used as controls. Monolayers were washed in 100 mM PBS and incubated for 1 h with MTT solution (0.5 mg/mL MTT in PBS, 100 µl per well in 96 well plate) at 37°C with 5% CO_2 to determine cell viability. Intracellular insoluble purple formazan salt is formed by reduction of MTT by NADPH dependent enzymes in metabolising cells. Formazan was solubilised using acidified isopropanol 50 µl/well. The optical density of the solution was measured at 540 nm with a reference at 630 nm, using a Tecan Infinite® 200 PRO series spectrophotometer. Optical density values for treated cells were normalised to untreated control, to produce percentage survival.

Table 2.5 Drug concentrations and equivalent vehicle control percentages

Drug	Drug concentration (μM)	DMSO (%)
GW4869	10	0.1
	50	0.5
	100	1
DMA	1	0.01
	10	0.1
	50	0.5

2.6.1.2 PrestoBlue® cell viability assay

In order to quantify viability in 3D models, we utilised PrestoBlue® Cell Viability reagent (Life technologies) as it can be added to models and washed away without toxic effects. PrestoBlue® was diluted 1:10 in Green's medium and 100 μl of this solution was added on top of the model. After 30 mins incubation at 37°C, 200 μl of media from the basal side of the model was taken and added to a clear 96 well plate. Triplicates for each biological repeat were used. PresoBlue® utilises resazurin that is reduced to resorfurin in viable cells during respiration. This reduction causes a colour change from blue to red, which we measured using a using a Tecan Infinite® 200 PRO series spectrophotometer at an excitation of 535nm and emission of 615nm. Relative fluorescence units (RFU) are directly proportional to cell metabolism, and we corrected for background using a media only control to normalise samples.

2.6.2 Scratch migration assay

A scratch assay was used to determine migration of NOF following incubation with EVs. NOF were seeded at a density of 0.5 x 10^6 in 13 mm culture dishes and allowed

to adhere over-night. Following this, cells were serum starved for 24 h to induce cell synchronisation. Cells were then treated with 5 µg/mL mitomycin C for 1 h to inhibit proliferation and ensure closure of wound due to migration only. A scratch wound was created using a 10 µl pipette tip and the cells were washed three times with PBS to remove detached cells before treatment with recombinant human transforming growth factor (rhTGF)-β (5 ng/mL) or EVs at a dose of 50 x concentration in conditioned media according to cell type. Cells were imaged using a Leica THUNDER live cell imaging system, taking an image every 15 min at 3 positions per treatment. Wound area closing was analysed using ImageJ. For analysis of motility, all images for each timepoint for each condition were compiled and analysed using Tracking Tool™ PRO software. For each technical repeat three cells from either side of the scratch were tracked. Rose plots were calculated from the cell trajectories using the same Tacking Tool™ PRO software.

2.6.3 Collagen contraction assay

NOF were seeded at a density of 0.5 x 10^6 in culture flasks (25 cm^2) and allowed to adhere for 24 h. Cells were cultured for 24 h in the absence of serum prior to treatment with 5 ng/mL rhTGFβ or EVs as previously described (Section 2.7.1) for 48 h. Following this, cells were trypsinised and seeded into 1 mL rat tail collagen per condition, prepared according to Table 2.1, with the exception of FBS. The collagen-cell mixture was then added to a well of a 48-well plate and incubated at 37°C 5% CO_2. Images were taken at 24, 48 and 72 h using a GelDoc Go imaging system (BioRad) and diameter shrinkage over time was measured using ImageJ.

2.7 Protein extraction and analysis

2.7.1 Protein extraction of whole cell lysate and EVs

EV pellets purified by SEC or ultracentrifugation were suspended in radioimmunoprecipitation assay (RIPA) buffer containing complete mini ethylenediaminetetraacetic acid (EDTA)-free ease protease inhibitors (Roche). Cell lines or NOFs were cultured as previously described (Sections 2.2.1 and 2.2.2) in either 6 well plates or flasks (75 cm^2) to confluency. On ice, culture media was removed and cells were washed twice with PBS before RIPA buffer containing complete mini EDTA-free ease protease inhibitors (Roche) was added. After 5 min cells were scraped, transferred to a microcentrifuge tube and clarified by centrifugation at 12,000 x *g* for 15 min at 4°C. The supernatant was transferred to a fresh tube and stored at -80°C. EV pellets were resuspended in up to 50 µl RIPA buffer before storage at -80°C.

2.7.2 Protein quantification

A bicinchoninic acid protein assay (BCA) kit (Thermo-Fisher Scientific) was used to assess protein concentration of samples. Bovine serum albumin (BSA) standards were made in PBS, to concentrations of 0.2, 0.4, 0.6, 0.8, 1, 2 mg/mL. 10 µl of sample or BSA standard was added to 200 µl BCA working reagent in a 96-well plate in duplicate. The plate was incubated at 37°C for 30 min. The absorbance of each well was measured at 562 nm using a Tecan Infinite® 200 PRO series spectrophotometer. Protein concentration of unknown samples were estimated by generating a curve of known standards (µg) versus absorbance.

2.7.3 Protein gel electrophoresis

Sodium dodecyl sulphate polyacrylamide gel electrophoresis (SDS-PAGE) gels of 1 mm thickness were made using a standard protocol using reagents listed in Table 2.6.

Table 2.6. The components and quantity of reagents for 12% SDS-PAGE gel

	Reagent	**Volume**
Stacking gel	40% acrylamide	0.975 mL
	Upper tris buffer (0.5 M tris base, 14 mM SDS, pH 6.8)	2.1 mL
	dH_2O	4.725 mL
	10% (v/v) Ammonium persulphate solution (APS)	100 µl
	TEMED	10 µl
Resolving gel	40% acrylamide	3 mL
	Lower tris buffer (1.5 M tris base, 14 mM SDS, pH 8.8)	2.5 mL
	dH_2O	4.3 mL
	10% (v/v) Ammonium persulphate solution (APS)	200 µl
	TEMED	5 µl

Resolving gel was poured between two glass plates and isopropanol overlayed on top to smooth the surface. After the resolving gel was set, stacking gel was added on top and a sample comb inserted before allowing the gel to polymerise. After this the comb was removed and each well was washed with distilled water.

Sample volumes were equalised to the same concentration in 20 µl with 1 X RIPA buffer, containing protease inhibitors, before the addition of 5 µl 5X loading buffer. The samples were heated at 95ºC for 5 min. Samples were then separated by 12% polyacrylamide SDS-PAGE in electrophoresis chambers (Biorad) filled with 1X Running buffer (88 g glycine, 10% (w/v) SDS and 32 g tris base in 1 L distilled water). 20 µl of sample was loaded in each well, with 5 µl Precision Plus pre-stained protein ladder (Biorad) added to the outside wells. Separation was performed at 110-120 V for 60-70 min and then at 120-150 V until the dye had run to the bottom of the glass plates.

2.7.4 Western blotting

Proteins separated by SDS-PAGE were transferred to nitrocellulose membranes using the Trans-Blot®Turbo™ system (Biorad). Membranes were incubated with blocking buffer (5% (w/v) dried milk powder in tris-buffered saline and 0.1% (w/v) Tween 20 (TBST)) at RT for 1 h with agitation. Primary antibody was diluted in blocking buffer according to Table 2.7 and the membrane incubated overnight at 4°C with agitation. Membranes were then washed three times in TBST for 10 min per wash. HRP-conjugated secondary antibody was diluted in blocking buffer and incubated with the membrane for 1 h at RT with agitation, followed by washing 3 times in TBST for 10 min each. Chemiluminescence substrate, WESTAR® Supernova (Geneflow) or SuperSignal™ West Pico PLUS (ThermoFisher) were added to the membrane as per manufacturer's instructions and protein bands were visualised using either X-ray film and a Compact X4 automatic processor (Xograph Imaging Systems) or LI-COR C-DiGit Chemiluminescence Western Blot Scanner.

Table 2.7. Antibodies used in immunoblotting.

Antibody target	Species (catalogue number)	Manufacturer	Expected weight (kDa)
CD63	Rabbit monoclonal (ab134045)	Abcam	26-65
TSG101	Mouse monoclonal (2918209)	BS Biosciences	44
HGS	Rabbit polyclonal (ab155539)	Abcam	86
GAPDH	Mouse monoclonal (50004-1-1a)	Proteintech	36
GFP	Mouse monoclonal	Santa Cruz	26
α-SMA	Rabbit monoclonal (ab124964)	Abcam	30-65
Anti-rabbit IgG	7076S	Cell signalling	
Anti-mouse IgG	7074S	Cell signalling	

2.7.5 Enzyme linked immunosorbent assay (ELISA)

FNB6, H357 and H357$^{\Delta HGS}$ cells were seeded at a density of 6 x 10^6 per T175 flask and after 24 h the medium was removed, and the flask washed three times with PBS before the addition of serum-free media. After another 24 h the conditioned media was removed, and EVs isolated by SEC as previously described (Section 2.5.2).

The DuoSet® Human TGF-β1 ELISA kit (R&D systems) was used to detect TGF-β1 concentrations in conditioned media and EV samples. Firstly, the capture antibody

was diluted in PBS to the working concentration (Table 2.8) and 100 µl per well was added to the 96-well microplate before being incubated overnight at RT. Following this, the plate was subject to a thrice repeated wash step involving filling each well with Wash Buffer using a squirt bottle and then inverting the plate onto blotting paper to remove liquid. Following this, plates were blocked with 300 µl blocking buffer (25% Tween 20 in PBS) and incubated for 1 h at RT. The plate was then subject to washing. Recombinant human TGF-β1 standard was diluted 2-fold in reagent diluent for seven concentrations and 100 µl of each were added to each well in duplicate. Samples were diluted in reagent diluent and/or activated using a TGF-β1 Sample Activation Kit (R&D systems) according to manufacturer's instructions. 100 µl of each sample was added per well in duplicate and incubated for 2 h at RT. Following another wash step, 100 µl detection antibody diluted in reagent diluent was added to each well and incubated for 2 h at RT. The plate was subject to another wash step and 100 µl Streptavidin-HRP was added per well and incubated for 20 min at RT without light. The plate was washed again and 50 µl Stop Solution (2N sulfuric acid) was added. The plate was then read using a Tecan Infinite® 200 PRO series spectrophotometer at a wavelength of 450 nm with a reference wavelength of 540nm.

Table 2.8. Working concentrations of antibodies used in DuoSet® Human TGF-β1 ELISA kit.

Reagent	**Working concentration**
Capture	2 µg/mL
Detection	50 ng/mL
Standard	31.2-2000 pg/mL
Streptavidin-HRP	40-fold dilution

2.8 Fluorescence Imaging

2.8.1 Immunofluorescence

In order to determine alpha smooth muscle actin (α-SMA) stress fibre formation, we used fluorescent staining. NOFs were fixed in methanol for 15 min at RT and washed three times with ice cold PBS. Cells were then permeabilised with 4 mM sodium deoxycholate in PBS for 10 min before washing three times with ice cold PBS. Cells were then incubated for 1 h at RT with blocking buffer consisting of 2.5% BSA in PBS (w/v) and washed again three times with ice cold PBS before the addition of primary antibody in blocking buffer overnight at 4°C. Antibody details are shown in Table 2.9. Following a further washing step, secondary antibody was added for 1 h at RT and washed once more. DAPI was diluted in PBS to a final concentration of 1 µg/mL and incubated for 10 min before washing and mounting onto glass coverslips with ProLong™ Glass Antifade Mountant. Coverslips were sealed with transparent nail varnish and stored at 4°C without light prior to imaging using a Leica THUNDER fluorescent microscope. For analysis, three random positions were imaged at 10x objective per technical repeat (27 total for three biological repeats). Representative images wee taken using a 20x objective lens. The percentage of area positive for fluorescence was calculated using ImageJ software.

Table 2.9. Immunofluorescence antibody details and dilutions.

Antibody	Host species	Manufacturer	Blocking buffer	Dilution buffer	Dilution
Anti-α-SMA	Mouse monoclonal (A2547)	Sigma	2.5% BSA (w/v) in PBS	2.5% BSA (w/v) in PBS	1:500
Anti-mouse FITC	Goat polyclonal (F-2761)	Sigma			1:500
Anti-EEA1	Rabbit polyclonal (ab70521)	Abcam	1% BSA (w/v), 10% normal goat serum (NGS) (v/v), 0.3 M glycine (w/v) dissolved in 0.1% PBST	1% BSA in 0.1% PBST	1:1000
Anti-rabbit Alexa Fluor 594	Donkey polyclonal (A32744)	ThermoFisher Scientific			1:1000

2.8.2 H357$^{CD63\text{-}GFP}$ EV uptake

NOFs were seeded onto glass coverslips at a density of 3 x 10^4 cells per well, in a 12 well plate, and allowed to adhere overnight. EVs were isolated by SEC (Section 2.5.2) from H357$^{CD63\text{-}GFP}$ cells, generated by methods described in Section 2.11. Particle number was quantified by NTA (Section 5.2.3) and 50-fold the number of particles secreted into conditioned medium by H357 cells (4 x 10^{10}/mL) was treated onto NOFs in serum free media. NOFs were then fixed at time points of 0.5, 1, 2, 4, 6 h in a solution of 4% paraformaldehyde (PFA) dissolved in PBS (w/v), for 10 min at RT. Cells were then permeabilised with 0.1% Triton X-100 (v/v) in PBS for 10 min before

washing three times with ice cold PBS. Cells were then incubated for 1 h at RT with blocking buffer consisting of 1% BSA, 10% normal goat serum (NGS), 0.3 M glycine dissolved in 0.1% PBST, and washed three times with PBS. Primary EEA1 antibody in 1% BSA in 0.1% PBST was incubated overnight at 4°C. Antibody details are shown in Table 2.9. Following washing three times with PBS, secondary antibody anti-rabbit Alexa Fluor 594 diluted in 1% BSA in 0.1% PBST was added for 1 h at RT before a further three repetition wash step with PBS. DAPI was diluted in PBS to a final concentration of 1 µg/mL and incubated for 10 min before washing and mounting onto glass coverslips with ProLong™ Glass Antifade Mountant. Coverslips were sealed with nail varnish and kept at 4°C without light prior to imaging with Leica THUNDER fluorescent microscope using a 100x oil objective lens. Software used for image processing was Leica Application Suite X (LAS X). ImageJ software plugin Coloc2 was utilised to determine correlation coefficient on 1 cell per technical repeat (9 total for 3 biological repeats).

2.9 RNA extraction and analysis

2.9.1 RNA extraction

Media was aspirated, and cells washed twice in PBS, 300 µl of RNA lysis buffer was added and cells harvested by using a cell scraper. RNA was extracted using the Monarch Total RNA MiniPrep Kit (NEB) according to the manufacturer's instructions. RNA concentrations were calculated using a NanoDrop™ 1000 spectrophotometer based on absorbance at 260nm and calculated using Beer's Law. RNA purity was assessed by the ratio of sample absorbance at 260 and 280 nm, whereby a ratio of 2 was considered ''pure''.

2.9.2 Complimentary DNA (cDNA) synthesis

RNA was normalised to 100 ng in dH_2O to a total volume of 10 µl. This was then combined with an RT-PCR mixture (2 µl 10x RT Buffer, 0.8 µl 25x dNTP Mix 100 mM, 2 µl 10x RT Random primers, 1 µl Multiscribe reverse transcriptase, 4.2 µl nuclease-free water). cDNA synthesis was performed using a 2720 Thermal Cycler (Applied Biosystems™).The thermal cycling program used is described in Table 2.10.

Table 2.10. RT-PCR thermocycling programme.

	Step 1	**Step 2**	**Step 3**	**Step 4**
Temperature (ºC)	25	37	85	4
Time (mins)	10	120	5	∞

2.9.3 Quantitative real-time PCR

0.5 µl of cDNA from each sample was added to 9.5 µl of PCR reagent mixture (5 µl of mastermix, 0.5 µl of GAPDH control probe (Hs99999905_m1), 0.5 µl of target probe, 3.5 µl of nuclease-free water). The Taqman target probes used were: α-SMA (ACTA2), Hs00426835_g1; FAP, Hs00990806_m1; and HGS, Hs00610371_m1. The 10 µl mixture was centrifuged for 1 min at 13,000 x *g* before undergoing the PCR reaction using a Rotor-gene Q 5plex or 2plex machine (QIAGEN). The thermal cycling program is described in Table 2.11.

Table 2.11. qPCR thermocycling schedule.

	Step 1	Step 2	Step 3 (Repeated for 40 cycles)		Step 4	
Temperature (ºC)	50	95	95	60	95	60
Time	2 min	10 min	15 secs	1 min	0.15 secs	0.15 secs

2.10 Preparation of plasmid DNA

2.10.1 Bacterial transformation

The plasmids used in this work were CD63-GFP (SBI System Bioscience) and mCherry-Tsg101 as a gift from James Hurley (Addgene plasmid #21505) first described in (Lee et al., 2008).

The pCT-CD63-GFP plasmid DNA is a Human Immunodeficiency Virus (HIV) lentiviral vector that contains a C-terminal copGFP reporter under the control of a CMV promoter and a puromycin selectable marker under the control of an EF1 alpha promoter. mCherry is cloned at the N-terminus of TSG101 under a CMV promotor and a neomycin selectable marker under the control of an SV40 promotor. The details of each plasmid are displayed in figure 2.2.

A

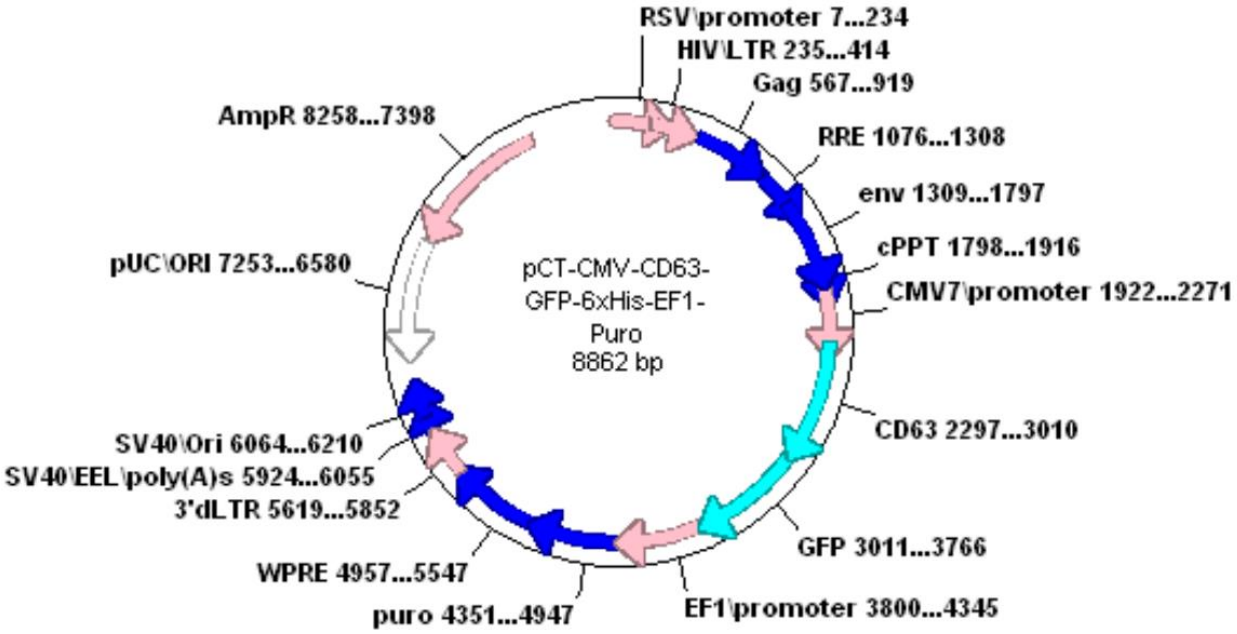

B

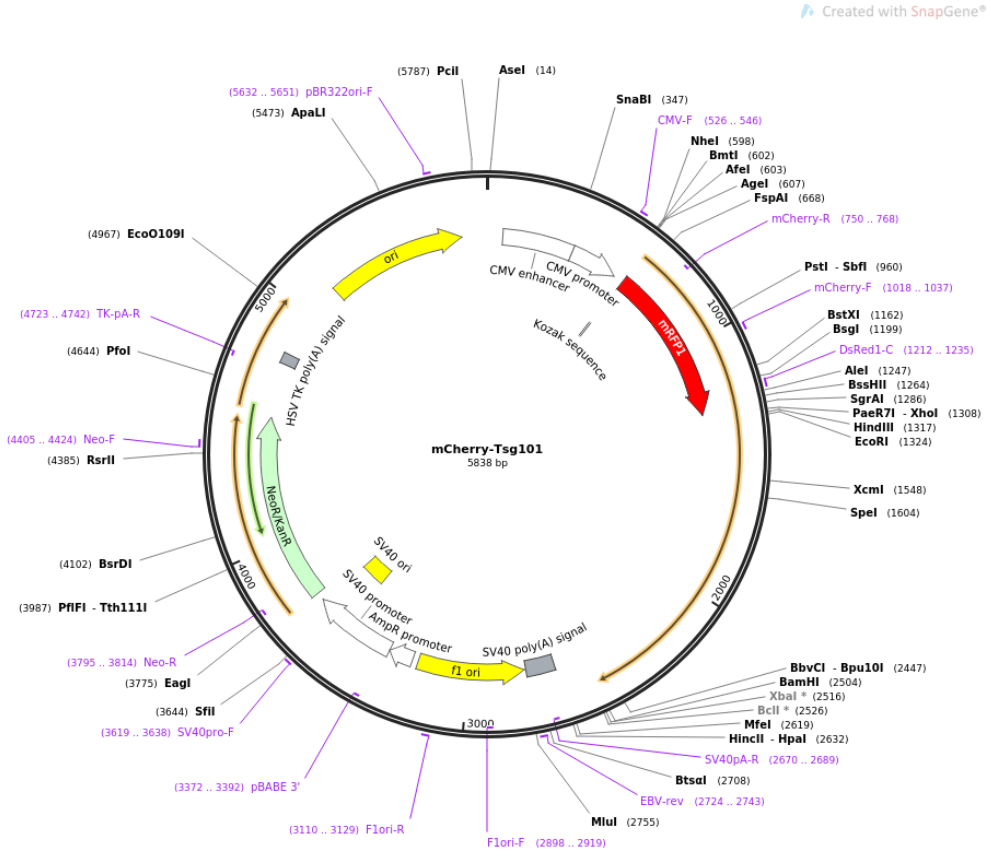

Figure 2.2 Plasmid constructs (A) CD63-GFP provided by SBI System Bioscience (B) TSG101-mCherry taken from Addgene.(https://www.addgene.org/21505/).

5-alpha Competent *Escherichia coli* cells (New England BioLabs) were thawed on ice for 10 min and 1 ng of plasmid DNA added. The mixture was then placed on ice for 30 min and heat shocked at 42°C for 30 s. The mixture was returned to ice for 5 min. 950 µl of RT Super Optimal broth with Catabolite repression (SOC) medium was added to the mixture and incubated at 37°C for 60 min with shaking. Following this, cells were diluted to 1:2, 1:5 and 1:10 and spread onto either kanamycin (50 µg/mL) or ampicillin (100 µg/mL) selection plates. Plates were incubated overnight at 37°C.

2.10.2 Plasmid DNA midiprep

Single colonies from transformation plates (Section 2.10.1) were picked and spread onto fresh agar plates with appropriate selection antibiotic and grown overnight at 37ºC. Following this, 5 mL of Luria Broth (LB) plus appropriate antibiotic was inoculated with a single colony and grown at 37°C for 16 h in a shaking incubator. Cells were harvested by centrifugation at 6000 x *g* for 15 min at 4ºC. Plasmid DNA was purified using the QIAGEN Plasmid Midiprep kit according to the manufacturer's instructions. DNA concentration was determined using a NanoDrop® ND-1000 UV-Vis Spectrophotometer.

2.11 Generation of stable cell line

2.11.1 FuGENE® HD transfection optimisation

H357 cells were seeded at a density of 2.5 x 10^4 in glass bottom Nunc™ Lab-Tek™ chambers and allowed to adhere overnight. For successful transfection of DNA into

cultured cells, the ratio of FuGENE transfection reagent:DNA required optimisation. The ratios chosen were 1:2, 1:3 and 1:4, as this in line with the manufacturer's recommended range. 2 µg/100 µl of DNA in total was used for each transfection condition, diluted in low serum Opti-MEM® medium (Invitrogen). We performed both single and co-transfections with TSG101-mCherry and CD63-GFP plasmids, meaning that 1 µg/100 µl of each plasmid DNA was used in the co-transfection conditions. FuGENE was added to the diluted DNA mixture at the correct ratio and incubated for 15 mins at RT to allow DNA complexes to form. 10 µl of the this mixture was then added to each well in a dropwise manner. Fluorescent positive cells were visualised using a ZOE fluorescent cell imager microscope (BioRad) and quantified using ImageJ.

2.11.2 Lipofectamine 2000 transfection

H357 cells were seeded at a density of 3 x 10^5 per well in 6 well cell culture plates. Initial optimisation included using volumes of 6, 9, 12 and 15 µl Lipofectamine 2000 with the same quantity of DNA (2500 ng). Cells were co-transfected meaning 1250 ng of Tsg101-mCherry and CD63-GFP plasmids were used, diluted in Opti-MEM® medium to a final volume of 150 µl. DNA mixture was added to Lipofectamine diluted in Opti-MEM® medium to a final volume of 300 µl and incubated at RT for 5 min. The DNA-lipid complex was then added directly into each well. Fluorescent positive cells were visualised using a ZOE fluorescent cell imager microscope (BioRad) and quantified using ImageJ.

For larger scale transfection we moved forward with 9 µl Lipofectamine per condition in 6 well plates. After 24 h each 6 well was split into a culture flask (25cm^2), and after

another 24 h antibiotic selection media containing 400 µg/mL G418 and/or 2.5 µg/mL puromycin (Gibco) were added. Selection media was changed every 3 days until surviving colonies expanded.

2.11.3 Fluorescence-activated cell sorting (FACS)

Surviving colonies (Section 2.11.2) were then trypsinised and resuspended in Green's media at a maximum concentration of 1 x 10^7 cells/mL. Single H357 cells were seeded into 96 well plates, using a BD FACSMelody™ Cell Sorter (BD Biosciences). Those transfected with CD63-GFP were sorted using a 488 nm laser, and those transfected with TSG101-mCherry were sorted using 587nm excitation.

2.12 Statistical analysis

Statistical analysis was carried out using GraphPad Prism (Version 8.0), with data presented as mean ± standard deviation (SD).

Shapiro-Wilk normality test was conducted to determine normal distribution and data sets normally distributed were analysed using ordinary one-way ANOVA with Dunnett's multiple comparisons to correct for variance with multiple comparisons or Student's t-test. Data sets not normally distributed were analysed by non-parametric Kruskal-Wallis test with Benjamini, Krieger and Yekutieli (BKY) correction for multiple comparisons or Wilcoxon signed rank test. Experimental repeats denoted as ''N'' refers to biological repeats and ''n'' denotes technical repeats.

3 Investigating chemical modulators of extracellular vesicle release

3.1 Introduction

Extracellular vesicles are key mediators of cell-cell communication between multiple cell types in the TME. Cancer-derived EVs have been demonstrated to be critical messengers in contributing to stromal reprogramming, immune evasion, neovascularisation and metastasis making them a favourable drug target (Cho et al., 2011; Lundholm et al., 2014; Conigliaro et al., 2015; Chen et al., 2021). Inhibiting EV release and uptake is a useful tool to investigate their functional role within the TME and is a potential novel therapeutic strategy (Richards et al., 2017).

As outlined previously, there are multiple modes of biogenesis for subpopulations of EVs (Chapter 1.2.1), making the development a single small molecule that can completely inhibit EV production or uptake unlikely. However, success has been attained by targeting the broad categories; inward budding of MVBs, exosome release by regulation of calcium or acidification, MV release and EV uptake (Catalano et al., 2020). The mechanism of action of the small molecules used to alter EV release in this chapter are highlighted in figure 3.1.

The most abundant membrane lipid, sphingomyelin, is hydrolysed into ceramide and phosphorylcholine by membrane neutral sphyingomyelinases (nSMase) (Clarke et al., 2006). These ceramides are an important component of large lipid raft domains that are involved in exosome shedding (Trajkovic et al., 2008). The cell permeable GW4869 is a non-competitive inhibitor of nSMase 1 and 2 and has been shown to

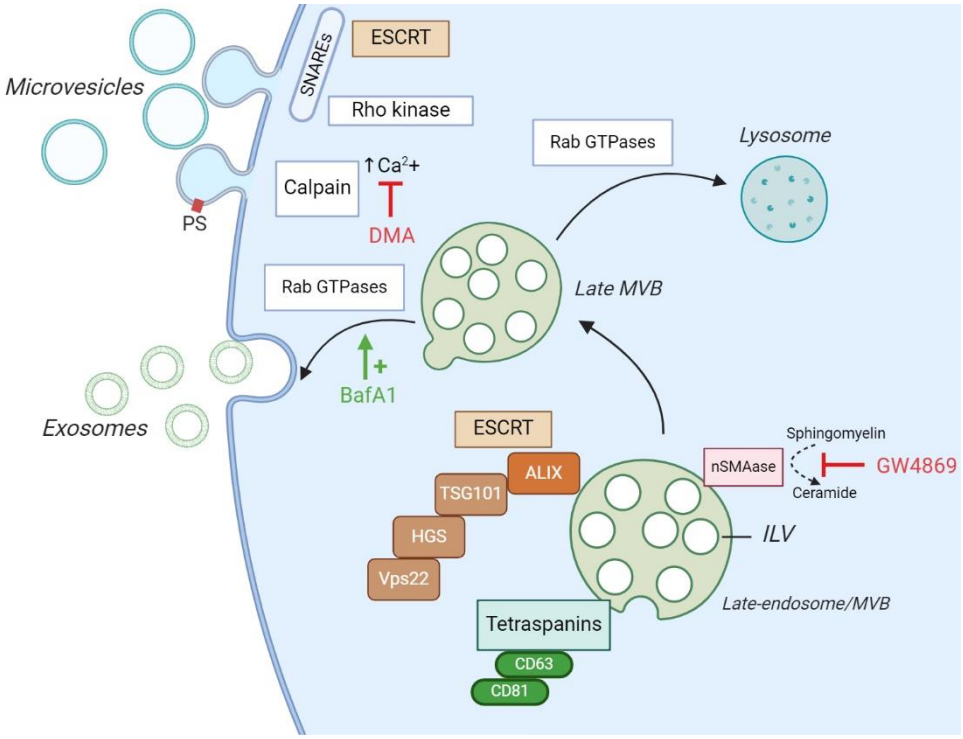

Figure 3.1 Summary of small molecule targets for modulation of EV biogenesis. Red arrows indicate inhibition and green arrows with plus sign indicate stimulation.

significantly reduce exosome release via inhibiting ceramide-dependent budding of ILVs into the lumen of MVBs (Trajkovic et al., 2008). nSMase associate with the plasma membrane, however, they also function in other organelles and have been shown to be involved in generation of Golgi apparatus derived vesicles, where both nSMAse 1 and 2 localise (Deng et al., 2016). GW4869 has been shown to significantly reduce the production of small vesicles in multiple cell types *in vitro* and has been used to demonstrate the role of EVs in cancer progression (Richards et al., 2016; Matsumoto et al., 2017; Gurunathan et al., 2021) For example, treatment of CAFs with GW4869 reduced their ability to confer gemcitabine resistance to colorectal cancer stem cells (Richards et al., 2016).

Another mechanism by which EV release can be altered is by calcium homeostasis due to intracellular Ca^{2+} modulating lipid translocases that maintain membrane phospholipid asymmetry (Hugel et al., 2005). When intracellular calcium is increased,

this asymmetry is disrupted and calpain is activated which cleaves cytoskeletal components. This disruption of the cytoskeletal-membrane attachment causes outward budding, forming plasma membrane EVs (Taylor et al., 2020). Dimethyl amiloride (DMA) is a derivative of amiloride, a drug clinically approved to treat high blood pressure because of its ability to block H^+/Na^+ and Na^+/Ca^{2+} channels. DMA has therefore been implicated in EV reduction due to its interference with Ca^{2+} levels (Savina et al., 2003; Chalmin et al., 2010). Chalmin *et al* completed a comprehensive assessment of DMA, showing that upon treatment, exosome secretion was reduced in CT26 (mouse colon carcinoma), EL4 (mouse lymphoma) and H23 (human lung adenocarcinoma) as well as in the bloodstream of tumour bearing mice (Chalmin et al., 2010). Savina *et al* used DMA to demonstrate that exosome release is regulated by a calcium-dependent mechanism, whereby exosome and large MV formation was blocked in a human erythroleukemia cell line following DMA treatment (Savina et al., 2003). Pharmacological inhibition of endocytic pathways has demonstrated that DMA inhibits micropinocytosis and could therefore reduce internalisation and sorting into early and late endosomes, therefore reducing EV formation (Plummer et al., 2012).

An as alternative to EV inhibiting compounds, we also aimed to test the proposed EV stimulating drug Bafilomycin A1 (BafA1). BafA1 is a macrolide antibiotic that potently inhibits the vacuolar ATPase (V-ATPase) proton pump (Shacka et al., 2006). Most widely used as an autophagy inhibitor, BafA1 blocks V-ATPase to prevent endosomal and lysosomal acidification and therefore fusion of lysosomes and autophagosomes (Shacka et al., 2006). The exact mechanisms are unclear, however it has been shown that BafA1 stimulates exosome release from MVBs, independently from endosomal pH neutralisation (Bebelman et al., 2023). This could be in part due to increased MVB-

plasma membrane fusion, as observed in HEK293 cells using live fluorescent imaging of CD63 tagged with a pH-sensitive reporter (Bebelman et al., 2023).

3.2 Results

3.2.1 Cell viability and particle release in response to GW4869

We first sought to determine the effect of GW4869 on cell viability for cells grown in monolayer. This would allow us to empirically determine an effective concentration, that does not affect cell viability, for future experiments. FNB6 (an immortalised normal oral keratinocyte cell line) and H357 (an OSCC cell line) were selected to represent normal and cancerous epithelial cells, respectively. Primary patient derived NOF and CAF cells were used to represent the normal and cancer associated underlying stroma, respectively.

FNB6 cells challenged with GW4869 demonstrated less sensitivity than H357; at 24 h cell survival was not significantly reduced at doses lower than 100 µM (46.9%) ($p < 0.0001$). At 48 h, unlike H357, there was no significant change in survival at the 10 µM dose, however the 50 µM and 100 µM concentrations further reduced survival to 57.7% and 25.1% ($p < 0.05$ and $p < 0.001$, respectively) (Figure 3.2B). IC_{50} values calculated from two repeats however show that a higher dose was needed to have the same cytotoxic effect at 24 h, with IC_{50} = 265.45 µM (SD ± 33.05) at 24 h and reducing to 43.25 µM (SD ± 10.62) at 48 h.

There was a similar trend in H357 cells treated with GW4869 for 24 h remained statistically unchanged compared to the untreated control from 0.01 – 10 µM, however there was significant decrease to 77.2% survival at the 50 µM dose ($p < 0.05$) and a decrease to 52.1% at the 100 µM concentration ($p < 0.0001$) (Figure 3.2C). There was a greater cytotoxic effect at 48 h with the 10 µM causing a significant ($p < 0.05$) reduction in survival. The 50 µM and 100 µM doses were reduced to 56.9% and 25.4%

survival at this timepoint ($p < 0.001$ and $p < 0.0001$, respectively) (Figure 3.2C). At 24 h cells displayed an IC_{50} value of 48.78 µM (SD ± 3.22), increasing to 80 µM (SD ± 13.47) at 48 h (based on two repeats).

Due to the low solubility of GW4869 in DMSO, the volume of DMSO used to solubilise higher concentrations of the drug could likely result in toxic effects in cells alone. To assess whether the change in survival was due to the GW4869 or DMSO, cells were treated with GW4869 (dissolved in DMSO) or an equivalent volume of DMSO only; 0.1% (10 µM drug), 0.5% (50 µM drug) and 1% (100 µM drug). At both 24 h and 48 h there is no significant difference in cell survival for either FNB6 or H357 cells treated with GW4869 and DMSO vehicle compared to DMSO alone, for all concentrations (Figure 3.2B and D, respectively).

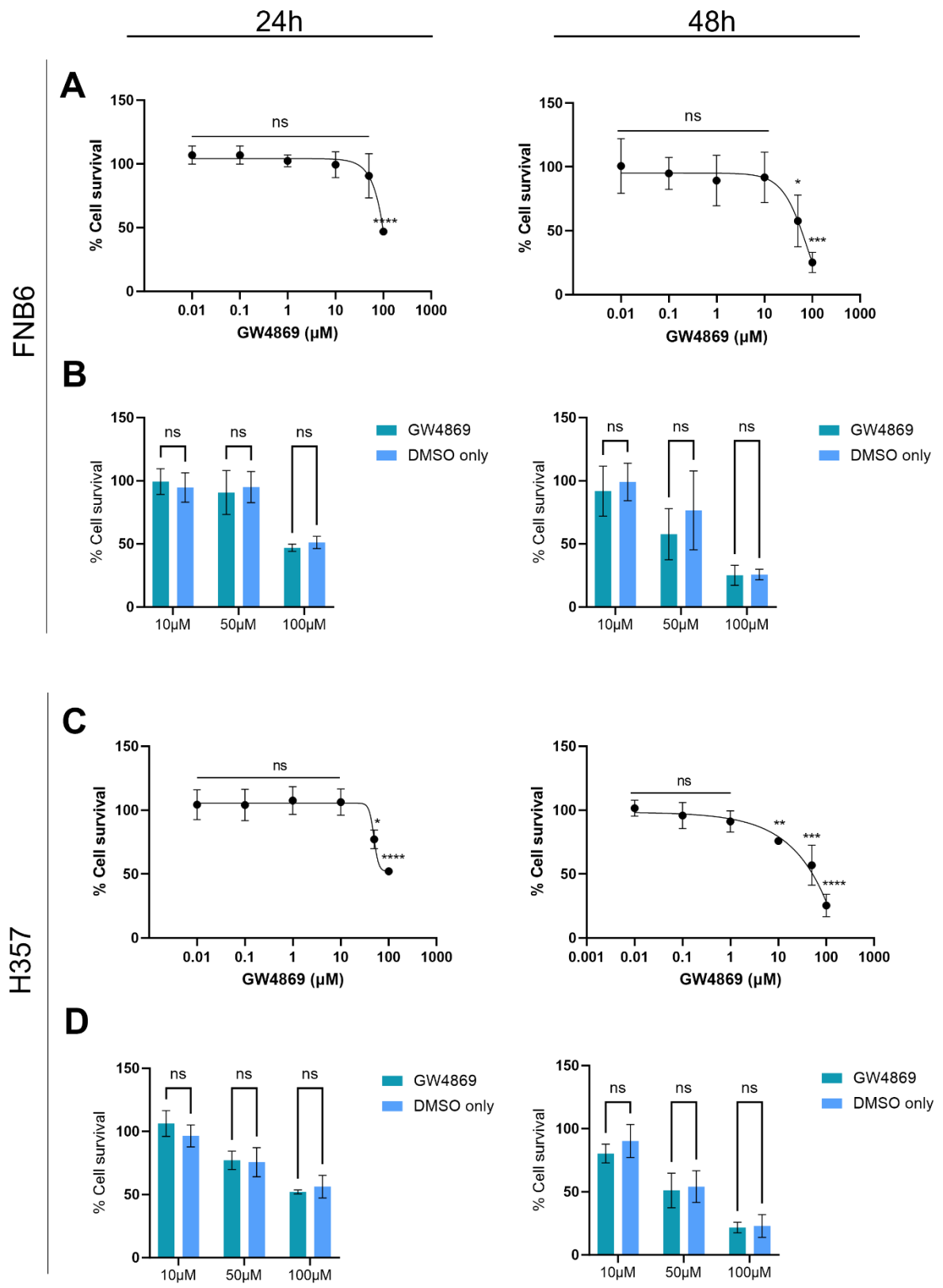

Figure 3.2 Cell survival of FNB6 and H357 cells in response to treatment with GW4869. Cells were seeded at a density of 5000 cells/well in 96-well plates, treated with (A,C) 0.01, 0.1, 1, 10, 50 and 100 μM GW4869 (DMSO vehicle) and cultured for 24 and 48 h. (B,D) 10, 50 and 100 μM GW4869 and equivalent DMSO vehicle control % were directly compared. Cell viability was assessed using an MTT assay. Data is presented as mean ± SD (N=3, n=3). Statistics performed by one-way ANOVA and Dunnets multiple comparisons test. ns, non-significant, *p < 0.05, **p < 0.01, ***p < 0.001, ****p < 0.0001.

The survival of NOF cells treated with GW4869 for 24 h was reduced significantly at all doses except 0.1 µM (Figure 3.3A). The curve shows small changes in cell survival, with the lowest dose of 0.01 µM GW4869 significantly reducing cell survival to 86.3% ($p < 0.05$) and treatment with the highest dose of 100 µM causing a significant reduction to 76% survival ($p < 0.001$) (Figure 3.3A). A 48 h duration of treatment caused a more pronounced reduction in cell survival to 71.4%, 66.2% and 57.1% for 10, 50 and 100 µM, respectively ($p < 0.05$, $p < 0.05$ and $p < 0.01$, respectively). There was no significant decrease in cell survival for concentrations below 10 µM (Figure 3.3A).

There was no significant difference in cell survival between NOF treated with GW4869 and DMSO only at 24 h (Figure 3.3B). However, at 48 h, there was significantly more cell survival in the DMSO only control at the 50 µM equivalent (0.5%) compared to the GW4869 treatment, showing a 31.6% reduction ($p < 0.05$) (Figure 3.3B)

A similar trend is seen in CAF cells, whereby at 24 h 0.01 µM GW4869 caused a reduction to 79% cell survival ($p < 0.0001$) and this was reduced to 61.2% survival with 100 µM treatment (Figure 3.3C). Again, at 48 h the reduction is more prominent with a decrease to 47.7% survival at 100 µM ($p < 0.001$), however the two lowest doses were not significantly different from the untreated control (Figure 3.3C). In contrast to the NOF cells, CAF cell survival was reduced significantly by GW4869 treatment compared to DMSO only for all concentrations at both 24 h and 48 h timepoints (Figure 3.3D).

We intended to confirm the inhibition of EV release from cancer cells cultured in 2D monolayer. Therefore, we aimed to determine particle release from H357 cells following drug treatment. Cell culture medium usually contains FBS, which is a source of contaminating bovine EVs. Therefore, we used the ultrafiltration method developed by Kornilov *et al.* (2018) to deplete FBS of EVs. Nanoparticle tracking analysis (NTA) revealed that the concentration of EV-sized particles in FBS was reduced by nearly 200-fold (Figure 3.4). To assess optimal storage conditions, we measured EV-depleted FBS that had undergone one freeze-thaw cycle, which showed ~5.5-fold higher particle concentration than fresh EV-depleted FBS. Medium supplemented with 10% FBS showed around 13-fold fewer particles than pure FBS, however particle number was below the detection range for medium supplemented with EV depleted FBS (Figure 3.4), confirming we could move forward with this depletion method.

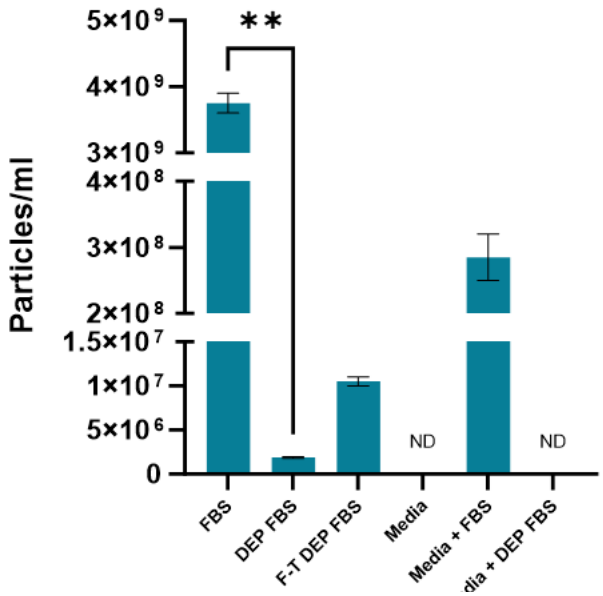

Figure 3.4 Analysis of particle number in EV-depleted fetal bovine serum (FBS). FBS was subject to 3,000 x g centrifugation in a 100 kDa MWCO column for 1 h. Flow through was then collected and measured on the same day (DEP FBS), or frozen at -20°C and thawed prior to measurement (F-T DEP FBS). FBS and EV DEP FBS was added to media at a final volume of 10%. NTA was performed using a ZetaView®. ND = not detected. Data presented as ± SEM for 6 technical repeats. $p < 0.01$.

For GW4869 treatment we selected the doses 5 µM and 10 µM as they showed no significant reduction in cell survival at 24 h compared to the untreated control and had low DMSO final concentrations. Treatment with either 5 µM or 10 µM GW4869 failed to significantly reduce particle release from H357 cells (Figure 3.5A). NTA revealed a similar size distribution of particles released from cells treated with 5 µM and 10 µM GW4859 as well as the untreated control (Figure 3.5A). There was no significant difference in mean particle size after GW4869 treatment, being 176.8 nm (SD ± 55.95) and 178.9 nm (SD ± 54.27) for 5 µM and 10 µM doses, respectively (Table 3.1).

Table 3.1 Mean size of particles analysed from GW4869 treated H357 cells.

	Untreated	5 µM	10 µM
Mean size (nm)	177.6	176.8	178.9
±*SD*	55.95	54.27	59.13

We also determined that there was no significant difference in particle release between cells treated with 5 µM and 10 µM GW4869 and equivalent DMSO concentrations, 0.05% and 0.1%, respectively (Figure 3.5B). Again, we saw no significant difference in mean particle size between GW4869 treatment and equivalent DMSO controls (Table 3.2).

Table 3.2 Mean size of particles analysed from GW4869 and equivalent DMSO control treated H357 cells.

	5µM	5µM DMSO	10µM	10µM DMSO
Mean size (nm)	185.6	204.7	192.3	184.4
±*SD*	59.67	65.05	59.80	55.22

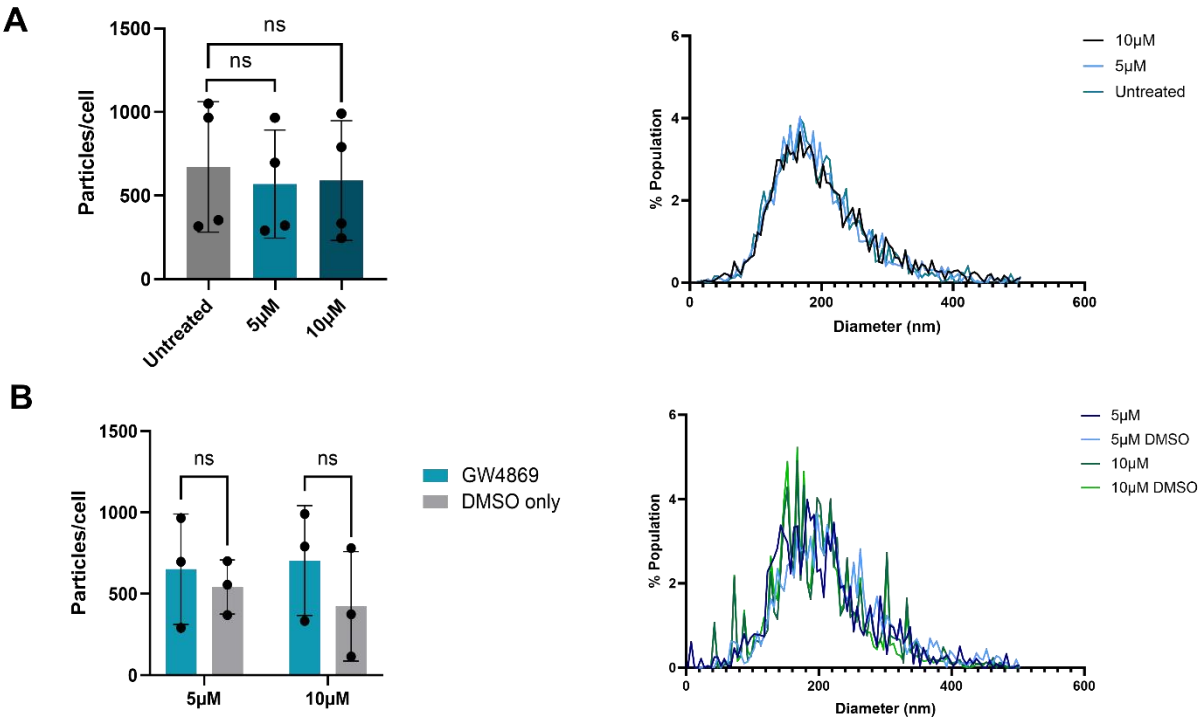

Figure 3.5 Nanoparticle tracking analysis of particle release from H357 cells following GW4869 treatment. Cells were seeded at a density of $2x10^5$ cells per well in a 6 well plate and incubated for 24 h before treatment with (A) 5 and 10 μM GW4869 and (B) equivalent vehicle control in EV depleted FBS supplemented media for 24h. NTA was carried out by injecting 2 ml of conditioned media into ZetaView measuring 11 positions across the cell. Data is presented as mean ± SD for (A) N=4, n=3 and (B) N=3, n=3. Statistics performed by one-way ANOVA and Dunnett's multiple comparisons . ns, non-significant.

3.2.2 Cell viability and particle release in response to DMA

In an attempt to characterise an alternative small molecule inhibitor that should significantly reduce particle release from H357 cells, we tested DMA in a similar manner to GW4869. To identify a non-toxic dose we again measured cell survival in response to increasing drug concentrations (Figure 3.6A). DMA concentrations of 0.1 – 50 µM at 24 h did not significantly reduce survival compared to the untreated control. Only the highest dose of 100 µM significantly reduced survival to 43.7% ($p < 0.001$). There was a comparable trend at 48 h where 0.1 – 10 µM did not significantly alter survival, however 50 µM and 100 µM show a significant ($p < 0.001$) reduction to 32.9% and 14.8%, respectively. Furthermore, IC_{50} values were similar at both treatment times, displaying values of 49.44 µM (SD ± 3.52) at 24 h and 42.51 µM (SD ± 3.03) at 48 h.

Particle release was again assessed by NTA of conditioned media (Figure 3.5B). DMA at non-toxic concentrations of 1, 10 and 50 µM failed to significantly reduce particle release in H357 cells and moreover, there was no significant difference between the highest drug dose and equivalent DMSO vehicle control (Figure 3.6B). The size distribution profile of particles released from DMA treated cells was similar with mean sizes ranging from 187.7 - 202.3 nm, however there was no significant differences in mean particle size between treatment groups and the control (Figure 3.6B).

NTA is useful for an overall particle release quantification, however in order to give a better indication of change in EV release we looked specifically at the protein abundance of the EV marker TSG101 in nanoparticle preparations from H357 cells treated with DMA (Figure 3.6C). We removed the 50 µM dose due to a marked decrease in survival, which is significantly reduced at 48 h. Neither 1 µM or 10 µM

DMA significantly reduced TSG101 protein abundance, suggesting it has no effect on EV release. Furthermore, there was no statistical difference between 10 μM DMA and the equivalent DMSO dose (0.1%) (Figure 3.6C).

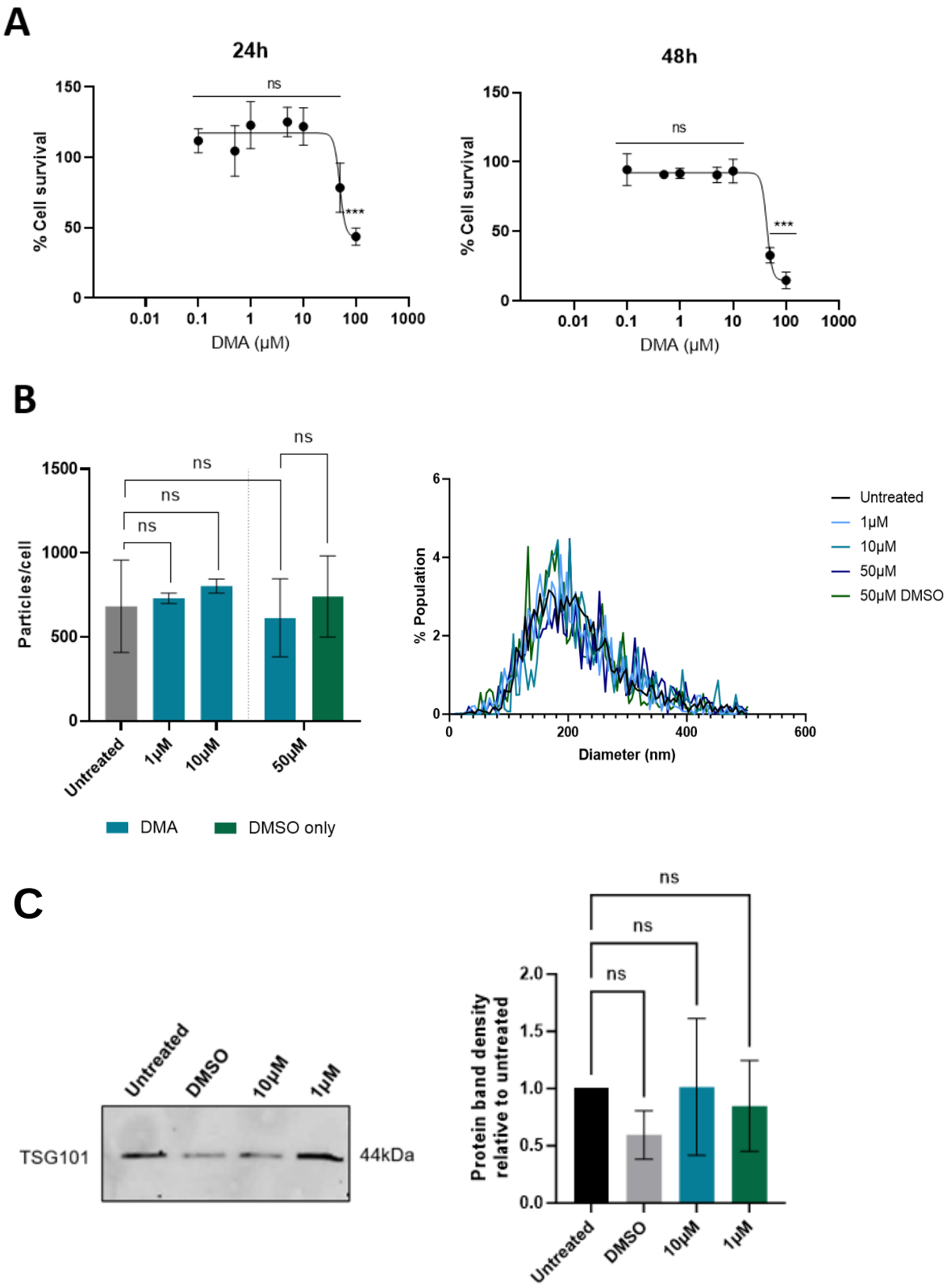

Figure 3.6 H357 cell survival, particle release and EV marker abundance in response to dimethyl amiloride (DMA) in DMSO vehicle. (A) H357 were treated with DMA and cultured for 24 and 48 h prior to MTT assay. (B) Cells were treated with 1, 10 and 50 μM DMA and equivalent DMSO vehicle control % in EV depleted FBS supplemented media for 24 h. NTA was carried out by injecting 2 ml of conditioned media into the ZetaView measuring 11 positions per sample. (C) TSG101 protein abundance was determined following treatment of cells with 1 and 10 μM DMA and equivalent DMSO vehicle control. Conditioned media from each group was subject to differential and ultra-centrifugation to collect an EV pellet that was lysed using RIPA buffer prior to western blot. Protein bands were quantified using ImageJ. Data is presented as mean ± SD for N=3, n=3. Statistics performed by one-way ANOVA with Dunnet's multiple comparisons, Student's t-test and Wilcoxon test. ns, non-significant, ***p < 0.001.

Table 3.3 Mean size of particles in conditioned media from DMA in DMSO vehicle treated H357 cells.

	Untreated	1 μM	10 μM	50 μM	50 μM DMSO
Mean size (nm)	194.1	190.9	200.7	202.3	187.7
±*SD*	62.74	64.95	60.71	81.82	63.92

We theorised that DMSO may be causing a confounding effect on the mechanism of action of DMA and therefore tested DMA dissolved in PBS vehicle (Figure 3.7A). DMA in PBS vehicle caused no significant reduction in cell survival until reaching doses of 50 and 100 μM ($p < 0.01$, $p < 0.001$). In order to confirm that the PBS vehicle did not have an inhibitory effect on cells, we compared untreated cells to those treated with PBS at the equivalent volume as the highest drug concentration (Figure 3.7A). H357 displayed a significant reduction in cell survival at doses of 50 μM and higher, with an IC_{50} value averaged from two repeats of 79.32 μM (SD ± 24.33). However, there was no significant reduction in cell survival after 24 h when treated with PBS compared to the untreated control (Figure 3.7A).

Quantifying particle release by NTA from cells treated with DMA in PBS vehicle, we saw no significant reduction in release between untreated cells and those treated with both 1 μM and 10 μM DMA (Figure 3.7B). DMA treatment did not significantly alter the mean size of particles released from H357 cells compared to the untreated control (Table 3.4). Moreover, there was no significant difference between 10 μM treatment and equivalent PBS vehicle only control (Figure 3.7C). Similarly, the abundance of TSG101 protein was not reduced following either 1 μM or 10 μM treatment. However,

no statistical analysis could be performed as this experiment was not repeated. The lack of EV protein detected in the untreated and PBS treated cells indicates that either this method of EV isolation produces inconsistent EV concentrations or protein contaminants

Table 3.4 Mean size of particles in conditioned media from DMA in PBS vehicle treated H357 cells.

	Untreated	1 μM	10 μM	10 μM PBS
Mean size (nm)	138.0	139.8	141.6	143.4
±*SD*	56.87	53.54	56.55	52.38

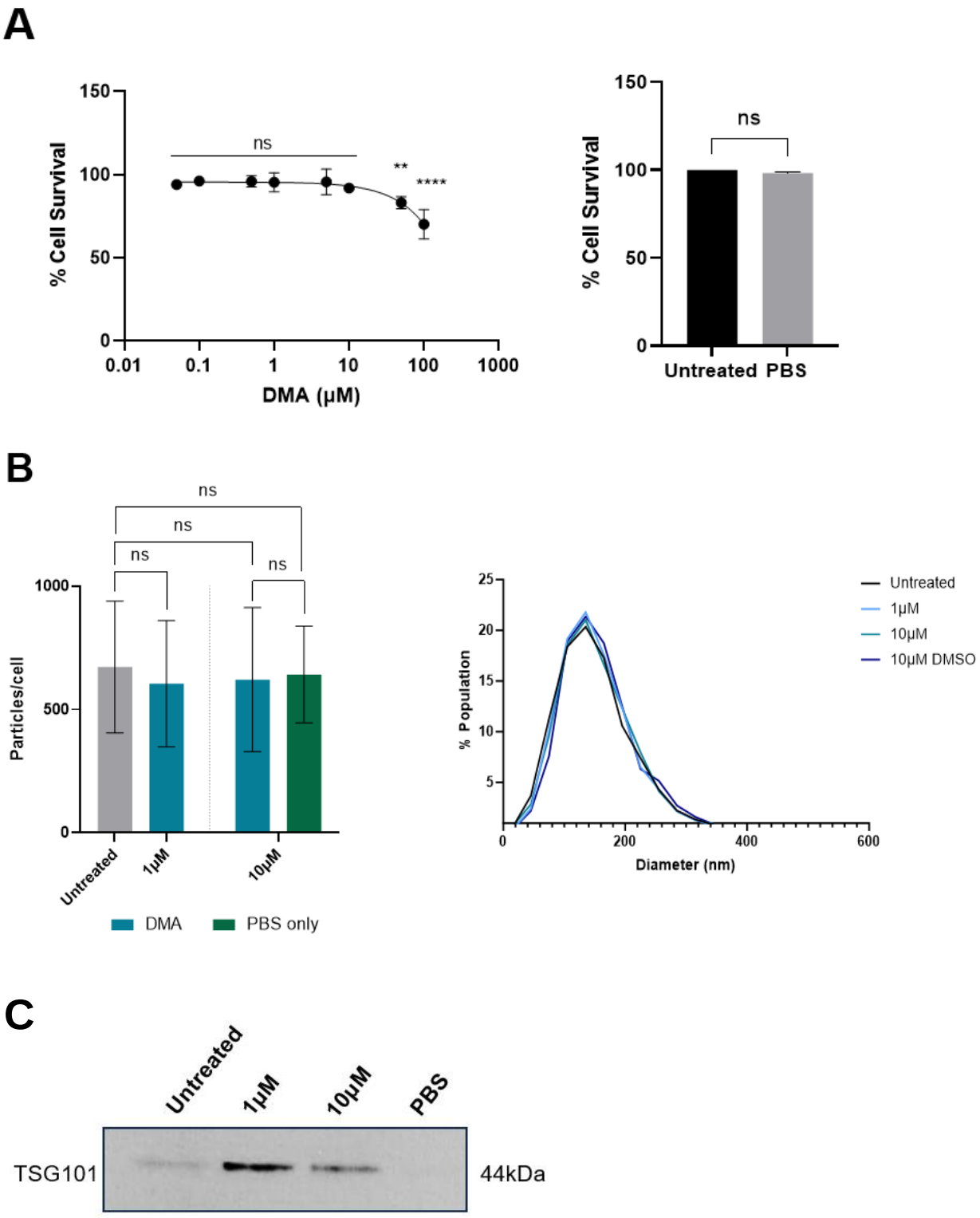

Figure 3.7 H357 cell survival, particle release and EV marker expression in response to dimethyl amiloride (DMA) in PBS vehicle. H357 were treated with increasing doses of DMA (A) or highest dose equivalent % PBS vehicle (B) and cultured for 24 h prior to MTT assay. (C) Cells were treated with 1, 10 and 50 μM DMA and equivalent PBS vehicle control % in EV depleted FBS supplemented media for 24 h. NTA was carried out by injecting 2 ml of conditioned media into the ZetaView measuring 11 positions per sample. (C) TSG101 protein expression was determined following treatment of cells with 1 and 10 μM DMA and equivalent PBS vehicle control. Conditioned media from each group was subject to differential and ultra-centrifugation to collect an EV pellet that was lysed using RIPA buffer prior to western blot. Data is presented as mean ± SD for N=3 (n=3) except for (C) where N=1 (n=1). Statistics performed by one-way ANOVA wjth Dunnets multiple comparisons test and Wilcoxon test. ns, non-significant, **p < 0.01, ****p < 0.001.

3.2.3 Cell viability and particle release in response to Bafilomycin A1

H357 cells treated with increasing doses (100,000 nM – 0.0001 nM) of Bafilomycin (BafA1) for 24 h showed no significant decrease in cell survival (Figure 3.8). However, the IC_{50} was determined to be 53 nM. At 48 h incubation with BafA1 we observed a more pronounced decrease in survival following doses higher than 10 nM (Figure 3.8). 10,000 1,000 and 100 nM doses showed a reduction to 48%, 45.3% and 49.2%, respectively ($p > 0.001$, $p < 0.01$, $p < 0.001$, respectively) (Figure 3.8). The increased incubation time was associated with an increased sensitivity to BafA1 treatment, with an IC_{50} of 12 nM.

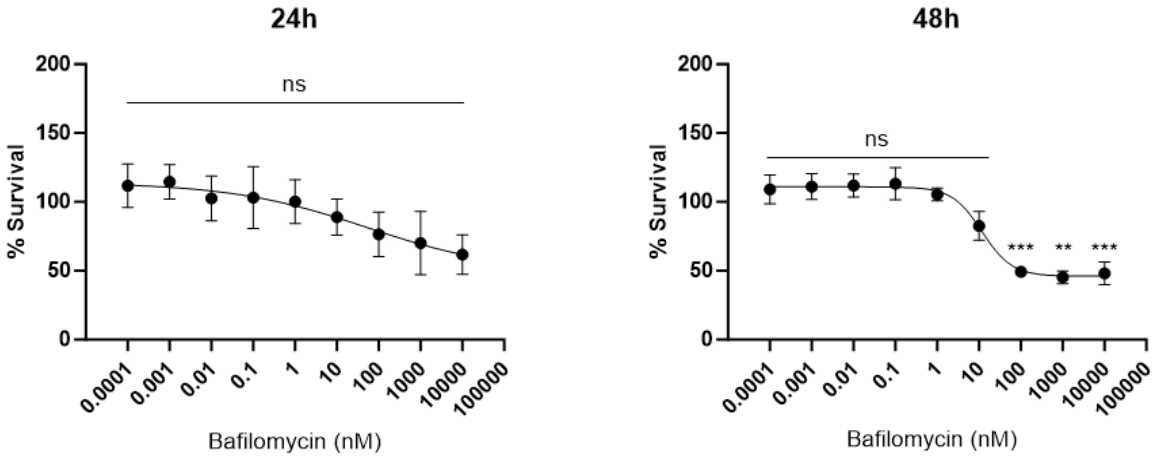

Figure 3.8 Dose response of H357s treated with BafA1. H357 cells were treated with increasing doses of BafA1 and incubated for 24 and 48 h prior to MTT assay. Data is presented as mean ± SD for N=3, n=3. Statistics performed by one-way ANOVA with Dunnet's multiple comparisons. ns, non-significant, **p < 0.01, ****p < 0.001.

NTA revealed no significant difference in particle release from H357 cells treated with 5, 50, or 100 nM BafA1 (Figure 3.9A). There was no significant difference in particle release from cells treated with 100 nM BafA1 and an equivalent DMSO vehicle control (0.1%). Mean particle diameter remained similar across all treatments, with no significant difference between BafA1 treated, vehicle control and untreated control (Figure 3.9B)(Table 3.5).

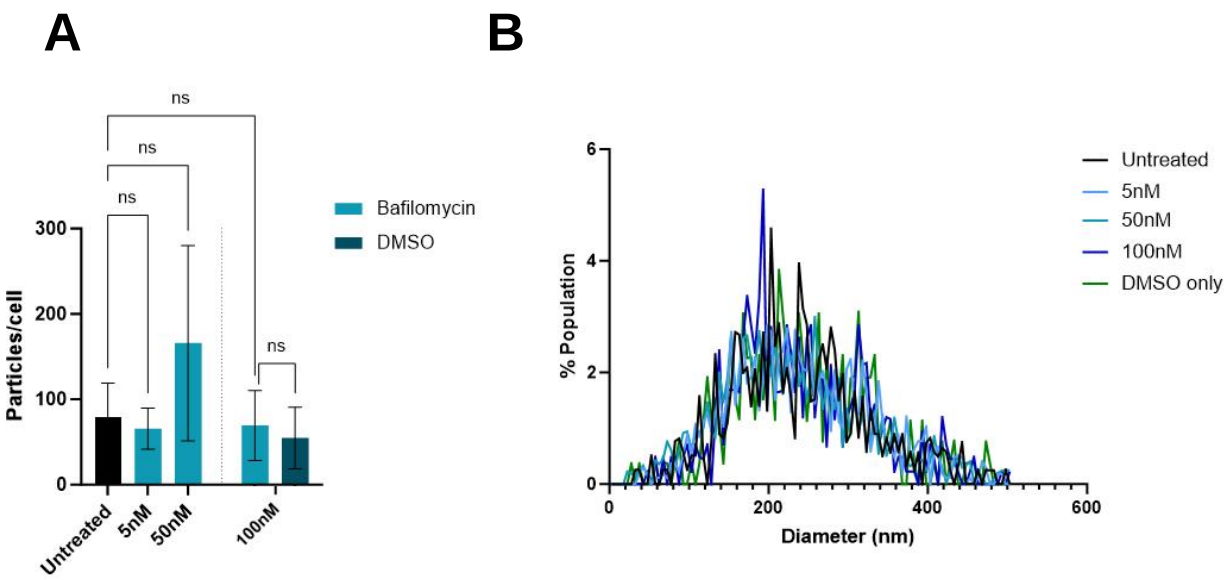

Figure 3.9 Particle release from H357 cells treated with BafA1. H357 cells were treated with 5, 50 and 100 nM BafA1 in EV depleted media and incubated for 24 h. NTA was performed by ZetaView across 11 positions. Data is presented as mean ± SD for N=3, n=3. Statistics performed by one-way ANOVA with Dunnet's multiple comparisons and Student's t-test . ns, non-significant.

Table 3.5 Mean particle size in conditioned media from BafA1 treated H357 cells.

	Untreated	5 nM	50 nM	100 nM	DMSO only
Mean size (nm)	227.4	228.9	215.4	225.2	235.1
± SD	79.48	90.18	87.52	82.12	88.61

3.3 Discussion

3.3.1 Cell viability and particle release in response to GW4869

Concentrations of GW4869 greater than 50 µM at 24 hours caused significant reduction in survival of H357 cells. These concentrations are similar to doses previously used in cancer cell lines, where 20 µM GW4869 significantly reduced cell survival compared to vehicle control in a prostate cancer cell line at 24 and 48 hours (Panigrahi et al., 2018). In the same study, 10 and 20 µM GW4869 also reduced clonogenicity of the same cell line over a longer period of 7-8 days (Panigrahi et al., 2018).

FNB6 cell survival was significantly reduced by doses ≥100 µM and 50 µM at 24 and 48 hours, respectively. This indicates that FNB6 may be slightly less sensitive to GW4869 than H357 cells. This could be due to H357 having a faster growth rate (previous data in shown in Hunt Lab), which may make them more vulnerable to drug inhibitors (Malhotra et al., 2003). Of note, nSMase, inhibited by GW4869, has been linked to the regulation of apoptosis in response to a range of stimuli in breast cancer cells and hepatoma cells (Ogretmen et al., 2004). Testai *et al* showed that nSMAse is activated by caspase 8 and signals downstream via caspase 3 in neuronal tumour cell lines (Testai et al., 2004). It could be argued that nSMase inhibition by GW4869 would reduce apoptotic signalling and lead to increased survival in H357 cells.

There was no significant difference in cell survival between GW4869 treated H357 and equivalent dose DMSO controls, suggesting that the DMSO vehicle was responsible for the inhibitory effect on cells. In the OSCC cell line SCC7, 2.5 µM GW4869 was shown to significantly reduce both cell proliferation and migration compared to untreated controls after 24 hours (Li et al., 2023). However, the authors did not indicate

the vehicle used to dissolve the drug or if the untreated control was a vehicle only treatment. This could have a significant impact on the conclusions drawn, due to DMSO having been shown to significantly reduce proliferation, migration and colony formation in cancer cells through stimulating tumour suppressor protein HLJ1 (Hajighasemi et al., 2017).Furthermore, Matsumoto *et al* showed that 5 µg/ml GW4869 treatment for 24 hours significantly reduced the survival of B16BL6 melanoma cells compared to untreated and DMSO-treated cells (Matsumoto et al., 2017). Interestingly, the 5 µg/ml dose equates to 6.8 µM GW4869, at which we saw no reduction in survival for both FNB6 and H375. Moreover, the authors stated that there was no significant difference in cell survival between 5% DMSO (vehicle) and untreated cells (Matsumoto et al., 2017). However, this contrasts many studies showing that this dose of DMSO is toxic to cells, therefore the reason for this inconsistency is unclear (Trivedi et al., 1990; Galvao et al., 2014; Hajighasemi et al., 2017).

In comparison to the two cell lines, primary fibroblasts show generally less sensitivity to GW4869 with minimal reduction in percentage survival compared to H357 and FNB6. This seems to be consistent with previous findings that treatment of muscle-derived fibroblasts showed no significant change in survival when treated with a range of 0-20 µM GW4869 (Zanotti et al., 2018). This could be attributed to differences in ceramide to sphingomyelin ratios in lipid metabolism. It has been reported that ceramide family proportions between dermal keratinocytes and fibroblasts are distinct, with fibroblasts having a higher abundance of ceramides with sphingosine base and non-hydroxy fatty acid (CER[NS]) and alpha-hydroxy—phytoceramides (CER[AP]), sub-classes of ceramides, than keratinocytes (Łuczaj et al., 2020).

Interestingly, we also see differences between fibroblasts and the cell lines when we compare equivalent doses of DMSO to the GW4869: for the cell lines there is no significant difference in cell survival compared to DMSO controls. However, there is significantly decreased survival in the drug treatment groups of NOFs treated with 50 µM for 48 hours and all treatment conditions for CAFs. Fibroblasts may have reduced sensitivity to DMSO compared to the cell lines, as it has been shown that low concentrations of DMSO can promote fibroblast proliferation in a Akt/mTOR mediated manner (Guo et al., 2020).

We selected the highest doses of GW4869 that did not cause a significant reduction in H357 cell survival, to determine if the drug could inhibit EV release. Our data showed that there was no significant decrease in particle release in treated cells compared to vehicle control, which is in contrast with a large body of literature (Riches et al., 2014; Menck et al., 2017; Peng et al., 2022).

The reason for this discrepancy may lie in differences in EV isolation methods, as this can influence the populations of EV separated (Théry et al., 2018). Here, we measured all particles released from cells into conditioned medium meaning a broad range of EV populations and other nanoparticles were likely present. This could account for the lack of difference in particle count between the drug treated and controls, as it has previously been reported that GW4869 has a contrasting effect on different EV populations (Menck et al., 2017). Menck *et al* analysed EV population size changes in response to GW4869 treatment from cell conditioned medium pelleted at 14,000 x *g* and 100,000 x *g*; with the aim to differentiate effects on ‘’microvesicles’’ and ‘’exosome’’ populations. Interestingly, GW4869 increased the number of larger EVs (100-200nm) in the 14,000 x *g* pellet, but reduced smaller EVs (<100nm) in 100,00 x g pellets, indicating that GW4869 has different effects on secretion of different sized

EV population (Menck et al., 2017). We saw no significant difference in mean particle size between treatment groups. However, our NTA data collection parameters were set to detect small particles (~100 nm), which means that larger particles were discounted.

3.3.2 Cell viability and particle release in response to DMA

Our data indicated that GW4869 treatment did not inhibit EV release in the cell lines tested. Therefore, we sought to characterise another small molecule inhibitor of EV release and focused on H357 cells only. H357 cells demonstrated an IC_{50} of 49.44 µM and 42.51 µM, at 24 and 48 hours, respectively. An IC_{50} of 106 µM has been reported in HUVEC cells, indicating that H357s may be more sensitive to DMA (Park et al., 2009). However, Rojas *et al* demonstrated in myeloma cell lines that DMA significantly decreased viability at the lowest tested concentration of 100 µM, which is consistent with our data at 48 hours (Rojas et al., 2017). However, another study has shown that 5 µg/ml DMA significantly reduces survival of a paclitaxel-resistant prostate cancer cell line (Kumar et al., 2022).

We selected DMA doses (1 µM, 10 µM and 50 µM) that caused no significant decrease in cell survival for further testing, but we observed no significant reduction in particle release from H357 cells compared to the untreated or DMSO vehicle controls. This is in contrast to data from Chalmin *et al*, showing that that in a mouse lymphoma cell line, DMA significantly reduced acetylcholinesterase (AChE) activity, which is a proposed generic marker for small EVs ((Chalmin et al., 2010). Although no DMA dose was stated for 2D cell treatment, this effect was mirrored in a lymphoma mouse model by treatment with 1 µmol/kg DMA daily for one week.

DMA dissolved in PBS also failed to inhibit particle release. The highly cited Savina *et al* study demonstrating that DMA blocks ‘’exosome’’ and ‘’gigantic Ca^{2+}-filled MVB’’ formation utilises stimulation by ionophore treatment prior to EV quantification and may not be comparable to our untreated condition. This stimulation treatment causes swelling of endosomes and lysosomes and may therefore effect EV subtype formation. Furthermore, the decrease in ‘’exosomes’’ that they observed may overlap with other EV populations, due to the exosome quantification and characterisation methods.

Both Chalmin *et al* and Savina *et al* utilise AChE activity for EV quantification, however this is an indirect measure and has previously been shown not to correlate with particle number (Liao et al., 2019). The MISEV 2018 guidelines (Théry et al., 2018) recommended further characterisation by protein markers, however the use of Hsc70 as a marker by Savina *et al* is also not exosome specific due to its promiscuous incorporation into EVs. Therefore, it is difficult to pinpoint which populations may be inhibited by DMA treatment. Indeed, we saw no reduction in TSG101 protein levels, possibly indicating that affected EV populations are produced via ESCRT-independent mechanisms. However, this contrasts data from Liu *et al* showing that TSG101 levels are attenuated in kidney proximal tubular cells following DMA treatment (Liu et al., 2020). This could be attributed to the higher dose of 388 μM DMA used, indicating that our doses were not in the range to have an inhibitory effect. However, there is no indication of vehicle control used making it difficult to confirm the reduction in TSG101 is due to DMA alone.

3.3.3 Cell viability and particle release in response to BafA1

BafA1 treatment caused no adverse effects on cell survival at 24 hours for all doses up to the highest dose of 10 μM. However, doses of 0.1 μM and higher caused a significant decrease in cell survival at 48 hours. This is similar to previous data, where in human neuroblastoma and embryonic kidney cells there was no significant decrease in survival following 24 hours treatment with 200 nM and 100 nM BafA1, respectively (Alvarez-Erviti et al., 2011; Joshi et al., 2020). However, a more prolonged exposure of 72 hours at a dose of 200 nM saw a marked decrease in survival (Alvarez-Erviti et al., 2011). Moreover, Yan *et al* tested up to 100 nM doses of BafA1 in a range of cell lines and found that there was no difference in survival for treatment at 24 hours, matching our findings (Yan et al., 2016). However, a dose of 5 nM reduced survival for 48 and 72 hours treatments (Yan et al., 2016).

In contrast to previous reports (Guo et al., 2017; Cashikar et al., 2019; Wang et al., 2022), we observed no increase in particle release in BafA1 treated cells. In agreement with these reports, Bebelman *et al* noted a 30% increase in particles released from HEK293 cells treated for 16 hours with 100 nM BafA1 (Bebelman et al., 2023). Moreover, this increase rose to 800% after 24 hours of treatment (Bebelman et al., 2023). In hindsight, it might have been better to quantify EV marker positive particles rather than relying on NTA to determine drug efficacy. This would have allowed discrimination between EVs and other nanoparticles present in conditioned medium samples. Indeed, Cashikar *et al* found increased levels of CD9, CD63, flotillin 2 and syntenin in HEK293 cells treated with 200 nM BafA1 (Cashikar et al., 2019). Of note, Hikita *et al* showed that a cell panel released more particles upon BafA1 treatment, however the same cells showed reduced particle release when cultured in hypoxia (Hikita et al., 2018). It would be interesting to see the effect on particle release

on cells cultured in hypoxia and treated with BafA1 to determine how alterations in culture conditions can vary particle release.

We might have expected an altered nanoparticle size profile due to BafA1 treatment causing increase of small EV/exosome release (Bebelman et al., 2023), however we observed no significant difference from treated or untreated H357 cells. Wang *et al* similarly observed no difference in particle size determined by NTA of BafA1 treated neuroblastoma cells compared to untreated (Wang et al., 2022). In contrast, work from another group showed that 100 Nm BafA1 treatment for 16 hours caused release of smaller EVs, as measured by NTA and electron microscopy (Mathieu et al., 2021). This effect was seen in pellets isolated from conditioned media by centrifugation at 200,000 x *g*, however there were no differences in size seen in the 10,000 x *g* pellet, indicating enrichment for smaller EV populations is necessary to examine specific size changes (Mathieu et al., 2021).

3.3.4 Conclusion

In summary, we have identified doses of GW4869, DMA and BafA1 that significantly decrease cell survival. Quantification of particle release in H357 cell conditioned medium and TSG101 marker abundance in EV pellets treated with either GW4859 and DMA revealed no significant reduction compared to the DMSO vehicle control. Particle release from H357 cells was not significantly increased when treated with EV stimulator, BafA1.

4 Development and characterisation of genetically altered OSCC cell lines for the study of EV biogenesis and uptake

4.1 Introduction

Genetic targeting is a useful alternative for inhibiting EV biogenesis components that currently do not have small molecule inhibitors. RNA interfering tools have been widely utilised to dissect mechanisms of EV biogenesis. In a landmark study, Stuffers *et al* was able to demonstrate ESCRT independent MVB formation through siRNA depletion of ESCRT subunits HGS, TSG101, Vps22 and Vps24 (Stuffers et al., 2009). Another study showed the role of GTPases in exosome production and ILV budding, using siRNA targeting ARF6 and its effector PLD2 (Ghossoub et al., 2014). However, it has also been reported that the use of transient transfection reagents can cause artefacts in downstream EV characterisation experiments (McConnell et al., 2022). This can be overcome by utilising techniques such as CRISPR/Ca9 genome editing. A study that created an MMP3 knockout (KO) in a murine metastatic tumour cell line showed that there was reduced EV protein release from these cells as well as reduced CD9 and CD63 abundance in EV fractions (Taha et al., 2020). MMP3-KO cell tumouroid formation and proliferation was reduced compared to the MMP3+ tumouroids and this effect was rescued by treatment with EVs (Taha et al., 2020).

Due to the lack of success of GW4869 and DMA to significantly reduce particle release in H357 cells (Chapter 3), in this chapter we utilised an alternate tool to perturb EV release. Here, we validate a CRISPR/cas9 edited H357 derivative cell line targeting HGS (termed H357$^{\Delta HGS}$), a master regulator of ESCRT-dependent EV biogenesis, for gene and protein silencing as well as the effect on EV release.

Cell-to-cell communication via EVs is a critical aspect of cancer progression, making it essential to understand how EVs interact with recipient cells (El Andaloussi et al., 2013). Various techniques exist to monitor EV uptake, biodistribution, and release. Among these, fluorescence-based detection is widely used. To stain EVs after isolation, lipophilic fluorescent dyes such as DiR, DiO, DiD, CFSE, PKH-26, and PKH-67 are commonly employed (Chuo et al., 2018). For example, DiR staining has been successfully used to label EVs in conditioned media from different cell types and demonstrating patterns of biodistribution and accumulation *in vivo* (Wiklander et al., 2015) Moreover, DiD labelled EVs have been shown to be detectable up to 24 hours post injection in mice (Grange et al., 2014). However, a significant drawback is their non-specific binding nature, as their lipophilic nature means all lipid-containing particles, vesicles, and cellular membranes are susceptible to labelling. This can lead to background noise in cellular assays and false positive signals, particularly because these stains may form micelles or aggregates in certain buffers, resembling the physiological properties of EVs (Takov et al., 2017).

A more specific method of EV visualisation is to label EVs by cloning specific EV markers into reporter vectors that are tagged with a fluorescent protein. Transfection of these vectors produces cells which release fluorescently tagged EVs. A number of studies have utilised the fusion of tetraspanin CD63 and GFP to study EV communication between cells (Maida et al., 2016; Sadovska et al., 2018; Levy et al., 2020). Koumangoye *et al* used this approach to tag breast cancer tumour cell exosomes and demonstrate that disruption of lipid rafts inhibited the internalisation of exosomes as well as annexin-mediated uptake (Koumangoye et al., 2011). Another study used a CD63-GFP producing prostate cancer cell line, cultured in a 3D heterotypic spheroid model with peripheral blood mononuclear cells (PBMCs). This

co-culture method showed different interactions with EVs, dependent on cell type. For example, EVs were mostly found on the surface of B-cells rather than internalised and CD3+ T-cells interacted with EVs at a greater capacity compared to CD8+ T-cells (Sadovska et al., 2018).

Here, we aimed to develop an OSCC cell line producing dual fluorescence labelled EVs to demonstrate cancer-derived EV association with stromal fibroblasts. H357 cells were transfected to stably express CD63-GFP (to label the EV membrane), as well as TSG101-mCherry (to label luminal EV cargo).

4.2 Results

4.2.1 Validation of HGS CRISPR/cas9 knockout

The H357$^{\Delta HGS}$ cell line was recently created by another member of our research group (Jiang., 2023) and so we first sought to validate the cell line before conducting further experiments. Comparing HGS mRNA transcript levels between H357 wildtype (WT) and the H357$^{\Delta HGS}$ cell line there was a significant reduction in relative expression ($p <$ 0.01), with the H357$^{\Delta HGS}$ cell line displaying a 4.6-fold lower transcript expression than H357^{WT} (Figure 4.1A). To confirm knockdown at the protein level we quantified protein

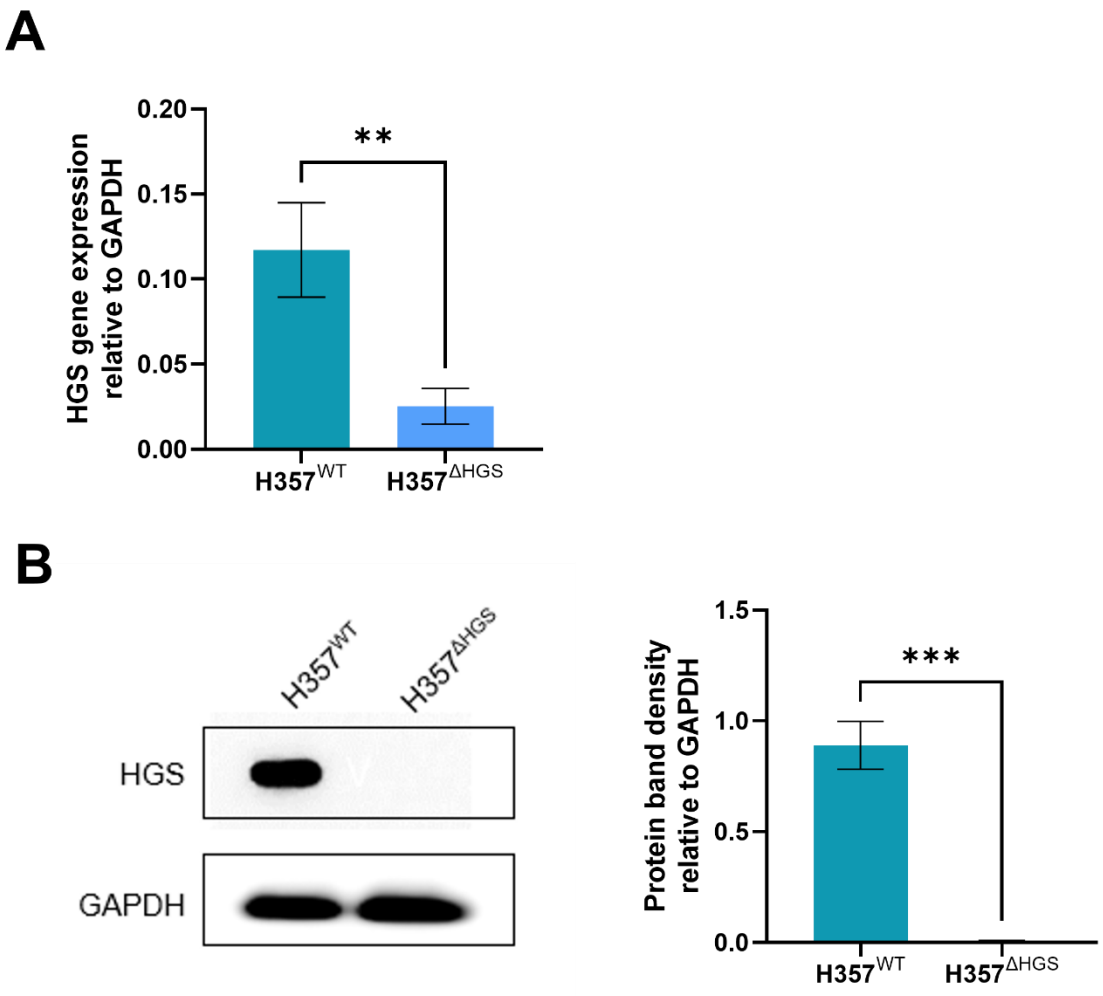

Figure 4.1 Validation of HGS knockout in H357 cells by transcript and protein quantification. Cells were grown to 80% confluency and RNA or protein extracted using an appropriate lysis buffer. (A) HGS cDNA was produced by RT-PCR and transcript levels quantified by qPCR (B) HGS protein levels were measured by western blot and densitometry was conducted using ImageJ. Data is expressed relative to GAPDH endogenous control. Data is presented as mean ± SD for N=3, n=3. Statistics performed by Student t-test. **p < 0.01, ***p > 0.001.

abundance by western blot. HGS protein levels were significantly lower ($p < 0.001$) in the $H357^{\Delta HGS}$ cell line compared to $H357^{WT}$, with no protein band detectable (Figure 4.1B).

Table 4.1 Average diameter of particles released into conditioned media from $H357^{WT}$ or $H357^{\Delta HGS}$ cells.

	$H357^{WT}$	**$H357^{\Delta HGS}$**
Mean diameter (nm)	153.3	150.4
±SD	51.87	48.75

To investigate whether knockout of HGS in these cells influenced EV release, we measured particles in conditioned media from the $H357^{\Delta HGS}$ cell line (Figure 4.2). There were 1,120 fewer particles released per $H357^{\Delta HGS}$ cell compared to $H357^{\Delta WT}$, equating to a significantly ($p < 0.01$) reduced amount. The size profiles of particles analysed from both cell lines were very similar, with no significant difference in mean particle diameter (Figure 4.2A)(Table 4.1). We then enriched EVs present in conditioned media by ultracentrifugation and compared the EV marker TSG101 in the cell lysate and in EV preparations from both cell lines. There was no significant difference in TSG101 levels in cell lysate from either cell line, however there was a 3.7-fold reduction ($p < 0.05$) in $H357^{\Delta HGS}$ EV pellets compared to $H357^{WT}$ (Figure 4.2B.

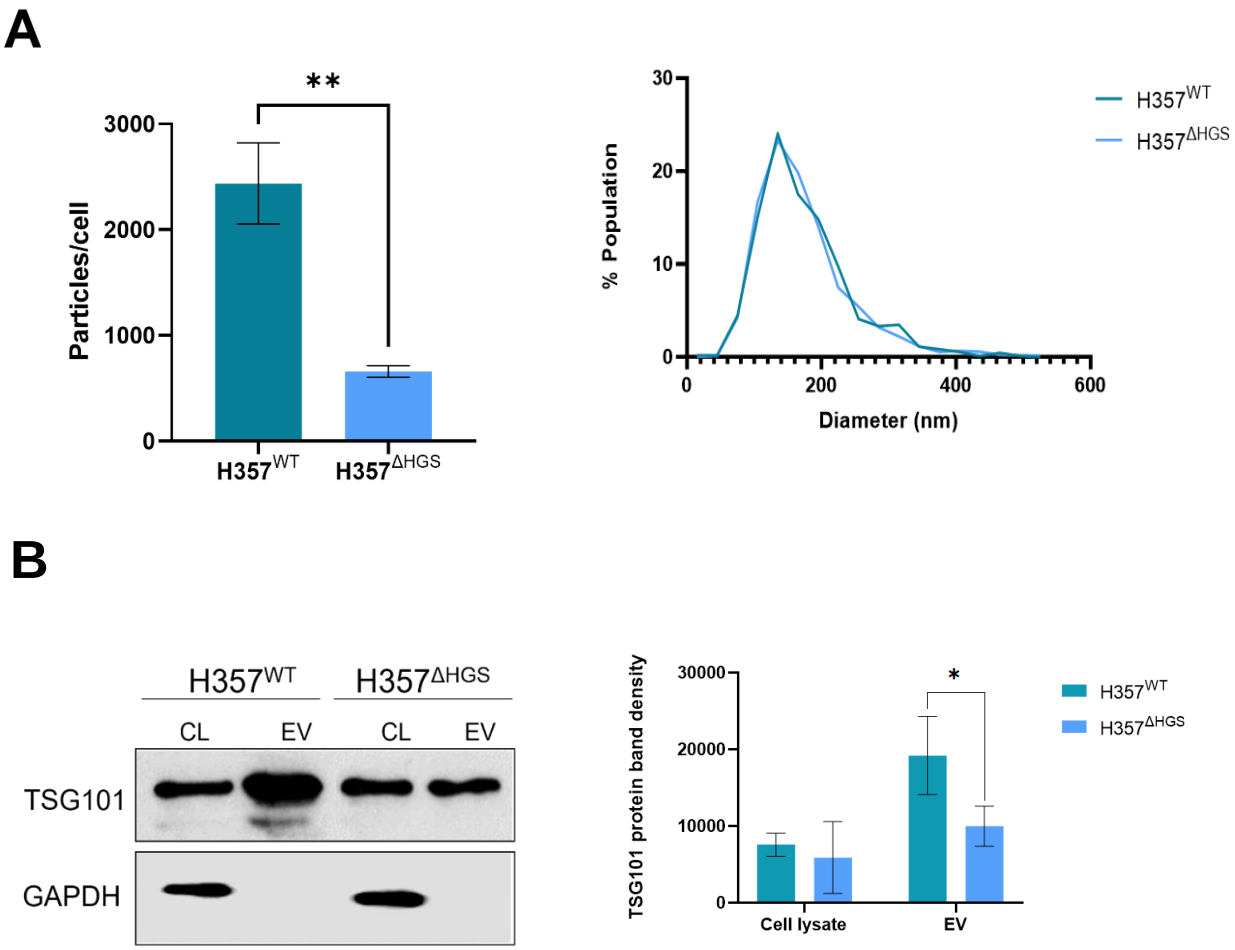

Figure 4.2 Evaluating functional EV knockdown in H357$^{\Delta HGS}$. (A) Particle release and size was quantified using NTA in conditioned media from WT and ΔHGS H357 cells (B) Representative blot of TSG101 protein level in cell lysate (CL) and EV preparations. Densitometry was conducted using ImageJ, and data is expressed as TSG101 band intensity relative to H357^{WT}. Data is presented as mean ± SD for N=3, n=3. Statistics performed by Student t-test. *p < 0.05.

4.2.1.1 H357$^{\Delta HGS}$ in 3D co-culture models

3D models are a useful tool to study interactions between multiple cell types in a more physiologically relevant system. In this system, modelling the oral mucosa, we cultured fibroblasts in a collagen matrix with keratinocytes seeded on top at an air to liquid interface (ALI). We hypothesised that the loss of HGS in H357 cells would interfere with EV mediated communication between the OSCC cells and fibroblasts. Models using H357^{WT} show a distinct epithelial layer when in combination with either NOFs or CAFs, however this epithelial layer is not present when H357$^{\Delta HGS}$ are incorporated (Figure 4.3A). Furthermore, it may be suggested that the models incorporating H357$^{\Delta HGS}$ cells display diminished viability compared to those with wildtype cells, however there is insufficient data to draw statistical conclusions. To determine whether the difference in model structure was due to EV knockdown interfering with intercellular communication, we looked at the ability of H357$^{\Delta HGS}$ to form epithelial only layers (Figure 4.3C). H357^{WT} form multi-cell layers, whereas H357$^{\Delta HGS}$ only formed layers of 1-2 cell thickness.

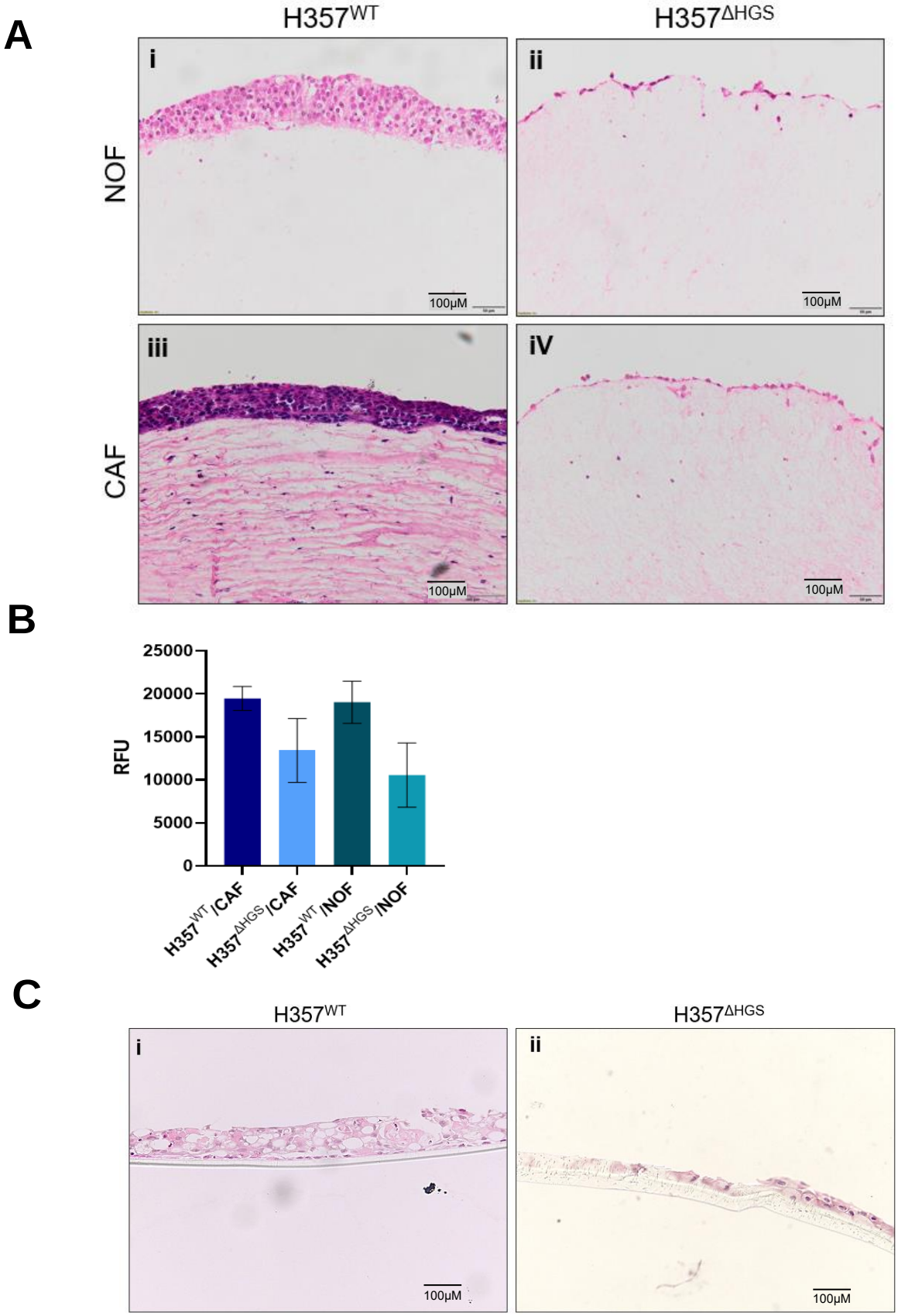

Figure 4.3 3D models of the oral mucosa using H357$^{\Delta HGS}$. (A) Representative images of 3D models generated using NOFs and CAFs seeded in collagen, in combination with H357^{WT} and H357$^{\Delta HGS}$ seeded on top and cultured at an air to liquid interface (ALI) for 10 days. (B) The viability of cells in the 3D collagen models was measured indirectly using PrestoBlue® where relative fluorescence units (RFU) is equivalent to viability. (C) Epithelial layers generated by seeding H357WT and H357ΔHGS into transwell inserts and culturing for 48h submered in media and then a further 48h at ALI. 3D and epithelial models were stained using H&E. Data represented as ±SEM for N=2, n=3.

4.2.2 Development of H357$^{CD63\text{-}GFP}$ cell line

4.2.2.1 Transfection reagent optimisation

Achieving successful transfection depends on various factors, including the transfection reagent, cell confluency, cell viability, quantity of nucleic acid, and the presence or absence of serum (Chong et al., 2021). To increase the likelihood and quantity of cells effectively incorporating plasmid DNA into their genome, it is essential to optimise the conditions for high transfection efficiency and minimal cell toxicity (Chong et al., 2021).

FuGENE ®, a non-liposomal transfection reagent, was used in the first instance; comparing different ratios of FuGENE (µl) to plasmid DNA (µg), as recommended by the manufacturer. We compared transfection efficiencies of CD63 and TSG101 fluorescent protein fused constructs used in single transfection or simultaneously (dual transfection) (Figure 4.4). After 24h incubation, transfection efficiency was determined by fluorescence microscopy. Overall transfection efficiency was low, with the highest TSG101-mCherry efficiency (2.9%) observed using a 2:1 ratio FuGENE:DNA (Figure 4.4B). There was a trend showing a larger proportion of fluorescent cells using a single TSG101-mCherry transfection, compared to CD63-GFP and dual transfection, across all ratios. Furthermore, transfecting both plasmid DNAs reduced the positive population compared to single transfected conditions. There was no significant difference in fluorescent positive populations for all FuGENE ratios using either single construct or dual transfection methods (Figure 4.4B).

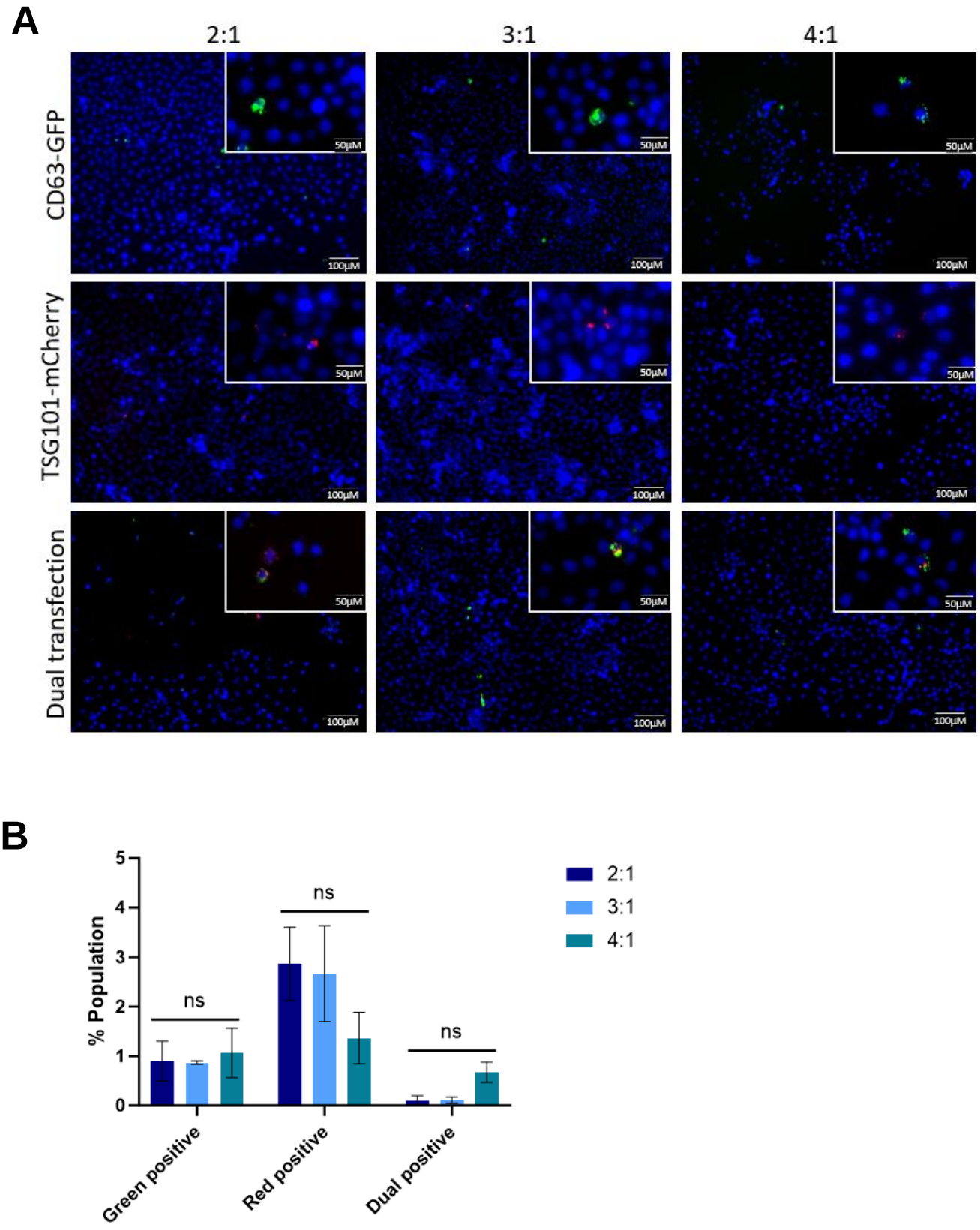

Figure 4.4 Transfection optimisation using FuGENE in H357 cells. Cells were seeded into glass bottom wells and transfected with either CD63-GFP, TSG101-mCherry, or both plasmid DNA in complex with FuGENE® at different ratios. After 24h cells were imaged using a Zoe™ Fluorescent Imaging System. (A) Representative images of single and dual transfections (B) Quantification of positive fluorescence analysed using ImageJ. Data is presented as mean ± SEM for N=1, n=3. Statistics performed by Dunnett's multiple comparisons t-test. ns, non-significant.

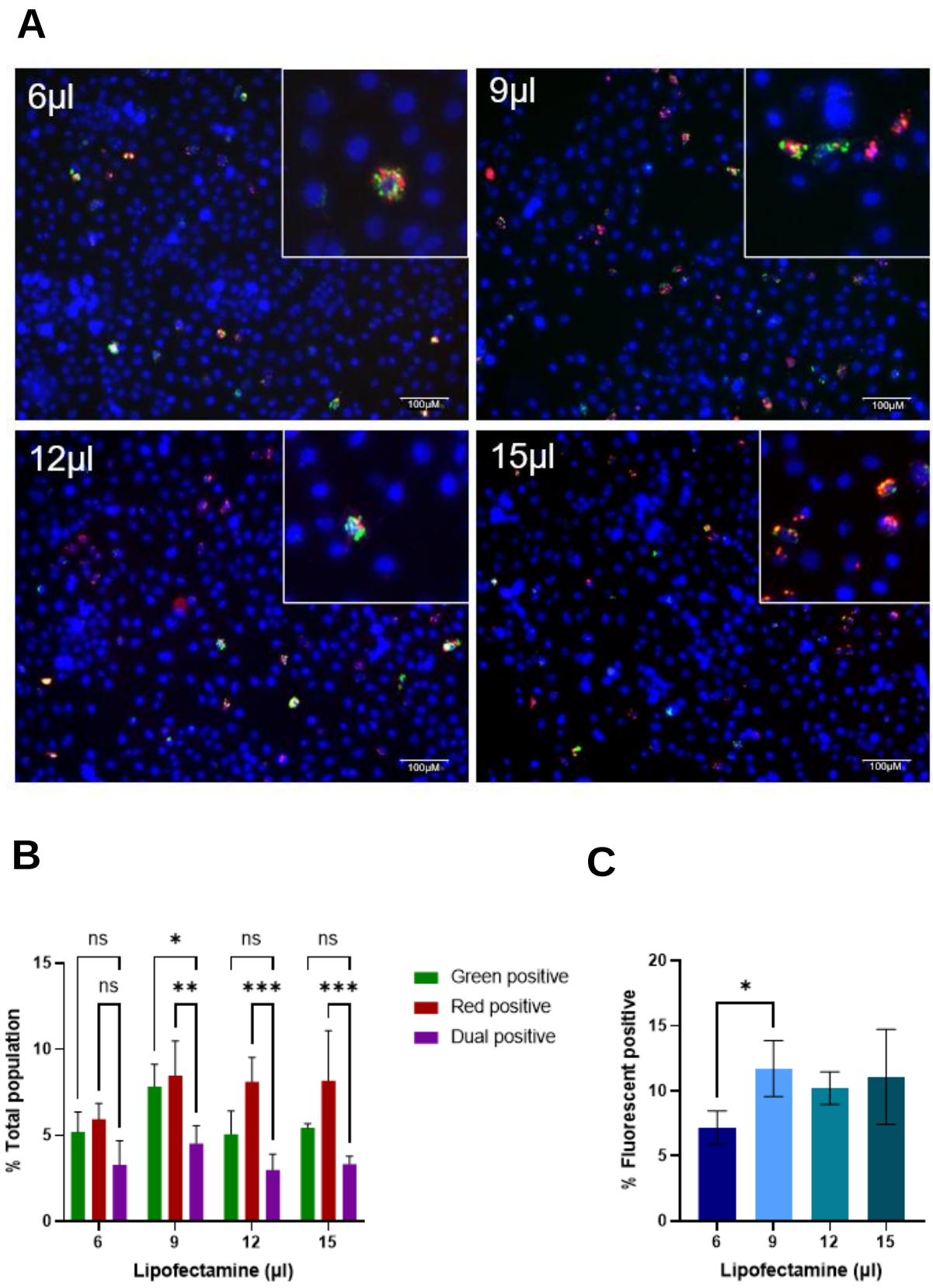

Figure 4.5 Dual transfection optimisation using Lipofectamine 2000 in H357 cells. Cells were seeded into glass bottom wells and incubated with CD63-GFP and TSG101-mCherry plasmid DNA in complex with 6, 9, 12, or 15 µl lipofectamine. After 24h cells were imaged using a Zoe™ Fluorescent Imaging System. (A) Representative images of single and dual transfections. Quantification of (B) Positive fluorescence for GFP, mCherry or both and (C) total fluorescence in each lipofectamine volume was analysed using ImageJ. Data is presented as mean ± SEM for N=1, n=3. Statistics performed by Dunnett's multiple comparisons t-test. ns, non-significant, *p < 0.05, **p< 0.01, ***p<0.001.

Due to the low transfection efficiency of FuGENE, we sought to optimise another type of transfection reagent, Lipofectamine 2000, which encapsulates nucleic acids in liposomes to be taken into the cell by endocytosis. Lipofectamine optimisation methods are based on transfection reagent volume rather than ratios with DNA.

We observed greater levels of transfection with Lipofectamine at all volumes used, compared to FuGENE. Volumes of 9, 12 and 15 µl showed a significantly higher percentage of red fluorescent compared to dual fluorescent cells (Figure 4.5B). Only the 9 µl volume showed a significantly higher percentage of green fluorescent cells compared to dual fluorescent (Figure 4.5B). When comparing the total proportion of fluorescent cells, cells transfected with 9 µl Lipofectamine showed the highest percentage (11.7%), which was significantly higher ($p < 0.05$) than cells transfected with 6 µl Lipofectamine (7.2%) (Figure 4.5C).

4.2.2.2 Isolating and expanding stable clones.

Moving forward with the 9 µl lipofectamine transfection conditions, we used single and dual plasmid transfection methods followed by antibiotic selection. Following this, colonies of surviving cells were cultured and sorted into single cells by FACS. Although the proportion of positive cells was low (Table 4.2), we were able to sort single cells from CD63-GFP and TSG101-mCherry transfected populations.

Table 4.2 Percentage of fluorescently positive cells in polyclonal H357 populations.

	Positive	
	% Parent	% Total
CD63-GFP	0.2	0.08
TSG101-mCherry	0.37	0.09
Dual transfected	0	0

Monoclonal populations were expanded from single cells positive for CD63-GFP, however there were no surviving TSG101-mCherry positive colonies. Fluorescence microscopy of stable clones showed punctate green fluorescence, indicating expression of CD63-GFP in internal compartments (Figure 12). Interestingly, some cells (Figure 4.6i) showed brighter GFP signal than others (Figure 4.6ii).

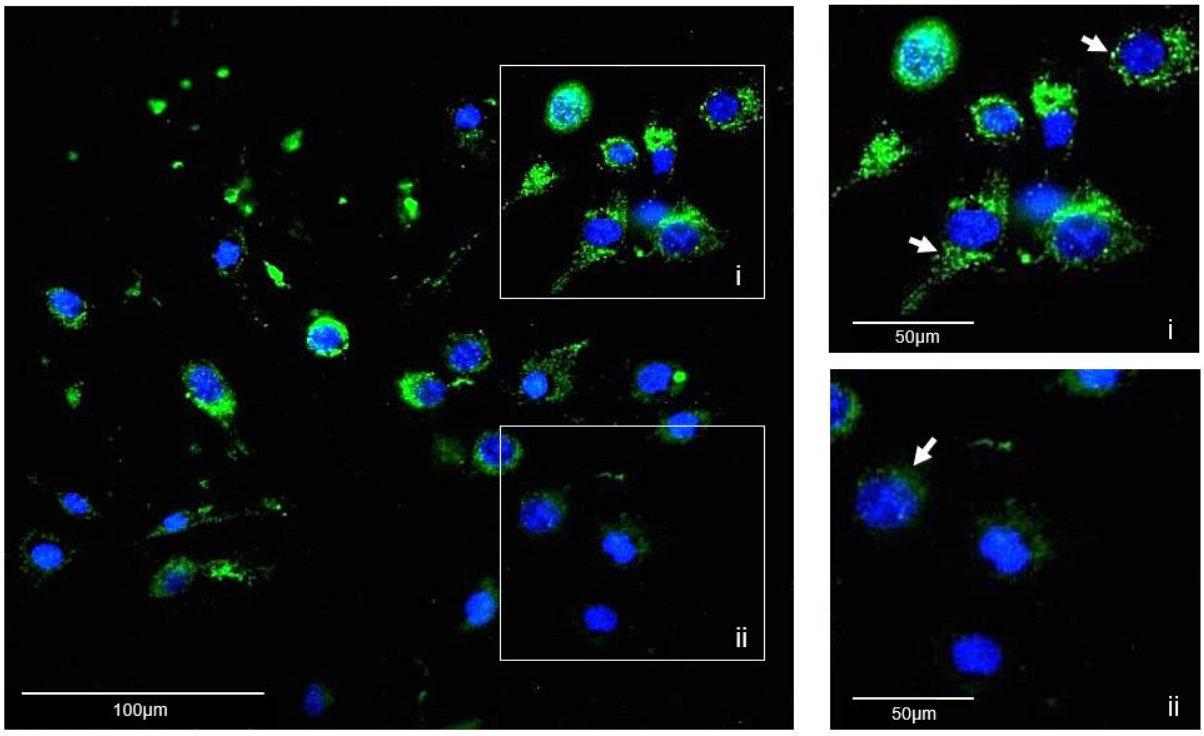

Figure 4.6 Imaging of CD63-GFP expressing H357 cells. Representative images of an expanded clone of H357 cells expressing CD63-GFP (green) and counterstained nuclei with DAPI (blue) at first expansion. Arrows in magnified images (i) and (ii), indicate examples of punctate fluorescence. Images were taken using a Leica Thunder fluorescent microscope. N=1.

4.2.2.3 Validation of H357$^{CD63\text{-}GFP}$

We further sought to confirm cellular GFP-CD63 protein expression after multiple passages by western blotting (Figure 4.7). Western blotting confirmed the presence of GFP in H357$^{CD63\text{-}GFP}$ whole cell lysates and importantly, the absence in wildtype cells (Figure 4.7A). To determine if there was co-localisation of endogenous CD63 with GFP-CD63 in our H357$^{CD63\text{-}GFP}$ cell line, cells were fixed and labelled with an anti-

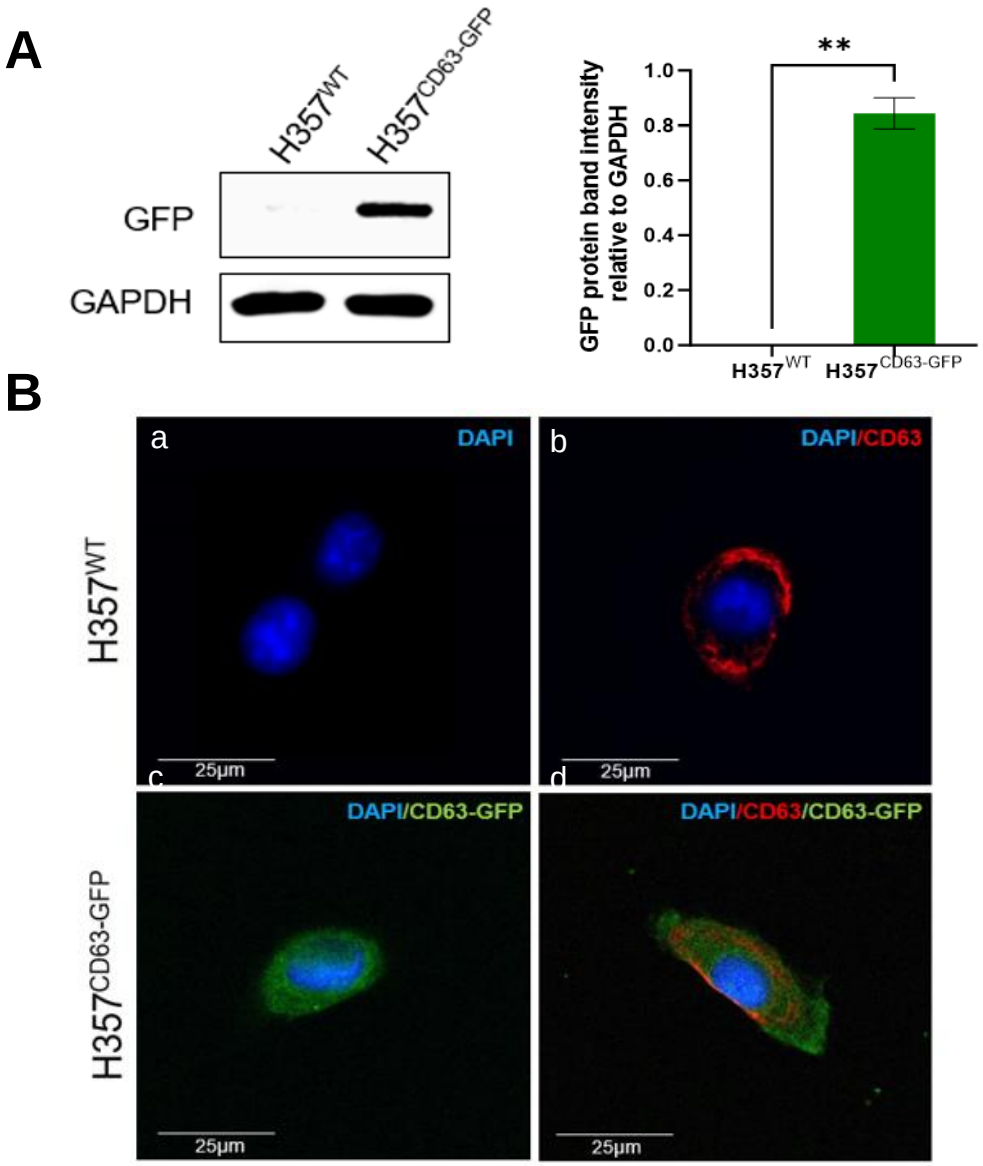

Figure 4.7 Validating GFP expression in H357$^{CD63\text{-}GFP}$ whole cells. (A) Representative western blot indicating GFP protein expression. Densitometry was performed using ImageJ and data is expressed as band density relative to endogenous control, N=2, n=1 (B) Images of H357 cells fixed and stained with DAPI only (a and c) or DAPI and an anti-CD63 antibody (b and d), DAPI stained nuclei depicted in blue, CD63 in red and CD63-GFP in green. Images were taken using a Nikon A1 Confocal microscope, N=1. Data presented as ± SEM **p<0.01.

CD63 antibody (Figure 4.7B). We observe incomplete co-localisation of endogenous CD63 with CD63-GFP in the stable cell line (Figure 4.7B).

4.2.2.4 Characterisation of H357$^{CD63\text{-}GFP}$

To determine if expression of CD63-GFP in H357 cells alters proliferation, we examined H357$^{CD63\text{-}GFP}$ cell growth compared to H357^{WT} and observed no significant difference between cell lines at any time point (Figure 4.8A). There was also no significant difference in doubling time between H357$^{CD63\text{-}GFP}$ and H357^{WT} (Figure 4.8B).

ESCRT-independent EV biogenesis has previously been shown to be driven in a CD63-dependent manner (van Niel et al., 2011). We therefore hypothesised that H357$^{CD63\text{-}GFP}$ might release increased numbers of EVs due to overexpression of CD63-GFP (via a constitutive cytomegalovirus promoter). NTA indicated no significant difference in particle secretion from H357$^{CD63\text{-}GFP}$compared to H357^{WT}

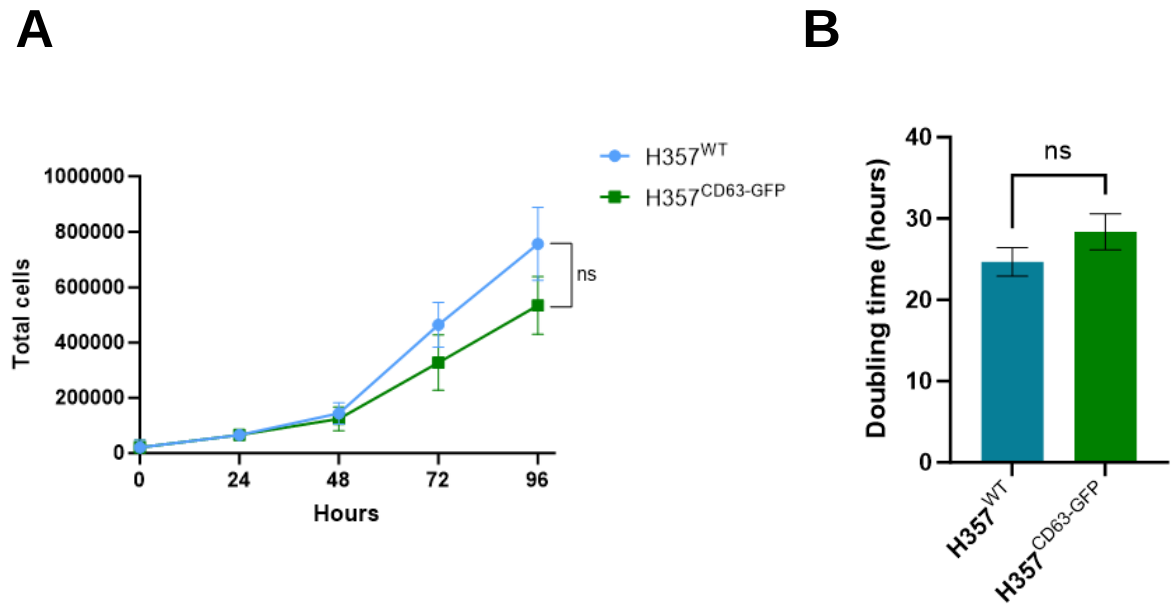

Figure 4.8 Growth analysis of H357$^{CD63\text{-}GFP}$. (A) 50,000 cells were seeded per well in a 6 well plate and counted using a haemocytometer every 24h for up to 96h. (B) Time taken for each cell line to double in number. Data is presented as mean ± SD for N=3, n=3. Statistics performed by Student t-test. Ns, no significance.

(Figure 4.9A). The largest proportion of particles (4.6%) released from H357^{WT} had a diameter of 135 nm, compared to 3.9% of the population of H357$^{CD63\text{-}GFP}$. The particles released from H357$^{CD63\text{-}GFP}$ showed a slight shift to smaller diameters (Figure 4.9B). However, there is no difference in mean average diameter (Table 4.3).

Table 4.3 Table 8. Comparison of mean diameter of particles in conditioned media from H357^{WT} and H357$^{CD63\text{-}GFP}$.

	H357^{WT}	**H357$^{CD63\text{-}GFP}$**
Mean diameter (nm)	139.7	127.0
± SD	49.62	34.67

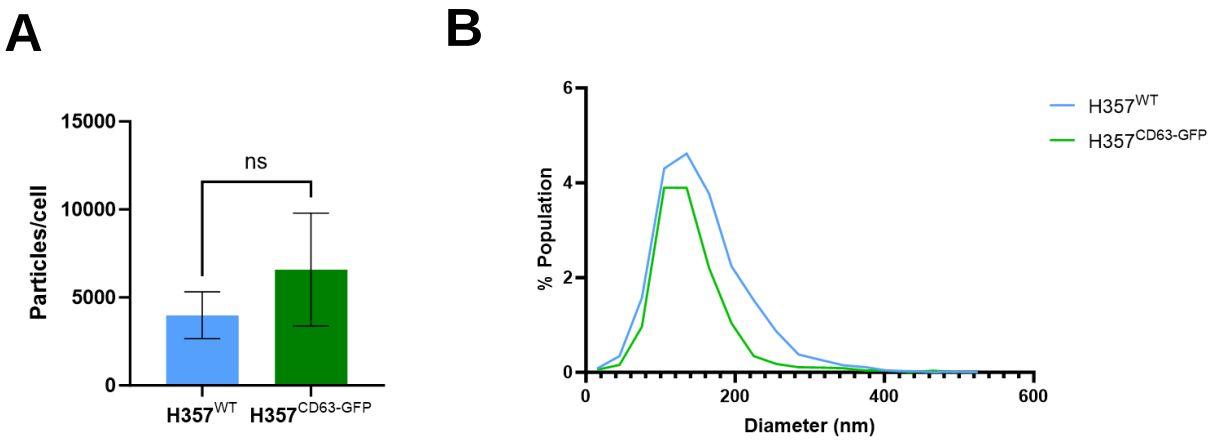

Figure 4.9 Nanoparticle tracking analysis of H357$^{CD63\text{-}GFP}$ secreted particles. 2x10^5 cells were seeded per well in 6 well plates and after 24h media was changed to EV-depleted FBS supplemented media. (A) Particle release and size was quantified from 24h conditioned media from WT and ΔHGS H357 cells using NTA (ZetaView®). Data is presented as mean ± SD for N=3, n=3. Statistics performed by Student t-test. Ns, no significance.

4.3 Discussion

4.3.1 HGS CRISPR/Cas9 knockout in H357 cell line

We predicted that knockout of HGS would result in reduced EV release, due to its assembly in ESCRT-0 machinery and initiating the ESCRT pathway responsible for EV biogenesis. We have demonstrated clear transcript and protein knockdown in H357$^{\Delta HGS}$ cells, which resulted in significantly reduced particle release in comparison to the wildtype. This observation is aligned with previous reports of reduced EV release following HGS knockdown (Tamai et al., 2010; Hoshino et al., 2013; Colombo, Moita, Van Niel, Kowal, Vigneron, Benaroch, Manel, Luis F. Moita, et al., 2013). Moreover, in our work, the EV specific marker TSG101 was significantly reduced in EV pellets from H357$^{\Delta HGS}$ cells. This is concurrent with other investigations utilising shRNA depletion of HGS, whereby TSG101 protein abundance was shown to be reduced in ‘’exosome’’ fractions from dendritic and breast cancer cells (Tamai et al., 2010; Hoshino et al., 2013) Further supporting evidence comes from Columbo *et al* who confirmed reduction of exosomes from HGS depleted HeLa cells by demonstrating reduced MHC II and CD63 protein levels in exosome fractions (Colombo, Moita, Van Niel, Kowal, Vigneron, Benaroch, Manel, Luis F. Moita, et al., 2013). HGS knockdown in endothelial cells has been shown to impair trafficking from early endosomes to lysosomes as well as recycling of endosomes to the plasma membrane, it therefore would be reasonable to assume that EV formation and release would also be altered (Yu et al., 2021).

Due to a major component of the ESCRT-dependent pathway being impaired, it can be hypothesised that other mechanisms of EV biogenesis may be upregulated to compensate. Indeed, it has been shown that knockdown of classical exosome marker TSG101 did not induce decreased EV release in HRAS-overexpressing epithelial

mammary cells, however the decrease in exosomal markers CD81, Alix and syntenin-1 was compensated via an increase in clathrin and Cav2-enriched EVs (Kilinc et al., 2021). This indicates that depletion of markers involved in EV biogenesis can induce EV release from alternate pathways (Kilinc et al., 2021). It follows that we might see a shift in EV sizes present in conditioned medium from H357$^{\Delta HGS}$ compared to wildtype cells. However, we saw no significant differences in particle size. This is in contrast to previous data showing that there was an increased proportion of smaller vesicles (<50 nm) in cells treated with shRNA against HGS (Colombo, Moita, Van Niel, Kowal, Vigneron, Benaroch, Manel, Moita, et al., 2013). This may be accounted for by differences in isolation and quantification methods, as NTA does not detect particles below 70 nm. The same trend was also seen in a colorectal cancer HGS knockout cell line using both electron micrographs and NTA, however interestingly, mean diameters measured by NTA were around double those measured by TEM (Sun et al., 2016) Bachurski *et al* observed substantially larger EV diameters when quantifying using NTA compared to TEM (Bachurski et al., 2019). This is due to dehydration during the TEM preparation process leading to shrinkage of up to 21%, meaning TEM may not be the most accurate method for assessment of EV size (Bachurski et al., 2019). Methods to quantify smaller diameters may be useful to distinguish further discrepancies in EV populations.

We observed a lack of epithelial layer in oral mucosa models incorporating H357$^{\Delta HGS}$ as well as thin epithelial-only layers compared to H357^{WT}. This observation poses questions relating to the role of HGS in epithelial cell-cell adhesion, especially as other regulators of endocytosis have been to show be responsible for recycling of the adherens junctions (AJs) component E-cadherin and maintaining cell-cell junction integrity (Yamamura et al., 2008; Desclozeaux et al., 2008). Depletion of ESCRT

subunits, including HGS, in fibroblasts causes accumulation of integrins with activated Src at enlarged early endosomes which reduced focal adhesion (FA) turnover (Lobert et al., 2012). The formation and turnover of FAs is key for cellular adhesion to the ECM, which may explain why H357$^{\Delta HGS}$ cells did not adhere to the underlying collagen matrix.

Moreover, ESCRT components have been linked to the maintenance of epithelial cell and fibroblast polarity by regulating recycling of cytoskeletal and cell junctional molecules (Dukes et al 2011). Silencing of TSG101 in a human colorectal cancer cell line caused disruptions in apicobasal polarity of epithelial only layers as well as reduced transepithelial resistance, indicating a disturbance to the diffusion barrier (Dukes et al., 2011). The same study demonstrated that TSG101 knockdown interfered with cell polarity using a 3D model of epithelial cysts (Dukes et al., 2011). Yu *et al* generated HGS KO mice to study endothelial cell polarity and found that this lead to impaired apicobasal polarity and brain vessel collapse (Yu et al).Taken together this evidence suggests that ESCRT machinery plays a role in regulating cell adhesion and polarity meaning this could be disrupted in our H357$^{\Delta HGS}$ cell line.

Due to ESCRT machinery involvement with trafficking of growth factors, another explanation is that proliferation may have been attenuated due to HGS KO. A previous study has shown that depletion of HGS in HeLa cells via siRNA, lead to decreased proliferation and colony formation compared to non-depleted cells (Toyoshima et al). The authors conclude that HGS KD upregulates E-cadherin which pools beta-catenin in the cytoplasm reducing its nuclear signalling and suppressing cell growth. Further validation of alterations in proliferation and adhesion markers would be pertinent to distinguish these effects. As E-cadherin is known to play a critical role in cell adhesion

and epithelial polarity, as well as proliferation, it would be a potential candidate to investigate further.

4.3.2 Generation of a fluorescently labelled EV secreting OSCC cell line

We were able to successfully transfect H357 cells with CD63-GFP and expand colonies with stable expression. Interestingly, there was variation in GFP brightness between cells in monoclonal populations. This could be due to differences in cell division, as protein expression fluctuates dependent on cell cycle stage (Cooper, 2000). Furthermore, fluorescent proteins that are practical for neutral pH imaging are known to lose fluorescence in acidic conditions, meaning there may be loss of signal in internal compartments (Shinoda et al., 2018). This is especially relevant as CD63 is enriched in endosomes, lysosomes and intraluminal vesicles (Pols et al., 2009).

We did not see co-localisation of endogenous CD63 and expressed CD63-GFP in H357 cells. This could be due to the anti-CD63 antibody recognising an epitope that is altered in CD63 due to fusion with GFP on the C-terminus, however the endogenous CD63 is still labelled. Moreover, CD63 is a highly glycosylated protein, meaning some forms may go undetected using this single antibody labelling technique.

Multiple studies have shown that CD63 knockout leads to a significantly lower number of particles secreted from cells compared to controls (Hurwitz et al., 2016b; Gauthier et al., 2017). However, our observations are more complementary to data produced by Corso *et al* who observed that CD63-GFP transiently transfected cells had similar

EV protein composition and size distribution (50-140 nm) compared to untransfected cell EVs despite non-physiological levels of CD63 (Corso et al., 2019).

Interestingly, the H357$^{CD63\text{-}GFP}$ cell line showed a shift towards releasing smaller particles compared to the wildtype. One study found that knockout of CD63 reduced the secretion of small EVs (<150 nm) from HEK293 cells but had no effect on large EVs (>150 nm), suggesting that CD63 primarily plays a role in small EV or exosome biogenesis (Hurwitz et al., 2016). This is supported by the knowledge that CD63 forms a complex with syntenin and Alix which recruits ESCRT to the endosomal membrane and promotes ILV formation, which are then released as exosomes (Baietti et al., 2012).

Furthermore, we observed no significant difference in doubling time of H357$^{CD63\text{-}GFP}$ compared to the wildtype. There is conflicting evidence surrounding the contribution of CD63 to cancer progression with both overexpression and knockdown causing reduced proliferation in in hepatocellular carcinoma and breast cancer cells, respectively, indicating that its effect may be context dependent (Tominaga et al., 2014; S. Yu et al., 2021). In HNSCC cell lines, overexpression of CD63 led to an increased proportion of cells in S phase of the cell cycle, thereby blocking cell cycle progression and diminishing proliferation (Huang et al., 2023). This mechanism was found to be related to CD63 interaction with keratin 1 (KRT1), both of which were under-expressed in HNSCC tumour tissue compared to normal tissue (Huang et al., 2023).

4.3.3 Conclusion

Validation of H357$^{\Delta HGS}$ showed a significant reduction in HGS transcript and protein level. Moreover, H357$^{\Delta HGS}$ released significantly fewer particles and had significantly reduced TSG101 marker abundance in EV pellets. 3D OSCC models generated with H357$^{\Delta HGS}$ failed to form full epithelial layers, however further validation and experimental repeats are required. We identified optimal transfection conditions for stable expression of CD63-GFP in H357 cells. FACS sorting to generate single colonies generated H357$^{CD63\text{-}GFP}$ cells showing green fluorescent punctate. GFP protein could be identified in cell lysate by western blot. H357$^{CD63\text{-}GFP}$ cells did not show significant differences in proliferation or particle release compared to the wildtype.

5 Oral cancer derived EVs promote an activated phenotype in normal oral fibroblasts in a TGF-β dependent manner.

5.1 Introduction

Transforming growth factor-β (TGF-β) signalling acts as a key regulator of numerous cellular processes including growth, differentiation and migration (Pickup et al., 2013). Its role in cancer is conflicting and highly context-dependent, having been shown to function as a tumour suppressor in early stages of oncogenesis and a tumour promotor in later stages (Meulmeester et al., 2011).

TGF-β is a member of a superfamily of regulatory cytokines including, bone morphogenetic proteins (BMPs), activins and growth and differentiation factors (Kubiczkova et al., 2012). There are three isoforms of TGF-β in humans; TGF-β1, TGF-β2 and TGF-β3, which function through the same receptor signalling pathways. TGF-β is secreted as part of an inactive latent complex that consists of an N-terminal latency-associated peptide and a C-terminal mature TGF-β monomer. Subsequent binding to the latent TGF-β-binding protein (LTBP) leads to formation of the large latency complex (LLC) which can be released into the extracellular matrix (Kubiczkova et al., 2012). TGF-β is activated by a variety of factors including integrins, proteases, matrix metalloproteases and acidic environments (Meulmeester et al., 2011). Active TGF-β signals through TGF-β type I and type II receptors (TGF-βRI and TGF-βRII, respectively). Binding of TGF-β with TGF-βII causes formation of a complex with TGF-βRI and its subsequent phosphorylation (Huang et al., 2012). Canonical signalling involves mothers against decapentaplegic homolog (SMAD) proteins, of which there are eight categorised into three subtypes (Guo et al., 2023). Following receptor

phosphorylation, receptor-regulated Smad (R-Smad) proteins are recruited and associate with Smad4 to form hetero-trimers. This complex translocates to the nucleus where it binds to Smad-binding elements to regulate TGF-β responsive genes in collaboration with cofactors such as zinc finger and forkhead. Non-canonical signalling includes activation of PI3K/Akt, MAPK and Ras homolog gene family A (Meng et al., 2016).

There is increasing evidence to suggest that TGF-β1 promotes OSCC progression via induction of EMT, matrix remodelling, proliferation and modulation of the extracellular microenvironment (Lu et al., 2004; Qiao et al., 2010; Richter et al., 2011) Increased levels of TGF-β1 have been observed in HNSCCs compared to normal control human tissues, and overexpression of TGF-β1 in transgenic mice was shown to result in enhanced proliferation of head and neck epithelia as well as inflammation and angiogenesis (Lu et al., 2004). TGF-β has also been implicated in EMT in OSCC via Snail and Slug, causing upregulation of matrix metalloprotease 9 (MMP-9) levels (Sun et al., 2008; Joseph et al., 2009). siRNA against Snail in an OSCC cell line attenuated MMP-9 expression and Matrigel invasion mediated by TGF-β1, indicating a potential role in OSCC matrix remodelling to allow dissemination from the primary site (Sun et al., 2008). Furthermore, TGFβ stimulated OSCC cells have been shown to display greater adhesion to type I-IV collagens which is believed to play a role in metastasis by allowing cancer invasion into the basement membrane (Richter et al., 2011).

TGF-β is well documented in facilitating fibroblast activation and generating CAFs which can reciprocally enhance tumour progression (Wu et al., 2021). For example, the secretion of IL-1α from OSCC cells has been shown to increase CAF proliferation as well as enhance CCL7, CXCL1 and IL-8 cytokine secretion (Bae et al., 2014). These CAF derived cytokines increased the proliferation of OSCC cells,

thus demonstrating a positive feedback loop (Bae et al., 2014). CAFs have also been implicated in multiple cancer promoting mechanisms; remodelling the ECM to promote migration, EMT plasticity to enhance invasion, maintaining a metastatic niche, and inducing glycogen metabolism in cancer cells amongst others (Yoshida, 2020).

There is growing evidence for the role of EV-associated TGF-β in CAF differentiation and tumour progression (Webber et al., 2010; Gu et al., 2012; Goulet et al., 2018). The aim of this chapter was to determine if TGF-β released by OSCC is associated with EVs and to determine their role in NOF to CAF phenotypic switch.

5.2 Results

5.2.1 Co-culture of OSCC cells and NOFs

We first sought to determine the influence of OSCC cells on surrounding NOFs compared to normal oral keratinocytes, and if this communication was EV-dependent. We utilised a transwell co-culture system (Figure 2.1 and Figure 5.1), whereby NOF ''acceptor'' cells were seeded into a tissue culture well and ''donor'' oral cell lines; FNB6, H357^{WT} and H357$^{\Delta HGS}$ seeded in transwell inserts, were cultured on top.

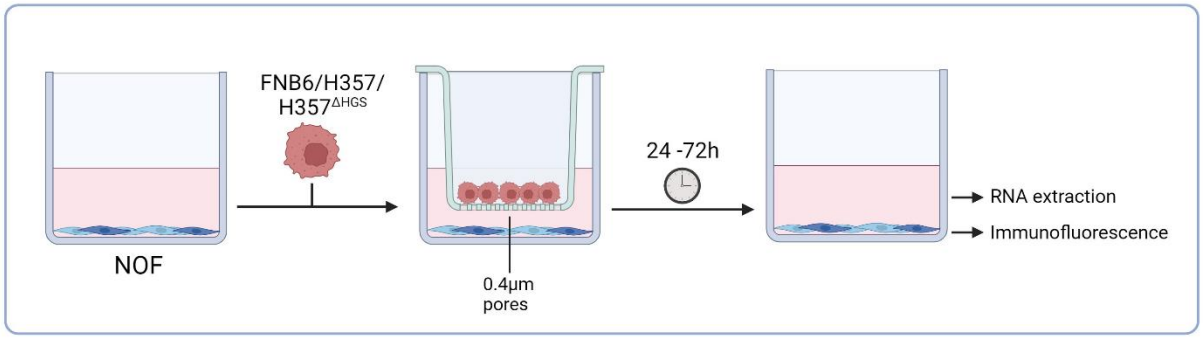

Figure 5.1 Schematic of transwell co-culture method.

The transcript expression of three common CAF markers were assayed by qPCR to determine if co-culture of NOF with oral keratinocytes led to their activation to a CAF-like phenotype. We chose two of the most highly cited CAF markers; α-smooth muscle actin (α-SMA), which is widely considered to be the most reliable, and fibroblast activation protein (FAP) which can also be expressed by epithelial cells undergoing EMT (Nurmik et al., 2020). In order to expand our selection we also chose a more novel marker, Collagen Type XI Alpha I chain (COL11A1), which has previously been shown to be highly specific to CAFs (Vázquez-Villa et al., 2015).

ACTA2, encoding for α-SMA protein, levels were not significantly increased in the positive control at both 24 and 48h (Figure 5.2A). NOFs co-cultured with FNB6, H357, H357$^{\Delta HGS}$ was also showed no significant difference compared to untreated cells at 24 and 48h (Figure 5.2A).

Similarly, both FAP and COLL11A1 transcript levels were not significantly altered upon TGF-β1 treatment at both 24 and 48h. There was also no significant change in FAP and COLL11A1 transcript levels in NOFs co-cultured with any of the keratinocyte cell lines (Figure 5.2.B and C).

A CAF phenotype is often characterised by stress fibre formation, therefore we imaged α-SMA fibre formation by immunofluorescence microscopy in NOFs using the same co-culture method (Figure 5.2 and 5.3). Compared to the untreated control, there was significantly higher positive fluorescent area in the positive control ($p < 0.05$), however no difference when NOF were co-cultured with any of the keratinocytes for 48h (Figure 5.3). However, at 72h co-culture we observed a significant increase in positive fluorescent area for both TGF-β1 treated NOF ($p < 0.01$) and those co-cultured with H357 WT ($p < 0.05$) (Figure 5.4). Co-culture with H357 induced a 10% increase of

fluorescent area, whereas TGF-β1 treatment increased this to 22%. No significant change was observed in NOFs co-cultured with FNB6 and H357$^{\Delta HGS}$ compared to the untreated control.

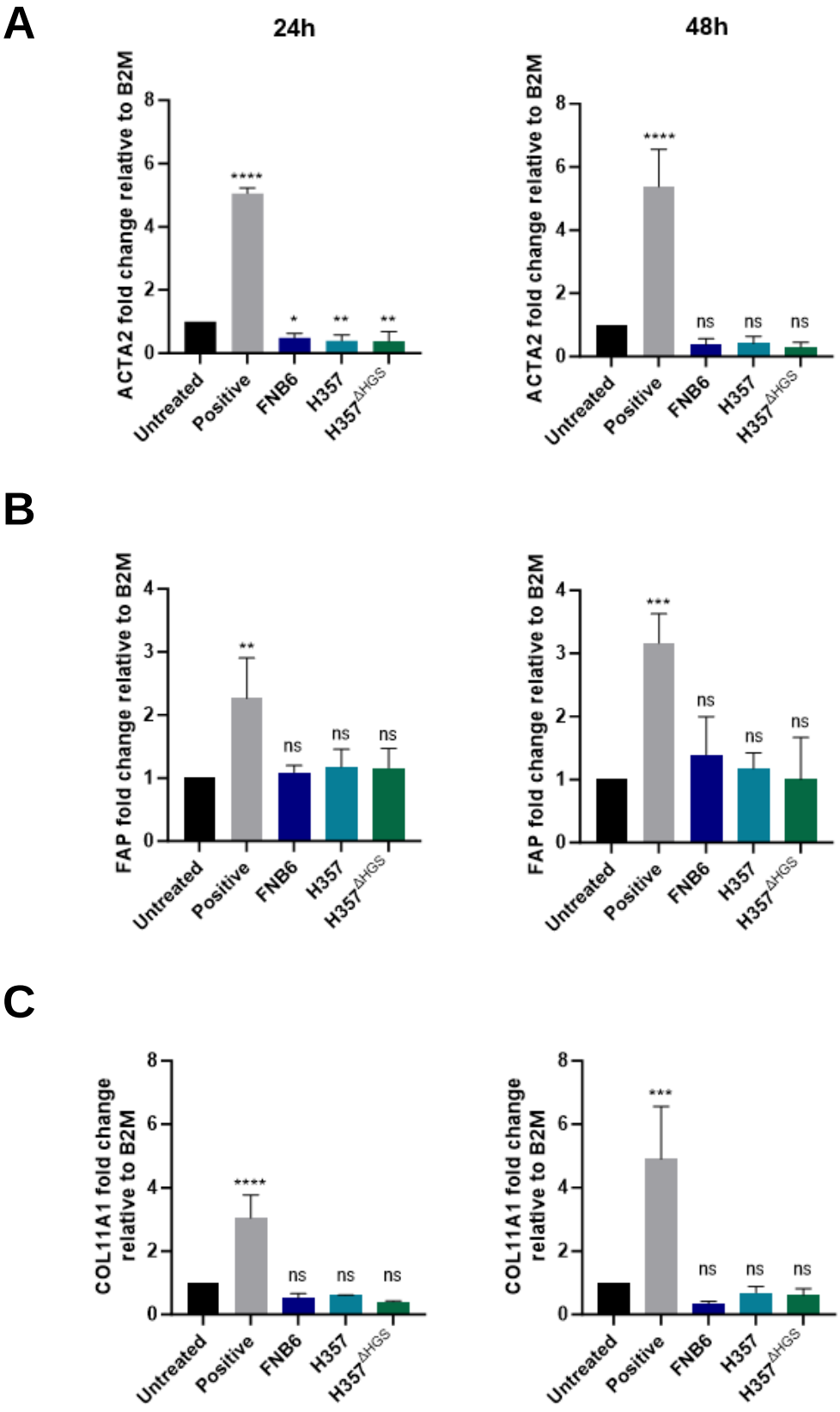

Figure 5.2 Cancer associated fibroblast marker transcript levels in normal oral fibroblasts co-cultured with oral keratinocytes. RNA was isolated from primary NOFs co-cultured with FNB6, H357 or H357$^{\Delta HGS}$ for 24 or 48h, and converted to cDNA by RT-PCR. Transcript levels of CAF markers (A) ACTA2 (B) FAP and (C) COLL11A1 were measured using qPCR. Positive control refers to NOF treated with 5 ng/mL TGF-β1. Data was normalised to the housekeeping gene B2M and expressed as relative to untreated control. Data is presented as mean ± SD for N=3, n=3. Statistics performed by Kruskall-Wallis with BKY multiple comparisons. ns, non-significant.

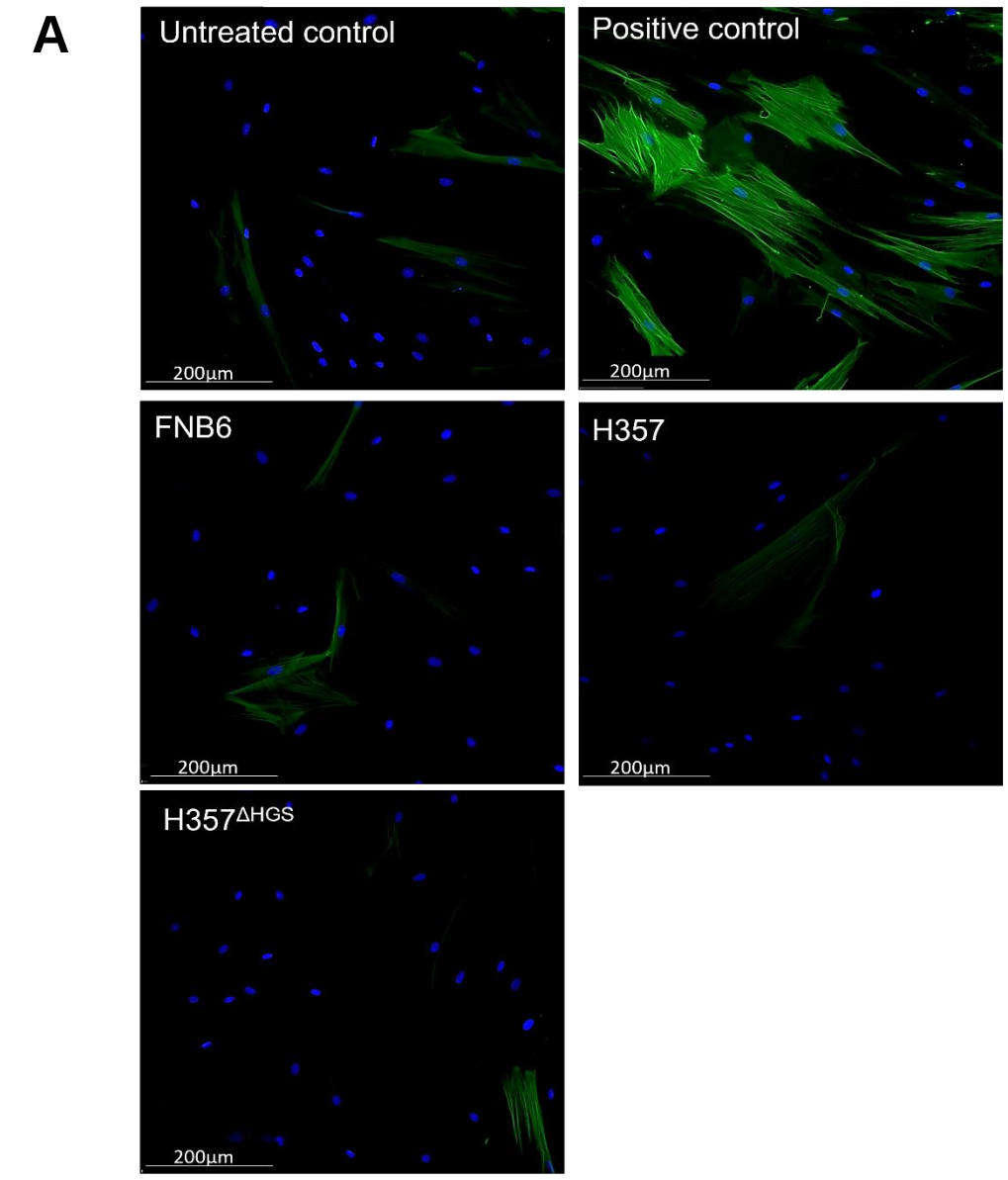

Figure 5.3 α-SMA stress fibre formation in NOFs co-cultured with keratinocytes for 48h. (A) Representative images were taken using a Leica THUNDER fluorescent microscope. Green staining indicates α-SMA and blue stains for DAPI (B) Fluorescence area percentage was measured using ImageJ. Positive controls refers to NOF treated with 5 ng/mL TGF-β1. Data is presented as mean ± SD for N=3, n=3. Statistics performed by Kruskall-Wallis test with BKY multiple comparison. ns, non-significant, **p<0.01 ***p<0.001 ****p<0.0001.

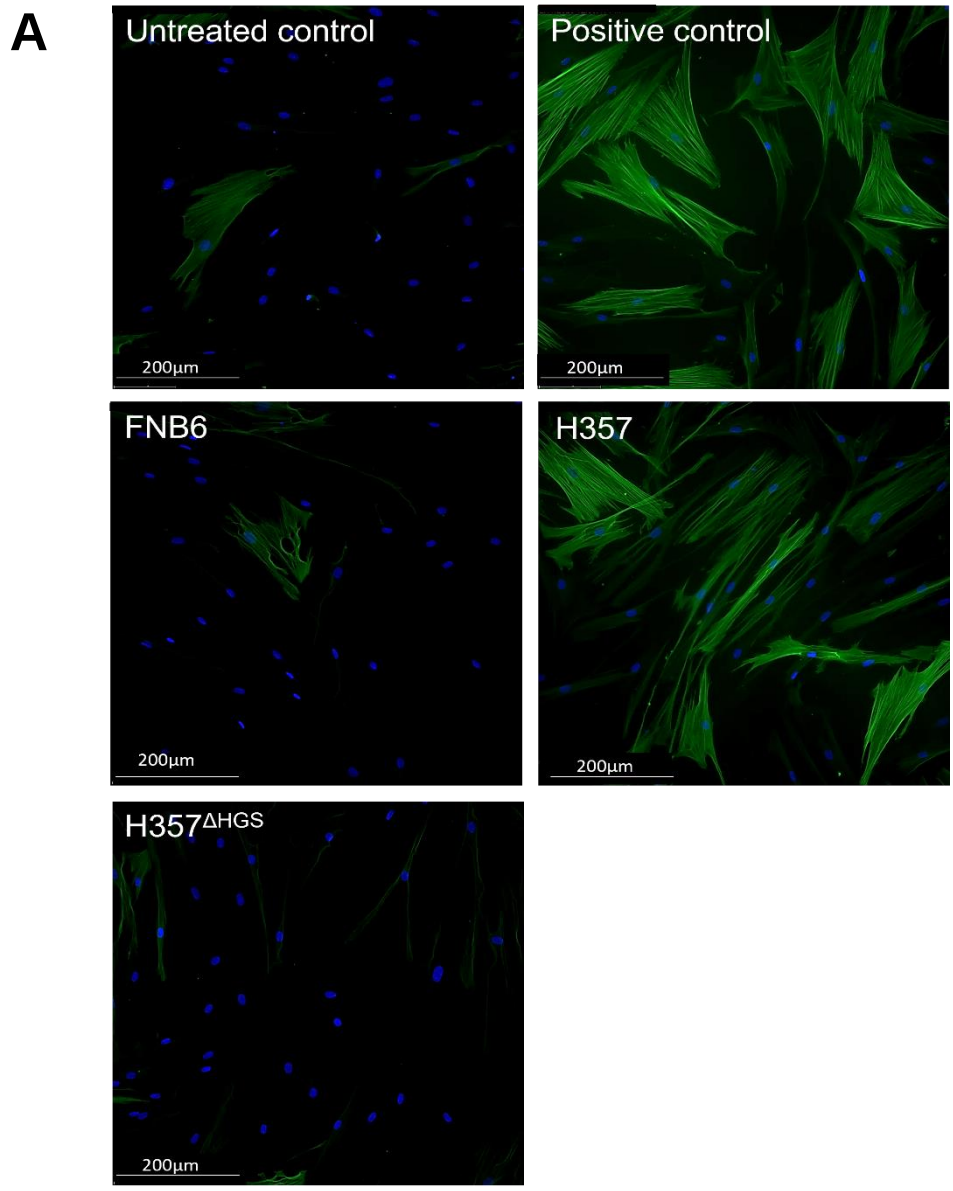

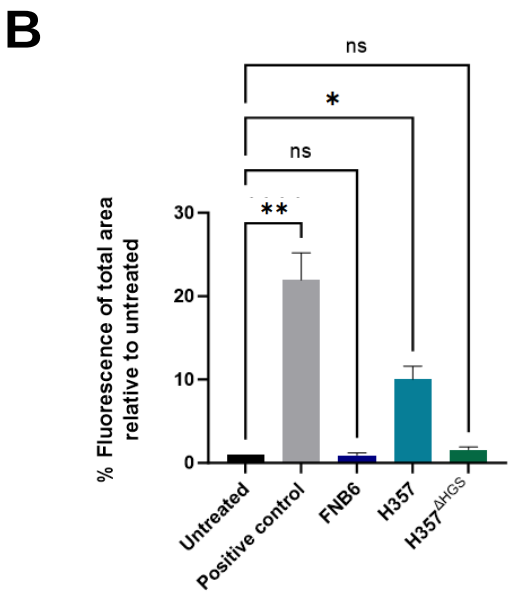

Figure 5.4 α-SMA stress fibre formation in NOFs co-cultured with keratinocytes for 72h. (A) Representative images were taken using a Leica THUNDER fluorescent microscope. Green staining indicates α-SMA and blue stains for DAPI (B) Fluorescence area percentage. Positive control refers to NOF treated with 5 ng/mL TGF-β1. Data is presented as mean ± SD for N=3, n=3. Statistics performed by Kruskall-Wallis test with BKY multiple comparison. ns, non-significant, *p<0.05 **p<0.01.

5.2.2 Isolation and characterisation of cell line EVs

The reduced ability of H357$^{\Delta HGS}$ to induce stress fibre formation in contrast to the wildtype suggested that EVs may play a role in NOF activation. We also hypothesised that H357^{WT} EVs were enriched with TGF-β, leading to the enhanced activation of NOF in the co-culture model. To investigate this we first compared the number of EV sized particles in conditioned media from FNB6, H357 and H357$^{\Delta HGS}$ cell lines, which would be useful for EV treatment experiments (Figure 5.5). H357^{WT} cells released 3.1 fold (p < 0.001) more particles per cell than both FNB6 and H357$^{\Delta HGS}$ (Figure 5.5). FNB6 and H357$^{\Delta HGS}$ released a similar number of particles into conditioned medium (598.3 and 658.3 particles per cell, respectively).

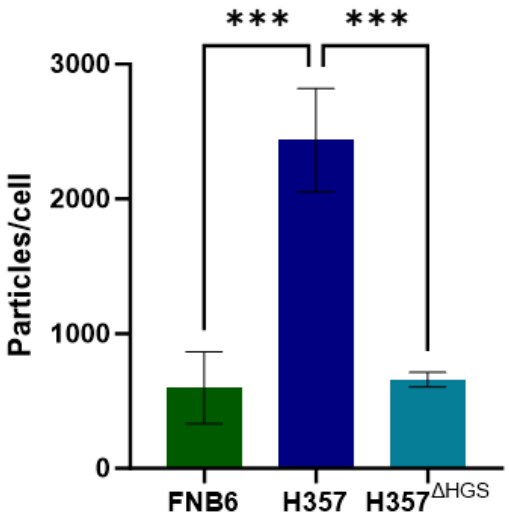

Figure 5.5 Characterisation of particles released from FNB6, H357^{WT} and H357$^{\Delta HGS}$. Particle concentration in 24 h conditioned media was measured via NTA using a ZetaView instrument. Data is presented as mean ± SD for N=3, n=3. Statistics performed by one-way ANOVA with Dunnett's multiple comparison. ***p<0.001.

Following this, we aimed to test if an enrichment of EVs was correlated with an enrichment in TGF-β1. EVs were enriched by SEC and a small amount of each preparation was used to calculate total protein concentration by BCA assay. The

remaining volume was used to calculate TGF-β1 concentration by sandwich ELISA. Each sample was analysed in acidified and non-acidified conditions, which allowed the determination of total TGF-β1 (latent and active) and active TGF-β1, respectively. Unfractionated conditioned media was analysed in the same way.

EV preparations for all cell lines showed higher levels of TGF-β1 compared to conditioned media (Figure 5.6). FNB6 EV preparations showed 4.7-fold ($p < 0.01$) more total TGF-β1 than in conditioned media, however differences in active TGF-β1 cannot be quantified as the levels in CM were undetectable with ELISA. H357 EV preparations had a 37.3-fold and 66.5-fold increase in total and active TGF-β1, respectively ($p < 0.01$, $p < 0.01$). $H357^{\Delta HGS}$ also showed significantly higher total TGF-β in EV preparations compared to conditioned media with a 6.3-fold increase ($p < 0.05$), and there was a 9.6-fold increase in active TGF-β1 compared to the conditioned media, however this was not statistically significant.

H357 EV preparations showed 5.8-fold ($p < 0.001$) and 2.9-fold ($p < 0.05$) more total TGF-β1 protein than those from FNB6 and $H357^{\Delta HGS}$, respectively (Figure 5.6). There was no significant difference in active TGF-β1 levels between FNB6, H357 and $H357^{\Delta HGS}$ EV preparations.

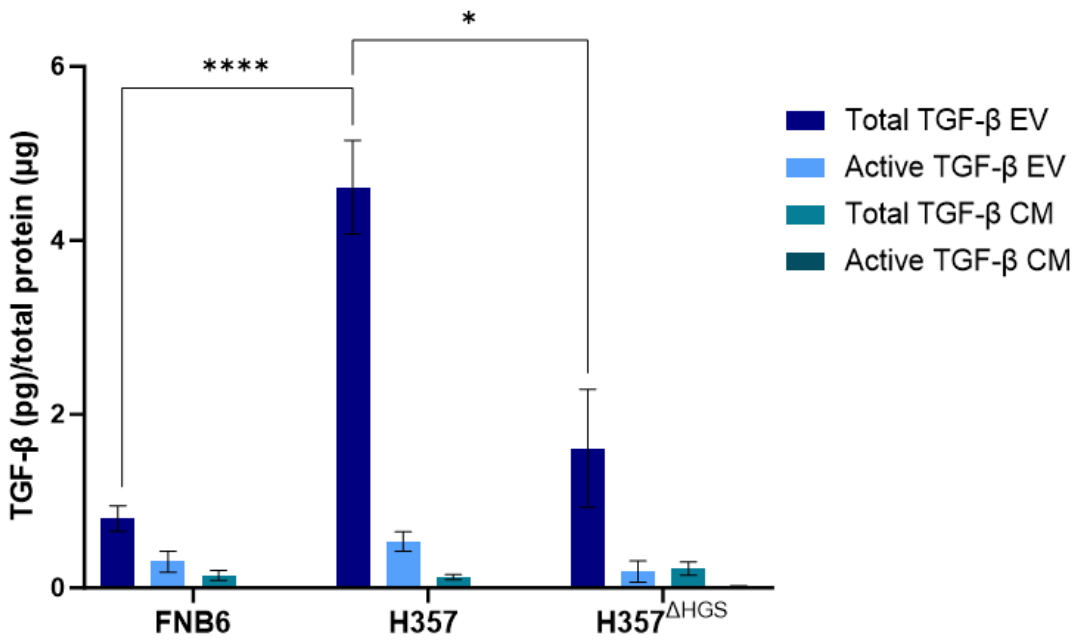

Figure 5.6 TGF-β1 protein levels in oral cell line conditioned media and EVs. Cells were cultured in serum free medium for 24h before medium was collected and subject to differential centrifugation. Conditioned media samples were taken post cell debris removal. EVs were isolated by SEC, pelleted by ultracentrifugation and re-suspended in PBS. Samples were activated by HCl addition prior to NaCl neutralisation. TGF-β1 levels were quantified by sandwich ELISA (R&D) and protein was quantified by BCA assay. Data represents ± SD for N=3, n=3. Statistics performed by one-way ANOVA and student's t-test. *p<0.05, **p<0.0001.

Having confirmed that enrichment of EVs led to an enrichment of TGF-β1, we next attempted to determine if the TGF-β1 was actually associated with EV-sized particles. Again, we enriched EVs by size exclusion chromatography prior to conducting Nano-Flow Cytometry. EV preparations were labelled with a cocktail of red-fluorescent antibodies against tetraspanins (CD63, CD81 and CD9) and a green-fluorescent antibody against TGF-β1. This dual labelling approach allowed detection of TGF-β1 on the surface of EVs and colocalisation with tetrapsanins positive EV populations (Figure 5.7).

The proportion of tetraspanin positive EVs was highest in FNB6 EV preparations, with 23.3% of the population showing positive staining (Figure 5.7). $H357^{\Delta HGS}$ had the second largest tetraspanin positive population (19.9%) and $H357^{WT}$ showed the least

positive staining (16.3%). FNB6 preparations also had the largest proportion of TGF-β positive EVs at 8.2%, followed by H357^{WT} and then H357$^{\Delta HGS}$ showing 6% and 2.1%, respectively. The percentage population that were both tetraspanin and TGF-β positive was low. The proportion showing dual positivity was 1.3% in FNB6 EV preparations, 1.2% in H357 and 0.8% in H357$^{\Delta HGS}$. This preliminary data is from one biological repeat and therefore we cannot conduct statistical analysis to draw firm conclusions. However, it does indicate that TGF-β1 is associated with EV-sized particles, a small proportion of which are also positive for tetraspanins.

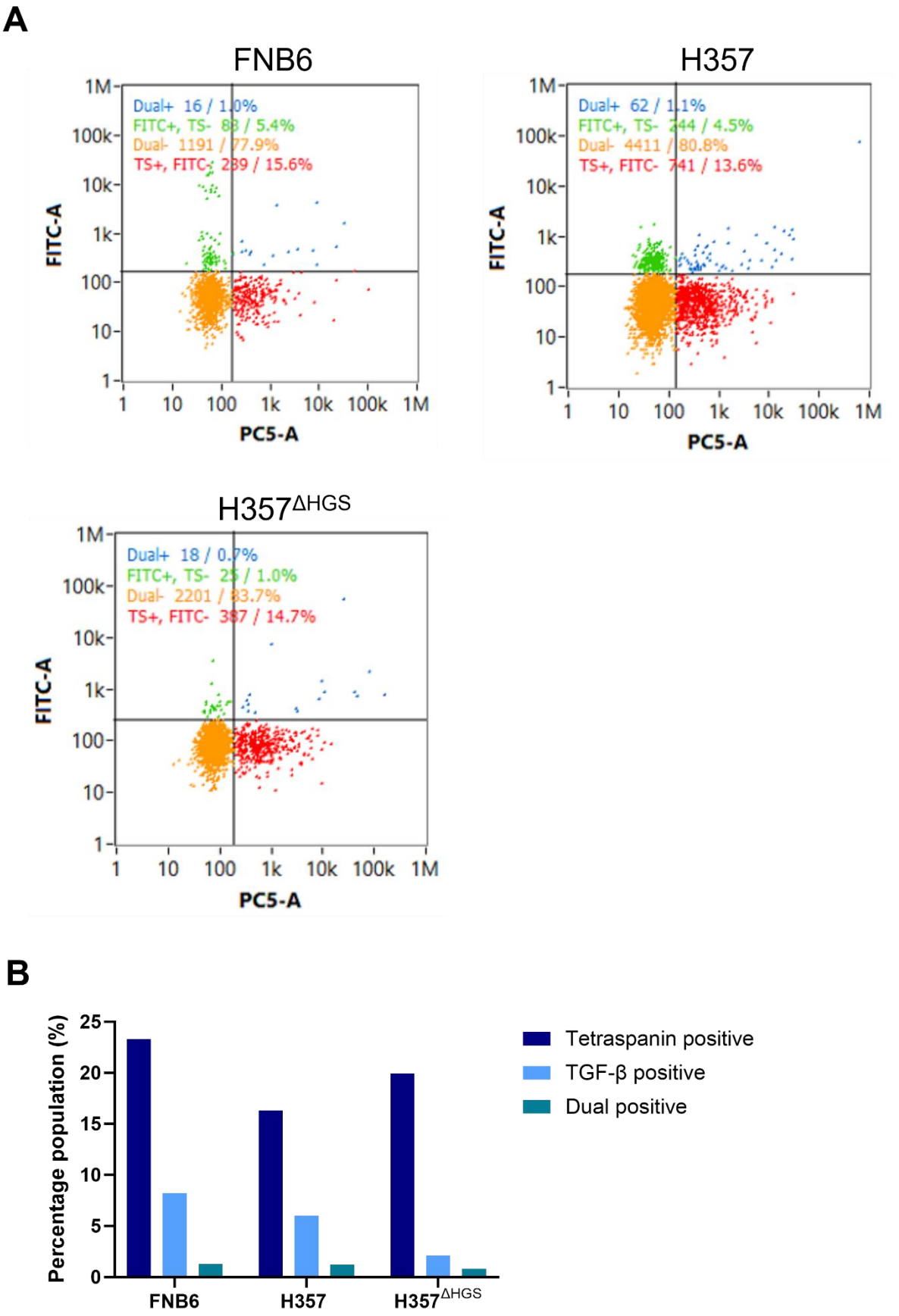

Figure 5.7 EV characterisation using Nano-Flow Cytometry. EVs were enriched from cell conditioned media using SEC, prior to staining with an anti-tetraspanin antibody cocktail including CD9, CD81 and CD63 conjugated to APC (red). Anti-TGF-beta antibody conjugated to AlexaFluor 488 (green). Analysis was conducted using a NanoAnalyzer U30 instrument. (A) Scatter plots were generated by the nFCM Professional Suite v2.0 software (B) Percentage positivity for tetraspanins and/or TGF-β in EV preparations from FNB6, H357 and H357$^{\Delta HGS}$. N=1.

5.2.3 EV association with NOFs

EVs have been shown to exert their effects via cell uptake and association with the recipient cell surface (Kwok et al., 2021). We therefore examined if OSCC EVs interacted with NOFs, using EVs derived from our H357$^{CD63\text{-}GFP}$ cell line, by fluorescence microscopy. H357$^{CD63\text{-}GFP}$ EVs were enriched by SEC and analysed by NTA to determine size and concentration (Figure 4.9). EVs were incubated with NOFs at increasing time points (Figure 5.8). Green fluorescence accumulated over time (Figure 5.8A) and there was significantly more colocalisation with the early endosome marker EEA1 at 1 and 6 hours incubation compared to 30 minutes (Figure 5.8B). However, there was no significant difference at 4 hours.

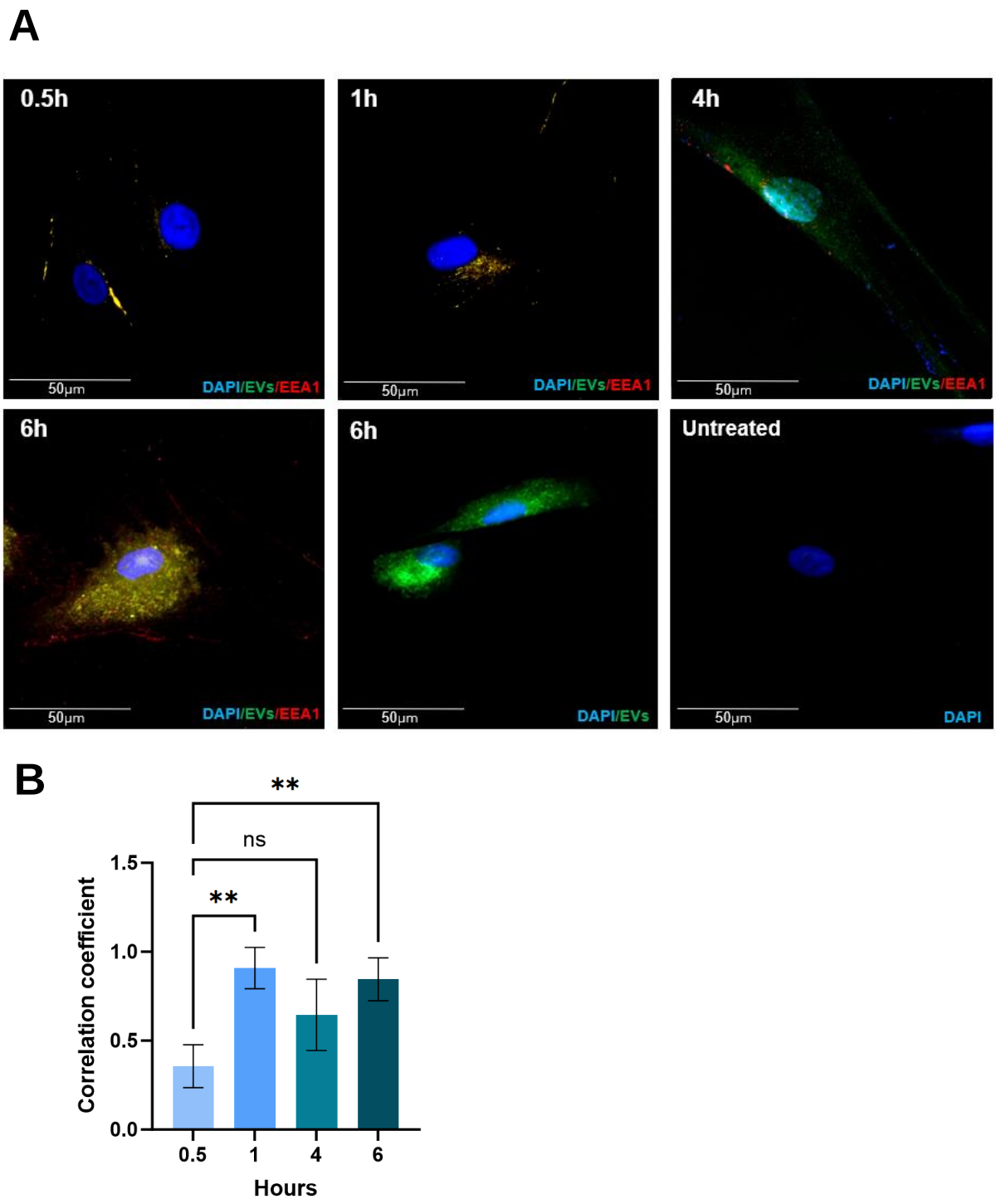

Figure 5.8 Association of H357$^{CD63\text{-}GFP}$ EVs with NOFs. H357$^{CD63\text{-}GFP}$ EVs were isolated by SEC, counted by NTA and diluted at a concentration of 50x conditioned media. EVs were incubated with NOFs for 0.5, 1, 4 and 6h. Cells were fixed and stained with primary EEA1, then secondary Alexa 568-conjugated secondary antibody (red). Cell nuclei were stained with DAPI (blue). Images were taken using a Leica THUNDER fluorescent microscope. (B) Co-localisation between EVs and EEA1 was quantified using ImageJ to determine Pearson's R value. Data is represented as ± SD for N=3, n=3. Statistics performed by one-way ANOVA with Dunnett's multiple comparison. ns, non-significant, **p<0.01.

5.2.4 OSCC derived EVs drive a CAF-like phenotype in NOFs.

After showing that OSCC derived EVs associate with NOFs, we next investigated whether OSCC-derived EVs play a role in the NOF-CAF switch. We again looked at transcript levels of three CAF markers; α-SMA, FAP and COL11A1 in NOFs incubated with EVs for 24 and 48h. TGF-β1 treatment induced a 5.3 and 5.1-fold increase in α-SMA ($p < 0.05$ and $p < 0.01$) at 24h and 72h, respectively. Although there was a2.2 and 2.7- fold increase in FAP at 24h and 48h respectively, this was not significantly different to the untreated. COL11A1 transcript levels increased 1.7 ($p < 0.001$) and 2.9-fold (ns) at 24 and 48h, respectively. However, NOFs incubated with FNB6, H357 or H357$^{\Delta HGS}$ EVs displayed no significant change in α-SMA, FAP or COL11A1 transcript expression at either time point(Figure 5.9).

In contrast to transcript expression, when looking specifically at stress fibre formation, we observed significantly ($p < 0.05$ and $p < 0.01$) higher overall α-SMA staining in NOFs treated with 10x and 50x dose of H357 EVs at 48h compared to the untreated control (Figure 5.10). Treatment of NOF with FNB6 and H357$^{\Delta HGS}$ EVs did not induce any significant change in α-SMA fibre formation at 48h (Figure 5.7). There were insufficient FNB6 EVs to allow treatment of NOF with the highest (50x) dose.

NOFs treated with 50x H357 EVs for 72h show significantly ($p < 0.05$) increased α-SMA staining, rising to 14.4% from 8.2% at 48h (Figure 5.11). For NOFs treated with H357 EVs we observed a dose dependent trend, although doses of H357 1x and 10x were not significantly different from the untreated. Similarly to 48h, FNB6 and H357$^{\Delta HGS}$ EVs did not induce significant change in α-SMA stress fibre formation in NOFs.

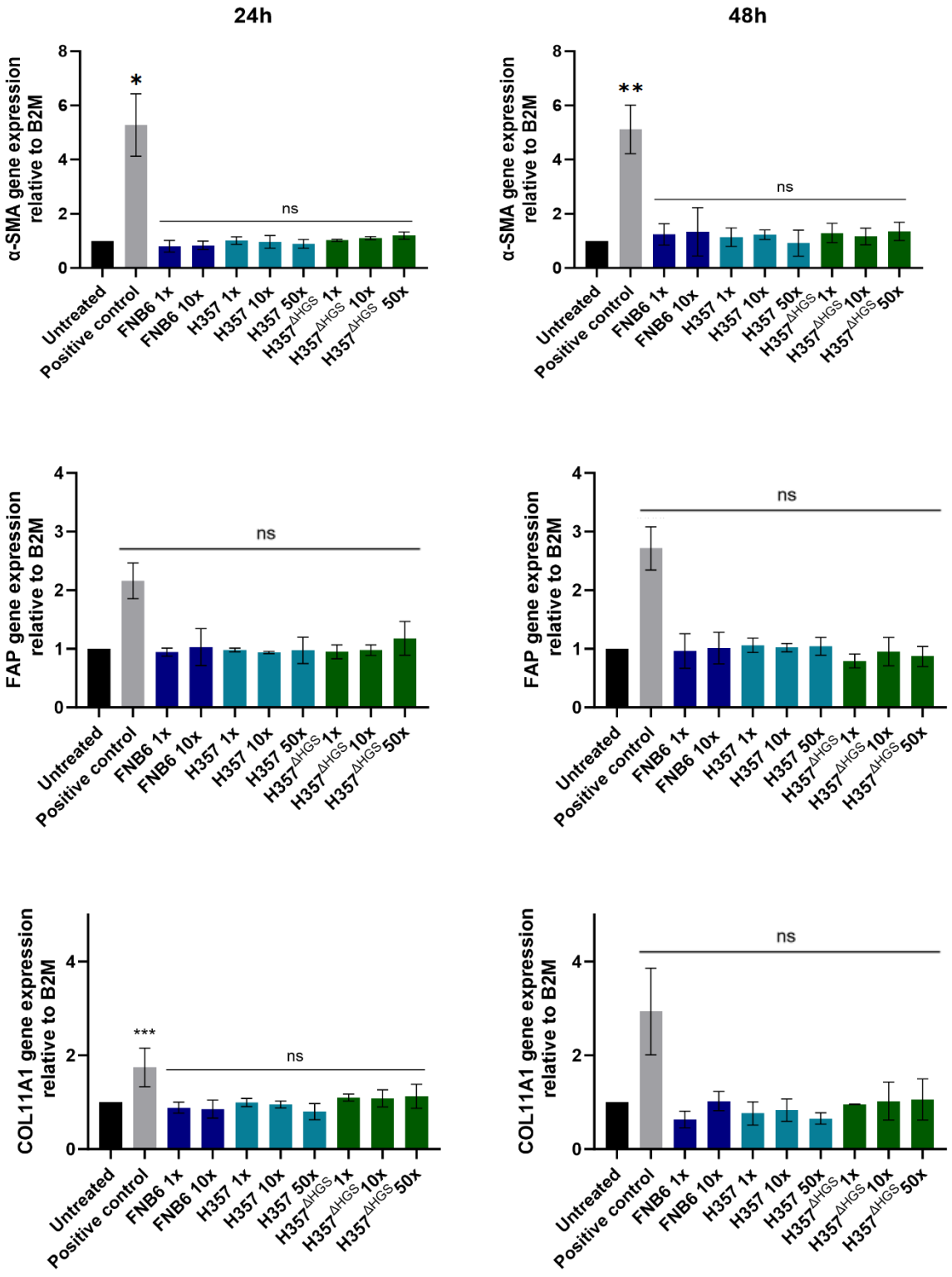

Figure 5.9 Cancer associated fibroblast markers transcript levels in normal oral fibroblasts treated with EVs. RNA was isolated from primary NOFs co-cultured with FNB6, H357 or H357$^{\Delta HGS}$ -derived EVs for 24 or 48h. Doses were calculated based on the average number of secreted particles/cell in conditioned medium from each cell line. Transcript levels of (A) ACTA2 (B) FAP and (C) COLL11A1 were measured using qPCR. Positive control refers to NOF treated with 5 ng/mL TGF-β1. Data is expressed as fold change relative to the housekeeping gene B2M. Data is presented as mean ± SD for N=3, n=3. Statistics performed by Kruskall-Wallis test with BKY multiple comparison. ns, non-significant.

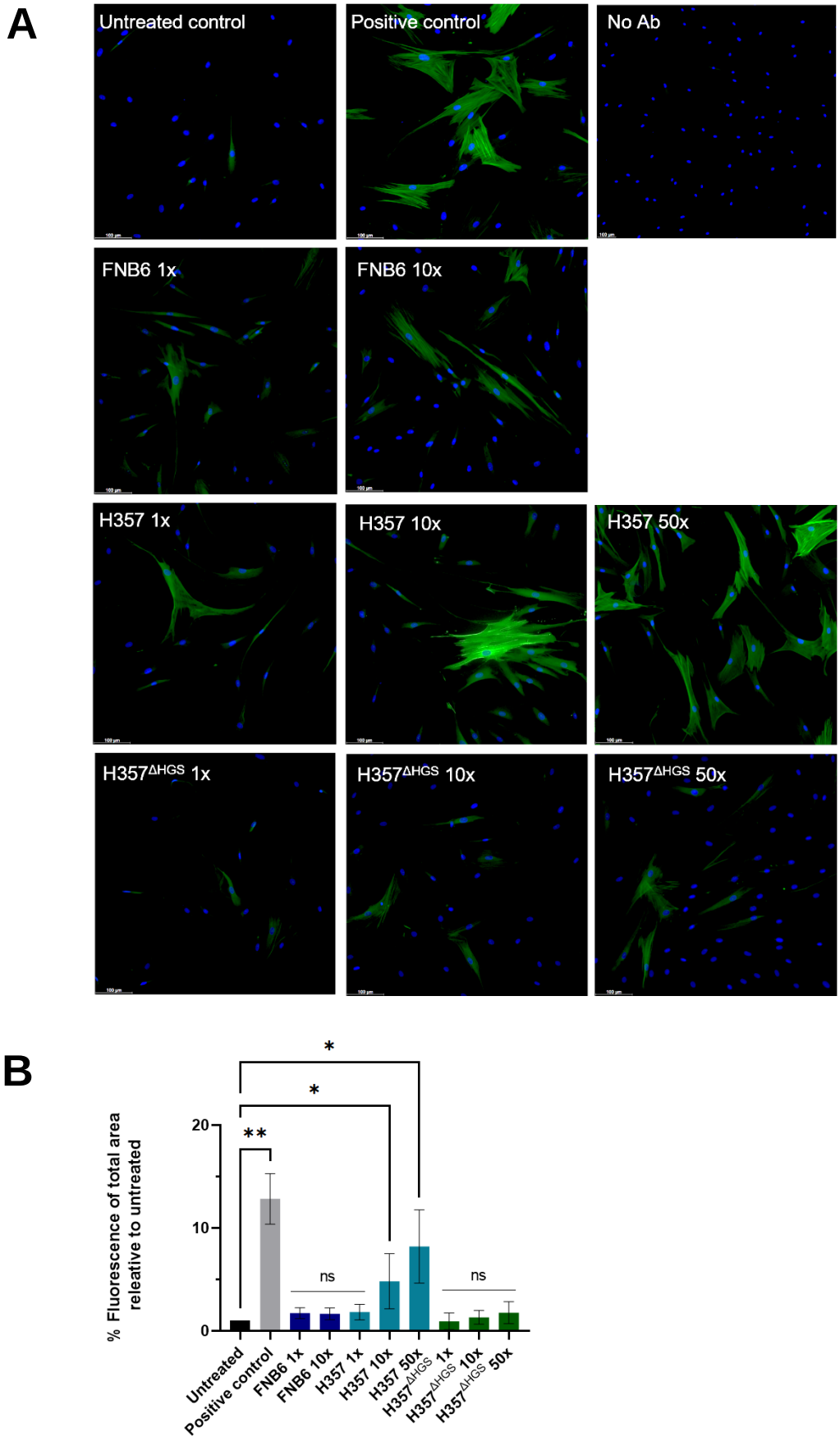

Figure 5.10 α-SMA stress fibre formation in normal oral fibroblasts treated with EVs for 48h. NOFs were seeded onto glass-coverslips and cultured without serum for 24h before incubation with FNB6, H357 or H357$^{\Delta HGS}$-derived EVs for 48h. Doses were calculated based on the average number of secreted particles/cell in conditioned medium from each cell line (A) Representative images where green staining indicates α-SMA and DAPI stains nuclei blue (B) Fluorescence area percentage was calculated using ImageJ from 3 random areas per well at a lower objective . Positive control refers to NOF treated with 5 ng/mL TGF-β1. Images were taken using a Leica THUNDER fluorescent microscope. Data is presented as mean ± SD for N=3, n=3. Statistics performed by Kruskall-Wallis test with BKY multiple comparison. ns, non-significant, *p<0.05, **p<0.01.

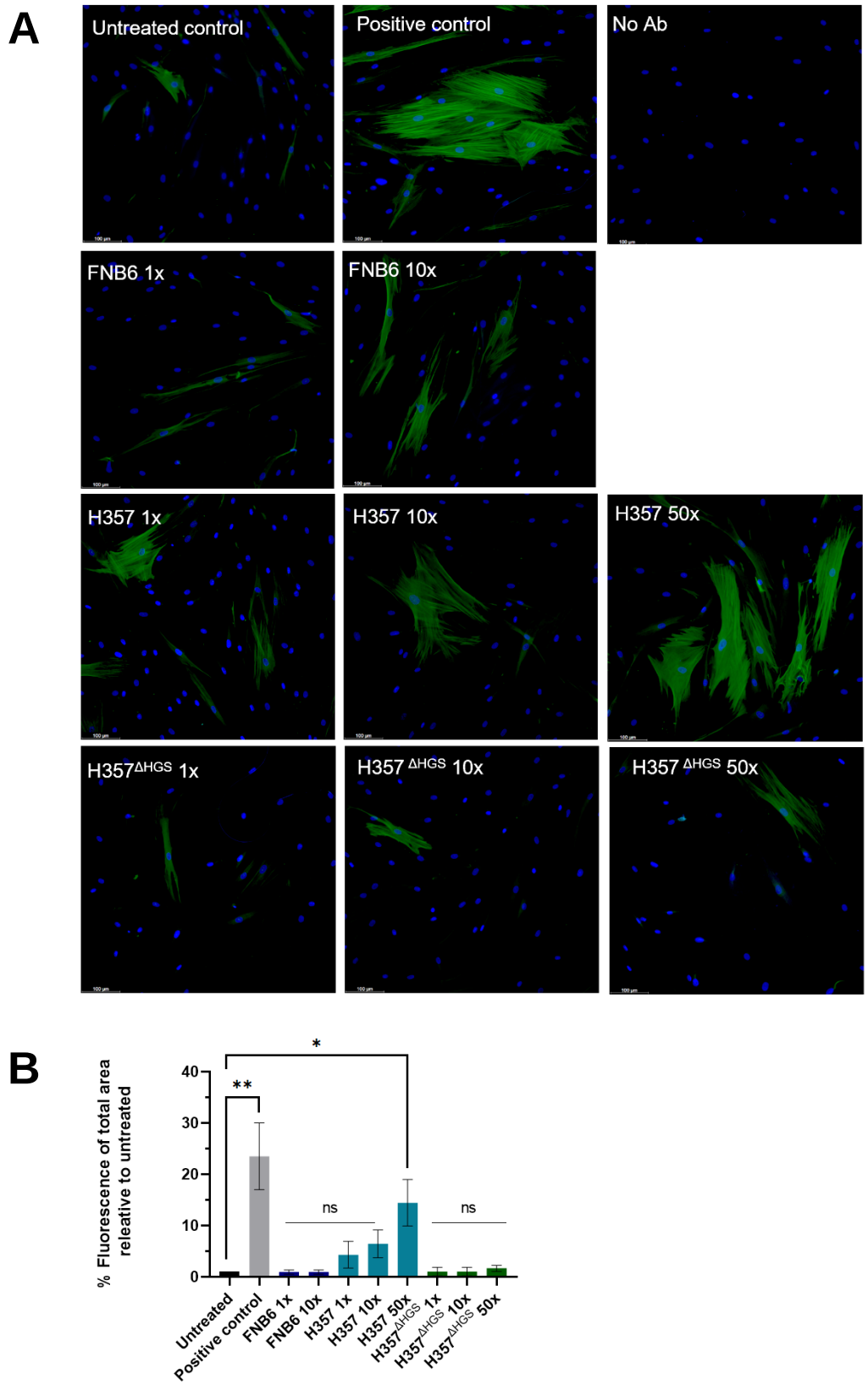

Figure 5.11 α-SMA stress fibre formation in normal oral fibroblasts treated with EVs for 72h. NOFs were seeded on glass-coverslips and cultured without serum for 24h before incubation with FNB6, H357 or H357$^{\Delta HGS}$-derived EVs for 72h. Doses were calculated based on the average number of secreted particles/cell in conditioned medium from each cell line (A) Representative images where green staining indicates α-SMA and DAPI stains nuclei blue (B)Fluorescence area percentage was calculated using ImageJ from 3 random areas per well at a lower objective . Positive control refers to NOF treated with 5 ng/mL TGF-β1. Images were taken using a Leica THUNDER fluorescent microscope. Data is presented as mean ± SD for N=3, n=3. Statistics performed withKruskall-Wallis test using BKY multiple comparisons. ns, non-significant, *p<0.05, **p<0.01.

Treatment of NOF with soluble TGF-β1 and H357 EVs (50x) both induced significantly greater fluorescent area compared to the untreated control. To determine potential differences in stress fibre conformation we quantified aspect ratio, the ratio of width to height, for NOFs in each treatment group (Figure 5.12). At 48h, H357 EV treatment there appears to be a larger population of cells with a greater aspect ratio compared to the positive control, however with averages shown to be 4.3 and 4.5 respectively, there is no significant difference. At 72h treatment both conditions show more cells with a greater aspect ratio and there is no significant difference between treatment groups.

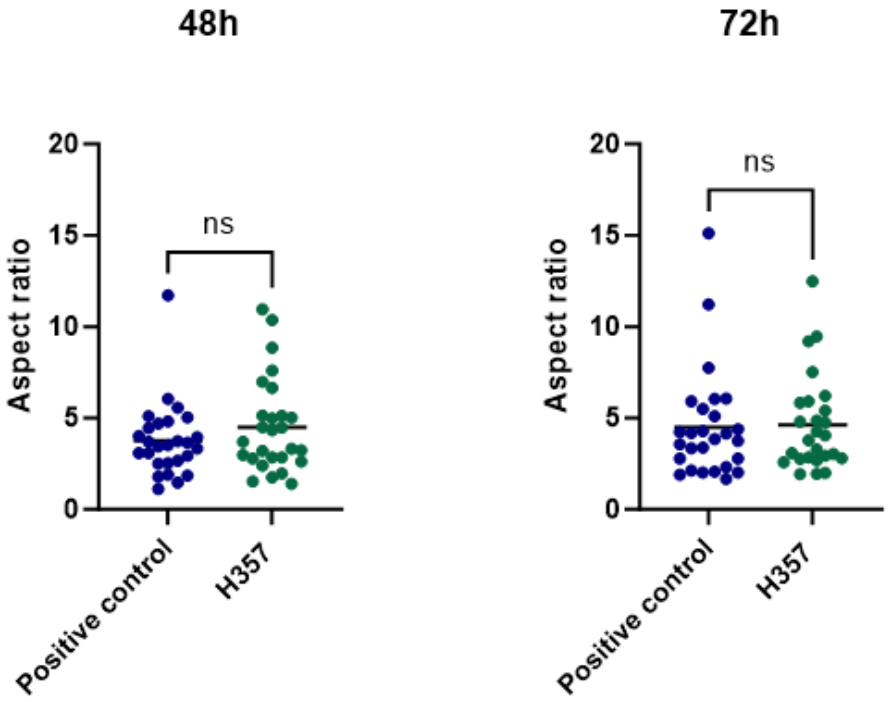

Figure 5.12 Aspect ratio of NOFs treated with H357 EVs. Aspect ratio was quantified using ImageJ based on α-SMA staining. Each dot represents an individual cell. Data is presented as mean ± SD for N=3, n=3. Statistics performed by Student's t-test. ns, non-significant.

5.2.5 OSCC EVs increase α-SMA expression in NOFS in TGF-β dependent manner.

As we have shown significantly higher levels of TGF-β1 associated with H357 EVs compared to FNB6 (by ELISA), we investigated whether the observed increase in α-SMA stress fibre formation in NOFs upon H357 EV treatment was attenuated with TGF-β blocking.

Compared to the untreated control, we observed significantly increased levels of α-SMA staining with TGF-β1 ($p < 0.01$), TGF-β1 + IgG control and H357 EV ($p < 0.05$) treated NOFs, showing 25.6%, 24.5% and 15% positive fluorescent area, respectively (Figure 5.13). The addition of TGF-β neutralising antibody to TGF-β1 treatment caused a 23.2% reduction in fluorescent area. Moreover, TGF-β blocking significantly ($p < 0.05$) attenuated the increase in α-SMA fibres caused by H357 EV treatment by 10.5% fluorescent area.

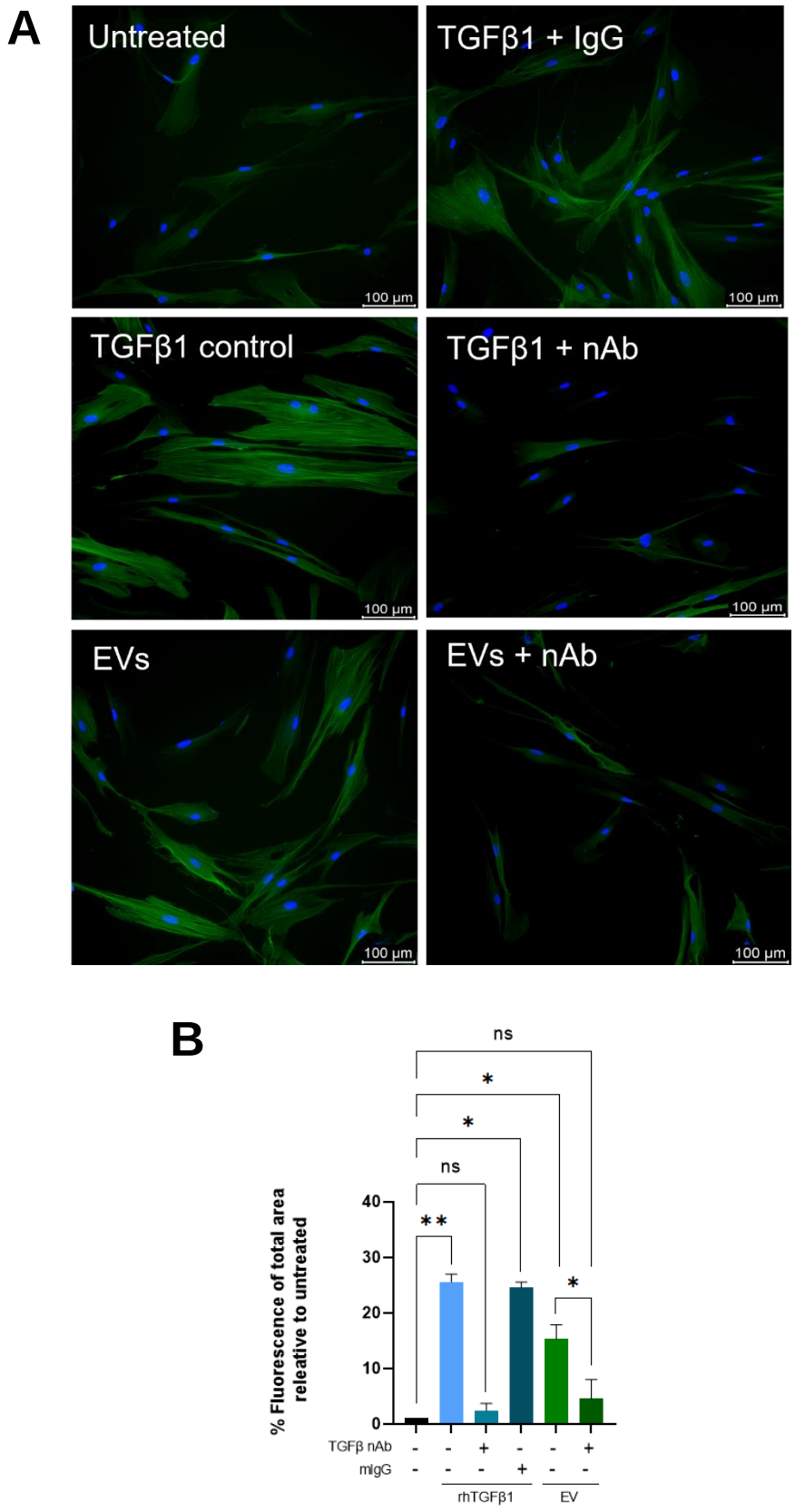

Figure 5.13 α-SMA fibre formation in OSCC EV treated NOFs with TGFβ blocking. NOFs were growth arrested for 24h before incubation with H357 EVs (50x conditioned media dose) or TGF-β1 in the presence or absence of TGF-β1–neutralizing antibody (at 10 µg/mL) or IgG isotype-matched antibody (at 10 µg/mL) for 72h. (A) Representative images where green staining indicates α-SMA and DAPI stains nuclei blue (B) Fluorescence area percentage was measured using ImageJ. Images were taken using a Leica THUNDER fluorescent microscope. Data is presented as mean ± SD for N=3, n=3. Statistics performed byKruskall-Wallis test with BKY multiple comparisons and Wilcox t-test. ns, non-significant, *p<0.05, ****p<0.01.

5.2.6 Functional effects of NOF treatment with OSCC-derived EVs

The expression of α-SMA by myofibroblasts has been linked directly to wound contraction (Jester et al., 1995). As we have demonstrated significant increase in α-SMA stress fibres with 50x conditioned medium dose of H357 EVs, we next sought to investigate the effect of this treatment on NOF contraction. NOFs were pre-incubated with EVs for 24h prior to being mixed with collagen I and allowed to set to observe collagen contraction over 72h. Compared to the untreated control, H357 EV treated NOFs caused significantly increased collagen contraction over 48 and 72h ($p < 0.01$), with an overall reduction in area to 0.43 that of the untreated (Figure 5.14). This is comparable to the positive control, which had an area 0.4 relative to the untreated at 72h.FNB6 EV treatment did not induce a significant change in area compared to the untreated control at any time point and showed an area of 0.93 relative to the untreated control at 72h. At 24h and 48h there was significantly ($p < 0.05$) greater contraction in NOFs treated with H357 EVs than FNB6 EVs.

We next looked at the ability of EVs to induce wound healing in NOFs, as myofibroblasts have been shown to generate the contractile forces required for wound closure and healing (Garrett et al., 2004). After 24h incubation with TGF-β1, NOFs displayed significantly ($p < 0.01$) more wound closure compared to the untreated control (Figure 5.15). H357 EV treatment for 24h induced wound closure by 28.2% which was significantly different to the untreated ($p < 0.05$). FNB6 EVs induced wound closure by 13.1%, which was not significantly different to the untreated (Figure 5.15).

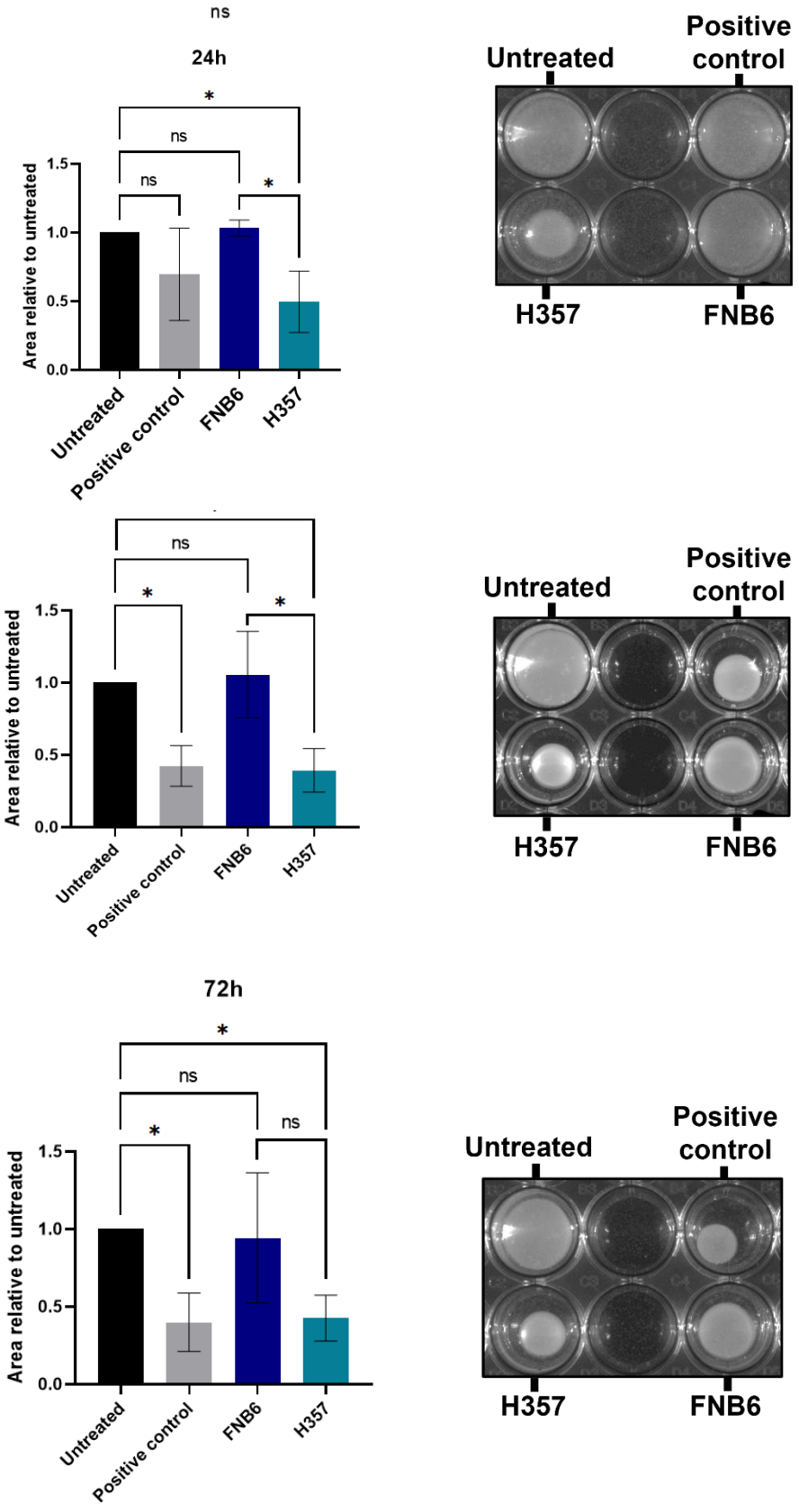

Figure 5.14 Collagen contraction ability of NOFs cultured with oral cell derived EVs. NOFs were cultured without serum for 24h prior to incubation for a further 24h with 50x the conditioned media dose of H357 EVs, 10x the conditioned media dose for FNB6 EVs or 5 ng/mL TGF-β1. NOFs were seeded into rat tail collagen (5 mg/mL), allowed to set and incubated at 37°C, 5% CO_2 for 24, 48 and 72h. Gel area was calculated using Image J. Data represents ± SD for N=3, n=3. Statistics performed by one-way ANOVA with Dunnet's multiple comparisons. ns, non-significant, *p<0.05..

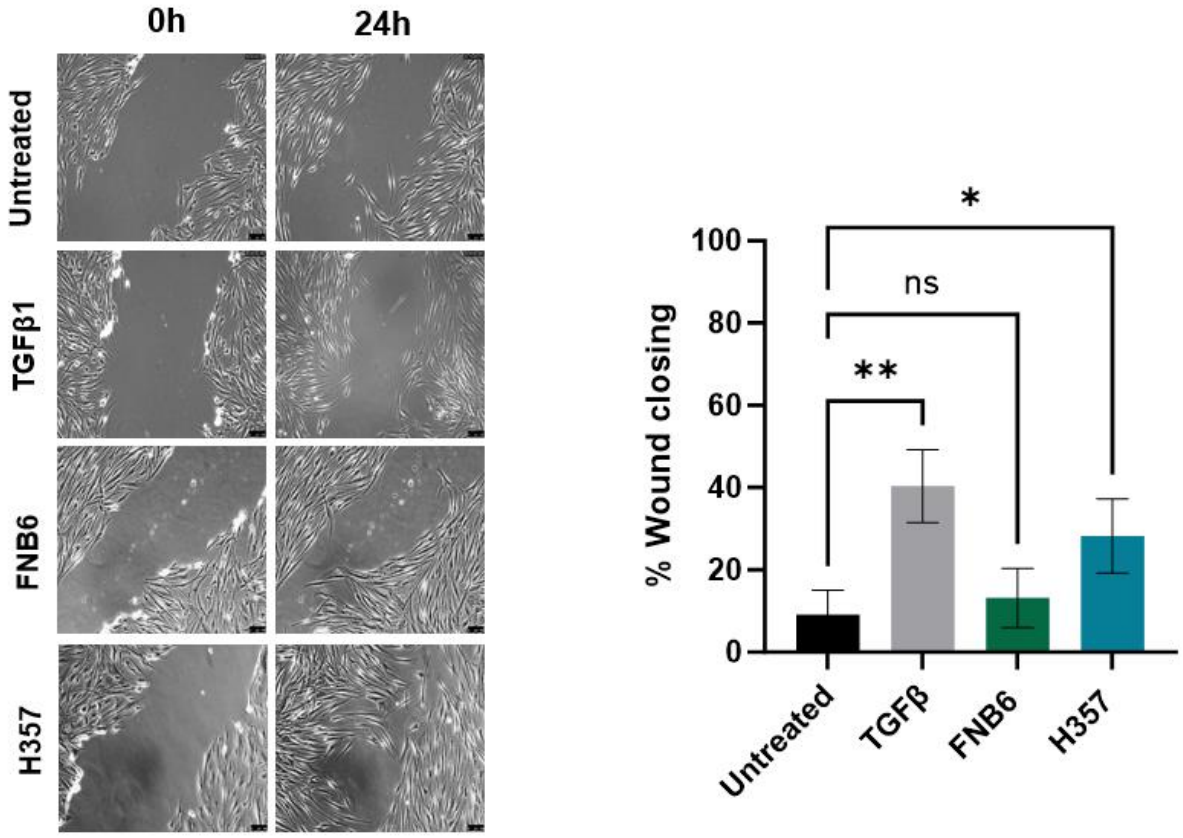

Figure 5.15 Wound healing assessment of NOFs treated with oral cell derived EVs. NOFs were cultured without serum for 24h and incubated for 1h with Mitomycin C to inhibit proliferation. A scratch was made across the well and cells were incubated for 24h with 50x the conditioned media dose of H357 EVs, 10x the conditioned media dose for FNB6 EVs or 5ng/mL TGF-β1. Three positions across random points of the scratch were imaged every 15 mins for 24h using a Leica THUNDER live imaging platform. Wound area closure was calculated using Image J. Data represents ± SD for N=3, n=3. Statistics performed by one-way ANOVA with Dunnet's multiple comparisons. ns, non-significant, *p<0.05, **p<0.01.

We also tracked and quantified the differences in motility of NOFs treated with EVs (Figure 5.16 and 5.17). NOFs treated with H357 EVs generated 200µm more accumulated distance and 135.3µm more Euclidian distance (distance between the starting and final point) than FNB6 EV treated NOFs (Figure 5.16A and B). Complimentary to the wound healing, compared to the untreated, accumulated and Euclidian distance in the H357 EV treated NOFs was significantly different ($p < 0.01$, $p < 0.001$, respectively), However, there was no significant difference with FNB6 EV treatment compared to the untreated (Figure 5.16A and B). TGF-β1 and H357 EV treated NOFs moved similar distances, migrating 297 ± 41 µm and 299.5 ± 71.5 µm in accumulated distance and 217.6 ± 18.6 µm and 216.8 ± 38.2 µm in Euclidian distance, respectively. Moreover, both TGF-β1 and H357 EV treated NOFs showed a significantly higher rate of velocity compared to the untreated ($p < 0.05$, $p < 0.01$, respectively), whereas there was no significant difference for FNB6 EV treatment.

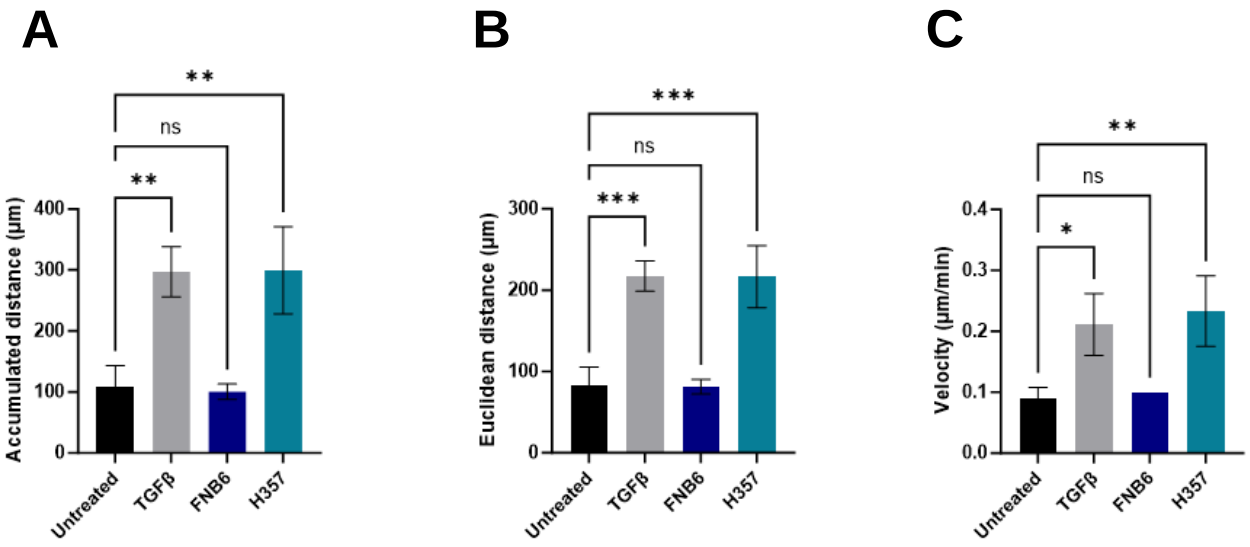

Figure 5.16 Motility of NOF treated with oral cell derived EVs. (A) Accumulated distance (B) Euclidian distance and (C) Velocity of NOFs treated with EVs during wound healing assay. 3 cells from either side of the scratch (6 total) were tracked using Tracking Tool™ PRO software for each technical repeat. Data represents ± SD for N=3, n=3. Statistics performed by one-way ANOVA with Dunnett's multiple comparison. ns, non-significant, *p<0.05, **p<0.01, ***p<0.001

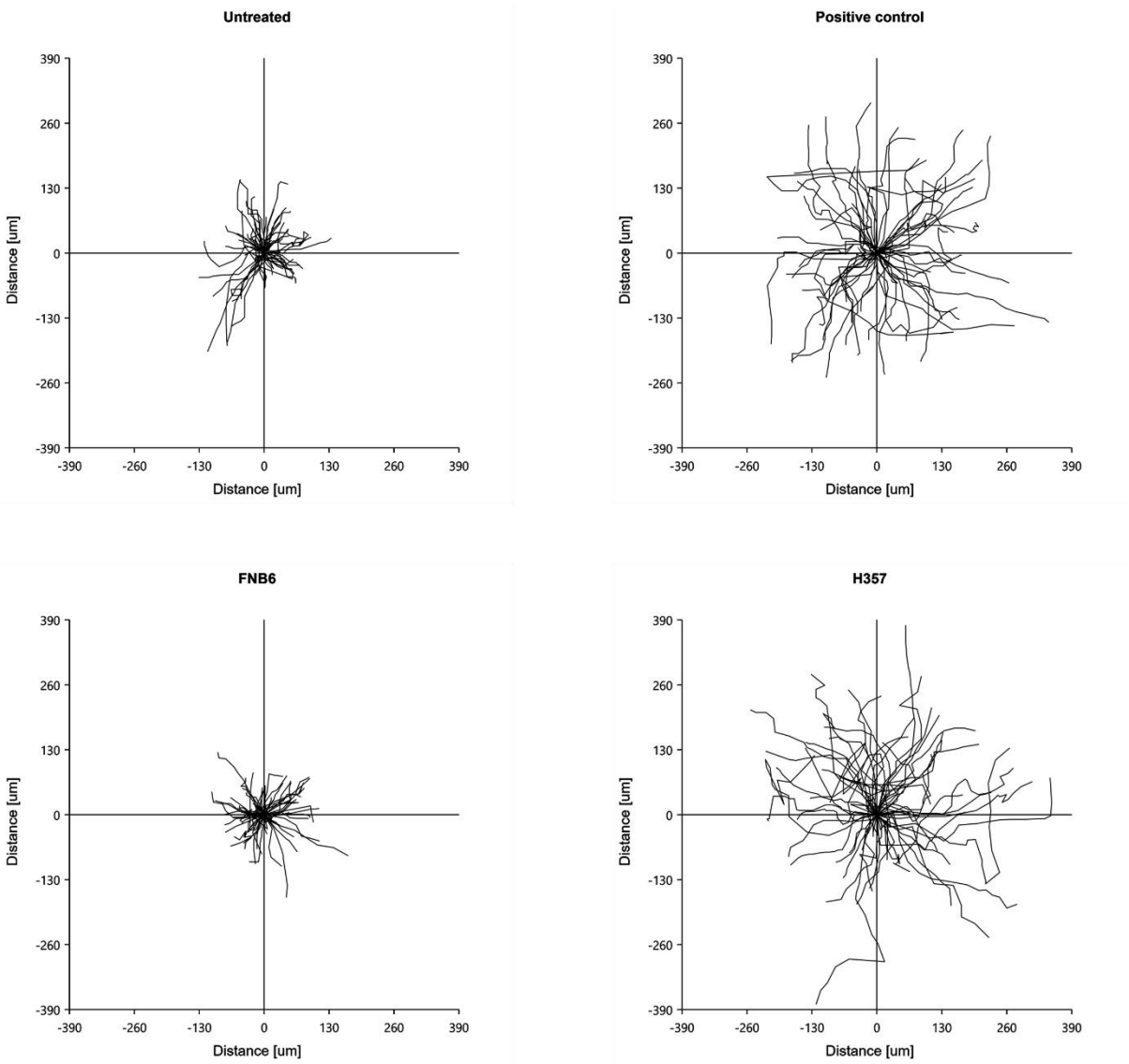

Figure 5.17 Representative rose plots depicting total path of EV treated NOFs. 3 cells from either side of the scratch (6 total) were tracked using Tracking Tool™ PRO software for each technical repeat. Data represents ± SD for N=3, n=3.

5.3 Discussion

5.3.1 CAF marker transcript levels are not altered with oral cell co-culture or EV treatment

In this chapter we first assessed changes in CAF marker gene expression in NOFs co-cultured with FNB6, H357 and H357$^{\Delta HGS}$ cells and EVs. We observed no significant change in α-SMA, FAP or COL11A1 transcript levels for any treatment condition. Shepard *et al* conducted a similar experiment, co-culturing normal keratinocytes directly with human dermal fibroblasts for four days and demonstrated a 2.4-fold increase in α-SMA gene expression in fibroblasts (Shephard et al., 2004). This effect was shown to be dependent on fibroblast proximity to keratinocytes, as α-SMA levels were similar to the untreated control when cells were separated via a transwell (Shephard et al., 2004). Furthermore, we observed no change in CAF marker transcript levels in our co-culture at 24 and 48 hour time points, however another study used a similar transwell system to demonstrate increased FAP transcript levels in normal human dermal fibroblasts co-cultured with primary and metastatic melanoma cells for 72 hours (Mazurkiewicz et al., 2022). Thus, indicating that longer time points may be necessary to observe significant change. Interestingly, an siRNA screen of ESCRT components identified that downregulation of ESCRT machinery increased the outputs of TGF-β signalling by trapping receptors in internal compartments and increased α-SMA expression in a mouse epithelial cell line (Miller et al., 2018). Therefore, we might expect increased TGF-β signalling in H357$^{\Delta HGS}$ cells and enhanced TGF-β1 due to autocrine signalling in cancer cells, thus leading to greater NOF activation (Ungefroren, 2021). However, we saw no significant increase,

indicating that HGS KO may not affect TGF-β secretion in our cell line, or that the reduction in particle release is a greater effector of α-SMA.

Despite no change in transcript level, we observed a significant increase in α-SMA stress fibre formation in NOFs co-cultured with H357 cells for 72 hours. Although, Fozzatti *et al* demonstrated by western blotting an increase in α-SMA by ~4-fold after co-culturing with 8505c (thyroid carcinoma) cells for only 24 hours (Fozzatti et al., 2019). Furthermore, fibroblasts treated with conditioned media from 8505c for 24 hours, showed increased α-SMA, platelet derived growth factor receptor (PDGFR)-β and vimentin protein levels (Fozzatti et al., 2019). This may indicate cancer cells can affect fibroblasts in a paracrine like manner. Similar results have been shown in the context of oral cancer. Al-Magsoosi *et al* generated conditioned media from oral cancer cell lines induced into cancer stem cells by adherence to fibronectin or cisplatin resistance. Exposure of NOFs to this conditioned media for 48 hours increased the transcript expression and protein abundance of α-SMA and interleukin (IL)-6 (Al-Magsoosi et al., 2021).

Similar to the transwell system, EV treatment induced no change in CAF marker transcript levels relative to the untreated control. Most investigations into the role of cancer derived EVs in fibroblast activation have looked solely at CAF marker protein level (Webber et al., 2010; Purushothaman et al., 2016; Yeon et al., 2018; Huang et al., 2021). However, Gu *et al* looked at the ability of gastric cancer cell line derived EVs to promote a CAF-like phenotype in human mesenchymal stem cells. After 36 hours treatment with 800 μg/mL EVs, MSCs displayed significantly higher levels of FAP, IL-6 and α-SMA mRNA (Gu et al., 2012).

One explanation for the lack of change in transcript expression, despite an increase in stress fibre formation in both co-culture and EV treatment conditions could be due to fibroblast heterogeneity in primary cultures. Distinct CAF populations in OSCC have been grouped according to differential single cell gene expression into: mesenchymal CAFs, inflammatory CAFs and cycling CAFs (Sun et al., 2023). Gene set enrichment analysis showed that mesenchymal CAFs had enriched TGF-β pathways, indicating that some fibroblasts may upregulate α-SMA more strongly than others (Sun et al., 2023). This single cell sequencing data may suggest that the increase in mRNA expression for our chosen CAF markers is masked when mRNA levels are averaged over the entire treatment population.

Moreover, there may be differences in EV uptake mechanisms. Single cell sequencing of skin fibroblasts has identified six subpopulations of fibroblasts with distinct genetic signatures (Vorstandlechner et al., 2020). Some of the most highly differentially expressed mRNAs were ECM components including collagens, elastin, fibronectin (FN) and fibrillin (Vorstandlechner et al., 2020). EV docking and entry into cells is known to involve ECM components, for example, FN has been shown to bind to the herparan sulfate proteoglycan on exosomal surfaces and facilitate their uptake into cells (Purushothaman et al., 2016; Buzás et al., 2018). Therefore, differential secretion of ECM molecules may cause differences in uptake and subsequently signal transduction in certain fibroblast populations, meaning that only a subset of cells respond significantly to EV treatment.

5.3.2 OSCC EVs associate with NOFs

Colocalisation analysis with early endosome marker EEA1, showed that CD63-GFP labelled H357 EVs were taken up into NOFs as early as 30 minutes after treatment.

We observed an increase in co-localisation after 1 hour, however a decrease at 4 hours before an increase again at 6 hours. This matches observations in breast cancer cells, whereby CD63-GFP labelled exosomes were shown to colocalise with EEA1 after 30 minutes (Koumangoye et al., 2011). After 1 hour exosomes were in late endosomes, as marked by CD71, for at least 2 hours. Following this, at 4 hours the exosomes colocalised with recycling endosomes, as indicated by LAMP1 positivity (Koumangoye et al., 2011). This may suggest that the decrease in EEA1 colocalisation we see at 4 hours is due to EVs moving out of early endosomes and being recycled and targeted to the lysosome, however late endosomal marker staining would be necessary to confirm this. An increase in colocalisation again at 6 hours may be due to more EVs being internalised and localising within early endosomes. The number of EVs taken up by cells over time may be better investigated using flow cytometry to confirm fluorescence intensity in recipient cells. This method has previously been used to demonstrate that prostate cancer EV uptake increased over time up to 12 hours (Lázaro-Ibáñez et al., 2017). Colocalisation with EEA1 may suggest that CD63 positive EVs are taken up by clathrin-mediated endocytosis, as shown in ovarian cancer cells, however further investigation by blocking this uptake mechanism would be useful in confirming this (Escrevente et al., 2011).

5.3.3 OSCC EVs increase α-SMA in a TGFβ dependent manner

We showed that TGF-β1 is present in higher levels on the surface of OSCC-derived EVs compared to normal oral keratinocytes. TGF-β has been shown to exist bound on the vesicle surface or within the soluble compartment, depending on the cancer of

origin. Goulet *et al* utilised proteinase K digestion, which degrades only proteins localised to the EV surface, to show that TGF-β levels in bladder cancer-derived EVs were not reduced upon treatment, indicating localisation in the lumen (Goulet et al., 2018). However, in both prostate and melanoma cancer derived-EVs TGFβ has been shown to be more greatly associated with the EV membrane (Webber et al., 2010; Yeon et al., 2018). In contrast to our findings, another study investigating HNSCC-derived EVs showed that TGF-β1 was primarily located in the EV lumen rather than the surface, however it was not clear which form of TGF-β1 they were detecting. Interestingly, we observed greater proportions of latent TGF-β than its active form, giving rise to questions about the conformation required for signalling.

Although preliminary data, in contrast to this, analysis of enriched SEC preparation by Nano-Flow Cytometry showed similar proportions of TGF-β1 positive particles from FNB6 and H357 cells. The anti-TGF-β1 antibody used detects both latent and active form, whereas the ELISA detects only the active form, meaning it is necessary to activate latent TGF-β1using HCl. It may be the case that the antibody detecting only the active form is more specific, whereas the latent and active binding antibody may not be able to detect latent TGF-β1 held in a different configuration on the EV surface. Nevertheless, NTA suggests that H357 release more particles than FNB6, meaning that we can assume more EV associated TGF-β1 is released by H357 cells. Moreover, the colocalisation of TGF-β1 with tetraspanins was low, suggesting that TGF-β1 may be more enriched in different EV populations. As this analysis does not take into account the number of TGF-β1 molecules per particle, there may be populations with a high number of TGFβ1 molecules compared to others. Furthermore, we cannot distinguish between the three tetraspanins, meaning any preferred colocalisation of highly TGF-β1 associated EVs with one of the three tetraspanins cannot be identified.

We were able to demonstrate that upregulation of α-SMA stress fibres in NOFs is dependent on TGF-β1 associated OSCC-EVs. This has been shown in other cancer types, for example, uptake of bladder cancer exosomes by normal fibroblasts has been shown to increase their proliferation and upregulate the CAF markers α-SMA, FAP and galectin (Goulet et al., 2018). Incubation of exosomes with a TGF-β neutralising antibody prior to culturing with NOFs attenuated the increase in CAF markers (Goulet et al., 2018). The same findings were mirrored in prostate cancer whereby these EVs express latent TGF-β and initiate the SMAD3 signalling pathway to promote a CAF phenotypic switch in normal fibroblasts (Webber et al., 2010). Prostate cancer EVs also stimulated the formation of a hyaluronic acid pericellular coat around fibroblasts, which is a marker of myofibroblast phenotype (Webber et al., 2010) Huang *et al* had supporting findings in HNSCC, showing that TGF-β1 associated with EVs initiated CAF conversion, however they observed no change in the canonical TGFβ-SMAD signalling pathway (Huang et al., 2021). Proteomic analysis of NOFs treated with TGF-β overexpressing EVs showed that fibronectin was upregulated and its silencing in CAFs reduced α-SMA expression (Huang et al., 2021).

HNSCC-derived EVs have further been implicated in reprogramming the tumour microenvironment via TGF-β. Ludwig *et al* demonstrated that HNSCC patient plasma-derived exosomes associated with TGF-β at higher levels compared to healthy controls and interestingly, the level of active TGF-β correlated with tumour size (Ludwig et al., 2023). Furthermore, these EVs were able to reprogram macrophages and endothelial cells into a pro-angiogenic phenotype, upregulating SMAD2 in the latter (Ludwig et al., 2022, 2023).

5.3.4 OSCC EVs increase NOF contraction and migratory abilities

We observed that NOFs treated with OSCC-EVs had increased contraction compared to untreated controls. Remodelling of the TME by CAFs plays an important role in altering matrix stiffness and contributing to the development of solid tumours. Zhang *et al* demonstrated that HNSCC derived CAFs contracted collagen greater than NOFs, and that this was due to lysyl oxidase (LOX) catalysing collagen crosslinking and increasing matrix stiffness (Zhang et al., 2021b). Moreover, the collagen stiffness created by these CAFs promoted invasion in OSCC cells by activating the FAK phosphorylation pathway (Zhang et al., 2021).

Stiffness, as measured by increased collagen organisation, has been shown to correlate with advanced disease and shorter recurrence-free survival time in OSCC (Matte et al., 2019). One study looked at the role of stiffness and EVs in breast cancer (BC) and showed that stiff tissues secreted higher levels of EVs compared to soft adjacent tissue. EVs derived from BC cells grown on matrices modelling stiff tissues, termed ‘’stiff’’ EVs, had increased adhesion molecule presentation compared to soft normal tissue derived EVs (‘’soft EVs’’) (Sneider et al., 2023). The stiff EVs were able to aid cancer cell dissemination *in vivo*. ‘’Soft’’ EVs increased the expression of α-SMA, COL1A1 and VEGFA in lung fibroblasts compared to the stiff EVs and upregulated signalling proteins linked to primary tumour growth. The authors theorised that stiff EVs from the primary site promote migration towards secondary sites with softer matrices, whereby cancer cells release soft EVs and transform the surrounding stroma to promote tumour growth (Sneider et al., 2023). This implicates EV-delivered TGF-β in potentially maintaining a stiff TME and contributing to metastasis.

Furthermore, we observed that OSCC-EVs induced an increased migratory in fibroblasts compared to the untreated. Multiple EV cargos and mechanisms have been implicated in orchestrating this in other cancer types; annexin A2, MMP2, desmoyokin, FAK-integrin and STAT3/YAP signalling pathways (Zhang et al., 2013; Silva et al., 2016; McAtee et al., 2019; Chang et al., 2023). In HNSCC, Huang *et al* also showed that treatment of fibroblasts with EVs derived from a TGF-β overexpressing cancer cell line caused even greater migration than the wildtype cell line derived EVs, indicating a role for TGF-β in migration (Huang et al., 2021).

5.3.5 Conclusion

In this chapter we have demonstrated that co-culture of NOFs with OSCC cells causes significantly enhanced α-SMA expression, an effect which could not be replicated using H357$^{\Delta HGS}$, indicating a possible EV dependent mechanism. Isolation of EVs from FNB6, H357 and H357$^{\Delta HGS}$ revealed that TGF-β1 was present on the surface of EVs at greater levels than in the conditioned media and primarily in its latent form. Moreover, H357 EVs associated with significantly higher levels of latent TGF-β1 compared to FNB6 and H357$^{\Delta HGS}$. Treatment of NOFs with H357 EVs significantly increased the α-SMA stress fibres, which was abrogated by pre-treatment of EVs with a TGF-β blocking antibody, highlighting an EV-TGF-β1 dependent mechanism for fibroblast activation. Moreover, at 24 and 48h H357 EVs enhanced NOF contraction greater than FNB6 EVs.Both migration and contraction of NOFs was signficantly enhanced with treatment with H357 derived EVs compared to the untreated.

6 Final discussion

6.1 TGF-β's Latent Form: A Fascinating Bond with EVs

The majority of TGF-β1 we found in the conditioned medium of cancer cells was associated with EVs and in its latent form. This observation is in line with previous studies (Webber et al., 2010; Shelke et al., 2019), and raises questions: How is TGF-β1 is held in this conformation and why this is preferred?

Inactive TGF-β1 bound to LAP can associate with the extracellular matrix by binding to heparan sulphate glycoproteins (HSPGs) (Rider et al., 2017). Indeed, a correlation has been found between levels of TGF-β and betaglycan, also known as TGF-β type III (TGFβRIII), on cancer-derived EVs (Webber et al., 2010). Incubation of these EVs with mesothelioma cells in a betaglycan-cleaving microenvironment reduced exosomal associated TGF-β levels, thus implicating it in EV tethering (Webber et al., 2010). Further work has looked more specifically at the role of the heparan sulphate side chains of HSPGs in TGFβ1-EV tethering (Webber et al., 2015; Shelke et al., 2019). Shelke *et al* showed that treatment of EVs with heparinase-II reduced inactive TGF-β1 levels. EVs derived from mast cells treated with a proteoglycan synthesis inhibitor had reduced latent TGF-β1 levels, whereas levels of the active form remained the same (Shelke et al., 2019). When Webber *et al*. used the more specific heparinase III, which cleaves heparan sulphates from the proteoglycan backbone, the levels of EV-TGFβ1 were unchanged, indicating that it binds to the betaglycan backbone and not the side chains. However, treatment of these enzymatically digested EVs onto fibroblasts could not induce increased α-SMA expression as the untreated ones, indicating that these heparan sulphate side chains are still important for the signalling of TGF-β in target cells (Webber et al., 2010).

Glycoprotein A repetitions predominant (GARP) is a transmembrane cell surface docking receptor for latent TGF-β1, which has been studied predominantly for its ability to enhance latent TGF-β activation in Treg cells. However, the distinct mechanisms for this are unclear (Metelli et al., 2018). Recently, it has been shown that the latent TGFβ:GARP complex is tethered to small EVs produced by lymphocytes and becomes activated (Burlingham et al., 2023). As integrins αVβ6 and αVβ8 have been implicated in force-dependent activation of TGF-β from the GARP:TGFβ complex, it was proposed that EV bound GAP:TGFβ is incorporated into the surface membrane of a cell, followed by αVβ8 integrin on an opposing cell binding to the LAP molecule creating a pulling force that either releases free TGF-β1 or exposes TGF-β1 loosely bound to GARP:LAP to its receptor (Wang et al., 2012; Campbell et al., 2020; Burlingham et al., 2023). Although there are currently no studies showing the expression of GARP:TGFβ on cancer derived EVs, it is known that GARP is widely expressed in multiple cancer cell types, indicating the possibility of its tethering to their EVs (Bouchard et al., 2021). However, Xing *et al* demonstrated that mesenchymal stem cells (MSC) derived EVs express GARP, and its knockdown produced EVs that had a reduced ability to promote proliferation, migration and invasion of mouse colon cancer cells (Xing et al., 2020). This implicates EV associated GARP in pro-tumorigenic signalling. In addition, αVβ6 integrin expression on colorectal cancer cells has been implicated in fibroblast activation by activating TGF-β, thus contributing to the proposed GARP-integrin TGFβ activation mechanism.

Moreover, EV-associated LAP-TGFβ has been shown to be taken up into the endosomal compartment and have more sustained signalling effects compared to unbound soluble TGF-β1. The increase in SMAD2 phosphorylation at 60 minutes stimulation was abrogated by pretreatment of cells with an inhibitor of endo-lysomal

acidification, indicating that TGF-β1 is activated in internal compartments (Shelke et al., 2019).

Taken together, this data suggests that TGF-β1 is bound in latent form on EVs by HSPGs and GARP. This could be a mechanism which allows sequestering of low abundance bioactive molecules to facilitate their presentation at the cell surface, allowing sustained signalling and a positive feedback loop between cells. This may be an explanation as to why co-culture of the EV deficient cell line H357$^{\Delta HGS}$ with fibroblasts failed to induce α-SMA stress fibres, as there was a reduction of EVs available to increase the presentation and concentration of TGF-β1 at the cell surface. Future work could look at these potential tethering mechanisms of latent TGF-β1 on OSCC-EVs to determine their role in EV-mediated TGFβ signalling between cells in the TME. Knockdown of certain tethering molecules would give an indication if EV-bound TGF-β1 is the preferred mechanism of TGFβ signalling initiation by cancer cells compared to unbound active TGF-β1.

6.2 EV bound TGF-β1 as a therapeutic target?

In the context of cancer, TGF-β has dual tumour promotor and suppressor effects, meaning there have been challenges in targeting this therapeutically. However, TGF-β mediates most of its cancer promoting effects by tumour-stroma interactions, therefore its use as a TME targeting strategy may be more appropriate. Specific targeting of EV associated TGF-β1 which has both alternate conformation and signalling kinetics makes it a possible alternate target.

Chen *et al* investigated EVs derived from cancer stem cells (CSCs) and observed, amongst others, higher TGF β mRNA and protein cargo compared to OSCC cells

(Chen et al., 2020). Treatment with ovatodiolide (OV), an anti-inflammatory, and STAT3 knockdown was shown to reduce EV associated TGF-β levels. Functionally, treatment of CSC cells with OV reduced the ability of their EVs to increase secreted TGF-β from normal fibroblasts, an indicator of a CAF-like phenotype. Moreover, OV abrogated the increased OSCC cell colony formation and migration induced by CSC EV treatment, thus implicating it as a therapy to suppress both tumourigenesis and the TME (Chen et al., 2020).

Radiation is reported to promote TGF-β activation via reactive oxygen species (ROS) and this can contribute to resistance by creating an immunosuppressive environment. In their irradiated BC model, Zhang *et al* showed increased EV-TGF-β levels and Tregs via expression and phosphorylation of protein kinase (PK)-C- ζ (Zhang et al., 2023). Inhibiting PKC- ζ reduced EV-TGFβ1 secretion and improved radiotherapy efficacy by downregulating the radiation-activated superoxide-Zinc-PKC-ζ-TGF-β1 EV pathway. (Zhang et al., 2023). Indeed, it has been shown previously that PKCs may regulate the secretion of EVs, meaning PKC- ζ could be a potential drug target for specific reduction of EVs that associate with TGF-β1 (Simon et al., 1996; Siddiqi et al., 2008).

As discussed previously, molecules involved in binding latent TGF-β are another potential target. 264RAD is a human monoclonal antibody (mAb) targeting αvβ6 and αvβ8 integrins (Eberlein et al., 2013). Preclinical data showed that 264RAD inhibited cancer cell invasion and MMP-9 production, as well as activation of dermal skin fibroblasts, shown by reduction of fibronectin and α-SMA levels *in vivo* (Eberlein et al., 2013; Reader et al., 2019). Although this agent has not reached clinical trial stage, other blocking antibodies and small molecules against αvβ6 integrin are currently under investigation for treatment against solid tumours (Brzozowska et al., 2022).

As mentioned previously, latent TGF-β is bound to βglycan on the EV surface allowing for sustained signalling. However, targeting this interaction for anti-tumour therapy may be complex. It has been shown there is a loss of TGFβRIII in BC and a negative correlation between TGFβRIII expression and disease progression (Bandyopadhyay et al., 1999). Restoring βglycan expression in BC cells inhibited tumour invasiveness and metastasis *in vivo*. This mechanism appears to be due to ectodomain shedding of TGFβRIII producing soluble TGFβRIII which binds and sequesters TGF-β to decrease its signalling (Bandyopadhyay et al., 1999). It's possible that blocking the interaction of latent TGFPβ and βglycan could make it more susceptible to cleavage and release in the soluble form, thus increasing pro-cancer effects.

Targeting the GARP:TGFβ1 complex has mainly been investigated in the context of immune escape in cancer. The use of a mAb that blocks TGF-β1 activation by GARP-expressing Tregs, has been shown to be effective in reducing fibrosis and tumour burden in Primary myelofibrosis (PMF) murine models (Lecomte et al., 2023). Assessment of hallmark signatures from spleens of mAb treated PMF mouse models found reduced TGF-β1 signalling in CD4+ T-cells and fibroblasts in treatment responder groups (Lecomte et al., 2023). Moreover, in combination with cancer immunotherapy, anti-PD-1, anti-GARP:TGF-β1 mAb induced an immune-mediated rejection of colon carcinoma tumours *in vivo* (de Streel et al., 2020). This antibody is currently being tested in patients with locally advanced or metastatic solid tumours (ClinicalTrials.gov: NCT03821935). This data supports GARP as a compelling TME therapeutic target for both overcoming immune evasion and limiting pro-oncogenic fibroblast activation. Further work investigating blockade of EV associated GARP:TGF-β1 as a means to promote anti-tumour immunity would be pertinent.

6.3 Exploring EV associated TGF-β as a potential biomarker

Recent studies have indicated EVs as favourable diagnostic/prognostic tools due to their accessibility from minimally invasive patient bodily fluids, such as saliva (Zhang et al., 2023). In OSCC, EVs carry substances that contribute to cancer progression which could be used as disease predictors. There have been many EV cargos linked to predicted poor prognosis of OSCC; HSP90α, HSP90β, CD63, Laminin-332, ApoA1, CXCL7, PF4V1 and F13A1 to name a few (Zhang et al., 2023).

Akin to the complexity of its role in cancer, there is conflicting evidence for TGF-β as a cancer biomarker. There are studies indicating a link between increased TGF-β1 expression and reduced mortality and improved survival rate in OSCC and soft tissue sarcomas (Sorbye et al., 2012; Elahi et al., 2020). There is also data showing no link between TGF-β1 and survival in HNSCC (Logullo et al., 2003). However, in non-small cell lung cancer TGF-β1 expression in infiltrating lymphocytes was associated with reduced postoperative survival time, thus highlighting the importance of the TME (Sterlacci et al., 2012). Interestingly, latent transforming growth factor beta binding protein 2 (LTBP2) expression in pancreatic cancer has been correlated with higher tumour stage and poorer overall survival, indicating that the form of TGF-β may be important for disease prediction (Wang et al., 2017). Indeed, increased levels of TGF-β1 associated with HNSCC plasma derived EVs can distinguish between heathy and HNSCC patients and was related to increased tumour stage and tumour size (Huang et al., 2021). In addition, the diagnostic efficacy of EV-bound TGF-β1 was greater than that for total TGF-β1 in plasma (Huang et al., 2021), suggesting that EV associated TGF-β1 is a more appropriate biomarker than the unbound form. However, there are challenges in the use of EVs as biomarkers due to their heterogeneity, which is likely to be context and cell type specific. Coupled with this, there are likely to be changes

in cargo type and abundance during cancer progression from dysplasia through to metastasis.

Therefore, the future of EV research lies in determining new methods of characterizing the tissue/cellular source of circulating EVs to provide information about cellular functional state or cancer stage. Much like the rise in single-cell transcriptomics and proteomics, single EV evaluation could be the key to disseminating their heterogeneity and pin-pointing oncogenic indicators. Attempts have been made to map EV RNA sequencing profiles to their cell or tissue of origin, however predictions using computational methods have failed to be validated by EV flow cytometry (Li et al., 2020). Multiplexed analysis of single EV (MASEV) is a promising technique that utilises a flow cell to attach pre-purified EVs (Spitzberg et al., 2023). Antibodies labelled with fluorophores linked by cleavable biorthogonal linkers allow rapid destaining, meaning individual vesicles can be repeatedly stained. Spitzberg *et al* used this method to show that biomarker multiplexing permitted clear separation of EVs from cell origins. Moreover, the use of CD63 as a positive EV marker resulted in the loss of 80% of all oncogene-positive EVs detected from KRAS mutant cells, indicating affinity purification could be detrimental to detecting EVs with diagnostic potential (Spitzberg et al., 2023). These novel methods are in their infancy, however further development to distinguish changes in EV signatures during cancer progression would be especially important for disseminating context dependent alterations in TGF-β1.

6.4 Limitations

Attempts to perturb EV release using chemical inhibitors were unsuccessful, mainly due to the inability to distinguish effects between drugs and DMSO vehicle control. More work could have been done to study particle release from cells treated with our drugs in alternate vehicles, as well as testing other putative EV inhibitors. Furthermore, due to the lack of promise of GW4869 and DMA, the availability of H357$^{\Delta HGS}$ and lack of time we did not repeat certain western blots for EV markers which would have improved conclusions drawn. Although TSG101 is a widely used EV marker, a greater selection of markers would be necessary to more accurately determine EV abundance.

Another limitation is that we did not investigate CAF marker transcript levels at the 72 hour timepoint, which may have allowed us to see changes in abundance. Two earlier time-points of 24 and 48 hours were chosen due to the presumption that changes in mRNA transcription would be detected at an earlier timepoint than changes in protein synthesis.

Much of this project was affected by the COVID-19 pandemic, firstly by loss of access to labs for 4 months (March-July 2020) due to national lockdown. Following this there was partial laboratory reopening with restricted working hours for around one year. Due to social distancing regulations, gaining training and access to equipment was delayed; namely microscopes and histology equipment. In addition, there were delivery delays for essential consumables such as specialised media, transwell inserts, collagen and deep-well culture plates used for 3D model generation and culture. This had an impact on the use of 3D models in this study and affected our decision to work primarily in 2D.

6.5 Future work

The next stages of this project would be to utilise 3D models to investigate the role of EVs in crosstalk between OSCC and fibroblasts. Further optimisation of our 3D OSCC models using H357$^{\Delta HGS}$ would be necessary to examine the effects of perturbing EV release in a more physiologically relevant model. Measuring CAF marker abundance and model contraction would be good indicators of the ability of EVs to promote fibroblast activation and determine if our 2D work can be recapitulated in 3D. The development of these models using H357$^{CD63\text{-}GFP}$ would also be useful to investigate the distribution of EVs in the ECM and discern the level of dissemination from the producing cell and possible sequestering on cell surfaces.

Further work should include closer investigation of the role of TGF-β, as summarised in Figure 6.1. Firstly, determining how TGF-β1 is tethered to OSCC derived EVs would allow us to distinguish the roles of soluble TGF-β from EV delivered TGF-β. Blocking tethering mechanisms and investigating if cancer derived EVs still induce fibroblast activation would demonstrate that TGF-β1 conformation is important in the TME and is a potential therapeutic target. Investigations may focus on GARP and membrane associated proteoglycans as tethering candidates due to their previous associations with TGF-β1, as discussed previously. Secondly, it would be pertinent to examine EV-TGF-β signalling in fibroblasts, to determine if this occurs through canonical SMAD signalling or through non-canonical means (Figure 6.1). As it had been previously shown that EV associated TGF-β induce sustained SMAD signalling in MSCs (Shelke et al., 2019), analysing this in OSCC-EV activated fibroblasts could provide an explanation as to why TGF-β is preferentially bound to EVs in the TME.

To gain a more rounded view of the role of EVs in the OSCC TME, future work should include investigations into the reciprocal communication between activated fibroblasts and OSCC (Figure 6.1). It would be interesting to examine potential changes in release and TGF-β1 association of EVs from NOFs activated by OSCC EVs compared to normal fibroblasts. Preliminary investigations would include incubation of activated NOF EVs with OSCC cells, NOKs and NOFs to determine changes in proliferation, migration and cancer-associated markers, as well as potentially upregulated signalling pathways.

Although beyond the immediate scope of this project, but of high clinical relevance, is the potential of EV-associated TGF-β1 to induce immunosuppression. There is currently little evidence for this in OSCC, however previous work has indicated this possibility due to increased immune tolerance behaviours of T-cells via TGF-β tethered lymphocyte EVs (Burlingham et al., 2023). Indeed, it has been shown that TGF-β associated HNSCC EVs were able to reprogram macrophages to a pro-angiogenic phenotype (Ludwig et al., 2022); thus demonstrating the wide TME modulating potential of TGF-β associated EVs that warrant further investigation.

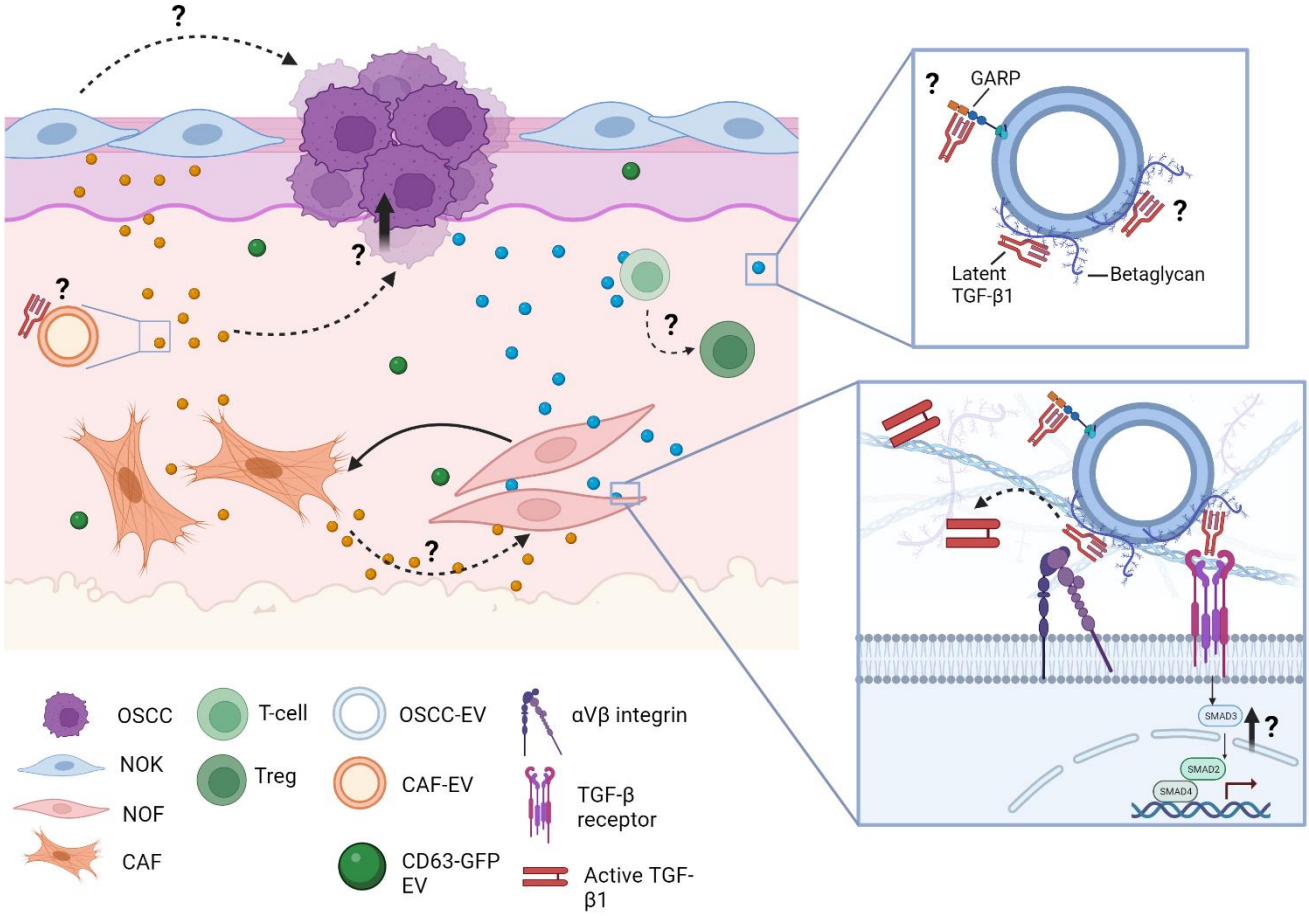

Figure 6.1 Schematic summary of proposed future work. The next steps of this work may focus on the tethering mechanisms of TGF-β1 to EVs, if traditional activation is necessary, and how signalling is maintained in recipient cells. Possible sequestering of EVs to cell surfaces or ECM components could be visualised with the use of H357CD63-GFP EVs in 3D models of OSCC. In addition, multiple directions of EV-mediated crosstalk in stromal cells could be further elucidated to gain a better understanding of possible therapeutic targets.

7 Supplementary materials

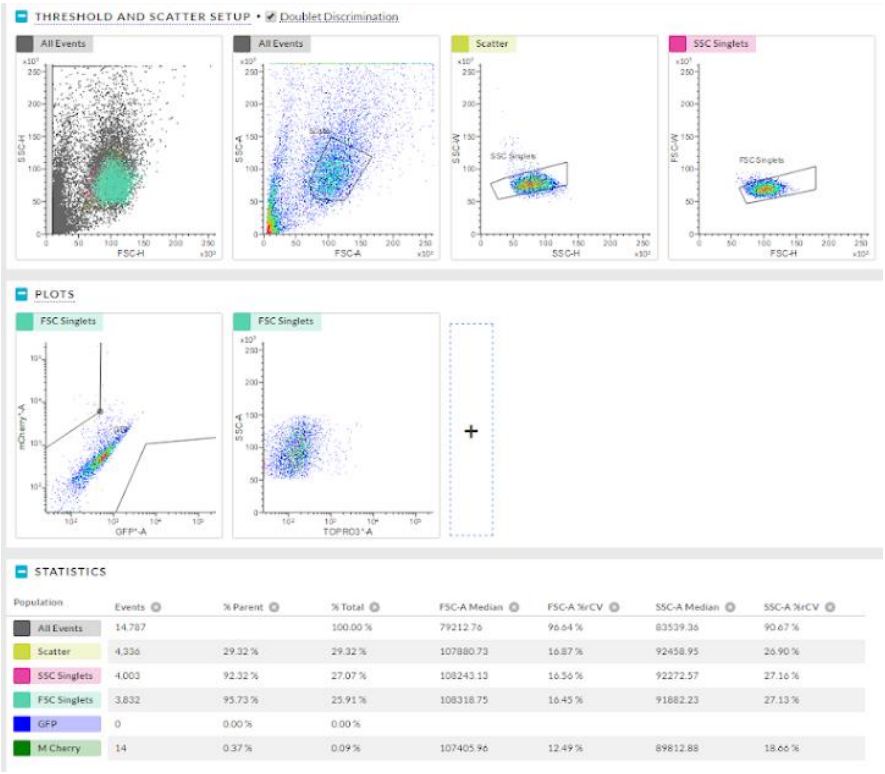

Population	Events	% Parent	% Total	FSC-A Median	FSC-A %rCV	SSC-A Median	SSC-A %rCV
All Events	14,787		100.00 %	79212.76	96.64 %	83539.36	90.67 %
Scatter	4,336	29.32 %	29.32 %	107880.73	16.87 %	92458.95	26.90 %
SSC Singlets	4,003	92.32 %	27.07 %	108243.13	16.56 %	92272.57	27.16 %
FSC Singlets	3,832	95.73 %	25.91 %	108318.75	16.45 %	91882.23	27.13 %
GFP	0	0.00 %	0.00 %				
M Cherry	14	0.37 %	0.09 %	107405.96	12.49 %	89812.88	18.66 %

Figure S. 1 FACS gating strategy representing GFP and mCherry positive single cells.

8 References

Aga, M., Bentz, G. L., Raffa, S., Torrisi, M. R., Kondo, S., Wakisaka, N., Yoshizaki, T., Pagano, J. S. and Shackelford, J. (2014), Exosomal HIF1α Supports Invasive Potential of Nasopharyngeal Carcinoma-Associated LMP1-Positive Exosomes. *Oncogene*, 33(37): 4613–4622.

Al-Magsoosi, Mohanad J.N., Lambert, Daniel W., Ali Khurram, Syed and Whawell, Simon A. (2021), Oral Cancer Stem Cells Drive Tumourigenesis through Activation of Stromal Fibroblasts. *Oral Diseases*, 27(6): 1383–1393.

Almangush, Alhadi, Mäkitie, Antti A., Triantafyllou, Asterios, de Bree, Remco, Strojan, Primož, Rinaldo, Alessandra, Hernandez-Prera, Juan C., Suárez, Carlos, Kowalski, Luiz P., Ferlito, Alfio and Leivo, Ilmo (2020), Staging and Grading of Oral Squamous Cell Carcinoma: An Update. *Oral Oncology*, 107: 104799.

Al-Nedawi, Khalid, Meehan, Brian, Micallef, Johann, Lhotak, Vladimir, May, Linda, Guha, Abhijit and Rak, Janusz (2008), Intercellular Transfer of the Oncogenic Receptor EGFRvIII by Microvesicles Derived from Tumour Cells. *Nature Cell Biology*, 10(5): 619–624.

Al-Samadi, Ahmed, Awad, Shady Adnan, Tuomainen, Katja, Zhao, Yue, Salem, Abdelhakim, Parikka, Mataleena and Salo, Tuula (2017), Crosstalk between Tongue Carcinoma Cells, Extracellular Vesicles, and Immune Cells in in Vitro and in Vivo Models. *Oncotarget*, 8(36): 60123–60134.

Alvarez-Erviti, Lydia, Seow, Yiqi, Schapira, Anthony H., Gardiner, Chris, Sargent, Ian L., Wood, Matthew J.A. and Cooper, J. Mark (2011), Lysosomal Dysfunction Increases Exosome-Mediated Alpha-Synuclein Release and Transmission. *Neurobiology of Disease*, 42(3): 360–367.

Alves, Alessandro Menna, Diel, Leonardo Francisco and Lamers, Marcelo Lazzaron (2018), Macrophages and Prognosis of Oral Squamous Cell Carcinoma: A Systematic Review. *Journal of Oral Pathology and Medicine*, 47(5): 460–467.

Amaral, Mariana Neves, Faísca, Pedro, Ferreira, Hugo Alexandre, Gaspar, Maria Manuela and Reis, Catarina Pinto (2022), Current Insights and Progress in the Clinical Management of Head and Neck Cancer. *Cancers*, 14(24).

Anand, Sushma, Samuel, Monisha, Kumar, Sharad and Mathivanan, Suresh (2019), Ticket to a Bubble Ride: Cargo Sorting into Exosomes and Extracellular Vesicles. *Biochimica et Biophysica Acta - Proteins and Proteomics*, 1867(12): 140203.

El Andaloussi, Samir, Mäger, Imre, Breakefield, Xandra O. and Wood, Matthew J.A. (2013), Extracellular Vesicles: Biology and Emerging Therapeutic Opportunities. *Nature Reviews Drug Discovery*, 12(5): 347–357.

de Andrade, A. L.D.L., de Oliveira, C. E., Dourado, M. R., Macedo, C. C.S., Winck, F. V., Paes Leme, A. F., Salo, T, Coletta, R. D., de Almeida Freitas, R and Galvão, H. C. (2018), Extracellular Vesicles from Oral Squamous Carcinoma Cells Display Pro- and Anti-Angiogenic Properties. *Oral Diseases*, 24(5): 725–731.

Ang, K. Kian, Harris, Jonathan, Wheeler, Richard, Weber, Randal, Rosenthal, David I., Nguyen-Tân, Phuc Felix, Westra, William H., Chung, Christine H., Jordan, Richard C., Lu, Charles, Kim, Harold, Axelrod, Rita, Silverman, C. Craig, Redmond, Kevin P. and Gillison, Maura L. (2010), Human Papillomavirus and Survival of Patients with Oropharyngeal Cancer. *The New England journal of medicine*, 363(1): 24.

Atkin-Smith, Georgia K. and Poon, Ivan K.H. (2017), Disassembly of the Dying: Mechanisms and Functions. *Trends in Cell Biology*, 27(2): 151–162.

Atkin-Smith, Georgia K., Tixeira, Rochelle, Paone, Stephanie, Mathivanan, Suresh, Collins, Christine, Liem, Michael, Goodall, Katharine J., Ravichandran, Kodi S., Hulett, Mark D. and Poon, Ivan K.H. (2015), A Novel Mechanism of Generating Extracellular Vesicles during Apoptosis via a Beads-on-a-String Membrane Structure. *Nature Communications*, 6(1): 1–10.

Bachurski, Daniel, Schuldner, Maximiliane, Nguyen, Phuong Hien, Malz, Alexandra, Reiners, Katrin S., Grenzi, Patricia C., Babatz, Felix, Schauss, Astrid C., Hansen, Hinrich P., Hallek, Michael and Pogge von Strandmann, Elke (2019), Extracellular Vesicle Measurements with Nanoparticle Tracking Analysis – An Accuracy and Repeatability Comparison between NanoSight NS300 and ZetaView. *Journal of Extracellular Vesicles*, 8(1).

Bae, Jung Yoon, Kim, Eun Kyoung, Yang, Dong Hyun, Zhang, Xianglan, Park, Young Jin, Lee, Doo Young, Che, Chung Min and Kim, Jin (2014), Reciprocal Interaction between Carcinoma-Associated Fibroblasts and Squamous Carcinoma Cells through Interleukin-1α Induces Cancer Progression. *Neoplasia (New York, N.Y.)*, 16(11): 928–938.

Baietti, Maria Francesca, Zhang, Zhe, Mortier, Eva, Melchior, Aurélie, Degeest, Gisèle, Geeraerts, Annelies, Ivarsson, Ylva, Depoortere, Fabienne, Coomans, Christien, Vermeiren,

Elke, Zimmermann, Pascale and David, Guido (2012), Syndecan-Syntenin-ALIX Regulates the Biogenesis of Exosomes. *Nature cell biology*, 14(7): 677–685.

Bandyopadhyay, Abhik, Zhu, Yong, Cibull, Michael L., Bao, Li Wei, Chen, Changguo and Sun, Lu Zhe (1999), A Soluble Transforming Growth Factor β Type III Receptor Suppresses Tumorigenicity and Metastasis of Human Breast Cancer MDA-MB-231 Cells. *Cancer Research*, 59(19): 5041–5046.

Bebelman, Maarten P, Crudden, Caitrin, Snieder, Bart, Thanou, Evangelia, Langedijk, Catharina J M, Viola, Margarida, Eleonora, Steven, Baginska, Urszula, Cotugno, Olaf, Paul, Jan, Bebelman, M, Van Eijndhoven, Monique A J, Bosch, Leontien, Li, Ka Wan, Smit, Martine J, Van Niel, Guillaume, Smit, August B, Verweij, Frederik J and Michiel, D (2023), Luminescence-Based Screening for Extracellular Vesicle Release Modulators Reveals a Role for PI4KIIIβ in Exosome Biogenesis upon Lysosome Inhibition. *bioRxiv*: 2023.02.23.529257.

Bebelman, Maarten P., Smit, Martine J., Pegtel, D. Michiel and Baglio, S. Rubina (2018), Biogenesis and Function of Extracellular Vesicles in Cancer. *Pharmacology and Therapeutics*, 188: 1–11.

Bhome, Rahul, Del Vecchio, Filippo, Lee, Gui Han, Bullock, Marc D., Primrose, John N., Sayan, A. Emre and Mirnezami, Alex H. (2018), Exosomal MicroRNAs (ExomiRs): Small Molecules with a Big Role in Cancer. *Cancer Letters*, 420: 228–235.

Bouchard, Alexanne, Collin, Bertrand, Garrido, Carmen, Bellaye, Pierre Simon and Kohli, Evelyne (2021), GARP: A Key Target to Evaluate Tumor Immunosuppressive Microenvironment. *Biology*, 10(9).

Bravo-Miana, Rocío del Carmen, Soler, María Florencia, Ceschin, Danilo Guillermo, Royo, Félix, Negretti-Borga, Dana María, Azkargorta, Mikel, Elortza, Félix, Montesinos, María del Mar, Pellizas, Claudia Gabriela, Falcón-Pérez, Juan Manuel and Donadio, Ana Carolina (2022), Extracellular Vesicles from Thyroid Cancer Harbor a Functional Machinery Involved in Extracellular Matrix Remodeling. *European Journal of Cell Biology*, 101(3): 151254.

Bray, Freddie, Ferlay, Jacques, Soerjomataram, Isabelle, Siegel, Rebecca L., Torre, Lindsey A. and Jemal, Ahmedin (2018), Global Cancer Statistics 2018: GLOBOCAN Estimates of Incidence and Mortality Worldwide for 36 Cancers in 185 Countries. *CA: A Cancer Journal for Clinicians*, 68(6): 394–424.

Brennan, K., Martin, K., FitzGerald, S. P., O'Sullivan, J., Wu, Y., Blanco, A., Richardson, C. and Mc Gee, M. M. (2020), A Comparison of Methods for the Isolation and Separation of

Extracellular Vesicles from Protein and Lipid Particles in Human Serum. *Scientific Reports*, 10(1): 1–13.

Brzozowska, Ewa and Deshmukh, Sameer (2022), Integrin Alpha v Beta 6 (Avβ6) and Its Implications in Cancer Treatment. *International Journal of Molecular Sciences*, 23(20).

Burlingham, William J., Jankowska-Gan, Ewa, Fechner, John H., Little, Christopher J., Wang, Jianxin, Hong, Seungpyo, Molla, Miraf, Sullivan, Jeremy A. and Foley, David P. (2023), Extracellular Vesicle–Associated GARP/TGFβ:LAP Mediates “Infectious” Allo-Tolerance. *Transplantation Direct*, 9(6).

Buzás, Edit I., Tóth, Eszter, Sódar, Barbara W. and Szabó-Taylor, Katalin (2018), Molecular Interactions at the Surface of Extracellular Vesicles. *Seminars in Immunopathology 2018 40:5*, 40(5): 453–464.

Cai, Jinghua, Qiao, Bin, Gao, Ning, Lin, Nan and He, Wei (2019), Oral Squamous Cell Carcinoma-Derived Exosomes Promote M2 Subtype Macrophage Polarization Mediated by Exosome-Enclosed MiR-29a-3p. *American Journal of Physiology - Cell Physiology*, 316(5): C731–C740.

Caillat, Christophe, Maity, Sourav, Miguet, Nolwenn, Roos, Wouter H. and Weissenhorn, Winfried (2019), The Role of VPS4 in ESCRT-III Polymer Remodeling. *Biochemical Society Transactions*, 47(1): 441–448.

Campbell, Melody G., Cormier, Anthony, Ito, Saburo, Seed, Robert I., Bondesson, Andrew J., Lou, Jianlong, Marks, James D., Baron, Jody L., Cheng, Yifan and Nishimura, Stephen L. (2020), Cryo-EM Reveals Integrin-Mediated TGF-β Activation without Release from Latent TGF-β. *Cell*, 180(3): 490-501.e16.

Cashikar, Anil G. and Hanson, Phyllis I. (2019), A Cell-Based Assay for CD63-Containing Extracellular Vesicles. *PLoS ONE*, 14(7).

Catalano, Mariadelva and O’Driscoll, Lorraine (2020a), Inhibiting Extracellular Vesicles Formation and Release: A Review of EV Inhibitors. *Journal of Extracellular Vesicles*, 9(1): 1703244.

Catalano, Mariadelva and O’Driscoll, Lorraine (2020b), Inhibiting Extracellular Vesicles Formation and Release: A Review of EV Inhibitors. *Journal of Extracellular Vesicles*, 9(1).

Chalmin, Fanny, Ladoire, Sylvain, Mignot, Grégoire, Vincent, Julie, Bruchard, Mélanie, Remy-Martin, Jean Paul, Boireau, Wilfrid, Rouleau, Alain, Simon, Benoit, Lanneau, David, De Thonel, Aurélie, Multhoff, Gabriele, Hamman, Arlette, Martin, François, Chauffert, Bruno, Solary, Eric, Zitvogel, Laurence, Garrido, Carmen, Ryffel, Bernhard, Borg, Christophe,

Apetoh, Lionel, Rébé, Cédric and Ghiringhelli, François (2010), Membrane-Associated Hsp72 from Tumor-Derived Exosomes Mediates STAT3-Dependent Immunosuppressive Function of Mouse and Human Myeloid-Derived Suppressor Cells. *The Journal of Clinical Investigation*, 120(2): 457–471.

Chang, Yu Ting, Peng, Hsuan Yu, Hu, Chun Mei, Tien, Sui Chih, Chen, Yi Ing, Jeng, Yung Ming and Chang, Ming Chu (2023), Pancreatic Cancer-Derived Small Extracellular Vesical Ezrin Activates Fibroblasts to Exacerbate Cancer Metastasis through STAT3 and YAP-1 Signaling Pathways. *Molecular oncology*, 17(8).

Chen, Bing, Sang, Yuting, Song, Xiaojin, Zhang, Dong, Wang, Lijuan, Zhao, Wenjing, Liang, Yiran, Zhang, Ning and Yang, Qifeng (2021), Exosomal MiR-500a-5p Derived from Cancer-Associated Fibroblasts Promotes Breast Cancer Cell Proliferation and Metastasis through Targeting USP28. *Theranostics*, 11(8): 3932–3947.

Chen, Bojie, Leung, Leanne Lee, Qu, Xinyu and Chan, Jason Ying Kuen (2023), Extracellular Vesicles as Biomarkers in Head and Neck Squamous Cell Carcinoma: From Diagnosis to Disease-Free Survival. *Cancers 2023, Vol. 15, Page 1826*, 15(6): 1826.

Chen, Jia Hong, Wu, Alexander T.H., Bamodu, Oluwaseun Adebayo, Yadav, Vijesh Kumar, Chao, Tsu Yi, Tzeng, Yew Min, Mukhopadhyay, Debabrata, Hsiao, Michael and Lee, Jih Chin (2020), Ovatodiolide Suppresses Oral Cancer Malignancy by Down-Regulating Exosomal Mir-21/STAT3/β-Catenin Cargo and Preventing Oncogenic Transformation of Normal Gingival Fibroblasts. *Cancers*, 12(1): 56.

Chen, Shunjin, Ying, Mingang, Lin, Xiuan, Zheng, Xiong, Liu, Chang and Liu, Hui (2015), Expression of MICA in Oral Squamous Carcinoma Cells and Its Effect on NK Cells. *International Journal of Clinical and Experimental Medicine*, 8(10): 18208–18212.

Chen, Xi, Liang, Hongwei, Zhang, Junfeng, Zen, Ke and Zhang, Chen Yu (2012), Secreted MicroRNAs: A New Form of Intercellular Communication. *Trends in Cell Biology*, 22(3): 125–132.

Cho, Jung Ah, Park, Ho, Lim, Eun Hye, Kim, Kye Hyun, Choi, Joong Sub, Lee, Jung Hoon, Shin, Jae Wook and Lee, Kyo Won (2011), Exosomes from Ovarian Cancer Cells Induce Adipose Tissue-Derived Mesenchymal Stem Cells to Acquire the Physical and Functional Characteristics of Tumor-Supporting Myofibroblasts. *Gynecologic oncology*, 123(2): 379–386.

Chong, Zhi Xiong, Yeap, Swee Keong and Ho, Wan Yong (2021), Transfection Types, Methods and Strategies: A Technical Review. *PeerJ*, 9.

Chowdhury, Ridwana, Webber, Jason P., Gurney, Mark, Mason, Malcolm D., Tabi, Zsuzsanna and Clayton, Aled (2015), Cancer Exosomes Trigger Mesenchymal Stem Cell Differentiation into Pro-Angiogenic and pro-Invasive Myofibroblasts. *Oncotarget*, 6(2): 715–731.

Chung, Christine H. and Gillison, Maura L. (2009), Human Papillomavirus in Head and Neck Cancer: Its Role in Pathogenesis and Clinical Implications. *Clinical Cancer Research*, 15(22): 6758–6762.

Chuo, Steven Ting Yu, Chien, Jasper Che Yung and Lai, Charles Pin Kuang (2018), Imaging Extracellular Vesicles: Current and Emerging Methods. *Journal of Biomedical Science*, 25(1): 1–10.

Ciferri, Maria Chiara, Quarto, Rodolfo and Tasso, Roberta (2021), Extracellular Vesicles as Biomarkers and Therapeutic Tools: From Pre-Clinical to Clinical Applications. *Biology*, 10(5).

Clarke, Christopher J., Snook, Christopher F., Tani, Motohiro, Matmati, Nabil, Marchesini, Norma and Hannun, Yusuf A. (2006), The Extended Family of Neutral Sphingomyelinases. *Biochemistry*, 45(38): 11247–11256.

Colombo, Marina, Moita, Catarina, Van Niel, Guillaume, Kowal, Joanna, Vigneron, James, Benaroch, Philippe, Manel, Nicolas, Moita, Luis F, Théry, Clotilde and Raposo, Graça (2013), Analysis of ESCRT Functions in Exosome Biogenesis, Composition and Secretion Highlights the Heterogeneity of Extracellular Vesicles. *Journal of Cell Science*, 126(24): 5553–5565.

Colombo, Marina, Moita, Catarina, Van Niel, Guillaume, Kowal, Joanna, Vigneron, James, Benaroch, Philippe, Manel, Nicolas, Moita, Luis F., Théry, Clotilde and Raposo, Graça (2013), Analysis of ESCRT Functions in Exosome Biogenesis, Composition and Secretion Highlights the Heterogeneity of Extracellular Vesicles. *Journal of cell science*, 126(Pt 24): 5553–5565.

Del Conde, Ian, Shrimpton, Corie N., Thiagarajan, Perumal and López, José A. (2005), Tissue-Factor-Bearing Microvesicles Arise from Lipid Rafts and Fuse with Activated Platelets to Initiate Coagulation. *Blood*, 106(5): 1604–1611.

Conigliaro, Alice, Costa, Viviana, Lo Dico, Alessia, Saieva, Laura, Buccheri, Simona, Dieli, Francesco, Manno, Mauro, Raccosta, Samuele, Mancone, Carmine, Tripodi, Marco, De Leo, Giacomo and Alessandro, Riccardo (2015), CD90+ Liver Cancer Cells Modulate Endothelial Cell Phenotype through the Release of Exosomes Containing H19 LncRNA. *Molecular Cancer*, 14(1).

Cooper, Geoffrey M (2000), *The Cell: A Molecular Approach* 2nd Edition. The Eukaryotic Cell Cycle.

Corso, Giulia, Heusermann, Wolf, Trojer, Dominic, Görgens, André, Steib, Emmanuelle, Voshol, Johannes, Graff, Alexandra, Genoud, Christel, Lee, Yi, Hean, Justin, Nordin, Joel Z, Wiklander, Oscar PB, El Andaloussi, Samir and Meisner-Kober, Nicole (2019), Journal of Extracellular Vesicles Systematic Characterization of Extracellular Vesicle Sorting Domains and Quantification at the Single Molecule-Single Vesicle Level by Fluorescence Correlation Spectroscopy and Single Particle Imaging.

Deng, Yongqiang, Rivera-Molina, Felix E., Toomre, Derek K. and Burd, Christopher G. (2016), Sphingomyelin Is Sorted at the Trans Golgi Network into a Distinct Class of Secretory Vesicle. *Proceedings of the National Academy of Sciences of the United States of America*, 113(24): 6677–6682.

Desclozeaux, Marion, Venturato, Juliana, Wylie, Fiona G., Kay, Jason G., Joseph, Shannon R., Le, Huong T. and Stow, Jennifer L. (2008), Active Rab11 and Functional Recycling Endosome Are Required for E-Cadherin Trafficking and Lumen Formation during Epithelial Morphogenesis. *American Journal of Physiology - Cell Physiology*, 295(2): 545–556.

Dourado, Mauricio Rocha, Korvala, Johanna, Åström, Pirjo, De Oliveira, Carine Ervolino, Cervigne, Nilva K., Mofatto, Luciana Souto, Campanella Bastos, Debora, Pereira Messetti, Ana Camila, Graner, Edgard, Paes Leme, Adriana Franco, Coletta, Ricardo D. and Salo, Tuula (2019), Extracellular Vesicles Derived from Cancer-Associated Fibroblasts Induce the Migration and Invasion of Oral Squamous Cell Carcinoma. *Journal of Extracellular Vesicles*, 8(1).

Dukes, Joseph D., Fish, Laura, Richardson, Judith D., Blaikley, Elizabeth, Burns, Samir, Caunt, Christopher J., Chalmers, Andrew D. and Whitley, Paul (2011), Functional ESCRT Machinery Is Required for Constitutive Recycling of Claudin-1 and Maintenance of Polarity in Vertebrate Epithelial Cells. *Molecular Biology of the Cell*, 22(17): 3192–3205.

Eberlein, C., Kendrew, J., McDaid, K., Alfred, A., Kang, J. S., Jacobs, V. N., Ross, S. J., Rooney, C., Smith, N. R., Rinkenberger, J., Cao, A., Churchman, A., Marshall, J. F., Weir, H. M., Bedian, V., Blakey, D. C., Foltz, I. N. and Barry, S. T. (2013), A Human Monoclonal Antibody 264RAD Targeting Avβ6 Integrin Reduces Tumour Growth and Metastasis, and Modulates Key Biomarkers in Vivo. *Oncogene*, 32(37): 4406–4416.

Elahi, Maryam and Rakhshan, Vahid (2020), MED15, Transforming Growth Factor Beta 1 (TGF-B1), FcγRIII (CD16), and HNK-1 (CD57) Are Prognostic Biomarkers of Oral Squamous Cell Carcinoma. *Scientific Reports 2020 10:1*, 10(1): 1–14.

Eldh, Maria, Olofsson Bagge, Roger, Lässer, Cecilia, Svanvik, Joar, Sjöstrand, Margareta, Mattsson, Jan, Lindnér, Per, Choi, Dong Sic, Gho, Song S. and Lötvall, Jan (2014), MicroRNA in Exosomes Isolated Directly from the Liver Circulation in Patients with Metastatic Uveal Melanoma. *BMC Cancer*, 14(1).

Escrevente, Cristina, Keller, Sascha, Altevogt, Peter and Costa, Júlia (2011), Interaction and Uptake of Exosomes by Ovarian Cancer Cells. *BMC Cancer*, 11(1): 1–10.

Fader, Claudio Marcelo, Sánchez, Diego Germán, Mestre, María Belén and Colombo, María Isabel (2009), TI-VAMP/VAMP7 and VAMP3/Cellubrevin: Two v-SNARE Proteins Involved in Specific Steps of the Autophagy/Multivesicular Body Pathways. *Biochimica et Biophysica Acta - Molecular Cell Research*, 1793(12): 1901–1916.

Filaci, Gilberto, Fenoglio, Daniela, Fravega, Marco, Ansaldo, Gianluca, Borgonovo, Giacomo, Traverso, Paolo, Villaggio, Barbara, Ferrera, Alessandra, Kunkl, Annalisa, Rizzi, Marta, Ferrera, Francesca, Balestra, Piercesare, Ghio, Massimo, Contini, Paola, Setti, Maurizio, Olive, Daniel, Azzarone, Bruno, Carmignani, Giorgio, Ravetti, Jean Louis, Torre, Giancarlo and Indiveri, Francesco (2007), CD8 + CD28 − T Regulatory Lymphocytes Inhibiting T Cell Proliferative and Cytotoxic Functions Infiltrate Human Cancers. *The Journal of Immunology*, 179(7): 4323–4334.

Fozzatti, Laura, Alamino, Vanina Alejandra, Park, Sunmi, Giusiano, Lucila, Volpini, Ximena, Zhao, Li, Stempin, Cinthia Carolina, Donadio, Ana Carolina, Cheng, Sheue yann and Pellizas, Claudia Gabriela (2019), Interplay of Fibroblasts with Anaplastic Tumor Cells Promotes Follicular Thyroid Cancer Progression. *Scientific Reports 2019 9:1*, 9(1): 1–15.

Fujiwara, Toshifumi, Eguchi, Takanori, Sogawa, Chiharu, Ono, Kisho, Murakami, Jun, Ibaragi, Soichiro, Asaumi, Jun ichi, Calderwood, Stuart K., Okamoto, Kuniaki and Kozaki, Ken ichi (2018), Carcinogenic Epithelial-Mesenchymal Transition Initiated by Oral Cancer Exosomes Is Inhibited by Anti-EGFR Antibody Cetuximab. *Oral oncology*, 86: 251–257.

Galati, Luisa, Chiocca, Susanna, Duca, Daria, Tagliabue, Marta, Simoens, Cindy, Gheit, Tarik, Arbyn, Marc and Tommasino, Massimo (2022), HPV and Head and Neck Cancers: Towards Early Diagnosis and Prevention. *Tumour Virus Research*, 14: 200245.

Galvao, Joana, Davis, Benjamin, Tilley, Mark, Normando, Eduardo, Duchen, Michael R. and Cordeiro, M. Francesca (2014), Unexpected Low-Dose Toxicity of the Universal Solvent DMSO. *The FASEB Journal*, 28(3): 1317–1330.

Garrett, Qian, Khaw, Peng T., Blalock, Timothy D., Schultz, Gregory S., Grotendorst, Gary R. and Daniels, Julie T. (2004), Involvement of CTGF in TGF-B1–Stimulation of Myofibroblast

Differentiation and Collagen Matrix Contraction in the Presence of Mechanical Stress. *Investigative Ophthalmology & Visual Science*, 45(4): 1109–1116.

Gauthier, Sébastien A., Pérez-González, Rocío, Sharma, Ajay, Huang, Fang Ke, Alldred, Melissa J., Pawlik, Monika, Kaur, Gurjinder, Ginsberg, Stephen D., Neubert, Thomas A. and Levy, Efrat (2017), Enhanced Exosome Secretion in Down Syndrome Brain - a Protective Mechanism to Alleviate Neuronal Endosomal Abnormalities. *Acta neuropathologica communications*, 5(1): 65.

Ghossoub, Rania, Lembo, Frédérique, Rubio, Aude, Gaillard, Carole Baron, Bouchet, Jérôme, Vitale, Nicolas, Slavík, Josef, Machala, Miroslav and Zimmermann, Pascale (2014), Syntenin-ALIX Exosome Biogenesis and Budding into Multivesicular Bodies Are Controlled by ARF6 and PLD2. *Nature Communications 2014 5:1*, 5(1): 1–12.

Goulet, Cassandra Ringuette, Bernard, Genevieve, Tremblay, Sarah, Chabaud, Stephane, Bolduc, Stephane and Pouliot, Frederic (2018), Exosomes Induce Fibroblast Differentiation into Cancer-Associated Fibroblasts through TGFβ Signaling. *Molecular cancer research : MCR*, 16(7): 1196–1204.

Grange, Cristina, Tapparo, Marta, Bruno, Stefania, Chatterjee, Devasis, Quesenberry, Peter J., Tetta, Ciro and Camussi, Giovanni (2014), Biodistribution of Mesenchymal Stem Cell-Derived Extracellular Vesicles in a Model of Acute Kidney Injury Monitored by Optical Imaging. *International Journal of Molecular Medicine*, 33(5): 1055.

Grant, Lois R., Milic, Ivana and Devitt, Andrew (2019), Apoptotic Cell-Derived Extracellular Vesicles: Structure–Function Relationships. *Biochemical Society Transactions*, 47(2): 509–516.

Gross, Julia Christina, Chaudhary, Varun, Bartscherer, Kerstin and Boutros, Michael (2012), Active Wnt Proteins Are Secreted on Exosomes. *Nature Cell Biology*, 14(10): 1036–1045.

Große-Thie, Christina, Maletzki, Claudia, Junghanss, Christian and Schmidt, Kathie (2021), Long-Term Survivor of Metastatic Squamous-Cell Head and Neck Carcinoma with Occult Primary after Cetuximab-Based Chemotherapy: A Case Report. *World Journal of Clinical Cases*, 9(24): 7092.

Gu, Jianmei, Qian, Hui, Shen, Li, Zhang, Xu, Zhu, Wei, Huang, Ling, Yan, Yongmin, Mao, Fei, Zhao, Chonghui, Shi, Yunyan and Xu, Wenrong (2012), Gastric Cancer Exosomes Trigger Differentiation of Umbilical Cord Derived Mesenchymal Stem Cells to Carcinoma-Associated Fibroblasts through TGF-β/Smad Pathway. *PLOS ONE*, 7(12): e52465.

Guo, Huishan, Chitiprolu, Maneka, Roncevic, Luc, Javalet, Charlotte, Hemming, Fiona J., Trung, My Tran, Meng, Lingrui, Latreille, Elyse, Tanese de Souza, Christiano, McCulloch, Danielle, Baldwin, R. Mitchell, Auer, Rebecca, Côté, Jocelyn, Russell, Ryan Charles, Sadoul, Rémy and Gibbings, Derrick (2017), Atg5 Disassociates the V1V0-ATPase to Promote Exosome Production and Tumor Metastasis Independent of Canonical Macroautophagy. *Developmental Cell*, 43(6): 716-730.e7.

Guo, Wei, Qiu, Wei, Ao, Xiang, Li, Weiqiang, He, Xiao, Ao, Luoquan, Hu, Xueting, Li, Zhan, Zhu, Ming, Luo, Donglin, Xing, Wei and Xu, Xiang (2020), Low-Concentration DMSO Accelerates Skin Wound Healing by Akt/MTOR-Mediated Cell Proliferation and Migration in Diabetic Mice. *British Journal of Pharmacology*, 177(14): 3327–3341.

Guo, Yuanyuan, Xu, Tiansong, Chai, Yujuan and Chen, Feng (2023), TGF-β Signaling in Progression of Oral Cancer. *International Journal of Molecular Sciences 2023, Vol. 24, Page 10263*, 24(12): 10263

Gurunathan, Sangiliyandi, Kang, Min Hee, Jeyaraj, Muniyandi and Kim, Jin Hoi (2021), Platinum Nanoparticles Enhance Exosome Release in Human Lung Epithelial Adenocarcinoma Cancer Cells (A549): Oxidative Stress and the Ceramide Pathway Are Key Players. *International Journal of Nanomedicine*, 16: 515.

Haddad, Robert I., Harrington, Kevin, Tahara, Makoto, Ferris, Robert L., Gillison, Maura, Fayette, Jerome, Daste, Amaury, Koralewski, Piotr, Zurawski, Bogdan, Taberna, Miren, Saba, Nabil F., Mak, Milena, Kawecki, Andrzej, Girotto, Gustavo, Alvarez Avitia, Miguel Angel, Even, Caroline, Toledo, Joaquin Gabriel Reinoso, Guminski, Alexander, Müller-Richter, Urs, Kiyota, Naomi, Roberts, Mustimbo, Khan, Tariq Aziz, Miller-Moslin, Karen, Wei, Li and Argiris, Athanassios (2023), Nivolumab Plus Ipilimumab Versus EXTREME Regimen as First-Line Treatment for Recurrent/Metastatic Squamous Cell Carcinoma of the Head and Neck: The Final Results of CheckMate 651. *Journal of Clinical Oncology*, 41(12): 2166.

Hadler-Olsen, Elin and Wirsing, Anna Maria (2019), Tissue-Infiltrating Immune Cells as Prognostic Markers in Oral Squamous Cell Carcinoma: A Systematic Review and Meta-Analysis. *British Journal of Cancer*, 120(7): 714–727.

Hajighasemi, Fatemeh and Tajik, Shaghayegh (2017), Hajighasemi F et al. Assessment of Cytotoxicity of Dimethyl Sulfoxide in Human Hematopoietic Tumor Cell Lines. *Iranian Journal of Blood and Cancer 48 IJBC*, 9(2): 48–53.

Haque, A. S.M.Rafiul, Moriyama, Masafumi, Kubota, Keigo, Ishiguro, Noriko, Sakamoto, Mizuki, Chinju, Akira, Mochizuki, Keita, Sakamoto, Taiki, Kaneko, Naoki, Munemura, Ryusuke, Maehara, Takashi, Tanaka, Akihiko, Hayashida, Jun Nosuke, Kawano, Shintaro, Kiyoshima,

Tamotsu and Nakamura, Seiji (2019), CD206+ Tumor-Associated Macrophages Promote Proliferation and Invasion in Oral Squamous Cell Carcinoma via EGF Production. *Scientific Reports*, 9(1).

Harari, Paul M., Harris, Jonathan, Kies, Merrill S., Myers, Jeffrey N., Jordan, Richard C., Gillison, Maura L., Foote, Robert L., Machtay, Mitchell, Rotman, Marvin, Khuntia, Deepak, Straube, William, Zhang, Qiang and Ang, Kian (2014), Postoperative Chemoradiotherapy and Cetuximab for High-Risk Squamous Cell Carcinoma of the Head and Neck: Radiation Therapy Oncology Group RTOG-0234. *Journal of clinical oncology : official journal of the American Society of Clinical Oncology*, 32(23): 2486–2495.

Harrington, Kevin J., Burtness, Barbara, Greil, Richard, Soulières, Denis, Tahara, Makoto, De Castro, Gilberto, Psyrri, Amanda, Brana, Irene, Basté, Neus, Neupane, Prakash, Bratland, Åse, Fuereder, Thorsten, Hughes, Brett G.M., Mesia, Ricard, Ngamphaiboon, Nuttapong, Rordorf, Tamara, Wan Ishak, Wan Zamaniah, Lin, Jianxin, Gumuscu, Burak, Swaby, Ramona F. and Rischin, Danny (2023), Pembrolizumab With or Without Chemotherapy in Recurrent or Metastatic Head and Neck Squamous Cell Carcinoma: Updated Results of the Phase III KEYNOTE-048 Study. *Journal of Clinical Oncology*, 41(4): 790.

Hassona, Y., Cirillo, N., Heesom, K., Parkinson, E. K. and Prime, S. S. (2014), Senescent Cancer-Associated Fibroblasts Secrete Active MMP-2 That Promotes Keratinocyte Dis-Cohesion and Invasion. *British Journal of Cancer*, 111(6): 1230–1237.

He, Shuqi, Zhang, Wu, Li, Xian, Wang, Junjie, Chen, Xufeng, Chen, Yu and Lai, Renfa (2021), Oral Squamous Cell Carcinoma (OSCC)-Derived Exosomal MiR-221 Targets and Regulates Phosphoinositide-3-Kinase Regulatory Subunit 1 (PIK3R1) to Promote Human Umbilical Vein Endothelial Cells Migration and Tube Formation. *Bioengineered*, 12(1): 2164–2174.

Hessvik, Nina Pettersen and Llorente, Alicia (2018), Current Knowledge on Exosome Biogenesis and Release. *Cellular and Molecular Life Sciences*, 75(2): 193–208.

Hikita, Tomoya, Miyata, Mamiko, Watanabe, Risayo and Oneyama, Chitose (2018), Sensitive and Rapid Quantification of Exosomes by Fusing Luciferase to Exosome Marker Proteins. *Scientific Reports*, 8(1).

Hoshino, Daisuke, Kirkbride, Kellye C., Costello, Kaitlin, Clark, Emily S., Sinha, Seema, Grega-Larson, Nathan, Tyska, Matthew J. and Weaver, Alissa M. (2013), Exosome Secretion Is Enhanced by Invadopodia and Drives Invasive Behavior. *Cell reports*, 5(5): 1159–1168.

Howren, M. Bryant, Christensen, Alan J., Karnell, Lucy H.ynds and Funk, Gerry F. (2013), Psychological Factors Associated with Head and Neck Cancer Treatment and Survivorship:

Evidence and Opportunities for Behavioral Medicine. *Journal of consulting and clinical psychology*, 81(2): 299–317.

Hsieh, Chia Hsin, Tai, Shyh Kuan and Yang, Muh Hwa (2018), Snail-Overexpressing Cancer Cells Promote M2-Like Polarization of Tumor-Associated Macrophages by Delivering MiR-21-Abundant Exosomes. *Neoplasia (United States)*, 20(8): 775–788.

Hsu, Chieh, Morohashi, Yuichi, Yoshimura, Shin Ichiro, Manrique-Hoyos, Natalia, Jung, Sang Yong, Lauterbach, Marcel A., Bakhti, Mostafa, Grønborg, Mads, Möbius, Wiebke, Rhee, Jeong Seop, Barr, Francis A. and Simons, Mikael (2010), Regulation of Exosome Secretion by Rab35 and Its GTPase-Activating Proteins TBC1D10A-C. *Journal of Cell Biology*, 189(2): 223–232.

Hu, Weilei, Wang, Guosheng, Huang, Dongsheng, Sui, Meihua and Xu, Yibing (2019), Cancer Immunotherapy Based on Natural Killer Cells: Current Progress and New Opportunities. *Frontiers in Immunology*, 10(MAY).

Huaitong, Xiao, Yuanyong, Feng, Yueqin, Tao, Peng, Zhao, Wei, Shang and Kai, Song (2017), Microvesicles Releasing by Oral Cancer Cells Enhance Endothelial Cell Angiogenesis via Shh/RhoA Signaling Pathway. *Cancer Biology and Therapy*, 18(10): 783–791.

Huang, Fei and Chen, Ye Guang (2012), Regulation of TGF-β Receptor Activity. *Cell and Bioscience*, 2(1): 1–10.

Huang, Qiang, Hsueh, Chi Yao, Guo, Yang, Wu, Xiu Fa, Li, Jiao Yu and Zhou, Liang (2020), Lack of MiR-1246 in Small Extracellular Vesicle Blunts Tumorigenesis of Laryngeal Carcinoma Cells by Regulating Cyclin G2. *IUBMB Life*, 72(7): 1491–1503.

Huang, Qiang, Hsueh, Chi Yao, Shen, Yu Jie, Guo, Yang, Huang, Jia Meng, Zhang, Yi Fan, Li, Jiao Yu, Gong, Hong Li and Zhou, Liang (2021a), Small Extracellular Vesicle-Packaged TGFβ1 Promotes the Reprogramming of Normal Fibroblasts into Cancer-Associated Fibroblasts by Regulating Fibronectin in Head and Neck Squamous Cell Carcinoma. *Cancer Letters*, 517: 1–13.

Huang, Qiang, Hsueh, Chi Yao, Shen, Yu Jie, Guo, Yang, Huang, Jia Meng, Zhang, Yi Fan, Li, Jiao Yu, Gong, Hong Li and Zhou, Liang (2021b), Small Extracellular Vesicle-Packaged TGFβ1 Promotes the Reprogramming of Normal Fibroblasts into Cancer-Associated Fibroblasts by Regulating Fibronectin in Head and Neck Squamous Cell Carcinoma. *Cancer Letters*, 517: 1–13.

Huang, Qiang, Shen, Yu-Jie, Hsueh, Chi-Yao, Zhang, Yi-Fan, Guo, Yang, Yuan, Xiao-Hui, Hu, Chun-Yan, Li, Jiao-Yu, Tao, Lei, Gong, Hong-Li, Zhang, Ming and Zhou, Liang (2023),

Tetraspanin CD63 Reduces the Progression and Metastasis of Head and Neck Squamous Cell Carcinoma via KRT1-Mediated Cell Cycle Arrest. *Heliyon*, 9(7): e17711.

Hugel, Bénédicte, Martínez, M. Carmen, Kunzelmann, Corinne and Freyssinet, Jean Marie (2005), Membrane Microparticles: Two Sides of the Coin. *Physiology*, 20(1): 22–27.

Hurwitz, Stephanie N., Conlon, Meghan M., Rider, Mark A., Brownstein, Naomi C. and Meckes, David G. (2016a), Nanoparticle Analysis Sheds Budding Insights into Genetic Drivers of Extracellular Vesicle Biogenesis. *Journal of Extracellular Vesicles*, 5(1).

Hurwitz, Stephanie N., Conlon, Meghan M., Rider, Mark A., Brownstein, Naomi C. and Meckes, David G. (2016b), Nanoparticle Analysis Sheds Budding Insights into Genetic Drivers of Extracellular Vesicle Biogenesis. *Journal of Extracellular Vesicles*, 5(1).

Jeong, Whun Kim, Wieckowski, Eva, Taylor, Douglas D., Reichert, Torsten E., Watkins, Simon and Whiteside, Theresa L. (2005), Fas Ligand-Positive Membranous Vesicles Isolated from Sera of Patients with Oral Cancer Induce Apoptosis of Activated T Lymphocytes. *Clinical Cancer Research*, 11(3): 1010–1020.

Jester, James V, Matthew Petroll, W, Barry, Patricia A and Dwight Cavanagh Jk, H (1995), Expression of Alpha-Smooth Muscle (Alpha-SM) Actin during Corneal Stromal Wound Healing. *Investigative Ophthalmology & Visual Science*, 36(5): 809–819.

Jiang, Erhui, Xu, Zhi, Wang, Meng, Yan, Tinglin, Huang, Chunming, Zhou, Xiaocheng, Liu, Qing, Wang, Lin, Chen, Yang, Wang, Hui, Liu, Ke, Shao, Zhe and Shang, Zhengjun (2019), Tumoral Microvesicle–Activated Glycometabolic Reprogramming in Fibroblasts Promotes the Progression of Oral Squamous Cell Carcinoma. *FASEB Journal*, 33(4): 5690–5703.

Jiang, Huaili, Zhou, Lei, Shen, Na, Ning, Xianhui, Wu, Daquan, Jiang, Kanglun and Huang, Xinsheng (2022), M1 Macrophage-Derived Exosomes and Their Key Molecule LncRNA HOTTIP Suppress Head and Neck Squamous Cell Carcinoma Progression by Upregulating the TLR5/NF-KB Pathway. *Cell Death & Disease 2022 13:2*, 13(2): 1–15.

Jie, H. B., Gildener-Leapman, N., Li, J., Srivastava, R. M., Gibson, S. P., Whiteside, T. L. and Ferris, R. L. (2013), Intratumoral Regulatory T Cells Upregulate Immunosuppressive Molecules in Head and Neck Cancer Patients. *British Journal of Cancer*, 109(10): 2629–2635.

Jin, Nuo, Jin, Nianqiang, Bu, Wenhuan, Li, Xing, Liu, Lili, Wang, Zilin, Tong, Jin and Li, Dechao (2020), Long Non-Coding RNA TIRY Promotes Tumor Metastasis by Enhancing Epithelial-to-Mesenchymal Transition in Oral Cancer. *Experimental Biology and Medicine*, 245(7): 585–596.

Johnson, Daniel E., Burtness, Barbara, Leemans, C. René, Lui, Vivian Wai Yan, Bauman, Julie E. and Grandis, Jennifer R. (2020), Head and Neck Squamous Cell Carcinoma. *Nature Reviews Disease Primers 2020 6:1*, 6(1): 1–22.

Johnstone, R. M., Adam, M., Hammond, J. R., Orr, L. and Turbide, C. (1987), Vesicle Formation during Reticulocyte Maturation. Association of Plasma Membrane Activities with Released Vesicles (Exosomes). *Journal of Biological Chemistry*, 262(19): 9412–9420.

Joseph, Mathew J., Dangi-Garimella, Surabhi, Shields, Mario A., Diamond, Michelle E., Sun, Limin, Koblinski, Jennifer E. and Munshi, Hidayatullah G. (2009), Slug Is a Downstream Mediator of Transforming Growth Factor-Beta1-Induced Matrix Metalloproteinase-9 Expression and Invasion of Oral Cancer Cells. *Journal of cellular biochemistry*, 108(3): 726–736.

Joshi, Bhagyashree S., de Beer, Marit A., Giepmans, Ben N.G. and Zuhorn, Inge S. (2020), Endocytosis of Extracellular Vesicles and Release of Their Cargo from Endosomes. *ACS nano*, 14(4): 4444–4455.

Kang, Seo Young, Lee, Eun Ji, Byun, Jung Woo, Han, Dohyun, Choi, Yoori, Hwang, Do Won and Lee, Dong Soo (2021), Extracellular Vesicles Induce an Aggressive Phenotype in Luminal Breast Cancer Cells Via PKM2 Phosphorylation. *Frontiers in Oncology*, 11: 785450.

Kawakubo-Yasukochi, Tomoyo, Morioka, Masahiko, Hazekawa, Mai, Yasukochi, Atsushi, Nishinakagawa, Takuya, Ono, Kazuhiko, Kawano, Shintaro, Nakamura, Seiji and Nakashima, Manabu (2018), MiR-200c-3p Spreads Invasive Capacity in Human Oral Squamous Cell Carcinoma Microenvironment. *Molecular Carcinogenesis*, 57(2): 295–302.

Kerr, Alexander Ross and Lodi, Giovanni (2021), Management of Oral Potentially Malignant Disorders. *Oral diseases*, 27(8): 2008–2025.

Kilinc, Seda, Paisner, Rebekka, Camarda, Roman, Gupta, Suprit, Momcilovic, Olga, Kohnz, Rebecca A., Avsaroglu, Baris, L'Etoile, Noelle D., Perera, Rushika M., Nomura, Daniel K. and Goga, Andrei (2021), Oncogene-Regulated Release of Extracellular Vesicles. *Developmental Cell*, 56(13): 1989-2006.e6.

King, Hamish W., Michael, Michael Z. and Gleadle, Jonathan M. (2012), Hypoxic Enhancement of Exosome Release by Breast Cancer Cells. *BMC Cancer*, 12(1): 421.

Kinnunen, P. K.J. and Holopainen, J. M. (2000), Mechanisms of Initiation of Membrane Fusion: Role of Lipids. *Bioscience Reports*, 20(6): 465–482.

König, Lisa, Kasimir-Bauer, Sabine, Bittner, Ann Kathrin, Hoffmann, Oliver, Wagner, Bettina, Santos Manvailer, Luis Felipe, Kimmig, Rainer, Horn, Peter A. and Rebmann, Vera (2017), Elevated Levels of Extracellular Vesicles Are Associated with Therapy Failure and Disease Progression in Breast Cancer Patients Undergoing Neoadjuvant Chemotherapy. *OncoImmunology*, 7(1).

Korrer, Michael J and Kim, Young (2019), Phenotypical and Functional Analysis of Natural Killer Cells from Primary Human Head and Neck Squamous Cell Carcinomas. *The Journal of Immunology*, 202(1 Supplement).

Koumangoye, Rainelli B., Sakwe, Amos M., Goodwin, J. Shawn, Patel, Tina and Ochieng, Josiah (2011a), Detachment of Breast Tumor Cells Induces Rapid Secretion of Exosomes Which Subsequently Mediate Cellular Adhesion and Spreading. *PLOS ONE*, 6(9): e24234.

Koumangoye, Rainelli B., Sakwe, Amos M., Goodwin, J. Shawn, Patel, Tina and Ochieng, Josiah (2011b), Detachment of Breast Tumor Cells Induces Rapid Secretion of Exosomes Which Subsequently Mediate Cellular Adhesion and Spreading. *PLoS ONE*, 6(9).

Kubiczkova, Lenka, Sedlarikova, Lenka, Hajek, Roman and Sevcikova, Sabina (2012), TGF-β - an Excellent Servant but a Bad Master. *Journal of Translational Medicine*, 10(1): 1–24.

Kumar, Ashish, Kumar, Pawan, Sharma, Mitu, Kim, Susy, Singh, Sangeeta, Kridel, Steven J. and Deep, Gagan (2022), Role of Extracellular Vesicles Secretion in Paclitaxel Resistance of Prostate Cancer Cells. *Cancer Drug Resistance*, 5(3): null.

Kumar, Ayan Tyagi, Knops, Alexander, Swendseid, Brian, Martinez-Outschoom, Ubaldo, Harshyne, Larry, Philp, Nancy, Rodeck, Ulrich, Luginbuhl, Adam, Cognetti, David, Johnson, Jennifer and Curry, Joseph (2019), Prognostic Significance of Tumor-Associated Macrophage Content in Head and Neck Squamous Cell Carcinoma: A Meta-Analysis. *Frontiers in Oncology*, 9.

Kwok, Zhi Hao, Wang, Chenghao and Jin, Yang (2021), Extracellular Vesicle Transportation and Uptake by Recipient Cells: A Process to Regulate Human Diseases. *Processes (Basel, Switzerland)*, 9(2): 1–16.

Languino, Lucia R, Singh, Amrita, Prisco, Marco, Inman, Gareth J, Luginbuhl, Adam, Curry, Joseph M and South, Andrew P (2016), Exosome-Mediated Transfer from the Tumor Microenvironment Increases TGFβ Signaling in Squamous Cell Carcinoma. *American Journal of Translational Research*, 8(5): 2432–2437.

Lázaro-Ibáñez, Elisa, Neuvonen, Maarit, Takatalo, Maarit, Thanigai Arasu, Uma, Capasso, Cristian, Cerullo, Vincenzo, Rhim, Johng S., Rilla, Kirsi, Yliperttula, Marjo and Siljander, Pia

R.M. (2017), Metastatic State of Parent Cells Influences the Uptake and Functionality of Prostate Cancer Cell-Derived Extracellular Vesicles. *Journal of Extracellular Vesicles*, 6(1).

Lecomte, Sara, Devreux, Julien, de Streel, Grégoire, van Baren, Nicolas, Havelange, Violaine, Schröder, David, Vaherto, Noora, Vanhaver, Christophe, Vanderaa, Christophe, Dupuis, Noémie, Pecquet, Christian, Coulie, Pierre G., Constantinescu, Stefan N. and Lucas, Sophie (2023), Therapeutic Activity of GARP:TGF-B1 Blockade in Murine Primary Myelofibrosis. *Blood*, 141(5): 490–502.

Lee, Ho Hyung, Elia, Natalie, Ghirlando, Rodolfo, Lippincott-Schwartz, Jennifer and Hurley, James H. (2008), Midbody Targeting of the ESCRT Machinery by a Noncanonical Coiled Coil in CEP55. *Science (New York, N.Y.)*, 322(5901): 576–580.

Lee, Tae Hoon, Chennakrishnaiah, Shilpa, Audemard, Eric, Montermini, Laura, Meehan, Brian and Rak, Janusz (2014), Oncogenic Ras-Driven Cancer Cell Vesiculation Leads to Emission of Double-Stranded DNA Capable of Interacting with Target Cells. *Biochemical and Biophysical Research Communications*, 451(2): 295–301.

Leemans, C. René, Braakhuis, Boudewijn J.M. and Brakenhoff, Ruud H. (2010), The Molecular Biology of Head and Neck Cancer. *Nature Reviews Cancer 2011 11:1*, 11(1): 9–22.

Levy, Daniel, Do, Mai Anh, Brown, Annie, Asano, Kyle, Diebold, David, Chen, Hanzhe, Zhang, Jiayi, Lawler, Brendan and Lu, Biao (2020), Genetic Labeling of Extracellular Vesicles for Studying Biogenesis and Uptake in Living Mammalian Cells. *Methods in enzymology*, 645: 1–14.

Li, B., Antonyak, M. A., Zhang, J. and Cerione, R. A. (2012), RhoA Triggers a Specific Signaling Pathway That Generates Transforming Microvesicles in Cancer Cells. *Oncogene*, 31(45): 4740–4749.

Li, Huan, Zhang, Ji, Chen, Shu Wei, Liu, Lu lu, Li, Lei, Gao, Fan, Zhuang, Shi Min, Wang, Li ping, Li, Yan and Song, Ming (2015), Cancer-Associated Fibroblasts Provide a Suitable Microenvironment for Tumor Development and Progression in Oral Tongue Squamous Cancer. *Journal of Translational Medicine*, 13(1): 198.

Li, Ling, Cao, Bangrong, Liang, Xinhua, Lu, Shun, Luo, Huaichao, Wang, Zhaohui, Wang, Shaoxin, Jiang, Jian, Lang, Jinyi and Zhu, Guiquan (2019), Microenvironmental Oxygen Pressure Orchestrates an Anti- and pro-Tumoral Γδ T Cell Equilibrium via Tumor-Derived Exosomes. *Oncogene*, 38(15): 2830–2843.

Li, Ling, Li, Chao, Wang, Shaoxin, Wang, Zhaohui, Jiang, Jian, Wang, Wei, Li, Xiaoxia, Chen, Jin, Liu, Kun, Li, Chunhua and Zhu, Guiquan (2016), Exosomes Derived from Hypoxic Oral

Squamous Cell Carcinoma Cells Deliver MiR-21 to Normoxic Cells to Elicit a Prometastatic Phenotype. *Cancer Research*, 76(7): 1770–1780.

Li, Ruowei, Zhou, Yifan, Zhang, Miaomiao, Xie, Ruiqi, Duan, Ning, Liu, Hong, Qin, Yao, Ma, Jingjing, Li, Zhiyuan, Ye, Pei, Wang, Wenmei and Wang, Xiang (2023), Oral Squamous Cell Carcinoma-Derived EVs Promote Tumor Progression by Regulating Inflammatory Cytokines and the IL-17A-Induced Signaling Pathway. *International Immunopharmacology*, 118: 110094.

Li, Xia, Xu, Qing, Wu, Yuhui, Li, Jinyun, Tang, Dongsheng, Han, Lu and Fan, Qinqiao (2014), A CCL2/ROS Autoregulation Loop Is Critical for Cancer-Associated Fibroblasts-Enhanced Tumor Growth of Oral Squamous Cell Carcinoma. *Carcinogenesis*, 35(6): 1362–1370.

Li, Yao yin, Tao, Yi wei, Gao, Shuo, Li, Pei, Zheng, Jian mao, Zhang, Si en, Liang, Jianfeng and Zhang, Yuejiao (2018), Cancer-Associated Fibroblasts Contribute to Oral Cancer Cells Proliferation and Metastasis via Exosome-Mediated Paracrine MiR-34a-5p. *EBioMedicine*, 36: 209–220.

Li, Yuchen, He, Xigan, Li, Qin, Lai, Hongyan, Zhang, Hena, Hu, Zhixiang, Li, Yan and Huang, Shenglin (2020), EV-Origin: Enumerating the Tissue-Cellular Origin of Circulating Extracellular Vesicles Using ExLR Profile. *Computational and Structural Biotechnology Journal*, 18: 2851–2859. a

Liang, Weilian, Chen, Yang, Liu, Hanzhe, Zhao, Hui, Luo, Tingting, Tang, Hokeung, Zhou, Xiaocheng, Jiang, Erhui, Shao, Zhe, Liu, Ke and Shang, Zhengjun (2022), Cancer Cells Corrupt Normal Epithelial Cells through MiR-Let-7c-Rich Small Extracellular Vesicle-Mediated Downregulation of P53/PTEN. *International Journal of Oral Science*, 14(1).

Liao, Zhaohao, Jaular, Lorena Martin, Soueidi, Estelle, Jouve, Mabel, Muth, Dillon C., Schøyen, Tine H., Seale, Tessa, Haughey, Norman J., Ostrowski, Matias, Théry, Clotilde and Witwer, Kenneth W. (2019), Acetylcholinesterase Is Not a Generic Marker of Extracellular Vesicles. *Journal of extracellular vesicles*, 8(1).

Lim, Kue Peng, Cirillo, Nicola, Hassona, Yazan, Wei, Wenbin, Thurlow, Johanna K., Cheong, Sok Ching, Pitiyage, Gayani, Parkinson, E. Ken and Prime, Stephen S. (2011), Fibroblast Gene Expression Profile Reflects the Stage of Tumour Progression in Oral Squamous Cell Carcinoma. *Journal of Pathology*, 223(4): 459–469.

Lin, Shih Shen, Peng, Chih Yu, Liao, Yi Wen, Chou, Ming Yung, Hsieh, Pei Ling and Yu, Cheng Chia (2018), MiR-1246 Targets CCNG2 to Enhance Cancer Stemness and Chemoresistance in Oral Carcinomas. *Cancers*, 10(8): 272.

Liu, Wei, Wu, Lan, Shen, Xue Min, Shi, Lin Jun, Zhang, Chen Ping, Xu, Li Qun and Zhou, Zeng Tong (2013), Expression Patterns of Cancer Stem Cell Markers ALDH1 and CD133 Correlate with a High Risk of Malignant Transformation of Oral Leukoplakia. *International journal of cancer*, 132(4): 868–874.

Liu, Xi, Miao, Jinhua, Wang, Cong, Zhou, Shan, Chen, Shuangqin, Ren, Qian, Hong, Xue, Wang, Yongping, Hou, Fan Fan, Zhou, Lili and Liu, Youhua (2020), Tubule-Derived Exosomes Play a Central Role in Fibroblast Activation and Kidney Fibrosis. *Kidney International*, 97(6): 1181–1195.

Lobert, Viola Hé Lène and Stenmark, Harald (2012), The ESCRT Machinery Mediates Polarization of Fibroblasts through Regulation of Myosin Light Chain. *Journal of Cell Science*, 125(1): 29–36.

Logozzi, Mariantonia, De Milito, Angelo, Lugini, Luana, Borghi, Martina, Calabrò, Luana, Spada, Massimo, Perdicchio, Maurizio, Marino, Maria Lucia, Federici, Cristina, Iessi, Elisabetta, Brambilla, Daria, Venturi, Giulietta, Lozupone, Francesco, Santinami, Mario, Huber, Veronica, Maio, Michele, Rivoltini, Licia and Fais, Stefano (2009), High Levels of Exosomes Expressing CD63 and Caveolin-1 in Plasma of Melanoma Patients. *PLoS ONE*, 4(4): e5219.

Logullo, Angela F., Nonogaki, Suely, Miguel, Roberto E., Kowalski, Luiz P., Nishimoto, Inês N., Pasini, Fátima S., Federico, Miriam H.H., Brentani, Ricardo R. and Brentani, M. Mitzi (2003), Transforming Growth Factor Beta1 (TGFbeta1) Expression in Head and Neck Squamous Cell Carcinoma Patients as Related to Prognosis. *Journal of oral pathology & medicine : official publication of the International Association of Oral Pathologists and the American Academy of Oral Pathology*, 32(3): 139–145.

Lu, Shi Long, Reh, Douglas, Li, Allen G., Woods, Jennifer, Corless, Christopher L., Kulesz-Martin, Molly and Wang, Xiao Jing (2004), Overexpression of Transforming Growth Factor Beta1 in Head and Neck Epithelia Results in Inflammation, Angiogenesis, and Epithelial Hyperproliferation. *Cancer research*, 64(13): 4405–4410.

Lu, Tingwei, Zhang, Zhen, Zhang, Jianjun, Pan, Xinhua, Zhu, Xueqin, Wang, Xu, Li, Zhihui, Ruan, Min, Li, Huasheng, Chen, Wantao and Yan, Ming (2022), CD73 in Small Extracellular Vesicles Derived from HNSCC Defines Tumour-associated Immunosuppression Mediated by Macrophages in the Microenvironment. *Journal of Extracellular Vesicles*, 11(5).

Łuczaj, Wojciech, Wroński, Adam, Domingues, Pedro, Rosário Domingues, M. and Skrzydlewska, Elżbieta (2020), Lipidomic Analysis Reveals Specific Differences between Fibroblast and Keratinocyte Ceramide Profile of Patients with Psoriasis Vulgaris. *Molecules*, 25(3).

Ludwig, Nils, Yerneni, Saigopalakrishna S., Azambuja, Juliana H., Pietrowska, Monika, Widłak, Piotr, Hinck, Cynthia S., Głuszko, Alicja, Szczepański, Mirosław J., Kärmer, Teresa, Kallinger, Isabella, Schulz, Daniela, Bauer, Richard J., Spanier, Gerrit, Spoerl, Steffen, Meier, Johannes K., Ettl, Tobias, Razzo, Beatrice M., Reichert, Torsten E., Hinck, Andrew P. and Whiteside, Theresa L. (2022), TGFβ+ Small Extracellular Vesicles from Head and Neck Squamous Cell Carcinoma Cells Reprogram Macrophages towards a Pro-angiogenic Phenotype. *Journal of Extracellular Vesicles*, 11(12): 12294.

Ludwig, Nils, Yerneni, Saigopalakrishna S, Razzo, Beatrice M and Whiteside, Theresa L (2018), Exosomes from HNSCC Promote Angiogenesis through Reprogramming of Endothelial Cells. *Molecular Cancer Research*, 16(11): 1798–1808.

Lundholm, Marie, Schröder, Mona, Nagaeva, Olga, Baranov, Vladimir, Widmark, Anders, Mincheva-Nilsson, Lucia and Wikström, Pernilla (2014), Prostate Tumor-Derived Exosomes down-Regulate NKG2D Expression on Natural Killer Cells and CD8+ T Cells: Mechanism of Immune Evasion. *PloS one*, 9(9).

Maida, Yoshiko, Takakura, Masahiro, Nishiuchi, Takumi, Yoshimoto, Tanihiro and Kyo, Satoru (2016), Exosomal Transfer of Functional Small RNAs Mediates Cancer-stroma Communication in Human Endometrium. *Cancer Medicine*, 5(2): 304.

Maity, Sourav, Caillat, Christophe, Miguet, Nolwenn, Sulbaran, Guidenn, Effantin, Gregory, Schoehn, Guy, Roos, Wouter H. and Weissenhorn, Winfried (2019), VPS4 Triggers Constriction and Cleavage of ESCRT-III Helical Filaments. *Science Advances*, 5(4): eaau7198.

Malhotra, Vikas and Perry, Michael C. (2003), Classical Chemotherapy: Mechanisms, Toxicities and the Therapeutc Window. *http://dx.doi.org/10.4161/cbt.199*, 2(4 Suppl 1).

Mathieu, Mathilde, Névo, Nathalie, Jouve, Mabel, Valenzuela, José Ignacio, Maurin, Mathieu, Verweij, Frederik J., Palmulli, Roberta, Lankar, Danielle, Dingli, Florent, Loew, Damarys, Rubinstein, Eric, Boncompain, Gaëlle, Perez, Franck and Théry, Clotilde (2021), Specificities of Exosome versus Small Ectosome Secretion Revealed by Live Intracellular Tracking of CD63 and CD9. *Nature Communications 2021 12:1*, 12(1): 1–18.

Matsumoto, Akihiro, Takahashi, Yuki, Nishikawa, Makiya, Sano, Kohei, Morishita, Masaki, Charoenviriyakul, Chonlada, Saji, Hideo and Takakura, Yoshinobu (2017), Accelerated Growth of B16BL6 Tumor in Mice through Efficient Uptake of Their Own Exosomes by B16BL6 Cells. *Cancer Science*, 108(9): 1803–1810.

Matte, Bibiana F., Kumar, Aditya, Placone, Jesse K., Zanella, Virgılio G., Martins, Manoela D., Engler, Adam J. and Lamers, Marcelo L. (2019), Matrix Stiffness Mechanically Conditions EMT and Migratory Behavior of Oral Squamous Cell Carcinoma. *Journal of Cell Science*, 132(1).

Maybruck, Brian T., Pfannenstiel, Lukas W., Diaz-Montero, Marcela and Gastman, Brian R. (2017), Tumor-Derived Exosomes Induce CD8+ T Cell Suppressors. *Journal for ImmunoTherapy of Cancer*, 5(1).

Mazurkiewicz, Justyna, Simiczyjew, Aleksandra, Dratkiewicz, Ewelina, Pietraszek-Gremplewicz, Katarzyna, Majkowski, Michał, Kot, Magdalena, Ziętek, Marcin, Matkowski, Rafał and Nowak, Dorota (2022), Melanoma Cells with Diverse Invasive Potential Differentially Induce the Activation of Normal Human Fibroblasts. *Cell Communication and Signaling*, 20(1): 1–19.

McAtee, Caitlin O., Booth, Christine, Elowsky, Christian, Zhao, Lei, Payne, Jeremy, Fangman, Teresa, Caplan, Steve, Henry, Michael D. and Simpson, Melanie A. (2019), Prostate Tumor Cell Exosomes Containing Hyaluronidase Hyal1 Stimulate Prostate Stromal Cell Motility by Engagement of FAK-Mediated Integrin Signaling. *Matrix biology : journal of the International Society for Matrix Biology*, 78–79: 165–179.

McConnell, Russell E., Youniss, Madeleine, Gnanasambandam, Bhargavee, Shah, Palak, Zhang, Wei and Finn, Jonathan D. (2022), Transfection Reagent Artefact Likely Accounts for Some Reports of Extracellular Vesicle Function. *Journal of extracellular vesicles*, 11(10).

Meliante, Piero Giuseppe, Zoccali, Federica, de Vincentiis, Marco, Ralli, Massimo, Petrella, Carla, Fiore, Marco, Minni, Antonio and Barbato, Christian (2023), Diagnostic Predictors of Immunotherapy Response in Head and Neck Squamous Cell Carcinoma. *Diagnostics*, 13(5).

Melo-Alvim, Cecília, Neves, Maria Eduarda, Santos, Jorge Leitão, Abrunhosa-Branquinho, André N., Barroso, Tiago, Costa, Luís and Ribeiro, Leonor (2023), Radiotherapy, Chemotherapy and Immunotherapy—Current Practice and Future Perspectives for Recurrent/Metastatic Oral Cavity Squamous Cell Carcinoma. *Diagnostics*, 13(1).

Menck, Kerstin, Sönmezer, Can, Worst, Thomas Stefan, Schulz, Matthias, Dihazi, Gry Helene, Streit, Frank, Erdmann, Gerrit, Kling, Simon, Boutros, Michael, Binder, Claudia and Gross, Julia Christina (2017), Neutral Sphingomyelinases Control Extracellular Vesicles Budding from the Plasma Membrane. *Journal of Extracellular Vesicles*, 6(1).

Meng, Xiao Ming, Nikolic-Paterson, David J. and Lan, Hui Yao (2016), TGF-β: The Master Regulator of Fibrosis. *Nature Reviews Nephrology 2016 12:6*, 12(6): 325–338.

Metelli, Alessandra, Salem, Mohammad, Wallace, Caroline H., Wu, Bill X., Li, Anqi, Li, Xue and Li, Zihai (2018), Immunoregulatory Functions and the Therapeutic Implications of GARP-TGF-β in Inflammation and Cancer. *Journal of hematology & oncology*, 11(1).

Meulmeester, Erik and Ten Dijke, Peter (2011), The Dynamic Roles of TGF-β in Cancer. *The Journal of pathology*, 223(2): 206–219.

Miller, Daniel S.J., Bloxham, Robert D., Jiang, Ming, Gori, Ilaria, Saunders, Rebecca E., Das, Debipriya, Chakravarty, Probir, Howell, Michael and Hill, Caroline S. (2018), The Dynamics of TGF-β Signaling Are Dictated by Receptor Trafficking via the ESCRT Machinery. *Cell Reports*, 25(7): 1841-1855.e5.

Momen-Heravi, Fatemeh and Bala, Shashi (2018), Extracellular Vesicles in Oral Squamous Carcinoma Carry Oncogenic MiRNA Profile and Reprogramme Monocytes via NF-KB Pathway. *Oncotarget*, 9(78): 34838–34854.

Morgan-Fisher, Marie, Wewer, Ulla M and Yoneda, Atsuko (2013), Regulation of ROCK Activity in Cancer. *Journal of Histochemistry and Cytochemistry*, 61(3): 185–198.

Morioka, Masahiko, Kawakubo-Yasukochi, Tomoyo, Hayashi, Yoshikazu, Nishinakagawa, Takuya, Hazekawa, Mai, Kawano, Shintaro, Nakamura, Seiji and Nakashima, Manabu (2016), The SQUU-B Cell Line Spreads Its Metastatic Properties to Nonmetastatic Clone SQUU-A from the Same Patient through Exosomes. *Journal of Oral Biosciences*, 58(1): 33–38.

Nabhan, Joseph F., Hu, Ruoxi, Oh, Raymond S., Cohen, Stanley N. and Lu, Quan (2012), Formation and Release of Arrestin Domain-Containing Protein 1-Mediated Microvesicles (ARMMs) at Plasma Membrane by Recruitment of TSG101 Protein. *Proceedings of the National Academy of Sciences of the United States of America*, 109(11): 4146–4151.

van Niel, Guillaume, Charrin, Stéphanie, Simoes, Sabrina, Romao, Maryse, Rochin, Leila, Saftig, Paul, Marks, Michael S., Rubinstein, Eric and Raposo, Graça (2011), The Tetraspanin CD63 Regulates ESCRT-Independent and Dependent Endosomal Sorting during Melanogenesis. *Developmental cell*, 21(4): 708.

Van Niel, Guillaume, D'Angelo, Gisela and Raposo, Graça (2018), Shedding Light on the Cell Biology of Extracellular Vesicles. *Nature Reviews Molecular Cell Biology*, 19(4): 213–228.

Nurmik, Martin, Ullmann, Pit, Rodriguez, Fabien, Haan, Serge and Letellier, Elisabeth (2020), In Search of Definitions: Cancer-associated Fibroblasts and Their Markers. *International Journal of Cancer*, 146(4): 895.

Ogretmen, Besim and Hannun, Yusuf A. (2004), Biologically Active Sphingolipids in Cancer Pathogenesis and Treatment. *Nature Reviews Cancer 2004 4:8*, 4(8): 604–616.

O'Higgins, Caoimhín, Ward, Frank J. and Eid, Rasha Abu (2018), Deciphering the Role of Regulatory CD4 T Cells in Oral and Oropharyngeal Cancer: A Systematic Review. *Frontiers in Oncology*, 8(OCT).

Oosting, Sjoukje F. and Haddad, Robert I. (2019), Best Practice in Systemic Therapy for Head and Neck Squamous Cell Carcinoma. *Frontiers in Oncology*, 9(AUG): 815.

Ostrowski, Matias, Carmo, Nuno B, Krumeich, Sophie, Fanget, Isabelle, Raposo, Graça, Savina, Ariel, Moita, Catarina F, Schauer, Kristine, Hume, Alistair N, Freitas, Rui P, Goud, Bruno, Benaroch, Philippe, Hacohen, Nir, Fukuda, Mitsunori, Desnos, Claire, Seabra, Miguel C, Darchen, François, Amigorena, Sebastian, Moita, Luis F and Thery, Clotilde (2010), Rab27a and Rab27b Control Different Steps of the Exosome Secretion Pathway. *Nature Cell Biology*, 12(1): 19–30.

Pai, Sara I. and Westra, William H. (2009), Molecular Pathology of Head and Neck Cancer: Implications for Diagnosis, Prognosis, and Treatment. *Annual Review of Pathology: Mechanisms of Disease*, 4(1): 49–70.

Pampaloni, Francesco, Reynaud, Emmanuel G. and Stelzer, Ernst H.K. (2007), The Third Dimension Bridges the Gap between Cell Culture and Live Tissue. *Nature Reviews Molecular Cell Biology*, 8(10): 839–845.

Pang, Xin, Tang, Ya Ling and Liang, Xin Hua (2018), Transforming Growth Factor-β Signaling in Head and Neck Squamous Cell Carcinoma: Insights into Cellular Responses. *Oncology Letters*, 16(4): 4799.

Panigrahi, Gati K., Praharaj, Prakash P., Peak, Taylor C., Long, Jessica, Singh, Ravi, Rhim, Johng S., Elmageed, Zakaria Y.Abd and Deep, Gagan (2018), Hypoxia-Induced Exosome Secretion Promotes Survival of African-American and Caucasian Prostate Cancer Cells. *Scientific Reports 2018 8:1*, 8(1): 1–13.

Park, K. S., Poburko, D., Wollheim, C. B. and Demaurex, N. (2009), Amiloride Derivatives Induce Apoptosis by Depleting ER Ca2+ Stores in Vascular Endothelial Cells. *British Journal of Pharmacology*, 156(8): 1296.

Parkin, D. M., Bray, F., Ferlay, J. and Pisani, P. (2005), Global Cancer Statistics, 2002. *CA: A Cancer Journal for Clinicians*, 55(2): 74–108.

Patil, Vijay Maruti, Noronha, Vanita, Menon, Nandini, Singh, Ajay, Ghosh-Laskar, Sarbani, Budrukkar, Ashwini, Bhattacharjee, Atanu, Swain, Monali, Mathrudev, Vijayalakshmi, Nawale, Kavita, Balaji, Arun, Peelay, Zoya, Alone, Mitali, Pathak, Shruti, Mahajan, Abhishek, Kumar, Suman, Purandare, Nilendu, Agarwal, Archi, Puranik, Ameya, Pendse, Shantanu, Reddy Yallala, Monica, Sahu, Harsh, Kapu, Venkatesh, Dey, Sayak, Choudhary, Jatin, Krishna, Madala Ravi, Shetty, Alok, Karuvandan, Naveen, Ravind, Rahul, Rai, Rahul, Jobanputra, Kunal, Chaturvedi, Pankaj, Pai, Prathamesh S., Chaukar, Devendra, Nair, Sudhir, Thiagarajan, Shivakumar and Prabhash, Kumar (2023), Results of Phase III Randomized Trial for Use of Docetaxel as a Radiosensitizer in Patients With Head and Neck Cancer, Unsuitable for Cisplatin-Based Chemoradiation. *Journal of clinical oncology : official journal of the American Society of Clinical Oncology*, 41(13): 2350–2361.

Peacock, Ben, Rigby, Alice, Bradford, James, Pink, Ryan, Hunter, Keith, Lambert, Daniel and Hunt, Stuart (2018), Extracellular Vesicle MicroRNA Cargo Is Correlated with HPV Status in Oropharyngeal Carcinoma. *Journal of Oral Pathology and Medicine*, 47(10): 954–963.

Peltanova, Barbora, Raudenska, Martina and Masarik, Michal (2019), Effect of Tumor Microenvironment on Pathogenesis of the Head and Neck Squamous Cell Carcinoma: A Systematic Review. *Molecular Cancer*, 18(1): 1–24.

Peng, Yilin, Zhao, Min, Hu, Yinying, Guo, Hongyan, Zhang, Yanyan, Huang, Yanqin, Zhao, Lin, Chai, Yong and Wang, Zhigang (2022), Blockade of Exosome Generation by GW4869 Inhibits the Education of M2 Macrophages in Prostate Cancer. *BMC Immunology*, 23(1).

Perez-Ordoñez, B., Beauchemin, M. and Jordan, R. C.K. (2006), Molecular Biology of Squamous Cell Carcinoma of the Head and Neck. *Journal of Clinical Pathology*, 59(5): 445.

Pickup, Michael, Novitskiy, Sergey and Moses, Harold L. (2013), The Roles of TGFβ in the Tumour Microenvironment. *Nature reviews. Cancer*, 13(11): 788.

Plummer, Emily M. and Manchester, Marianne (2012), Endocytic Uptake Pathways Utilized by CPMV Nanoparticles. *Molecular Pharmaceutics*, 10(1): 26–32.

Pols, Maaike S. and Klumperman, Judith (2009), Trafficking and Function of the Tetraspanin CD63. *Experimental cell research*, 315(9): 1584–1592.

Prime, Stephen S., Nixon, Sally V.R., Crane, Isabel J., Stone, Andrea, Matthews, John B., Maitland, Norman J., Remnant, Lucy, Powell, Susan K., Game, Stephen M. and Scully, Crispian (1990), The Behaviour of Human Oral Squamous Cell Carcinoma in Cell Culture. *The Journal of pathology*, 160(3): 259–269.

Principe, Simona, Mejia-Guerrero, Salvador, Ignatchenko, Vladimir, Sinha, Ankit, Ignatchenko, Alexandr, Shi, Willa, Pereira, Keira, Su, Susie, Huang, Shao Hui, O'Sullivan, Brian, Xu, Wei, Goldstein, David P., Weinreb, Ilan, Ailles, Laurie, Liu, Fei Fei and Kislinger, Thomas (2018), Proteomic Analysis of Cancer-Associated Fibroblasts Reveals a Paracrine Role for MFAP5 in Human Oral Tongue Squamous Cell Carcinoma. *Journal of Proteome Research*, 17(6): 2045–2059.

Purushothaman, Anurag, Bandari, Shyam Kumar, Liu, Jian, Mobley, James A., Brown, Elizabeth A. and Sanderson, Ralph D. (2016), Fibronectin on the Surface of Myeloma Cell-Derived Exosomes Mediates Exosome-Cell Interactions. *Journal of Biological Chemistry*, 291(4): 1652–1663.

Qadir, Fatima, Aziz, Mohammad Arshad, Sari, Chrisdina Puspita, Ma, Hong, Dai, Haiyan, Wang, Xun, Raithatha, Dhiresh, Da Silva, Lucas Girotto Lagreca, Hussain, Muhammad, Poorkasreiy, Seyedeh P., Hutchison, Iain L., Waseem, Ahmad and Teh, Muy Teck (2018), Transcriptome Reprogramming by Cancer Exosomes: Identification of Novel Molecular Targets in Matrix and Immune Modulation. *Molecular Cancer*, 17(1): 1–16.

Qiao, Bin, Johnson, Newell W and Gao, Jin (2010), Epithelial-Mesenchymal Transition in Oral Squamous Cell Carcinoma Triggered by Transforming Growth Factor-Beta1 Is Snail Family-Dependent and Correlates with Matrix Metalloproteinase-2 and -9 Expressions. *International journal of oncology*, 37(3).

Raposo, Graça, Nijman, Hans W., Stoorvogel, Willem, Leijendekker, Richtje, Harding, Clifford V., Melief, Cornelis J.M. and Geuze, Hans J. (1996), B Lymphocytes Secrete Antigen-Presenting Vesicles. *Journal of Experimental Medicine*, 183(3): 1161–1172.

Raposo, Graça and Stoorvogel, Willem (2013), Extracellular Vesicles: Exosomes, Microvesicles, and Friends. *Journal of Cell Biology*, 200(4): 373–383.

Razzo, Beatrice M, Ludwig, Nils, Hong, Chang-Sook, Sharma, Pryanka, Fabian, Kellsye P, Fecek, Ronald J, Storkus, Walkter J and Whiteside, Theresa L (2019), Tumor-Derived Exosomes Promote Carcinogenesis of Murine Oral Squamous Cell Carcinoma. *Carcinogenesis*.

Reader, Claire S., Vallath, Sabari, Steele, Colin W., Haider, Syed, Brentnall, Adam, Desai, Ami, Moore, Kate M., Jamieson, Nigel B., Chang, David, Bailey, Peter, Scarpa, Aldo, Lawlor, Rita, Chelala, Claude, Keyse, Stephen M., Biankin, Andrew, Morton, Jennifer P., Evans, TR Jeffry, Barry, Simon T., Sansom, Owen J., Kocher, Hemant M. and Marshall, John F. (2019), The Integrin Avβ6 Drives Pancreatic Cancer through Diverse Mechanisms and Represents an Effective Target for Therapy. *The Journal of pathology*, 249(3): 332–342.

Richards, K. E., Zeleniak, A. E., Fishel, M. L., Wu, J., Littlepage, L. E. and Hill, R. (2016), Cancer-Associated Fibroblast Exosomes Regulate Survival and Proliferation of Pancreatic Cancer Cells. *Oncogene 2017 36:13*, 36(13): 1770–1778.

Riches, Andrew, Campbell, Elaine, Borger, Eva and Powis, Simon (2014), Regulation of Exosome Release from Mammary Epithelial and Breast Cancer Cells - a New Regulatory Pathway. *European journal of cancer (Oxford, England : 1990)*, 50(5): 1025–1034.

Richter, Petra, Umbreit, Claudia, Franz, Marcus, Berndt, Angela, Grimm, Susanne, Uecker, Andrea, Böhmer, Frank D., Kosmehl, Hartwig and Berndt, Alexander (2011), EGF/TGFβ1 Co-Stimulation of Oral Squamous Cell Carcinoma Cells Causes an Epithelial-Mesenchymal Transition Cell Phenotype Expressing Laminin 332. *Journal of oral pathology & medicine : official publication of the International Association of Oral Pathologists and the American Academy of Oral Pathology*, 40(1): 46–54.

Rider, Chris C. and Mulloy, Barbara (2017), Heparin, Heparan Sulphate and the TGF-β Cytokine Superfamily. *Molecules 2017, Vol. 22, Page 713*, 22(5): 713.

Rocha, Sara, Carvalho, Joana, Oliveira, Patrícia, Voglstaetter, Maren, Schvartz, Domitille, Thomsen, Andreas R., Walter, Nadia, Khanduri, Richa, Sanchez, Jean Charles, Keller, Andreas, Oliveira, Carla and Nazarenko, Irina (2019), 3D Cellular Architecture Affects MicroRNA and Protein Cargo of Extracellular Vesicles. *Advanced Science*, 6(4): 1800948.

Rojas, Elizabeta A., Corchete, Luis Antonio, San-Segundo, Laura, Martínez-Blanch, Juan F., Codoñer, Francisco M., Paíno, Teresa, Puig, Noemí, García-Sanz, Ramon, Mateos, María Victoria, Ocio, Enrique M., Misiewicz-Krzeminska, Irena and Gutierrez, Norma C. (2017), Amiloride, an Old Diuretic Drug, Is a Potential Therapeutic Agent for Multiple Myeloma. *Clinical Cancer Research*, 23(21): 6602–6615.

Roseblade, Ariane, Luk, Frederick, Ung, Alison and Bebawy, Mary (2015), Targeting Microparticle Biogenesis: A Novel Approach to the Circumvention of Cancer Multidrug Resistance. *Current Cancer Drug Targets*, 15(3): 205–214.

Ruiz-Martinez, Marc, Navarro, Alfons, Marrades, Ramón M., Viñolas, Nuria, Santasusagna, Sandra, Muñoz, Carmen, Ramírez, Josep, Molins, Laureano and Monzo, Mariano (2016), YKT6 Expression, Exosome Release, and Survival in Non-Small Cell Lung Cancer. *Oncotarget*, 7(32): 51515–51524.

Sadovska, Lilite, Zandberga, Elīna, Sagini, Krizia, Jēkabsons, Kaspars, Riekstiņa, Una, Kalniņa, Zane, Llorente, Alicia and Linē, Aija (2018), A Novel 3D Heterotypic Spheroid Model for

Studying Extracellular Vesicle-Mediated Tumour and Immune Cell Communication. *Biochemical and biophysical research communications*, 495(2): 1930–1935.

Sakha, Sujata, Muramatsu, Tomoki, Ueda, Koji and Inazawa, Johji (2016), Exosomal MicroRNA MiR-1246 Induces Cell Motility and Invasion through the Regulation of DENND2D in Oral Squamous Cell Carcinoma. *Scientific Reports*, 6(1): 1–11.

Salo, Tuula, Sutinen, Meeri, Hoque Apu, Ehsanul, Sundquist, Elias, Cervigne, Nilva K., de Oliveira, Carine Ervolino, Akram, Saad Ullah, Ohlmeier, Steffen, Suomi, Fumi, Eklund, Lauri, Juusela, Pirjo, Åström, Pirjo, Bitu, Carolina Cavalcante, Santala, Markku, Savolainen, Kalle, Korvala, Johanna, Paes Leme, Adriana Franco and Coletta, Ricardo D. (2015), A Novel Human Leiomyoma Tissue Derived Matrix for Cell Culture Studies. *BMC Cancer*, 15(1): 1.

Savina, Ariel, Furlán, Marcelo, Vidal, Michel and Colombo, Maria I. (2003), Exosome Release Is Regulated by a Calcium-Dependent Mechanism in K562 Cells. *Journal of Biological Chemistry*, 278(22): 20083–20090.

Sebbagh, M., Renvoizé, C., Hamelin, J., Riché, N., Bertoglio, J. and Bréard, J. (2001), Caspase-3-Mediated Cleavage of ROCK I Induces MLC Phosphorylation and Apoptotic Membrane Blebbing. *Nature Cell Biology*, 3(4): 346–352.

Sedgwick, Alanna E. and D'Souza-Schorey, Crislyn (2018), The Biology of Extracellular Microvesicles. *Traffic*, 19(5): 319–327.

Sento, Shinya, Sasabe, Eri and Yamamoto, Tetsuya (2016), Application of a Persistent Heparin Treatment Inhibits the Malignant Potential of Oral Squamous Carcinoma Cells Induced by Tumor Cell-Derived Exosomes. *PLoS ONE*, 11(2): e0148454.

Shacka, John J., Klocke, Barbara J. and Roth, Kevin A. (2006), Autophagy, Bafilomycin and Cell Death: The 'A-B-Cs' of Plecomacrolide-Induced Neuroprotection. *Autophagy*, 2(3): 228–230.

Shan, Ying, You, Bo, Shi, Si, Shi, Wei, Zhang, Zhenxin, Zhang, Qicheng, Gu, Miao, Chen, Jing, Bao, Lili, Liu, Dong and You, Yiwen (2018), Hypoxia-Induced Matrix Metalloproteinase-13 Expression in Exosomes from Nasopharyngeal Carcinoma Enhances Metastases. *Cell Death and Disease*, 9(3): 382.

Shelke, Ganesh Vilas, Yin, Yanan, Jang, Su Chul, Lässer, Cecilia, Wennmalm, Stefan, Hoffmann, Hans Jürgen, Li, Li, Gho, Yong Song, Nilsson, Jonas Andreas and Lötvall, Jan (2019), Endosomal Signalling via Exosome Surface TGFβ-1. *Journal of Extracellular Vesicles*, 8(1).

Shephard, Pierre, Martin, Gail, Smola-Hess, Sigrun, Brunner, Georg, Krieg, Thomas and Smola, Hans (2004), Myofibroblast Differentiation Is Induced in Keratinocyte-Fibroblast Co-Cultures

and Is Antagonistically Regulated by Endogenous Transforming Growth Factor-β and Interleukin-1. *The American Journal of Pathology*, 164(6): 2055.

Shi, Zhihua, Jiang, Tao, Cao, Bingji, Sun, Xusheng and Liu, Jun Feng (2022), CAF-Derived Exosomes Deliver LINC01410 to Promote Epithelial-Mesenchymal Transition of Esophageal Squamous Cell Carcinoma. *Experimental Cell Research*, 412(2).

Shinoda, Hajime, Shannon, Michael and Nagai, Takeharu (2018), Fluorescent Proteins for Investigating Biological Events in Acidic Environments. *International Journal of Molecular Sciences*, 19(6).

Shuang, Yu, Yao, Xiaofeng, Liu, Jing, Niu, Juntao, Guo, Wenyu and Li, Chao (2022), Serum-Derived Extracellular Vesicles Mediate Smad4 Expression through Shuttling MicroRNA-27a in the Progression of Laryngeal Squamous Cell Carcinoma. *Human Cell*, 35(4): 1084–1099.

Siddiqi, Shadab A. and Mansbach, Charles M. (2008), PKC Zeta-Mediated Phosphorylation Controls Budding of the Pre-Chylomicron Transport Vesicle. *Journal of cell science*, 121(Pt 14): 2327–2338.

Silva, Thaiomara A., Smuczek, Basílio, Valadão, Iuri C., Dzik, Luciana M., Iglesia, Rebeca P., Cruz, Mário C., Zelanis, André, de Siqueira, Adriane S., Serrano, Solange M.T., Goldberg, Gary S., Jaeger, Ruy G. and Freitas, Vanessa M. (2016), AHNAK Enables Mammary Carcinoma Cells to Produce Extracellular Vesicles That Increase Neighboring Fibroblast Cell Motility. *Oncotarget*, 7(31): 49998.

Simon, Jean Pierre, Ivanov, Ivan E., Adesnik, Milton and Sabatini, David D. (1996), The Production of Post-Golgi Vesicles Requires a Protein Kinase C-like Molecule, but Not Its Phosphorylating Activity. *The Journal of cell biology*, 135(2): 355–370.

Skotland, Tore, Hessvik, Nina P., Sandvig, Kirsten and Llorente, Alicia (2019), Exosomal Lipid Composition and the Role of Ether Lipids and Phosphoinositides in Exosome Biology. *Journal of Lipid Research*, 60(1): 9–18.

Sneider, Alexandra, Liu, Ying, Starich, Bartholomew, Du, Wenxuan, Marar, Carolyn, Faqih, Najwa, Ciotti, Gabrielle E, Kim, Joo Ho, Krishnan, Sejal, Ibrahim, Salma, Igboko, Muna, Locke, Alexus, Lewis, Daniel M, Hong, Hanna, Karl, Michelle, Vij, Raghav, Russo, Gabriella C, Nair, Praful, Gómez-De-Mariscal, Estibaliz, Habibi, Mehran, Muñoz-Barrutia, Arrate, Gu, Luo, Karin Eisinger-Mathason, T S, Wirtz, Denis, Lewis, Daniel and Kim, Jooho (2023), Small Extracellular Vesicles Promote Stiffness-Mediated Metastasis. *bioRxiv*: 2023.07.01.545937.

Song, Jian, Zhang, Nian, Cao, Lideng, Xiao, Di, Ye, Xingchen, Luo, En and Zhang, Zhuang (2020), Down-Regulation of MiR-200c Associates with Poor Prognosis of Oral Squamous Cell Carcinoma. *International Journal of Clinical Oncology*, 25(6): 1072–1078.

Song, Lin, Tang, Shi, Han, Xiaolei, Jiang, Ziying, Dong, Lingling, Liu, Cuicui, Liang, Xiaoyan, Dong, Jixin, Qiu, Chengxuan, Wang, Yongxiang and Du, Yifeng (2019), KIBRA Controls Exosome Secretion via Inhibiting the Proteasomal Degradation of Rab27a. *Nature Communications*, 10(1): 1–13.

Song, Young Hye, Warncke, Christine, Choi, Sung Jin, Choi, Siyoung, Chiou, Aaron E., Ling, Lu, Liu, Han Yuan, Daniel, Susan, Antonyak, Marc A., Cerione, Richard A. and Fischbach, Claudia (2017), Breast Cancer-Derived Extracellular Vesicles Stimulate Myofibroblast Differentiation and pro-Angiogenic Behavior of Adipose Stem Cells. *Matrix Biology*, 60–61: 190–205.

Sorbye, Sveinung W., Kilvaer, Thomas K., Valkov, Andrej, Donnem, Tom, Smeland, Eivind, Al-Shibli, Khalid, Bremnes, Roy M. and Busund, Lill Tove (2012), Prognostic Impact of CD57, CD68, M-CSF, CSF-1R, Ki67 and TGF-Beta in Soft Tissue Sarcomas. *BMC clinical pathology*, 12.

Spitzberg, Joshua D., Ferguson, Scott, Yang, Katherine S., Peterson, Hannah M., Carlson, Jonathan C.T. and Weissleder, Ralph (2023), Multiplexed Analysis of EV Reveals Specific Biomarker Composition with Diagnostic Impact. *Nature Communications*, 14(1).

Sterlacci, William, Wolf, Dominik, Savic, Spasenija, Hilbe, Wolfgang, Schmid, Thomas, Jamnig, Herbert, Fiegl, Michael and Tzankov, Alexandar (2012), High Transforming Growth Factor β Expression Represents an Important Prognostic Parameter for Surgically Resected Non-Small Cell Lung Cancer. *Human pathology*, 43(3): 339–349.

de Streel, Grégoire, Bertrand, Charlotte, Chalon, Nicolas, Liénart, Stéphanie, Bricard, Orian, Lecomte, Sara, Devreux, Julien, Gaignage, Mélanie, De Boeck, Gitte, Mariën, Lore, Van De Walle, Inge, van der Woning, Bas, Saunders, Michael, de Haard, Hans, Vermeersch, Elien, Maes, Wim, Deckmyn, Hans, Coulie, Pierre G., van Baren, Nicolas and Lucas, Sophie (2020), Selective Inhibition of TGF-B1 Produced by GARP-Expressing Tregs Overcomes Resistance to PD-1/PD-L1 Blockade in Cancer. *Nature Communications 2020 11:1*, 11(1): 1–15.

Stuffers, Susanne, Sem Wegner, Catherine, Stenmark, Harald and Brech, Andreas (2009), Multivesicular Endosome Biogenesis in the Absence of ESCRTs. *Traffic*, 10(7): 925–937.

Sun, Li Ping, Xu, Kai, Cui, Jing, Yuan, Dao Ying, Zou, Bo, Li, Jun, Liu, Jian Lin, Li, Ke Yi, Meng, Zhen and Zhang, Bin (2019), Cancer-Associated Fibroblast-Derived Exosomal MiR-382-5p Promotes the Migration and Invasion of Oral Squamous Cell Carcinoma. *Oncology Reports*, 42(4): 1319–1328.

Sun, Limin, Diamond, Michelle E., Ottaviano, Adam J., Joseph, Mathew J., Ananthanarayan, Vijayalakshmi and Munshi, Hidayatullah G. (2008), Transforming Growth Factor-Beta 1 Promotes Matrix Metalloproteinase-9-Mediated Oral Cancer

Sun, Lulu, Kang, Xindan, Wang, Chong, Wang, Rui, Yang, Guizhu, Jiang, Wen, Wu, Qi, Wang, Yujue, Wu, Yaping, Gao, Jiamin, Chen, Lan, Zhang, Jie, Tian, Zhen, Zhu, Guopei and Sun, Shuyang (2023), Single-Cell and Spatial Dissection of Precancerous Lesions Underlying the Initiation Process of Oral Squamous Cell Carcinoma. *Cell Discovery 2023 9:1*, 9(1): 1–19.

Sun, Yulin, Zheng, Weiwei, Guo, Zhengguang, Ju, Qiang, Zhu, Lin, Gao, Jiajia, Zhou, Lanping, Liu, Fang, Xu, Yang, Zhan, Qimin, Zhou, Zhixiang, Sun, Wei and Zhao, Xiaohang (2016), A Novel TP53 Pathway Influences the HGS-Mediated Exosome Formation in Colorectal Cancer. *Scientific Reports*, 6.

Taha, Eman A., Sogawa, Chiharu, Okusha, Yuka, Kawai, Hotaka, Oo, May Wathone, Elseoudi, Abdellatif, Lu, Yanyin, Nagatsuka, Hitoshi, Kubota, Satoshi, Satoh, Ayano, Okamoto, Kuniaki and Eguchi, Takanori (2020), Knockout of MMP3 Weakens Solid Tumor Organoids and Cancer Extracellular Vesicles. *Cancers 2020, Vol. 12, Page 1260*, 12(5): 1260.

Takeshita, N., Hoshino, I., Mori, M., Akutsu, Y., Hanari, N., Yoneyama, Y., Ikeda, N., Isozaki, Y., Maruyama, T., Akanuma, N., Komatsu, A., Jitsukawa, M. and Matsubara, H. (2013), Serum MicroRNA Expression Profile: MiR-1246 as a Novel Diagnostic and Prognostic Biomarker for Oesophageal Squamous Cell Carcinoma. *British Journal of Cancer*, 108(3): 644–652.

Takov, Kaloyan, Yellon, Derek M. and Davidson, Sean M. (2017), Confounding Factors in Vesicle Uptake Studies Using Fluorescent Lipophilic Membrane Dyes. *Journal of extracellular vesicles*, 6(1).

Tamai, Keiichi, Tanaka, Nobuyuki, Nakano, Takashi, Kakazu, Eiji, Kondo, Yasuteru, Inoue, Jun, Shiina, Masaaki, Fukushima, Koji, Hoshino, Tomoaki, Sano, Kouichi, Ueno, Yoshiyuki, Shimosegawa, Tooru and Sugamura, Kazuo (2010), Exosome Secretion of Dendritic Cells Is Regulated by Hrs, an ESCRT-0 Protein. *Biochemical and Biophysical Research Communications*, 399(3): 384–390.

Tan, Yunhan, Wang, Zhihan, Xu, Mengtong, Li, Bowen, Huang, Zhao, Qin, Siyuan, Nice, Edouard C., Tang, Jing and Huang, Canhua (2023), Oral Squamous Cell Carcinomas: State of the Field and Emerging Directions. *International Journal of Oral Science 2023 15:1*, 15(1): 1–23.

Taylor, Jack, Azimi, Iman, Monteith, Gregory and Bebawy, Mary (2020), Ca2+ Mediates Extracellular Vesicle Biogenesis through Alternate Pathways in Malignancy. *Journal of Extracellular Vesicles*, 9(1).

Taylor, Jack and Bebawy, Mary (2019), Proteins Regulating Microvesicle Biogenesis and Multidrug Resistance in Cancer. *Proteomics*, 19(1–2): 1800165.

Testai, F. D., Landek, M. A. and Dawson, Glyn (2004), Regulation of Sphingomyelinases in Cells of the Oligodendrocyte Lineage. *Journal of neuroscience research*, 75(1): 66–74.

Théry, Clotilde, Witwer, Kenneth W., Aikawa, Elena, Alcaraz, Maria Jose, Anderson, Johnathon D., Andriantsitohaina, Ramaroson, Antoniou, Anna, Arab, Tanina, Archer, Fabienne, Atkin-Smith, Georgia K., Ayre, D. Craig, Bach, Jean Marie, Bachurski, Daniel, Baharvand, Hossein, Balaj, Leonora, Baldacchino, Shawn, Bauer, Natalie N., Baxter, Amy A., Bebawy, Mary, Beckham, Carla, Bedina Zavec, Apolonija, Benmoussa, Abderrahim, Berardi, Anna C., Bergese, Paolo, Bielska, Ewa, Blenkiron, Cherie, Bobis-Wozowicz, Sylwia, Boilard, Eric, Boireau, Wilfrid, Bongiovanni, Antonella, Borràs, Francesc E., Bosch, Steffi, Boulanger, Chantal M., Breakefield, Xandra, Breglio, Andrew M., Brennan, Meadhbh, Brigstock, David R., Brisson, Alain, Broekman, Marike L.D., Bromberg, Jacqueline F., Bryl-Górecka, Paulina, Buch, Shilpa, Buck, Amy H., Burger, Dylan, Busatto, Sara, Buschmann, Dominik, Bussolati, Benedetta, Buzás, Edit I., Byrd, James Bryan, Camussi, Giovanni, Carter, David R.F., Caruso, Sarah, Chamley, Lawrence W., Chang, Yu Ting, Chaudhuri, Amrita Datta, Chen, Chihchen, Chen, Shuai, Cheng, Lesley, Chin, Andrew R., Clayton, Aled, Clerici, Stefano P., Cocks, Alex, Cocucci, Emanuele, Coffey, Robert J., Cordeiro-da-Silva, Anabela, Couch, Yvonne, Coumans, Frank A.W., Coyle, Beth, Crescitelli, Rossella, Criado, Miria Ferreira, D'Souza-Schorey, Crislyn, Das, Saumya, de Candia, Paola, De Santana, Eliezer F., De Wever, Olivier, del Portillo, Hernando A., Demaret, Tanguy, Deville, Sarah, Devitt, Andrew, Dhondt, Bert, Di Vizio, Dolores, Dieterich, Lothar C., Dolo, Vincenza, Dominguez Rubio, Ana Paula, Dominici, Massimo, Dourado, Mauricio R., Driedonks, Tom A.P., Duarte, Filipe V., Duncan, Heather M., Eichenberger, Ramon M., Ekström, Karin, EL Andaloussi, Samir, Elie-Caille, Celine, Erdbrügger, Uta, Falcón-Pérez, Juan M., Fatima, Farah, Fish, Jason E., Flores-Bellver, Miguel, Försönits, András, Frelet-Barrand, Annie, Fricke, Fabia, Fuhrmann, Gregor, Gabrielsson, Susanne, Gámez-Valero, Ana, Gardiner, Chris, Gärtner, Kathrin, Gaudin, Raphael, Gho, Yong Song, Giebel, Bernd, Gilbert, Caroline, Gimona, Mario, Giusti, Ilaria, Goberdhan, Deborah C.I., Görgens, André, Gorski, Sharon M., Greening, David W.,

Gross, Julia Christina, Gualerzi, Alice, Gupta, Gopal N., Gustafson, Dakota, Handberg, Aase, Haraszti, Reka A., Harrison, Paul, Hegyesi, Hargita, Hendrix, An, Hill, Andrew F., Hochberg, Fred H., Hoffmann, Karl F., Holder, Beth, Holthofer, Harry, Hosseinkhani, Baharak, Hu, Guoku, Huang, Yiyao, Huber, Veronica, Hunt, Stuart, Ibrahim, Ahmed Gamal Eldin, Ikezu, Tsuneya, Inal, Jameel M., Isin, Mustafa, Ivanova, Alena, Jackson, Hannah K., Jacobsen, Soren, Jay, Steven M., Jayachandran, Muthuvel, Jenster, Guido, Jiang, Lanzhou, Johnson, Suzanne M., Jones, Jennifer C., Jong, Ambrose, Jovanovic-Talisman, Tijana, Jung, Stephanie, Kalluri, Raghu, Kano, Shin ichi, Kaur, Sukhbir, Kawamura, Yumi, Keller, Evan T., Khamari, Delaram, Khomyakova, Elena, Khvorova, Anastasia, Kierulf, Peter, Kim, Kwang Pyo, Kislinger, Thomas, Klingeborn, Mikael, Klinke, David J., Kornek, Miroslaw, Kosanović, Maja M., Kovács, Árpád Ferenc, Krämer-Albers, Eva Maria, Krasemann, Susanne, Krause, Mirja, Kurochkin, Igor V., Kusuma, Gina D., Kuypers, Sören, Laitinen, Saara, Langevin, Scott M., Languino, Lucia R., Lannigan, Joanne, Lässer, Cecilia, Laurent, Louise C., Lavieu, Gregory, Lázaro-Ibáñez, Elisa, Le Lay, Soazig, Lee, Myung Shin, Lee, Yi Xin Fiona, Lemos, Debora S., Lenassi, Metka, Leszczynska, Aleksandra, Li, Isaac T.S., Liao, Ke, Libregts, Sten F., Ligeti, Erzsebet, Lim, Rebecca, Lim, Sai Kiang, Linē, Aija, Linnemannstöns, Karen, Llorente, Alicia, Lombard, Catherine A., Lorenowicz, Magdalena J., Lörincz, Ákos M., Lötvall, Jan, Lovett, Jason, Lowry, Michelle C., Loyer, Xavier, Lu, Quan, Lukomska, Barbara, Lunavat, Taral R., Maas, Sybren L.N., Malhi, Harmeet, Marcilla, Antonio, Mariani, Jacopo, Mariscal, Javier, Martens-Uzunova, Elena S., Martin-Jaular, Lorena, Martinez, M. Carmen, Martins, Vilma Regina, Mathieu, Mathilde, Mathivanan, Suresh, Maugeri, Marco, McGinnis, Lynda K., McVey, Mark J., Meckes, David G., Meehan, Katie L., Mertens, Inge, Minciacchi, Valentina R., Möller, Andreas, Møller Jørgensen, Malene, Morales-Kastresana, Aizea, Morhayim, Jess, Mullier, François, Muraca, Maurizio, Musante, Luca, Mussack, Veronika, Muth, Dillon C., Myburgh, Kathryn H., Najrana, Tanbir, Nawaz, Muhammad, Nazarenko, Irina, Nejsum, Peter, Neri, Christian, Neri, Tommaso, Nieuwland, Rienk, Nimrichter, Leonardo, Nolan, John P., Nolte-'t Hoen, Esther N.M., Noren Hooten, Nicole, O'Driscoll, Lorraine, O'Grady, Tina, O'Loghlen, Ana, Ochiya, Takahiro, Olivier, Martin, Ortiz, Alberto, Ortiz, Luis A., Osteikoetxea, Xabier, Ostegaard, Ole, Ostrowski, Matias, Park, Jaesung, Pegtel, D. Michiel, Peinado, Hector, Perut, Francesca, Pfaffl, Michael W., Phinney, Donald G., Pieters, Bartijn C.H., Pink, Ryan C., Pisetsky, David S., Pogge von Strandmann, Elke, Polakovicova, Iva, Poon, Ivan K.H., Powell, Bonita H., Prada, Ilaria, Pulliam, Lynn, Quesenberry, Peter, Radeghieri, Annalisa, Raffai, Robert L., Raimondo, Stefania, Rak, Janusz, Ramirez, Marcel I., Raposo, Graça, Rayyan, Morsi S., Regev-Rudzki, Neta, Ricklefs, Franz L., Robbins, Paul D., Roberts, David D., Rodrigues, Silvia C., Rohde, Eva, Rome, Sophie, Rouschop, Kasper M.A., Rughetti, Aurelia, Russell, Ashley E., Saá, Paula, Sahoo, Susmita, Salas-Huenuleo, Edison, Sánchez, Catherine,

Saugstad, Julie A., Saul, Meike J., Schiffelers, Raymond M., Schneider, Raphael, Schøyen, Tine Hiorth, Scott, Aaron, Shahaj, Eriomina, Sharma, Shivani, Shatnyeva, Olga, Shekari, Faezeh, Shelke, Ganesh Vilas, Shetty, Ashok K., Shiba, Kiyotaka, Siljander, Pia R.M., Silva, Andreia M., Skowronek, Agata, Snyder, Orman L., Soares, Rodrigo Pedro, Sódar, Barbara W., Soekmadji, Carolina, Sotillo, Javier, Stahl, Philip D., Stoorvogel, Willem, Stott, Shannon L., Strasser, Erwin F., Swift, Simon, Tahara, Hidetoshi, Tewari, Muneesh, Timms, Kate, Tiwari, Swasti, Tixeira, Rochelle, Tkach, Mercedes, Toh, Wei Seong, Tomasini, Richard, Torrecilhas, Ana Claudia, Tosar, Juan Pablo, Toxavidis, Vasilis, Urbanelli, Lorena, Vader, Pieter, van Balkom, Bas W.M., van der Grein, Susanne G., Van Deun, Jan, van Herwijnen, Martijn J.C., Van Keuren-Jensen, Kendall, van Niel, Guillaume, van Royen, Martin E., van Wijnen, Andre J., Vasconcelos, M. Helena, Vechetti, Ivan J., Veit, Tiago D., Vella, Laura J., Velot, Émilie, Verweij, Frederik J., Vestad, Beate, Viñas, Jose L., Visnovitz, Tamás, Vukman, Krisztina V., Wahlgren, Jessica, Watson, Dionysios C., Wauben, Marca H.M., Weaver, Alissa, Webber, Jason P., Weber, Viktoria, Wehman, Ann M., Weiss, Daniel J., Welsh, Joshua A., Wendt, Sebastian, Wheelock, Asa M., Wiener, Zoltán, Witte, Leonie, Wolfram, Joy, Xagorari, Angeliki, Xander, Patricia, Xu, Jing, Yan, Xiaomei, Yáñez-Mó, María, Yin, Hang, Yuana, Yuana, Zappulli, Valentina, Zarubova, Jana, Žėkas, Vytautas, Zhang, Jian ye, Zhao, Zezhou, Zheng, Lei, Zheutlin, Alexander R., Zickler, Antje M., Zimmermann, Pascale, Zivkovic, Angela M., Zocco, Davide and Zuba-Surma, Ewa K. (2018), Minimal Information for Studies of Extracellular Vesicles 2018 (MISEV2018): A Position Statement of the International Society for Extracellular Vesicles and Update of the MISEV2014 Guidelines. *Journal of Extracellular Vesicles*, 7(1).

Thippabhotla, Sirisha, Zhong, Cuncong and He, Mei (2019), 3D Cell Culture Stimulates the Secretion of in Vivo like Extracellular Vesicles. *Scientific Reports*, 9(1): 1–14.

Tominaga, Naoomi, Hagiwara, Keitaro, Kosaka, Nobuyoshi, Honma, Kimi, Nakagama, Hitoshi and Ochiya, Takahiro (2014), RPN2-Mediated Glycosylation of Tetraspanin CD63 Regulates Breast Cancer Cell Malignancy. *Molecular Cancer*, 13(1): 1–11.

Trajkovic, Katarina, Hsu, Chieh, Chiantia, Salvatore, Rajendran, Lawrence, Wenzel, Dirk, Wieland, Felix, Schwille, Petra, Brügger, Britta and Simons, Mikael (2008), Ceramide Triggers Budding of Exosome Vesicles into Multivesicular Endosomes. *Science*, 319(5867): 1244–1247.

Trivedi, Alka Ben, Kitabatake, Naofumi and Doi, Etsushiro (1990), Toxicity of Dimethyl Sulfoxide as a Solvent in Bioassay System with HeLa Cells Evaluated Colorimetrically with 3-(4,5-Dimethyl Thiazol-2-Yl)-2,5-Diphenyl-Tetrazolium Bromide. *Biol. Chem*, 54: 2961–2966.

Ungefroren, Hendrik (2021), Autocrine TGF-β in Cancer: Review of the Literature and Caveats in Experimental Analysis. *International Journal of Molecular Sciences*, 22(2): 1–22.

Vázquez-Villa, Fernando, García-Ocaña, Marcos, Galván, José A., García-Martínez, Jorge, García-Pravia, Carmen, Menéndez-Rodríguez, Primitiva, Rey, Carmen González del, Barneo-Serra, Luis and de los Toyos, Juan R. (2015), COL11A1/(pro)Collagen 11A1 Expression Is a Remarkable Biomarker of Human Invasive Carcinoma-Associated Stromal Cells and Carcinoma Progression. *Tumour biology : the journal of the International Society for Oncodevelopmental Biology and Medicine*, 36(4): 2213–2222.

Vered, Marilena, Lehtonen, Meri, Hotakainen, Lari, Pirilä, Emma, Teppo, Susanna, Nyberg, Pia, Sormunen, Raija, Zlotogorski-Hurvitz, Ayelet, Salo, Tuula and Dayan, Dan (2015), Caveolin-1 Accumulation in the Tongue Cancer Tumor Microenvironment Is Significantly Associated with Poor Prognosis: An in-Vivo and in-Vitro Study. *BMC Cancer*, 15(1).

Vidal, Michel, Mangeat, Paul and Hoekstra, Dick (1997), Aggregation Reroutes Molecules from a Recycling to a Vesicle-Mediated Secretion Pathway during Reticulocyte Maturation. *Journal of Cell Science*, 110(16): 1867–1877.

Vigneswaran, Nadarajah, Beckers, Simone, Waigel, Sabine, Mensah, John, Wu, Jean, Mo, Juan, Fleisher, Kenneth E., Bouquot, Jerry, Sacks, Peter G. and Zacharias, Wolfgang (2006), Increased EMMPRIN (CD 147) Expression during Oral Carcinogenesis. *Experimental and Molecular Pathology*, 80(2): 147–159.

Villarroya-Beltri, Carolina, Gutiérrez-Vázquez, Cristina, Sánchez-Cabo, Fátima, Pérez-Hernández, Daniel, Vázquez, Jesús, Martin-Cofreces, Noa, Martinez-Herrera, Dannys Jorge, Pascual-Montano, Alberto, Mittelbrunn, María and Sánchez-Madrid, Francisco (2013), Sumoylated HnRNPA2B1 Controls the Sorting of MiRNAs into Exosomes through Binding to Specific Motifs. *Nature Communications*, 4: 2980.

Villasante, Aranzazu, Marturano-Kruik, Alessandro, Ambati, Srikanth R., Liu, Zen, Godier-Furnemont, Amandine, Parsa, Hesam, Lee, Benjamin W., Moore, Malcolm A.S. and Vunjak-Novakovic, Gordana (2016), Recapitulating the Size and Cargo of Tumor Exosomes in a Tissue-Engineered Model. *Theranostics*, 6(8): 1119–1130.

Vorstandlechner, Vera, Laggner, Maria, Kalinina, Polina, Haslik, Werner, Radtke, Christine, Shaw, Lisa, Lichtenberger, Beate Maria, Tschachler, Erwin, Ankersmit, Hendrik Jan and Mildner, Michael (2020), Deciphering the Functional Heterogeneity of Skin Fibroblasts Using Single-Cell RNA Sequencing. *The FASEB Journal*, 34(3): 3677–3692.

Wang, Cheng, Wang, Gang, Zhang, Lu, Pan, Jingen and Wei, Yajun (2017), Latent Transforming Growth Factor β Binding Protein 2 (LTBP2) as a Novel Biomarker for the Diagnosis and Prognosis of Pancreatic Carcinoma. *Medical Science Monitor : International Medical Journal of Experimental and Clinical Research*, 23: 3232.

Wang, Rui, Zhu, Jianghai, Dong, Xianchi, Shi, Minlong, Lu, Chafen and Springer, Timothy A. (2012), A Highlights from MBoC Selection: GARP Regulates the Bioavailability and Activation of TGFβ. *Molecular Biology of the Cell*, 23(6): 1129.

Wang, Ssu Han, Liou, Gunn Guang, Liu, Szu Heng, Chang, Jeffrey S., Hsiao, Jenn Ren, Yen, Yi Chen, Chen, Yu Lin, Wu, Wan Ling, Chang, Jang Yang and Chen, Ya Wen (2019), Laminin Γ2-Enriched Extracellular Vesicles of Oral Squamous Cell Carcinoma Cells Enhance in Vitro Lymphangiogenesis via Integrin A3-Dependent Uptake by Lymphatic Endothelial Cells. *International Journal of Cancer*, 144(11): 2795–2810.

Wang, Xiaoning, Qin, Xing, Yan, Ming, Shi, Jianbo, Xu, Qin, Li, Zhihui, Yang, Wenjun, Zhang, Jianjun and Chen, Wantao (2019), Loss of Exosomal MiR-3188 in Cancer-Associated Fibroblasts Contributes to HNC Progression. *Journal of Experimental and Clinical Cancer Research*, 38(1): 151.

Wang, Xiaowan, Berkowicz, Alexandra, King, Kirsten, Menta, Blaise, Gabrielli, Alexander P., Novikova, Lesya, Troutwine, Benjamin, Pleen, Joseph, Wilkins, Heather M. and Swerdlow, Russell H. (2022), Pharmacologic Enrichment of Exosome Yields and Mitochondrial Cargo. *Mitochondrion*, 64: 136–144.

Wang, Yingnan, Qin, Xing, Zhu, Xueqin, Chen, Wanjun, Zhang, Jianjun and Chen, Wantao (2018), Oral Cancer-Derived Exosomal NAP1 Enhances Cytotoxicity of Natural Killer Cells via the IRF-3 Pathway. *Oral Oncology*, 76: 34–41.

Webber, J. P., Spary, L. K., Sanders, A. J., Chowdhury, R., Jiang, W. G., Steadman, R., Wymant, J., Jones, A. T., Kynaston, H., Mason, M. D., Tabi, Z. and Clayton, A. (2015), Differentiation of Tumour-Promoting Stromal Myofibroblasts by Cancer Exosomes. *Oncogene*, 34(3): 319–333.

Webber, Jason, Steadman, Robert, Mason, Malcolm D., Tabi, Zsuzsanna and Clayton, Aled (2010), Cancer Exosomes Trigger Fibroblast to Myofibroblast Differentiation. *Cancer Research*, 70(23): 9621–9630.

Wiklander, Oscar P.B., Nordin, Joel Z., O'Loughlin, Aisling, Gustafsson, Ylva, Corso, Giulia, Mäger, Imre, Vader, Pieter, Lee, Yi, Sork, Helena, Seow, Yiqi, Heldring, Nina, Alvarez-Erviti, Lydia, Edvard Smith, C. I., Le Blanc, Katarina, Macchiarini, Paolo, Jungebluth, Philipp,

Wood, Matthew J.A. and El Andaloussi, Samir (2015), Extracellular Vesicle in Vivo Biodistribution Is Determined by Cell Source, Route of Administration and Targeting. *Journal of extracellular vesicles*, 4(2015): 1–13.

Wolf, P. (1967), The Nature and Significance of Platelet Products in Human Plasma. *British journal of haematology*, 13(3): 269–288.

Wu, Fanglong, Yang, Jin, Liu, Junjiang, Wang, Ye, Mu, Jingtian, Zeng, Qingxiang, Deng, Shuzhi and Zhou, Hongmei (2021), Signaling Pathways in Cancer-Associated Fibroblasts and Targeted Therapy for Cancer. *Signal Transduction and Targeted Therapy*, 6(1).

Xiao, Li, Hu, Qiannan, Peng, Yanshuang, Zheng, Kaiyue, Zhang, Ting, Yang, Lianjie, Wang, Zhi, Tang, Wanrong, Yu, Jie, Xiao, Qian, Zhang, Dandan, Zhang, Weifang, He, Chanjuan, Wu, Dengxun, Zheng, Yanyan and Liu, Ying (2021), TRAP1 Suppresses Oral Squamous Cell Carcinoma Progression by Reducing Oxidative Phosphorylation Metabolism of Cancer-Associated Fibroblasts. *BMC Cancer*, 21(1).

Xiao, Meng, Zhang, Jianjun, Chen, Wanjun and Chen, Wantao (2018), M1-like Tumor-Associated Macrophages Activated by Exosome-Transferred THBS1 Promote Malignant Migration in Oral Squamous Cell Carcinoma. *Journal of Experimental and Clinical Cancer Research*, 37(1).

Xie, N. N., Liu, Z. X., Wu, C., Wang, P. L., Song, G. T. and Chen, Z. (2018), MicroRNA-200c Suppresses Tumor Metastasis in Oral Squamous Carcinoma by Inhibiting Epithelial-Mesenchymal Transition. *European review for medical and pharmacological sciences*, 22(11): 3415–3422.

Xing, Haizhou, Liang, Chunyan, Xu, Xintong, Sun, Hui, Ma, Xiaojun and Jiang, Zhongxing (2020), Mesenchymal Stroma/Stem-like Cells of GARP Knockdown Inhibits Cell Proliferation and Invasion of Mouse Colon Cancer Cells (MC38) through Exosomes. *Journal of Cellular and Molecular Medicine*, 24(23): 13984–13990.

Yamamura, Rie, Nishimura, Noriyuki, Nakatsuji, Hiroyoshi, Arase, Seiji and Sasaki, Takuya (2008), The Interaction of JRAB/MICAL-L2 with Rab8 and Rab13 Coordinates the Assembly of Tight Junctions and Adherens Junctions. *Molecular biology of the cell*, 19(3): 971–983.

Yan, Yixuan, Yan, Fengzhi and Huang, Qun (2018), MiR-200c Inhibited the Proliferation of Oral Squamous Cell Carcinoma Cells by Targeting Akt Pathway and Its Downstream Glut1. *Archives of Oral Biology*, 96: 52–57.

Yan, Yumei, Jiang, Ke, Liu, Peng, Zhang, Xianbin, Dong, Xin, Gao, Jingchun, Liu, Quentin, Barr, Martin P., Zhang, Quan, Hou, Xiukun, Meng, Songshu and Gong, Peng (2016), Bafilomycin

A1 Induces Caspase-Independent Cell Death in Hepatocellular Carcinoma Cells via Targeting of Autophagy and MAPK Pathways. *Scientific Reports*, 6.

Yap, Tami, Pruthi, Neha, Seers, Christine, Belobrov, Simone, McCullough, Michael and Celentano, Antonio (2020), Extracellular Vesicles in Oral Squamous Cell Carcinoma and Oral Potentially Malignant Disorders: A Systematic Review. *International Journal of Molecular Sciences*, 21(4).

Yeon, Ju Hun, Jeong, Hyo Eun, Seo, Hyemin, Cho, Siwoo, Kim, Kimin, Na, Dokyun, Chung, Seok, Park, Jaesung, Choi, Nakwon and Kang, Ji Yoon (2018), Cancer-Derived Exosomes Trigger Endothelial to Mesenchymal Transition Followed by the Induction of Cancer-Associated Fibroblasts. *Acta Biomaterialia*, 76: 146–153.

Yoshida, Go J. (2020), Regulation of Heterogeneous Cancer-Associated Fibroblasts: The Molecular Pathology of Activated Signaling Pathways. *Journal of Experimental & Clinical Cancer Research 2020 39:1*, 39(1): 1–15.

You, Yiwen, Shan, Ying, Chen, Jing, Yue, Huijun, You, Bo, Shi, Si, Li, Xingyu and Cao, Xiaolei (2015), Matrix Metalloproteinase 13-Containing Exosomes Promote Nasopharyngeal Carcinoma Metastasis. *Cancer Science*, 106(12): 1669–1677.

You, Yuanhe, Tian, Zhuowei, Du, Zhong, Wu, Kailiu, Xu, Guisong, Dai, Meilu, Wang, Yan'an and Xiao, Meng (2022), M1-like Tumor-Associated Macrophages Cascade a Mesenchymal/Stem-like Phenotype of Oral Squamous Cell Carcinoma via the IL6/Stat3/THBS1 Feedback Loop. *Journal of Experimental & Clinical Cancer Research : CR*, 41(1): 10–16.

Yu, Chenhang, Li, Qiang, Zhang, Yu, Wen, Zhi Fa, Dong, Heng and Mou, Yongbin (2022), Current Status and Perspective of Tumor Immunotherapy for Head and Neck Squamous Cell Carcinoma. *Frontiers in Cell and Developmental Biology*, 10.

Yu, Shijun, Chen, Jingde, Quan, Ming, Li, Li, Li, Yandong and Gao, Yong (2021), CD63 Negatively Regulates Hepatocellular Carcinoma Development through Suppression of Inflammatory Cytokine-induced STAT3 Activation. *Journal of Cellular and Molecular Medicine*, 25(2): 1024.

Yu, Zhenyang, Zeng, Jian, Wang, Jun, Cui, Yaxiong, Song, Xiaopeng, Zhang, Yizhe, Cheng, Xuan, Hou, Ning, Teng, Yan, Lan, Yu, Chen, Yeguang and Yang, Xiao (2021), Hepatocyte Growth Factor-Regulated Tyrosine Kinase Substrate Is Essential for Endothelial Cell Polarity and Cerebrovascular Stability. *Cardiovascular Research*, 117(2): 533.

Zanotti, Simona, Gibertini, Sara, Blasevich, Flavia, Bragato, Cinzia, Ruggieri, Alessandra, Saredi, Simona, Fabbri, Marco, Bernasconi, Pia, Maggi, Lorenzo, Mantegazza, Renato and Mora, Marina (2018), Exosomes and Exosomal MiRNAs from Muscle-Derived Fibroblasts Promote Skeletal Muscle Fibrosis. *Matrix biology : journal of the International Society for Matrix Biology*, 74: 77–100.

Zhang, Fayun, Zheng, Zifeng, Wang, Luoyang, Zeng, Wenfeng, Wei, Wenjing, Zhang, Chunling, Zhao, Ziran and Liang, Wei (2023), PKC-ζ Mediated Reduction of the Extracellular Vesicles-Associated TGF-B1 Overcomes Radiotherapy Resistance in Breast Cancer. *Breast Cancer Research*, 25(1): 1–14.

Zhang, Jia Yi, Zhu, Wei Wen, Wang, Meng Yao, Zhai, Run Dong, Wang, Qiong, Shen, Wei Li and Liu, Lai Kui (2021a), Cancer-Associated Fibroblasts Promote Oral Squamous Cell Carcinoma Progression through LOX-Mediated Matrix Stiffness. *Journal of translational medicine*, 19(1).

Zhang, Jia-Yi, Wang, Ya-Min, Song, Le-Bin, Chen, Chen, Wang, Yi-Chun and Song, Ning-Hong (2016), Prognostic Significance of MicroRNA-200c in Various Types of Cancer: An Updated Meta-Analysis of 34 Studies. *Molecular and Clinical Oncology*, 4(6): 933–941.

Zhang, Wei, Zhao, Pu, Xu, Xiu Li, Cai, Lei, Song, Zhen Shun, Cao, Da Yong, Tao, Kai Shan, Zhou, Wen Ping, Chen, Zhi Nan and Dou, Ke Feng (2013), Annexin A2 Promotes the Migration and Invasion of Human Hepatocellular Carcinoma Cells In Vitro by Regulating the Shedding of CD147-Harboring Microvesicles from Tumor Cells. *PLOS ONE*, 8(8): e67268.

Zhang, Yanqi, Liu, Jianing, Liu, Shiyu, Yu, Lu, Liu, Siying, Li, Meng and Jin, Fang (2023), Extracellular Vesicles in Oral Squamous Cell Carcinoma: Current Progress and Future Prospect. *Frontiers in Bioengineering and Biotechnology*, 11.

Zhang, Yuan, Liu, Yunfeng, Liu, Haiying and Tang, Wai Ho (2019), Exosomes: Biogenesis, Biologic Function and Clinical Potential. *Cell and Bioscience*, 9(1).

Head and Neck Cancers Statistics | Cancer Research UK. available at https://www.cancerresearchuk.org/health-professional/cancer-statistics/statistics-by-cancer-type/head-and-neck-cancers#heading-Zero